Helwan University

Faculty of Engineering

Civil Engineering Department

Mattaria-Cairo

Behavior of GFRP- Reinforced Concrete Beams under Torsion

A Thesis

Submitted in Partial Fulfillment for the Requirements of the Degree of Master of Science in civil Engineering.

By

Eng. Abdullah Fares Nafez Sayed Emam

B.Sc.2017, Civil Engineering

Supervised by

Assoc. Prof. Hala Mamdouh Esmael

Assoc. Professor of civil Eng.

Faculty of Engineering Mataria

Helwan University

Assoc. Prof. Ahmed Mohammed Hassan Ali

Assoc. Professor of civil Eng.

Faculty of Engineering Mataria

Helwan University

2024

ACKNOWLEDGEMENTS

I would like to thank ALLAH for the blessings that ALLAH granted to me all the way till I finished this research, and all through my life.

I want to express this profound gratitude and deep appreciation to the supervisors and thank them for their great effort for solving all problems during the research and for direct supervisions and valuable advice and their continuous encouragement.

Associate.Prof. Dr. Hala Mamdouh Esmael,

Associate.Prof. Dr. Ahmed Mohammed Hassan Ali

I am writing to extend my deepest gratitude for the invaluable assistance and support of my supervisors and my family, have provided me with my research. their effort, guidance, and expertise have been instrumental in shaping the direction and quality of my work.

Their willingness to share their knowledge and provide thoughtful feedback has not only enhanced my research but also inspired me to strive for excellence. I am truly grateful for the time and energy they have dedicated to helping me.

Thank they once again for their unwavering support and encouragement. It has been an honor to learn from them, and I look forward to any future opportunities to collaborate.

I want to dedicate this thesis to my family and my friends for their love and continuous encouragement during my life and whatever I do for them not fulfilled their right and all what I hope is a pleasing ALLAH then my father and mother.

ABSTRACT

The thesis aims to study the behavior of concrete beams reinforced in longitudinal and transverse directions with GFRP under pure torsion and concrete beams without stirrups with longitudinal reinforcement only. The study based on nine concrete beams, controlled beam reinforced in longitudinal and transverse directions with steel reinforcement under pure torsion. Six beams were reinforced in longitudinal and transverse directions with GFRP, five of them were tested under pure torsion with increasing of stirrups, inclined stirrups, additional side bars, and increasing of concrete strength. Sixth beam was tested under combined torsional and bending moments with shear force. In addition to, two concrete beams reinforced with steel bars in longitudinal direction and without transverse reinforcement, one was tested under pure torsion and the other under combined torsional and bending moments with shear force. The beams tested with many variables and were compared with the steel reinforced concrete beams counterpart to GFRP. The variables were behavior of GFRP reinforcement under torsion, configuration of stirrups, changing of stirrups spacing, the difference loading, changing of concrete strength and influence of absent stirrups. The results show that all beams failed under torsional loading. The torsional capacity improved with increasing transverse reinforcement. The crack pattern was clear and over all beam for steel RC beams comparing to counterpart GFRP. The inclined stirrups method was not effective because the crack is parallel to the stirrups in addition to the weak bond between the beam and GFRP torsional reinforcement contributed to decrease the torsional strength capacity less than the initial torsional capacity for control beam. The increasing of concrete strength improved the bond so the concrete capacity increased. Using the $f_{ft} = 0.4f_{fv}$ mothed in CAN/CSA S806-12 was the better method to calculate the torsional strength,

but needed more modifications and the tensile strength of the bent GFRP stirrups method was less prediction of torsional strength of GFRP stirrups.

Table of content

List of Tables

List of Figures

CHAPTER ONE

INTRODUCTION

1.1 General.

Concrete is one of the most important building materials in modern era, especially with its reinforcement with steel to become reinforced concrete but corrosion of steel reinforcement is one of the main factors reducing the sustainability of reinforced concrete (RC) structures. Nevertheless, many existing concrete structures show significant corrosion, often when comparatively new, leading to the need for expensive repair.

In the construction of modern buildings, the world trends to use alternative to steel to overcome the corrosion of steel. Glass fiber reinforced polymer GFRP is the more common alternative in those days because it has a high resistance to corrosion (not permeable to salinity and alkaline), Light weight about 25% of the weight of the reinforcement steel rebar, long-term benefits of GFRP rebar, it is a cost-effective product as compared with epoxy-coated or stainless steel, GFRP rebar is non-conductive to electricity and heat, it is impervious to chloride ions and other chemical elements and It can be manufactured in custom lengths, bends, and shapes.

Torsional moment is common in many buildings. Torsion is one of the forces that beams may be subjected to this force, and it's explained as the twisting of an object due to an applied torque and it can exist in curved or circular beams, beams supporting a slab or a beam on one side only and beams supporting loads that act far away transverse to the longitudinal axis of the beam etc.

This thesis shows the experimental results obtained from an experimental investigation of nine specimens which present the beams were tested under

pure torsion or with combine forces with normal strength concrete or high strength concrete. One specimen was control beam reinforced with steel in transverse and longitudinal. Five specimens were reinforced with GFRP in transverse and longitudinal. Two specimens were reinforced with steel in longitudinal without stirrups. The experiment showed many parameters; effect of vary compressive strength of concrete and reinforcing material, configuration of stirrups effect of longitudinal bars, effect of spacing of the stirrups, loading types and the effect of absent of stirrups. This thesis discussed the behavior of GFRP- reinforced concrete beams under torsion.

1.2 Objectives.

The objectives of this study are to study the behaviour of GFRP reinforced beams under torsion. The use of FRP as reinforcement for concrete structures is widely increasing. Nevertheless, the torsional behavior of concrete members reinforced in longitudinal and transverse directions with GFRP has not yet been fully explored. Several codes and design guidelines addressing FRP as primary reinforcement for structural concrete have been published, but few codes (CSA S806-12) report the torsional design provisions incorporated in these codes and design guides are based on the design formulas of structure reinforced with conventional steel considering some modifications to account for the substantial differences between FRP and conventional reinforcement. Taking into account the empirical nature of most of the current shear design methods, investigations are required to examine the validity of these methods. The main objectives of this investigation can be summarized as follows:

1. Investigate the torsional behavior and failure mode mechanisms of beams reinforced with GFRP bars and stirrups under pure torsional loading.

2. Study the influence of concrete strength on the beams reinforced with GFRP bars and stirrups torsional reinforcement on the concrete torsion strength.
3. Study the influence of GFRP transverse reinforcement ratio on the concrete torsional strength.
4. Study the influence of using inclined GFRP transverse reinforcement on the concrete torsional strength.
5. Study the influence absent stirrups on the behavior of GFRP RC beams under pure torsion.
6. Study the influence difference loading on the behavior of GFRP RC beams and their torsional strength.
7. Assess the validity of the current FRP design provisions for estimating the concrete torsion strength, including ACI 318-19, CSA S806-12, and EGY 203-19.

1.3 Scope and contents.

scope of this work is to study the effect of bars and stirrups GFRP under torsion, and study the torsion under absenting of stirrups with using many parameters:

a- Behavior of GFRP reinforcement under torsion

b- Configuration of stirrups.

c- Changing of stirrups spacing.

d- The difference loading.

e- Changing of concrete strength.

f- Influence of absent stirrups.

This thesis consists of main seven chapters including available references, listing of Tables, listing of Figures and in the research field. The contents of

these chapters are as follows:

Chapter One: Introduction

This chapter consists of an introduction and definition of the problem, the objectives of the study, and the scope.

Chapter Two: Literature Review

This chapter presents the literature review, and backgrounds of the previous investigations were carried out on the solid section beams under torsion.

Chapter Three: Experimental Work

This chapter depicts the work program for the experiment which contains the details of tested R.C beams specimens, the materials properties and test set-up.

Chapter Four: Experimental Test Results

This chapter represents the results were analyzed under the effect of the parameters on the study individually. The behavior of the tested specimens was monitored for deflections, cracking and failure loads, the concrete and stirrups strains.

Chapter Five: Discussion and Analysis of Experimental Results

This chapter represents the analysis of all experimental results and the comparisons between behaviors of different test specimens.

Chapter Six: Analytical Equations and Comparison with Test Results

This chapter represents the design of tested beams using analytical equation of CSA S806-12, ECP and ACI codes and comparison with test results.

Chapter Seven: Conclusions and Recommendations

This chapter represents the main conclusions and recommendations based on the results of the experiment and suggestions for the future work and **References**.

CHAPTER TWO

LITERATURE REVIEW

2. 1 Introduction

Corrosion of steel reinforcement emerges as a huge factor affects badly in reinforced concrete structures. In the last years, the world went to have a new alternative for steel. One of those alternatives is glass fiber-reinforced polymer (GFRP). Currently, GFRP is used a lot as an alternative for steel. Currently several studies have been carried out to study the behavior of GFRP reinforced concrete structures under bending moment, shear and normal forces and a few studies in torsion. In this chapter, a literature review is presented for the previous research on the behavior of GFRP reinforced concrete beams under torsion.

2.2 Torsion in Beams

2.2.1General Behavior

A beam resists torsional moment (M_t) by shear flow within the effective thickness (t_d) from the outermost surface of member according to the thin-walled tube theory, as shown in Figure (2-1) (a) **[1]**. The equilibrium of the forces in the transverse direction among the shear elements of the thin-walled tubes with effective thickness t_d, as shown in Figure (2-1) (b) and (c), can be represented by considering the average compressive stress (σ_2) of the concrete compression strut and the stirrup stress and average tensile stress (σ_1) acting in a direction perpendicular thereto. According to thin-walled tube, torsion resists by the effective thickness t_d, so the core concrete cross section in a solid beam neglected. After cracking, the torsion forces resist by transverse and longitudinal reinforcement. The manner in which torsion failures can occur varies widely with the dimensions, outside perimeter of concrete cross section, loading, and properties of the members.

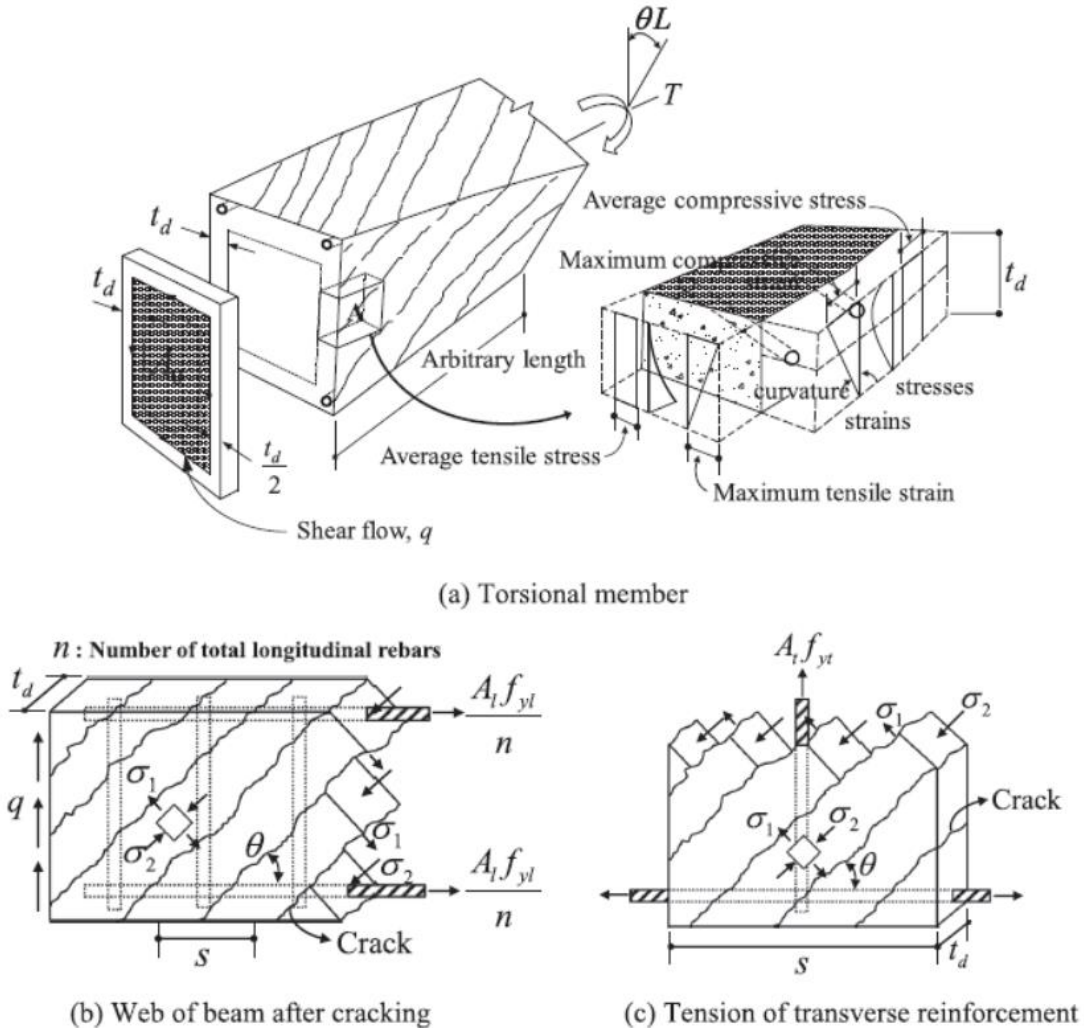

Figure (2-1): Equilibrium Conditions **[1]**

For this reason, there is no unique way to design for torsion. In design, the maximum reinforcement ratio is necessary to know, because of the torsion moment resists by reinforcement only. The maximum torsional reinforcement ratio that can ensure the yielding of the rebar before the compressive failure of the concrete struts to avoid the brittle torsional failure of reinforced concrete beams was derived based on the truss model. It was also designed to reflect the characteristics of torsional members and was presented in a very simple form to facilitate its practical application. In addition, the proposed model was verified by comparing its results with the experimental results of 98 specimens subjected to pure torsion, and the conclusions below were derived from the results.

- The strain gradients of the torsional members are related to the characteristics of reinforced concrete beams subjected to torsion, such as the tensile stress of concrete, the cross-sectional shape, the compressive softening phenomenon of concrete, and the average stress, and has the advantage that it can be applied to both transverse and longitudinal reinforcements.
- The CSA-14 provision estimated the yielding of the transverse rebars and the failure modes of the specimens with relatively good accuracy, but The ACI 318 code provided a conservative estimate of the maximum torsional reinforcement ratio, the EC2 code suggested a maximum torsional reinforcement ratio that was slightly on the unsafe side.

2.2.2 Torsion Cracking of Reinforced Concrete Beams

The major codes in world reveal the torsional design provisions that the members behave as thin-walled tube and when the torque is greater than cracking torque, the cracks present as a diagonal cracks spiraling around the tube wall Figure (2-2) **[2]**. At failure, the concrete cover on the exterior transverse torsion reinforcement, or hoops, is considered ineffective because it normally spalls off before failure.

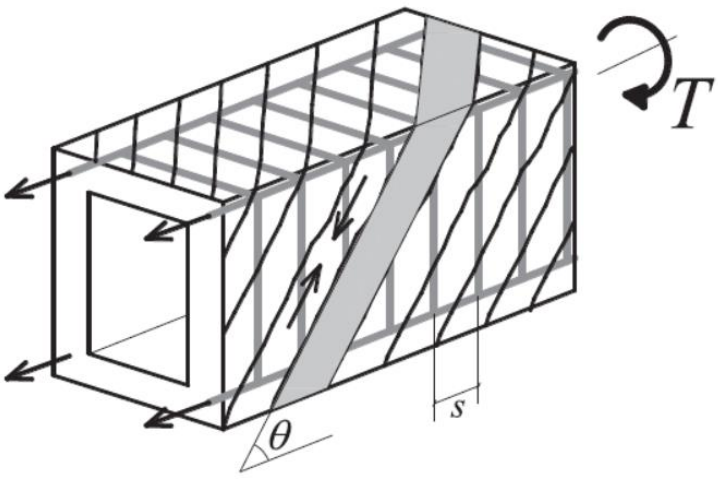

Figure (2-2): Cracked Section Under Torsion **[2]**

The torsional moment consists of tension and compression forces. The tension force is resisted by longitudinal and transverse reinforcements and the compression force is resisted by concrete struts, so the failure occurs by crushing concrete or yielding reinforcement. It is assumed that the centerline of tube-wall (t_w) is the centerline of stirrups, so some codes assumed that $A_o=0.85A_{oh}$ where A_o and A_{oh} are the areas enclosed by hollow tube and the centerlines of the hoops Figure (2-3).

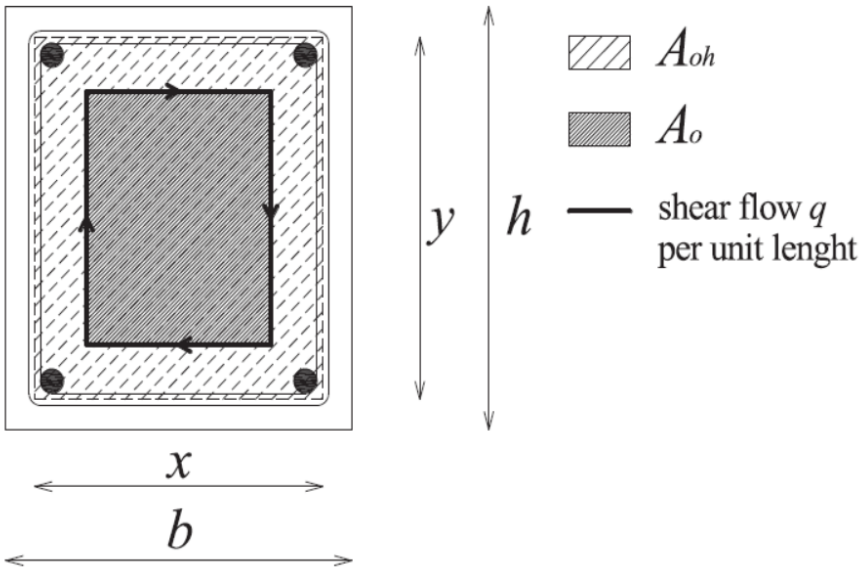

Figure (2-3): Cross Section of The Member **[2]**

When the reinforced bar is bent as stirrup or hoop, the axially stressed hoop will be subjected to radial compressive stress in its corner Figure (2-4) the ratio r_b/d_b and the magnitude of the axial stress in the bar govern the magnitude of stress in the corner (bending corner) where d_b and r_b are the diameter of bar and the radius of the bend. The stress at the corner is biaxial stress with is created from radial stress σ_r and axial stress σ_l.

The steel is isotropic and ductile which makes the axial stress is bigger than the radial stress generally, therefore, the radial stress is ignored. In the other hand, the radial stress in FRP is different because of the modulus and

strength of the bar (corner of FRP bent bar) is smaller than the longitudinal (circumferential) direction and the biaxial tensile compressive state of the stress at the bend. Therefore, the bent bar fails at small axial load than similar straight bar. The different also that the resin type and the bar fiber content have role in failure with the geometric parameter r_b/d_b.

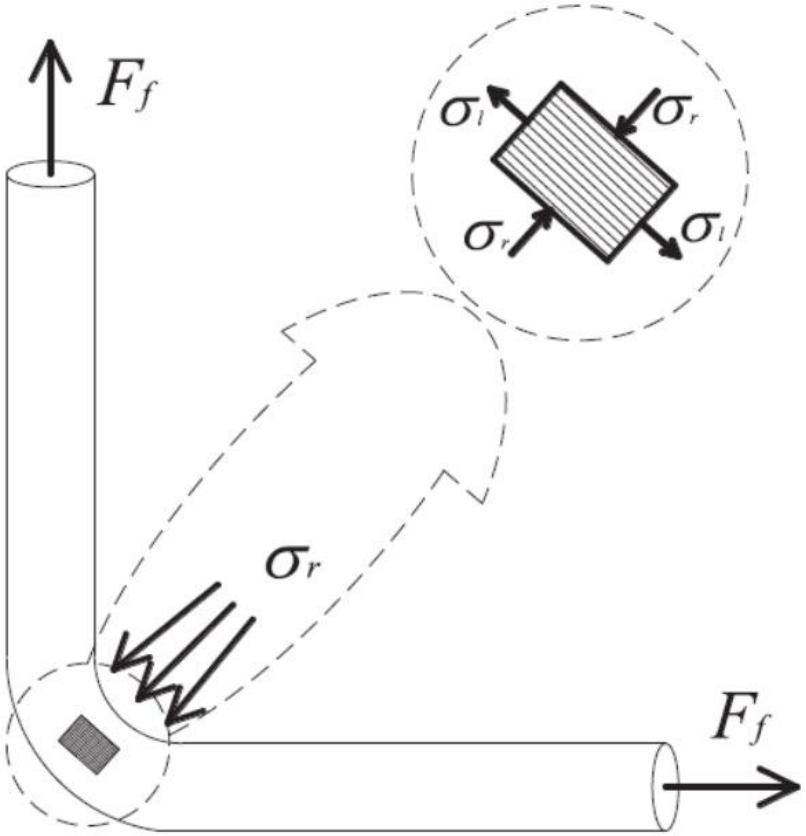

Figure (2-4): Corner of FRP Bent Bar **[2]**

Japan Society of Civil Engineers (JSCE) [3] suggested Equation (1), which was later adopted by ACI. By examining tested data using used the equation (1), too much data involved bars with r_b/d_b less than 5, but in case of $r_b/d_b > 5$ for GFRP and CFRP the Equation (1) would not be effective because the actual strength was smaller than the predicted strengths. On the other hand, for $r_b/d_b < 3$, the predicted strength was generally conservative, but in no case, irrespective of the bar size or material type, f_{bFu} was less than $0.4 f_{Fut}$. ACI 318 code states that the minimum bend diameter specified is 4-

6 times d_b up to 25 mm for reinforcement diameter. Considering reinforcement is generally not expected to be larger than 25 mm in diameter.

$$f_{bFu}=[0.05\frac{r_b}{d_b}+0.3]r_{Fut}$$ Equation (2-1)

Where

f_{Fut} = tensile strength of the FRP straight bar

f_{bFu} = tensile strength of the FRP bent bar

To prevent unacceptably wide diagonal cracks under service load, the **CSA S806 [4]** further limits the maximum strain in the FRP transverse reinforcement at ultimate state to 0.005, but it is recognized that the latter strain limit may be conservative when computing nominal torsional strength. Therefore, it is recommended here that when making comparison with experimental results, the transverse reinforcement stress at ultimate be assumed $0.4f_{Fut} \leq 1200$ MPa. Note that in the derivation of the **ACI 318 [5]** torsional design equations, to limit crack width, the maximum shear that can be resisted by concrete under torsion is limited to $0.833\sqrt{f'_c}$ where f'_c is in MPa, this limitation also leads to a conservative estimate of the ultimate strength.

It was stated earlier that the radial compressive stresses acting at the corner of the stirrup is mainly responsible for its lower strength compared to a companion straight bar. The works of **Imjai et al. [6-8]** supports this statement. They derived a macro-mechanical-based model, which considered the biaxial tension-compression state of stress at the stirrup bend and the longitudinal tensile and radial compressive strength of the bar, in conjunction with the Tsai-Hill failure criterion **[9]**. They arrived at the following equation for computing the stirrup strength.

$$f_{bFu}=\frac{f_{Fut}}{\sqrt{1+(\frac{r_b}{d_b})+(\frac{r_b}{d_b})^2\beta^2}}$$ Equation (2-2)

$$\beta = \frac{f_{Fut}}{f_{Fuc}}$$ Equation (2-3)

where f_{Fuc} is radial compressive strength of FRP bar.

At first glance at it may seem that the biaxial state of stress is not reflected by equation (2), but actually it is because from equilibrium of forces acting on the bar at the bend and assuming initially a uniform radial stress, one can express the results of this model are less conservative than those given by the empirical equation (1)

$$\frac{\sigma_l}{\sigma_r} = \frac{r_b}{d_b}$$ Equation (2-4)

The results of this model are less conservative than those given by the empirical equation (1) but follow the same basic trend. Hence, irrespective of the manufacturing process or other random phenomena, the bent bar strength is strongly reduced by the ratio of the bar diameter to bend radius. Furthermore, the somewhat higher strength predicted by equation (4) may be difficult to utilize in design because it may lead to wide cracks at the serviceability limit state.

2.2.3 Design for Torsion

2.2.3.1 American Code, ACI 318M-19[5]

The maximum torsion, T_u, in a beam must not exceed the design torsion capacity of the beam cross section, φT_n, where φ is 0.75 and T_n is the nominal torsional moment strength. The torsional moment is resisted by reinforcement only. Torsional moment must not exceed the torsional design strength.

In ACI 318M-19, the design for torsion is based on a thin-walled tube space truss analogy. The shear flow is constant at all points around the perimeter of the tube. Because of a lack of the test data and the practical experience with concretes have compressive strength greater than 70 MPa, the code imposes a maximum value of 8.3 MPa on $\sqrt{f'_c}$ for use in the calculation of

torsional strength. For control the diagonal crack width f_y and f_{yt} mustn't exceed 420 MPa. Threshold torsion is defined as one-fourth the cracking torsional moment T_{cr} where the cracking torsion is the cracking torsional moment under pure torsion, T_{cr}, is derived by replacing the exact section with an equivalent thin-walled tube with a wall thickness prior to cracking of 0.75 A_{cp} / p_{cp} and area enclosed by the wall centerline A_0 equal to $2A_{cp}/3$ where A_{cp} is area enclosed by outside perimeter of concrete cross section and P_{cp} is outside perimeter of concrete cross section where the tensile stress in concrete reaches to $0.33\sqrt{f'_c}$ the torsional cracking is assumed to accour, T_{cr}.

$$T_{cr}= 0.33\lambda\sqrt{f'_c}\left(\frac{A^2_{cp}}{P_{cp}}\right)$$ **ACI 318M-19** Equation (2-5)

$$T_{th}= 0.083\lambda\sqrt{f'_c}\left(\frac{A^2_{cp}}{P_{cp}}\right)$$ **ACI 318M-19** Equation (2-6)

Solid section

$$T_{th}= 0.083\lambda\sqrt{f'_c}\left(\frac{A^2_{g}}{P_{cp}}\right)$$ **ACI 318M-19** Equation (2-7)

Hollow section

Where A_g is gross area of concrete section mm^2 for hollow section, A_g is the area of concrete only doesn't include the area of the voids. If $A_g/A_{cp} \geq 0.95$, can be neglected when calculating T_{th}. The reinforcement resists the stress due to torsion, according to the space truss analogy in Figure (2-5) with compression diagonals at an angle θ. When the torsional stress exceeds to T_{cr} the torsional strength is provided mainly by outer closed stirrups, longitudinal reinforcement and compression diagonals.

By release shear flow due to torsion, an axial torsion force $N_i = V_i \cot\theta$ developed so it needed to resist by longitudinal reinforcement. axial torsion forces are assumed along the sides of the area Ao these sides form a perimeter length Po approximately equal to the length of the line

jointing the tube. For ease in calculation this has been replaced with the perimeter of the closed stirrups, Ph as shown in Figure (2-6).

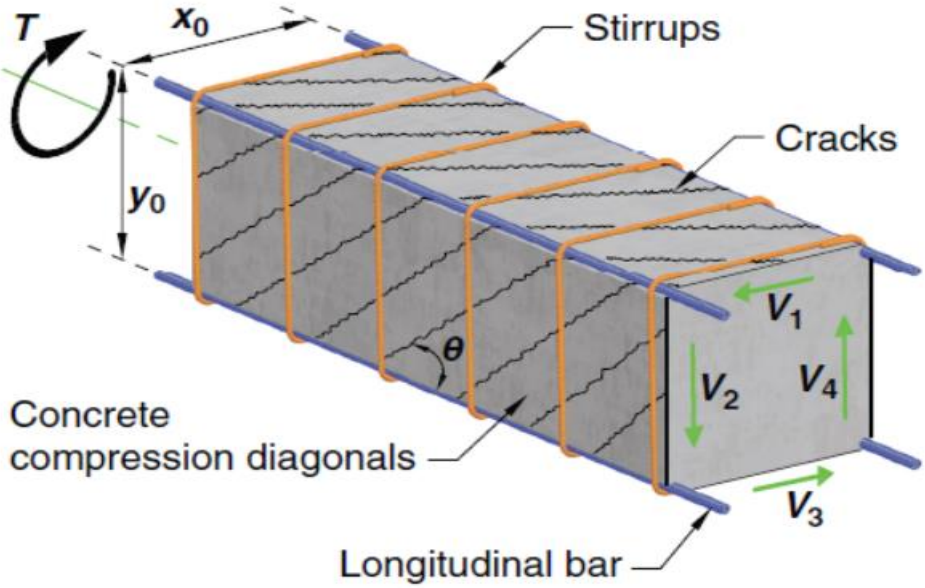

Figure (2-5): Space Truss Analogy **[5]**

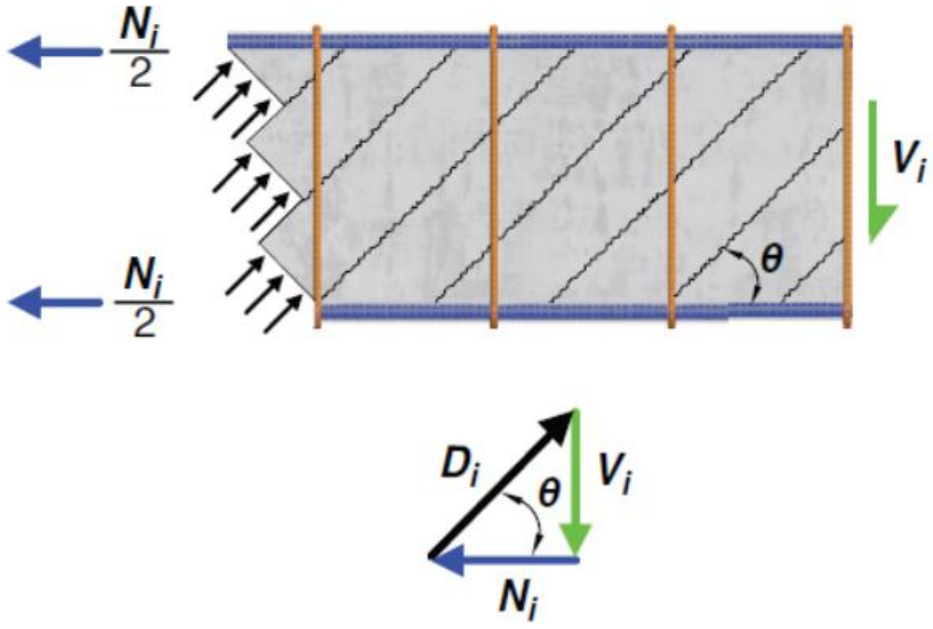

Figure (2-6): Resolution of Shear Force V_i into Diagonal Compression Force D_i and Axial Tension Force N_i in One Wall of Tube **[5]**

$T_n = \frac{2A_o A_t f_{yt}}{S} cot\,\theta$ **ACI 318M-19** Equation (2-8)

$T_n = \frac{2A_o A_l f_y}{P_h} cot\,\theta$ **ACI 318M-19** Equation (2-9)

θ = 45 for non-prestressed member.

Taking in account the cross-section limits.

$$\sqrt{(\frac{V_u}{b_w d})^2 + (\frac{T_u P_h}{1.7 A^2_{oh}})^2} \leq \varphi[\frac{V_u}{b_w d} + 0.66\sqrt{f'_c}]$$

ACI 318M-19 for solid section Equation 22.7.7.1 (a)

2.2.3.2 Egyptian Code, ECP 203-2019 [10]

Provisions of torsion design in Egyptian code of practice ECP 2019 are based on empirical equations and mix concrete characteristic strength is limited to 60 N/mm^2 and f_y = 400 N/mm^2. In ECP 2019 code, the basic design equations for the torsion capacity of concrete are…

$q_{tu} = \frac{M_{tu}}{2A_o t_e}$ **ECP** Equation (2-10)

$A_o = 0.85\,A_{oh}$

$t_e = A_{oh} / P_h$

If $q_{tu} \leq 0.06\sqrt{\frac{f_{cu}}{\gamma_c}}$ *N/mm^2* Neglect torsion design.

For solid section

$\sqrt{(q_u)^2 + (q_{tu})^2} \leq q_{umax}$ **ECP** Equation (2-11)

For hollow section

$q_u + q_{tu} \leq q_{umax}$ **ECP** Equation (2-12)

Where $q_{umax} = 0.7\sqrt{\frac{f_{cu}}{\gamma_c}}$ *N/mm^2* **ECP** Equation (2-13)

If $\sqrt{(q_u)^2 + (q_{tu})^2} \geq q_{umax}$ *or* $q_u + q_{tu} \geq q_{umax}$ increase section dimension taking in account the mix concrete characteristic strength is limited to 60 N/mm^2 and f_y = 400 N/mm^2

$q = q_u + q_{tu} - q_{cu}$ **ECP** Table (2-14)

$q_{cu} = 0.16\sqrt{\frac{f_{cu}}{\gamma_c}}$ (uncracked section) **ECP** Equation (2-15)

$A_{str(torsion)} = \frac{M_{tu}.S}{2A_o[\frac{f_{yst}}{\gamma_s}]}$ for torsion **ECP** Equation (2-16)

A_{str}(torsion) is subjected only outer of section (as outer stirrups) to resist the torsional moment.

$A_{str} = \frac{M_{tu}.S}{1.7(x_1.y_1)[\frac{f_{yst}}{\gamma_s}]}$ **ECP** Equation (2-17)

$A_{str(torsion)} + A_{st(shear)} \geq 0.4\ \frac{S.b}{f_{yst}}$ **ECP** Equation (2-18)

S$\leq$ 200mm or $\frac{P_h}{8}$

Additional longitudinal bars

$A_{sl} = [\frac{A_{str}.P_h}{S}] * [\frac{f_{yst}}{f_y}]$

Subject the additional longitudinal bars around all section.

$A_{sl.min} = \frac{0.4\sqrt{\frac{f_{cu}}{\gamma_c}}.A_{cp}}{\frac{f_y}{\gamma_s}} - \frac{A_{str}.P_h}{S} * \frac{f_{yst}}{f_y}$

$\frac{A_{str}}{S} \geq \frac{1}{6} * \frac{f_{yst}}{f_y}$

Noticed that torsional stirrups are closed stirrups.

2.2.4 Experimental Work on Torsion

M.R.Prakash, Sadanand P., Manjunath H.R., Jagadeesh Kumar B.G. and Prabhakara R. [11] examined to study the Torsional behavior of the Medium strength concrete (NSC) and High strength concrete (HSC) beams with the mix proportion of the concrete M50 –M80 grade and more than

M100 grade. Eighteen beams with varying longitudinal and transverse reinforcement ratio were tested under torsion. The result of experiment was compared with the different codal equations and also the equations given by researchers for 95 data collected from previous investigations. The study revealed that:

- The failure at the ultimate torsional moments for HSC beams is exploding type of failure, and the effect of the transverse reinforcement is more effective than the longitudinal reinforcement.
- The Torsional strength of beam increases with increasing in the compressive strength of concrete, So the HSC beams gives high torsional strength than NSC beams for same amount of reinforcement.
- The ductile for HSC and NSC is similar.
- The torsional strength of beam for NSC beams is increases with decreases the spacing of transverse reinforcement but was not clear in HSC beams. By observing, the torsional strength increases with increase in the span to depth ratio.
- The ultimate torsional strength increases with increasing in the percentage of longitudinal reinforcement for all the beams increased.
- Prediction for the skew bending theory for the value of torsional strength much better than the other codes for the experimental beams.
- The ultimate torsional strength increases with increasing in the depth for beams. Fourth root of depth has significant effect on the Torsional strength.
- The calculation tsorsional strength in codes and the theory is not considered for the longitudinal reinforcement, except European code, which predicted the values better when compared to other codes.

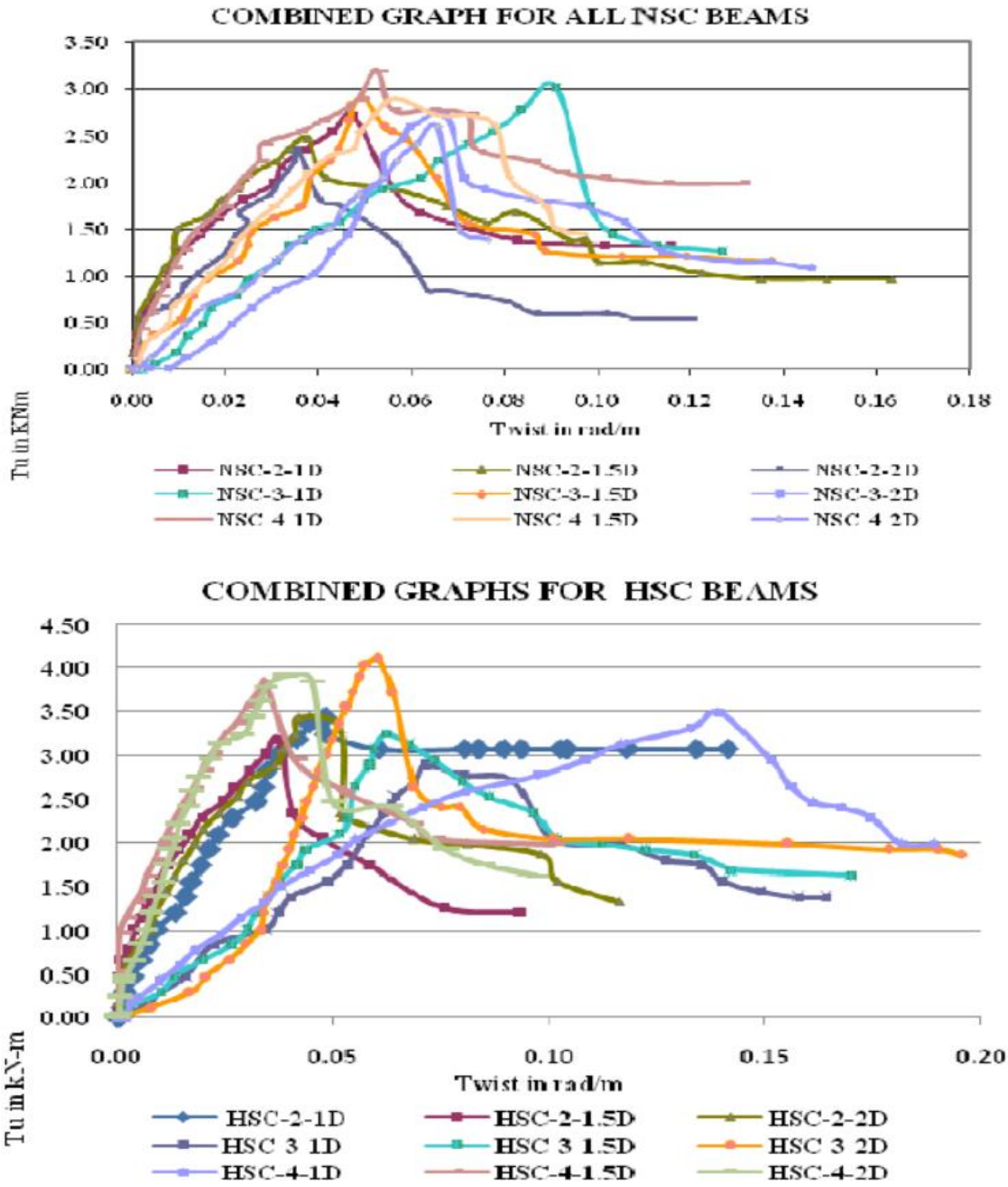

Figure (2-7): Torsional Moment V/S Twist Curve for all MSC & HSC Beams **[11]**

Eighteen beams made of 80 MPa concrete reinforced by high-strength bars with rectangular section and various test variables involving the minimum torsional reinforcement ratio, the transverse-to-longitudinal reinforcement ratio and the total reinforcement ratio were examined by **Changbin Joh, Imjong Kwahk, Jungwoo Lee, In-Hwan Yang and Byung-Suk Kim [12]**

to study the reduction of ductility resulting from the increasing in strength. The beams were examined under torsion and compared the results by regulations of Eurocode 2. Considering that this also concerns the design for torsion, this study intends to investigate the regulations related to the torsional minimum reinforcement ratio in view of the minimum ductility requirement with focus on Eurocode 2. From the experiment, for the high-strength concrete beams, the minimum torsional reinforcement ratio recommended by Eurocode 2 was insufficient to prevent the sudden loss of strength after the initiation of the torsional cracking), The adoption of $\rho_{v,min}$ recommended by EC2 secured enough deformability to allow the redistribution of the torsional moment for the statically indeterminate structure. Experimental data on the average gave conservative torsional cracking moment (T_{cr}) and torsional strength (T_n) reaching, respectively, 157% and 123% of the prediction from the formulae based on the thin-walled tube theory and space truss analogy with the effective thickness based on EC2.

Thirteen beams with full size were experimented by **Hao-Jan Chiu, I-Kuang Fang, Wen-Tang Young, Jyh-Kun Shiau [13]** to study the behavior of high-(HSC) and normal-strength concrete (NSC) with relatively low amounts of torsional reinforcement. primarily, the ratio of the transverse to the longitudinal reinforcement factors in addition to the total amounts of torsional reinforcement affected basically in low amounts of torsional reinforcement. From the experiment, the torsional cracking strengths of the specimens with hollow sections are smaller than those of the specimens with solid sections. The increase of the aspect ratio of the cross section decreases the cracking and ultimate strengths and increases the crack widths for the specimens with approximately the same amounts of torsional reinforcement. For the HSC and NSC specimens designed with lower amounts of torsional

reinforcement, the selection of equal percentages in the transverse and longitudinal directions provides adequately not only the post cracking reserve strength and torsional ductility needed, but also the crack width control necessary at service load level. With low amounts of torsional reinforcement for HSC beams, a brittle failure mode was occurred for $\rho_t f_{yv}/\rho_l f_{yl}$ = 0.19–0.27 and ρ_{total} = 0.95%. And a ductile failure mode was found for both HSC and NSC specimens designed with the ratios of $\rho_t f_{yv}/\rho_l f_{yl}$ ranging from 0.34 to 0.98, and ρ_{total} greater than 0.95% for HSC specimens and 0.87% for NSC specimens, respectively.

To reflect the actual behavior of the beams under torsion, **Luı´s F. A., Bernardo Se´rgio and M. R. Lopes [14]** made a theoretical study to predict the general behavior of reinforced concrete beams under torsion for both plain and hollow beams with normal strength. From the study. Before crack point (State I), when calculating the cracking torque, (T_{cr}), for plain sections beams, both Theory of Elasticity and Skew-Bending Theory give good Predictions and Bredt's Thin-Tube Theory gives the best predictions for hollow beams. The reducing factor K = 0.7 must be used to predict the torsional stiffness in State I ($(GC)^{I}$) because of, before the effective cracking of the beams, the microcracking of the concrete that takes place, and should not be neglected. After crack point. (State II), Both for plain and hollow beams, a three-dimensional truss model with concrete struts inclined by 45˚ is better to predict for the T–θ curves and the intersection with the T axis ($\rceil T_c$) and the rotational stiffness ($(GC)^{II}$) are very close to the experimental values. To consider that all the stresses take place in an outer concrete ring, neglecting the inner concrete core, the concrete core does not affect the ultimate strength, but it does affect the ultimate deformation. The plain beams give a big deformation whin compared with hollow beams.

A. Prabaghar, G. Kumaran investigated eight beams under torsion experimentally **[15]**. They studied the beams with difference in the concrete grade (20 M and 30 M) and variation in transverses (50mm and 75mm) and longitudinal (0.56% and 0.85%). From the exterminate, the torsional strength of the beams depended on the ratio of steel when starting to crack under increased load. When the steel ratio is lesser than 1% with more ratio (ie.0.56%), the beams are failed due to yielding of longitudinal and transverse reinforcements before crushing of concrete in compression. In the other side, beams with approximately closer to 1% (ie.0.86%) of steel reinforcement ratio are failed by crushing of concrete in compression before yielding of longitudinal or transverse reinforcements. With increasing in crack propagation and width, the reducing of the torsional stiffness has been completed with increasing twist and constant torque. For variable beams, the twist was higher for beams of M 30 grade than M 20 grade beams and the torque was lesser value for the two grades. As expected, when decreasing the spacing of stirrups, the torsional capacity increased. The increase in steel percentage and the grade of concrete made a rapid increase in the twist of specimen and torque.

According to the Egyptian Code of Practice recommendations (ECP 203) as it is based on the lower bound of the space truss theory, **Ahmed Hassan and Laila Abd-EL Hafez [16]** made theoretical study for investigating the torsional behavior of high-strength reinforced concrete sections. The study based on previous experimental studies. The reduction of steel, cross section, variable box section wall thickness and variable concrete compressive strength were the main parameters in the study. Test results showed that.

- More cracking, reduction the failure torque, decreasing angle of twist at cracking and increasing the failure with decreasing in steel reinforcement of section of a section subjected to torsion.
- Increasing cracking and decreasing failure torque with reducing the size of the concrete section. As Major degree than with a reduction in steel reinforcement, The failure and angle of twist at cracking increased.
- Ductility, cracking torque and ultimate torque improved with increasing the compressive strength of concrete for the same cross section. the failure torque increased by 40% with increasing the compressive strength by 30%.
- The first stage of loading wall thickness was affected more than the effect of the failure stage, for box sections.
- With the ultimate torque increasing by 15% for 1 N/mm^2 pressure, applying compression force on the cross section improves the cracking torque, ductility and ultimate torque for the same cross section.

Fourteen beams under pure torsion were studied theoretically based on previous experimental research by **Mostofinejad, D., Talaeitaba, S.** by using the smeared crack model **[17]**. The beams were one box-section, one T-section and 12 beams rectangular section. From using ANSYS was noticed that…

- The cracking and failure due to torques could be evaluated accurately. The torsional capacity with this method was even more precise than that obtained using the method explained in ACI 318.
- The crack developing trend and shape for the torsional cracking were predicted accurately up to the fracture threshold.

- As shown in Figure (2-8), the torque-rotation curves were consonant with those obtained from experiment for all specimens. However, in the post-cracking zone, in which torsional stiffness of the beam decreases

significantly, the analysis encountered convergence trouble. This happens because of the strict sensitivity of the "smeared cracks" model in nonlinear analysis under torsion, towards the shear transfer coefficient in open cracks, β_t . Small values of β_t induces severe reduction in shear stiffness in the stiffness matrix and shear instability on the crack surface. Another reason behind this trouble seems to be making use of the large deformation option in the analyses, which is inapplicable for the SOLID65 in ANSYS.

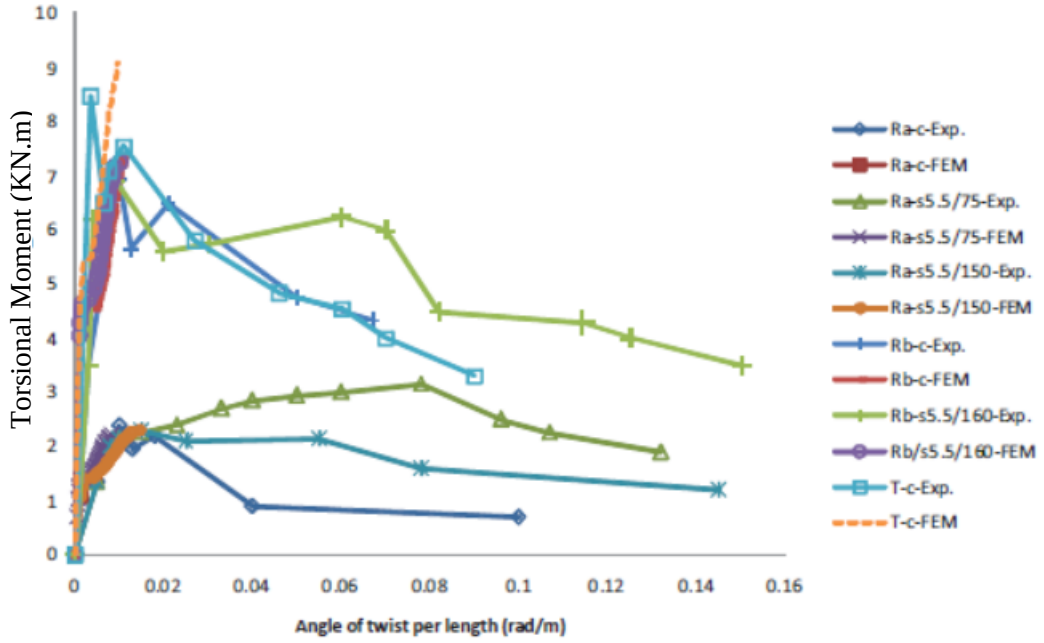

Figure (2-8): Torque-twist curve of the specimens **[17]**

Min-Jun Kim, Hyeong-Gook Kim, Yong-Jun Lee, Dong-Hwan Kim, Jung-Yoon Lee and Kil-Hee Kim [18] studied eleven specimens under pure torsion theoretically. The main parameters were 1- the yield strength of the torsional reinforcement, 2- the spacing of the torsional reinforcement, 3- the amount of arranged torsional reinforcement compared to that of the ACI 318-19 building code and 4- the properties of the solid and hollow cross sections. In the end of study was observed that

- with increasing the amount of transverse torsional reinforcement, the torsional stiffness and torsional strength increased reinforcement regardless of cross-sectional properties.
- After the occurrence of the first torsional crack, torsional stiffness and peak torsional strength were higher for hollow cross-sections Compared with solid cross sections.
- With comparing the results for compression strut angle h_{test} calculated using the space truss model, and the ACI 318-19 building code angle h_{ACI}, the ratio $h_{test}=h_{ACI}$ of the S-series averaged 0.95 with a coefficient of variation of 12.8%, and that of the H-series averaged 0.97 with a coefficient of variation of 11.6%.

Khaldoun N. Rahal studied 152 specimens theoretically based on previous studies **[19]**. The purpose of the study was to calculate the ultimate torsional moment in normal-strength and high-strength concrete beams. The researcher used the ACI and the CSA building code equations to compare the results. The main equation in the model relates the torsional strength to the amount and strength of the longitudinal and transverse reinforcement, the concrete compressive strength and the outer area of the cross section. By the results of another equation that estimates the strength when crushing of the concrete takes place before yielding in the steel Limited the calculated strength. A very good agreement was obtained by Checking The method results against the results for specimens from the previous studies and included the results from simple methods (the ACI and the CSA codes equations). The results showed that under-reinforced and over-reinforced beams, the normal-strength and high strength concrete beams were similar in the accuracy of the proposed method. When combined with the $1.7(A_{oh})^2/p_h$ factor, the ultimate crushing torsional stress of $0.25f'_c$ isn't fair for high-strength concrete in the CSA. So, for over

reinforcement the CSA provisions don't provide enough protection. But for under reinforced sections the calculation of the equation was generally satisfied more so in HSC. Clearly, for under-reinforced beams the CSA equation and the ACI equation were satisfied and limited the crack width and to provide a check against concrete crushing is very satisfied when used to estimate the maximum torsional moment over reinforced sections, particularly in HSC, the effect of amount of reinforcement on torsional strength shown in Figure (2-9).

Four beams tested under pure torsion to evaluate the torsional strength for the reinforced beams with different type of steel arrangement by **Mohammad Rashidi, Hana Takhtfiroozeh [20]**. beams were subjected without reinforcement in both longitudinal and transverse reinforcement, without transverse reinforcement and with both longitudinal and transverse reinforcement. The results showed that reinforcement lonely for longitudinal reinforcement or transverse reinforcement wasn't able to increase the torsional strength of RC beams. With increasing percentage reinforcement, the ductility factor increased comparing with the beams without reinforcement. The transverse reinforcement is essential in the ultimate torsional strength and ductility when comparing with longitudinal reinforcement. The ductility of reinforced concrete beams has been increased 95% and 50% for the beams with transverse and longitudinal reinforcement respectively with comparing the beams without reinforcement. Both longitudinal and transverse reinforcement together improved the torsional behavior well for reinforced concrete beams.

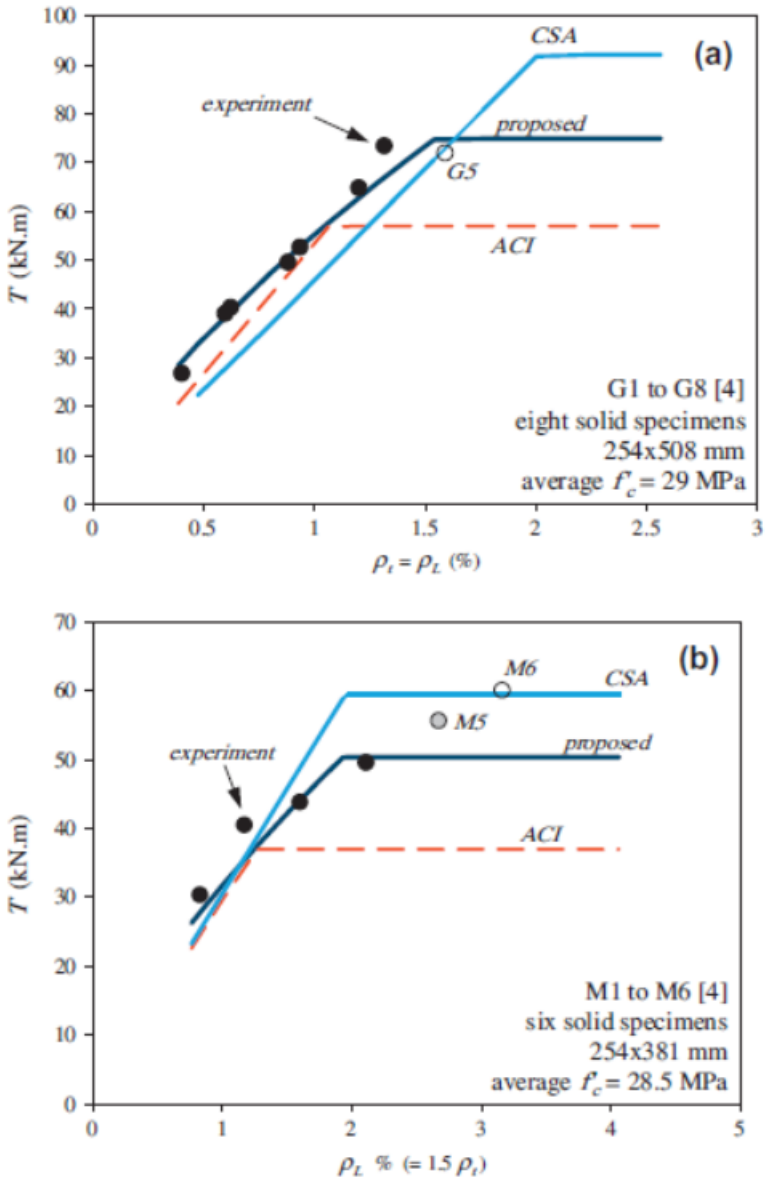

Figure (2-9): Effect of amount of reinforcement on torsional strength: (a) Series G and (b) Series M. **[19]**

2.3 Fibers

Fibers are the principal constituent in a fiber-reinforced composite material. They take up the largest volume fraction in a composite laminate and share a major part of the load acting on a composite structure. Suitable selection of the type, orientation and number of fibers is very important.

A fiber is a lengthy filament composed of a material. Surface flaws are more likely to occur with larger diameters. In continuous fibers, the length-to-

diameter aspect ratio can range from thousands to infinity. They typically take up 30-70 percent of the composite's volume and 50 percent of its weight. Fibers' primary tasks are to transport load and offer stiffness, strength, thermal stability, and other structural qualities to FRPs, **Tuakta, [21]**. Fibers in FRP composites must have a high modulus of elasticity, a high ultimate strength, low variation in strength among fibers, high strength stability during handling, and high uniformity of diameter and surface dimension among fibers in order to execute these roles.

2.3.1 Types of Fibers

The main classification of FRP composites is based on the type of fibers employed as reinforcement. The civil engineering sector is dominated by types of fibers: glass, carbon, and aramid fibers.

2.3.1.1 Glass Fibers

Glass fibers are a refined form of glass made from a combination of oxides (mainly silica oxide) and other raw materials (such as lime-stone, fluorspar, boric acid, clay). They are made by pulling melted oxides into filaments ranging in length from 3 to 24 meters. Chopped fibers, chopped strands, chopped strand mats, woven fabrics, and surface tissue are the five types of glass fibers used as matrix reinforcement. The most often employed forms in civil engineering applications are glass fiber strands and woven fabrics. E-glass fibers are the most often utilized fibers in the construction sector due to their low cost when compared to other types of fibers. Glass fibers' shortcomings include a low young's modulus, low humidity and alkaline resistance, and low long-term strength owing to stress rupture. A more alkaline resistant so-called AR fiber (also known as CemFil fiber) with higher zircon oxide content has been developed for concrete applications **Tuakta, [21]**.

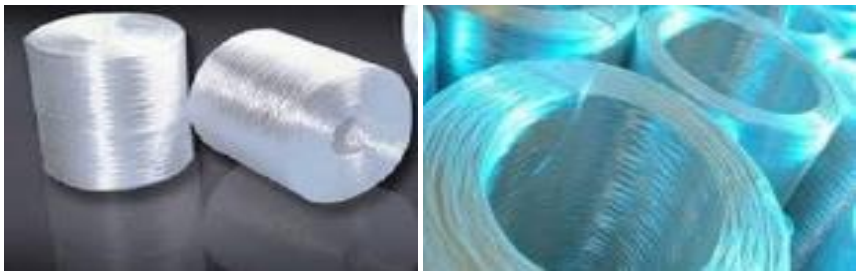

Figure (2-10): Glass Fibers **[22]**

2.3.1.2 Carbon Fibers

Carbon fibers are a type of high-performance fiber available for civil engineering application. They are manufactured by controlled pyrolysis and crystallization of organic precursors at temperatures above 2000°C. In this process carbon crystallites are produced and orientated along the fiber length. There are three choices of precursor used in manufacturing process of carbon fibers - rayon precursor's poly acrylo nitrile (PAN) precursors, and pitch precursor. PAN precursors are the major precursors for commercial carbon fibers. It yields about 50% of original fiber mass. Pitch precursors also have high carbon yield at lower cost. Carbon fibers have high elastic modulus and fatigue strength than those of glass fibers. Considering service life, studies suggests that carbon fiber reinforced polymer have more potential than aramid and glass fibers. Their disadvantages include inherent *-anisotropy (reduced radial strength), comparatively high energy requirements in their production as well as relatively high costs, **Tuakta, [21]** and **Zobel, [23].**

2.3.3 Aramid Fibers

Aramid or aromatic polyamide fiber is one of the two high performance fibers used in civil engineering application. It is manufactured by extruding a solution of aromatic polyamide at a temperature between -50°C and -80°C into a hot cylinder at200°C. Fibers left from evaporation are then stretched and drawn to increase their strength and stiffness. During this process, aramid molecules become highly oriented in the longitudinal direction.

Aramid fibers have high static, dynamic fatigue, and impact strengths. The disadvantages are: low compressive strength (500-1000 MPa), reduced long-term strength (stress rupture) as well as sensitivity to UV radiation. Another drawback of aramid fibers is that they are difficult for cutting and machining **Tuakta, [21]**.

2.3.4 Manufacturing of FRP Bars

2.3.4.1 Choosing the Method

When selecting a production process for Fiber Reinforced Composite elements, keep in mind the expected number of elements needed to achieve the desired shape and dimensions. Also important are criteria for tensile strength, young's modulus, and other qualities like as dimension accuracy, surface quality, and so on. The parameters of the reinforcement and the matrix, such as the coefficient of thermal expansion, must be carefully chosen in order to provide the highest possible mechanical compatibility, **Zobel, [23].**

Manufacturing can be done in a variety of ways, from manual to totally automated. Hand lay-up, spray-up, filament winding, resin transfer moulding, and pultrusion, **Tuakta, [21]** are five civil engineering procedures mentioned here.

2.3.4.2 Manual and Semi-Automated Methods

Hand lay-up and spray-up are examples of manual operations. One of the oldest composite production technologies is hand lay-up or wet lay-up. It's a time-consuming procedure that involves pouring liquid resin into the mould and manually placing fiber reinforcement on top. The fiber is impregnated with resin and any trapped air is removed using a metal laminating roller. A series of procedures is continued until the desired thickness is achieved. Hand lay-up has several drawbacks, including

inconsistent quality of manufactured parts, poor fiber volume fraction, and environmental and health concerns about styrene emissions. Figure (2-8) shows the hand lay –up process.

Table (2-1): Properties of Glass, Aramid and Carbon Fibers **Zobel, [23].**

Typical properties	Fibers					
	glass		Aramid		Carbon	
	E-Glass	S-Glass	Kevlar 29	Kevlar 49	HS (High Strength)	HM (High Modulus)
Density ρ [g/cm^3]	2.6	2.5	1.44	1.44	1.80	0.190
Young´s Modulus *E* [GPa]	72	87	100	124	230	370
Tensile strength Rm [MPa]	1.72	2.53	2.27	2.27	2.48	1.79
Extension [%]	2.40	2.90	2.80	1.80	11.00	0.50

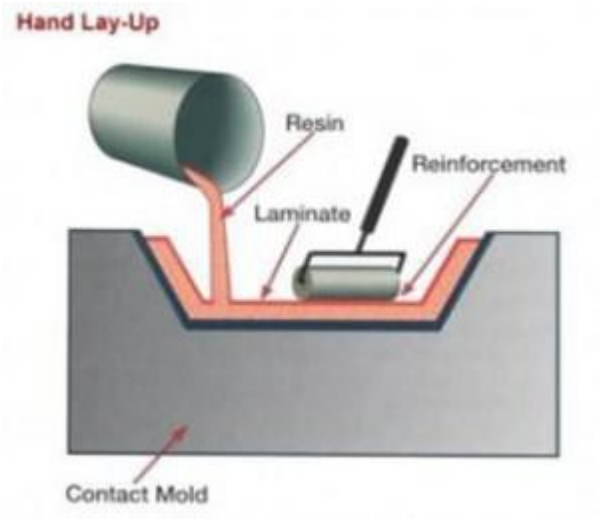

Figure (2-11): Hand Lay-up Process, Iimage from www.ale.nl **[22]**

The spray-up method is comparable to hand lay-up, however it is considerably faster and less expensive. A spray gun is used to apply resin and chopped reinforcements to the mould during this operation. As reinforcement, glass fibers cut to a length of 10 to 40 mm are commonly utilized. It's better for making non-structural pieces that don't require a lot of strength. Controlling the fiber volume fraction and thickness, on the other hand, is extremely difficult and requires a highly competent operator. As a result, this method is not suitable for parts that require dimensional precision. The spray up procedure tooling method is depicted in Figure (2-12).

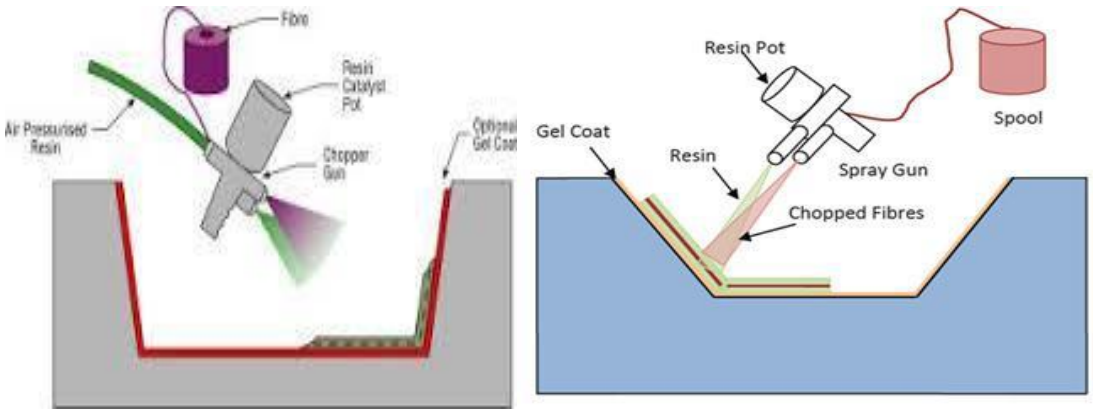

Figure (2-12): Spray-up Process, Image from www.ale.nl/ **[22]**

One of the semi-automated processes is resin infusion under flexible CFRP is commonly retrofitted to steel, cast iron, and concrete bridges using this technology. Fibers are prepared in a mould and transported to the site in this technique. The pre-form is then joined to the retrofitted structure and sealed with a resin supply using a vacuum bagging method. The pre-form is then injected with resin, which forms the composite material as well as the adhesive bond between the composite and the framework. This method produces a high fiber volume percentage of up to 55%.

2.3.4.3 Fully Automated Methods

2.3.4.3.1 Pultrusion

Pultrusion is a technology that allows for the continuous fabrication of FRP profiles with consistent cross sections and material qualities for specified applications, **Zobel, [23]**. Sources say it's the only known approach for ensuring sufficiently consistent quality thus far. The method has been utilized in its most basic version for about 60 years. The process of pultrusion according to **Kolding [24]** is given below.

Pultrusion is accomplished by continuously pulling reinforced material through a guide in which the fibers are precisely aligned with the profile cross section, then leading the fibers through processing equipment and impregnating them with the matrix material, pulling the combined mixture through heated equipment, and curing the profile into its final geometry. The fully cured profile is dragged forward and chopped into defined lengths by a floating suspended saw. When continuous fibers, complicated weaves, and mats are positioned in a profile, the type and number of continuous fibers, as well as the type and size of complex weaves and mats, are placed in a way that allows visual verification.

The Pultrusion method is depicted in Figure (2-13). The qualities and quality of the finished product are dependent on the precise positioning of fibers and mats in respect to the cross section of a pro-file. The matrix is injected into the reinforcement when it is pushed into the processing machinery.

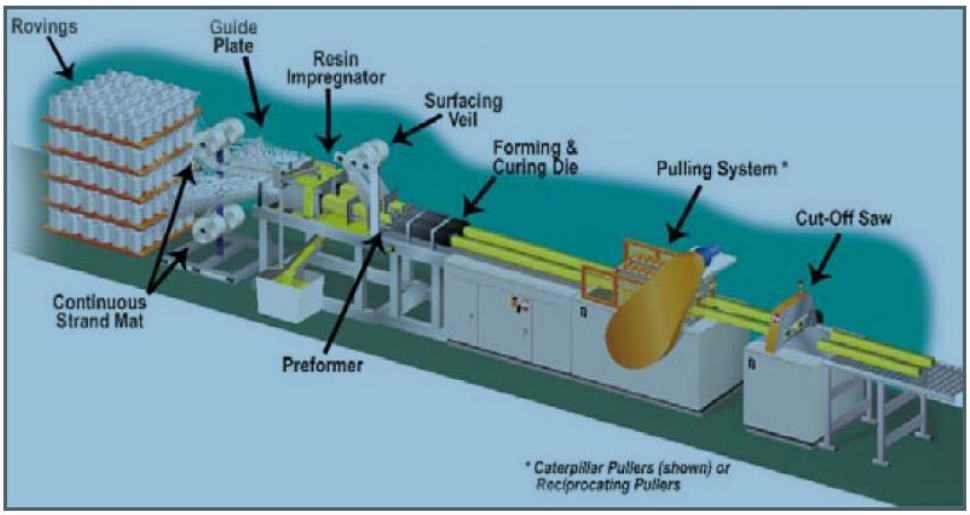

Figure (2-13): Pultrusion Process **[22]**

Pultrusion via injection is useful for managing and inspecting reinforcement, as well as speeding the transition from one profile to another and facilitating matrix changes during the process. Another important aspect affecting the end product's characteristics is the degree of impregnation of the fibers. Reinforcement is led through an open vat containing the matrix in classic pultrusion. The injection method, on the other hand, is a completely contained operation that minimizes solvent evaporation. After the fibers have been impregnated with the injected matrix, the entire product is moved to the next stage of the process, where the profile is heated, and curing is expedited. The final curing is done in the processing equipment's last segment. When a pro-file leaves the processing equipment, it is entirely cured and stable in form. Pullers situated outside the processing equipment give the pulling strength that overcomes friction in the equipment, and so provides the driving force in the process. Belts or reciprocal pullers can be used for pulling. A saw mounted to travel at the same speed as the profile

being pulled out of the equipment is used to shorten the profiles in the last step of the operation. This assures that the procedure is never interrupted.

2.3.4.3.2. Filament Winding

Filament winding is a method in which resin-impregnated fibers are wound at the desired angle over a rotating mandrel. As a result, continuous glass, carbon, or aramid fibers are used as starting materials in this technique. Epoxy, polyester, and vinyl ester are liquid thermoset resins utilized in this technique. After that, the composite unit is removed from the mandrel and cured for 8 hours in an oven enclosure at 60°C. Tubular constructions and pipelines are frequently manufactured using this method. Because low-cost materials and tooling are employed, it is a low-cost process. However, it is confined to manufacturing closed and convex structures, and the volume fraction of fibers produced is quite low. The filament winding procedure is depicted in Figures (2-14).

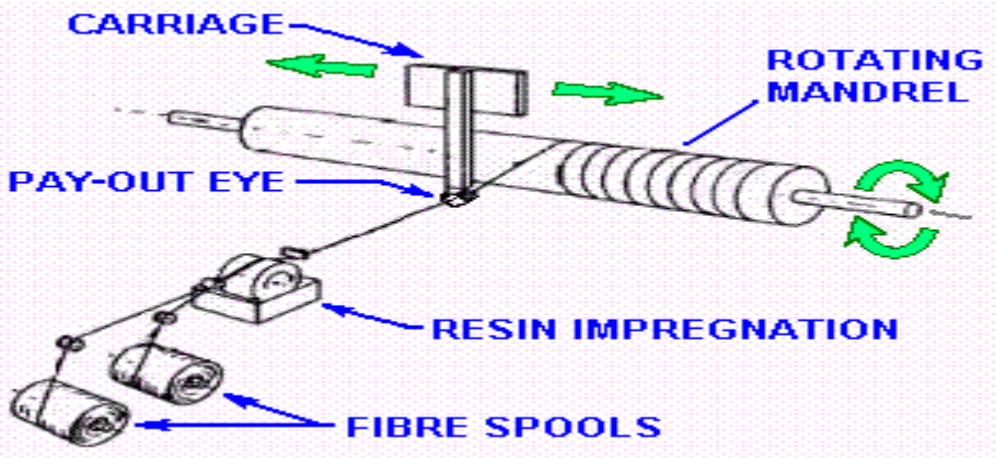

Figure (2-14): Filament Winding Process, Image from www.ale.nl/ **[22]**

2.3.4.3.3. Resin Transfer Moulding

Fabrics are laid out as a dry stack, sometimes pre-pressed to the mould shape, and kept together by a binder in resin transfer moulding. These acts can then be more readily inserted into the mould tool. A second mould tool is then clamped over the first, and structural pieces are formed by injecting

a pressured combination of thermoset resin, a catalyst, colour, filler, and other materials into the cavity using dispensing equipment. The resin inlets are closed, and the laminate is allowed to cure once all of the cloth has been soaked out. Both the injection and the cure can take place at room temperature or at a higher temperature. Figure (2-15) shows the resin transfer molding process.

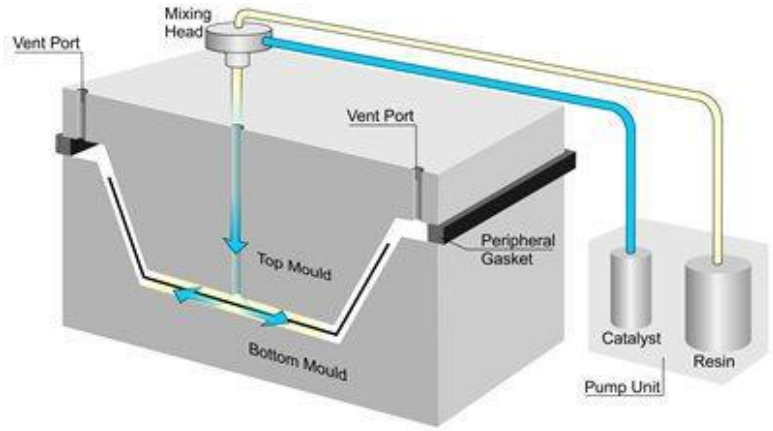

Figure (2-15): Resin Transfer Molding Process, Image from www.ale.nl/ **[22]**

This technology can be used to make little to medium-sized structures in low- to medium-volume quantities. Resin transfer moulding can make complex parts in intermediate volumes at a cost-effective rate, allowing restricted production to continue. This approach can achieve fiber volume fractions as high as 65 percent. Resin transfer moulding, on the other hand, has a variety of drawbacks. Tooling and equipment expenses are substantially larger and more complex than in the hand lay-up and spray-up processes, and dimensional tolerances are less adhered to than in the pultrusion method. Resins must have a low viscosity, which may compromise the completed composite's mechanical qualities resin transfer moulding comes in a variety of forms, each with its own mechanics for introducing resin to the reinforcement in the mould cavity. Vacuum infusion

to vacuum assisted resin transfer moulding are examples of these variations (VARTM).

2.3.4.3.4. Braidtrusion Method

The most common ways for making FRP are pultrusion, braiding, and filament winding. Pultrusion is a continuous manufacturing technique that produces unidirectional components with a constant cross-section and is often regarded as the most cost-effective and time-efficient method of producing prestress tendons and reinforcing bars. As a result, it is the most widely used process for producing FRP rebars. The FRP member's bond performance with concrete is the most important performance requirement for it to fulfil its duty inside concrete. Even though pultrusion has the advantage of manufacturing continuously parts with constant cross-section, since the produced member has a flat surface, an additional step is required to achieve concrete bond performance. To address this issue, a method that combines pultrusion and braiding has been developed by **Ko, F.K.; Somboonsong, W.; Harris, H.G. [25]**. This procedure, known as braidtrusion, adds braiding to the pultrusion process in order to create a net-like skin on the reinforced fiber bundle's surface. Thus, the braid trusion bears the continuous manufacture and preservation of a constant cross-section, as well as the rough surface or skin, as featured by the pultrusion. Due to the gaps created in the section by the air entrained during the resin impregnation of the relatively loose fiber bundles composing the rebar's core, the braidtruded FRP rebar loses its tensile performance. **KICT [26]** developed an improved braidtrusion process, as depicted in Figure (2-16), to eliminate voids inside the section.

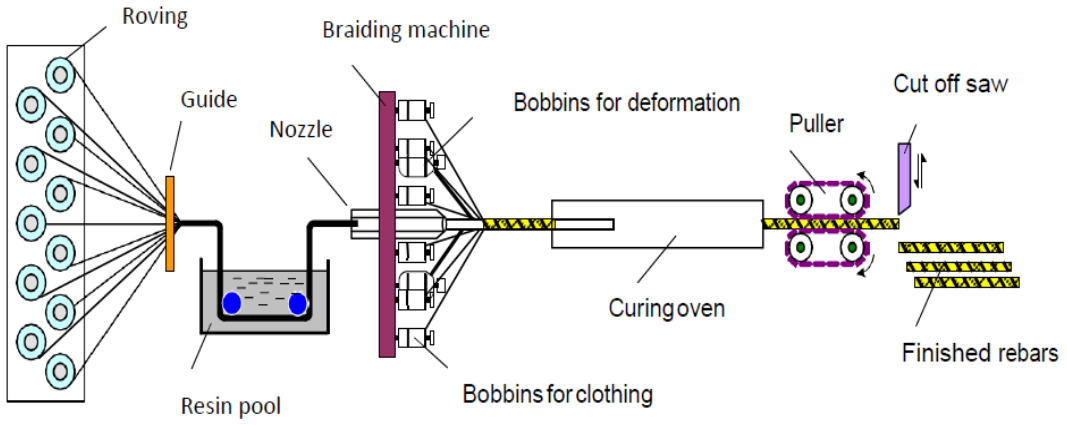

Figure (2-16): Modified Braidtrusion Process **[22]**

2.3.5 Experimental work on beams reinforced by GFRP under Torsion

Esam El-Awady, Mohamed Husain, Sayed Mandour [27] made experiment and theoretical study of the behavior of FRP-reinforced concrete beams under combined torsion and flexure. Eighteen beams tested experimentally, and ten beams were numerically analyzed via ANSYS software. All beam specimens are designed to fail in torsion and all tested beams failed in torsion as planned. The deflection was more in beams reinforced with GFRP then beams reinforced with steel, according to Figure (2-17) with basic flexure reinforcement only and the same result with Figure (2-18) with extra longitudinal torsion reinforcement.

Figure (2-19) introduces the obtained formula form the current study results. The torsion resistance is drawn against the ratio of the GFRP torsion longitudinal bars (U_f) in the tested and analyzed beams. These results show that the torsional resistance of the beams increased as the ratio of the additional GFRP longitudinal bars increased. It should be noted here that the study results did not find torsional resistance contribution to the GFRP stirrups formed by heating GFRP bars made with thermoplastic matrix. This Figure shows that at 0 % of the additional GFRP longitudinal bars, the tested

beams have a considerable torsional resistance (refer to B1 result), while the torsional resistance of the beams increased as the ratio of the additional GFRP longitudinal bars increased up to a certain level, using Microsoft Excel trendline formula by a polynomial trend the curve equation could be estimated as:

$T_u = 190 + 42 (U_f)^{0.8}$

The study made equation between torsion resistance and ratio of the GFRP torsion longitudinal bars for the tested and analyzed beams. The study showed that the increasing in ratio of the additional GFRP longitudinal bars increases torsional resistance. It was noted that the study results didn't find torsional resistance contribution to the GFRP stirrups formed by heating GFRP bars made with thermoplastic matrix. It was noted that the stirrups formed by heating GFRP bars made with thermoplastic resin are found ineffective in resisting torsion due to residual stresses on the corners arises during stirrup forming.

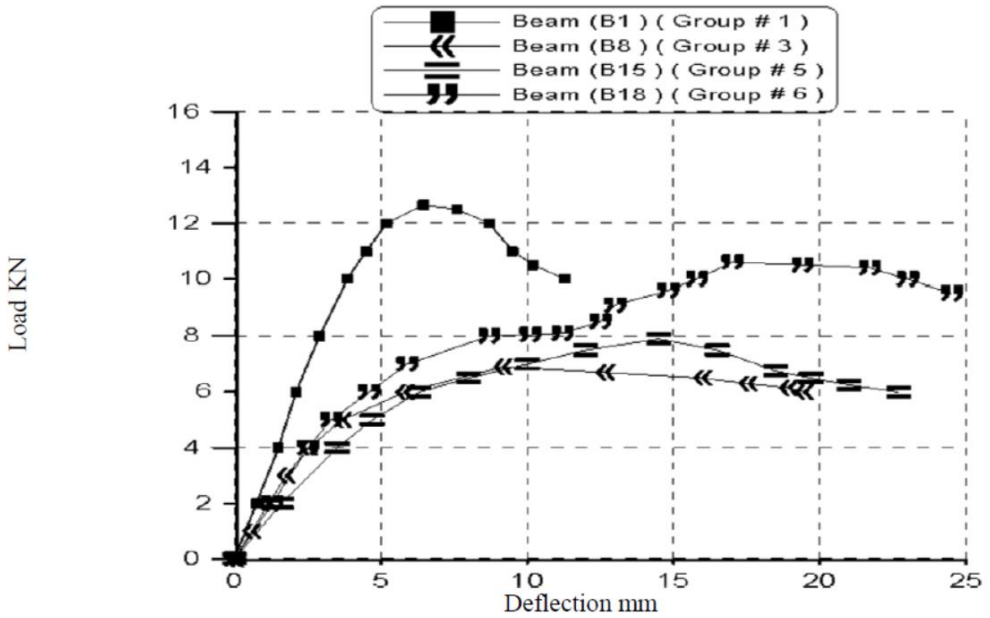

Figure (2-17): Load-Deflection Curves for B1, B8, B15, and B18 **[27]**

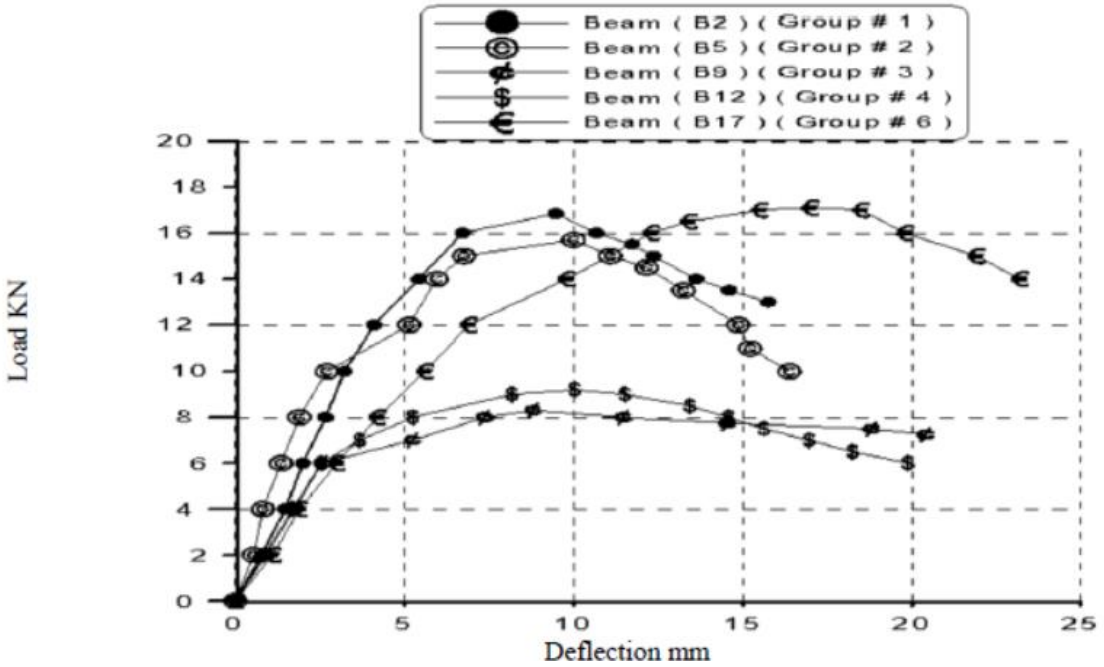

Figure (2-18): Load-Deflection Curves for B2, B5, B9, B12, and B17 **[27]**

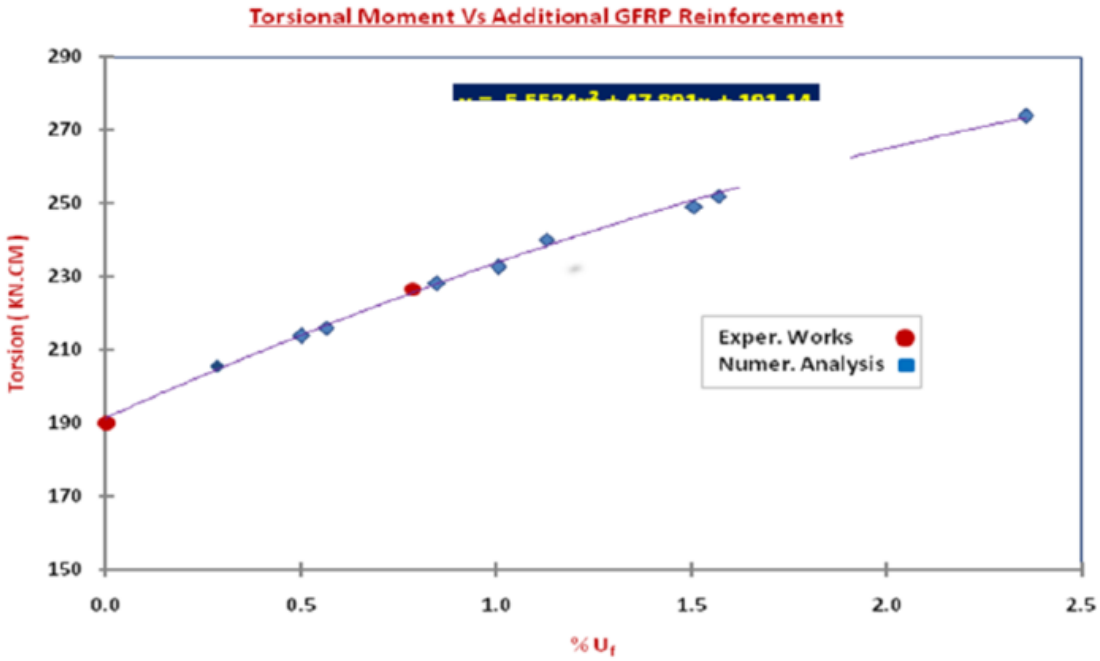

Figure (2-19): Torsion Moment Vs Ratio of the GFRP Bars (U_f) **[27]**

Hamdy M. Mohamed and Brahim Benmokrane [28] studied eight RC beams with full-scale under pure torsion. The main parameters were the type and ratio of torsional reinforcement. The study based on Sand-coated glass-FRP (GFRP) and carbon-FRP (CFRP) bars and stirrups but the steel

reinforcement was used to reinforce the control beams reinforced bars and stirrups. To determine the concrete contribution to torsional resistance, three beams were built without stirrups and the bars were steel, GFRP and CFRP. The beams failed as torsional failure. As result for this study

- The beams reinforced without stirrup had the same behavior however the beams reinforced with vary bars steel, GFRP and CFRP.
- The skew-bending theory provided overestimated values but the elasticity theory and ACI 318-14 design equation yielded good predictions of the experimental cracking torque of the tested GFRP RC beams.
- From the study, using of GFRP and CFRP stirrups as torsion reinforcement, in accordance with CSA S806-12 limitations, effectively provided torsion strength like that of the counterpart steel RC beam.
- Concrete splitting was controller for the beams reinforced without stirrup.
- Rupture of the FRP stirrups at the bent portion for the beams reinforced with a transverse-reinforcement ratio of 0.537% from GFRP and CFRP but with increasing the ratio of transverse reinforcement to 1.074% the failure was in concrete by crushing the concrete in diagonal strut for both GFRP and CFRP beams.
- Conservative predictions of the torsional capacity for the tested FRP RC beams with high transverse-reinforcement ratios were provided by use of CSA S806-12 torsion design provisions for the cross-sectional dimension limitation to avoid crushing.
- For the beams reinforced with GFRP and CFRP with high stirrup ratios, the failure was in the concrete by crushing in concrete and it was observed no rupture in the FRP stirrups after the test finish.

- Torsional failure was not triggered by the GFRP or CFRP bars rupturing because of the low strain at ultimate for GFRP and CFRP reinforcement.

Hamdy M. Mohamed and Brahim Benmokrane [29] investigated the strength and the torsional behavior for four beams reinforced with GFRP bars and stirrups and one control beam reinforced with conventional steel reinforcement under torsion. The parameters were the type and ratio of torsional reinforcement. All specimens failed due to diagonal torsional cracking with GFRP stirrup rupture. The strength and cracking behavior for the GFRP-reinforced concrete (RC) beam was similar with lower post peak torsional stiffness compared to the conventional steel RC beam. The torsional strength increased with decreasing the spacing of the GFRP stirrups and improvement in the post-peak stiffness. In the GFRP-RC beams with large stirrup spacing, the beams failed by stirrup rupture combined with concrete crushing. Contrariwise, in the GFRP-RC beams with lower stirrup spacing, the beams were imputed to the rupture of the GFRP stirrups at the bent portion, the effect of stirrup spacing on predicted torsion strength is shown in Figure (2-20). The hollow-tube, space-truss analogy with the 45-degree inclination of diagonal compressive stresses was acceptable with the observed diagonal torsion failure. The torsional strength ratio of the GFRP-reinforced beam to that of the steel-reinforced beam is directly proportional to the ratio of the bend strength of the GFRP stirrups multiplied by the GFRP torsional reinforcement ratio ($f_{ftb}\rho_{ft}$) to the yield strength of the steel stirrups multiplied by steel torsional reinforcement ratio ($f_y\rho_{st}$). providing conservative predictions of the torsional capacity by Using a 0.4 reduction factor in CAN/CSA S806-12 to account for the reduction in the tensile strength of the bent GFRP stirrups as a function of the tensile strength of the straight portion.

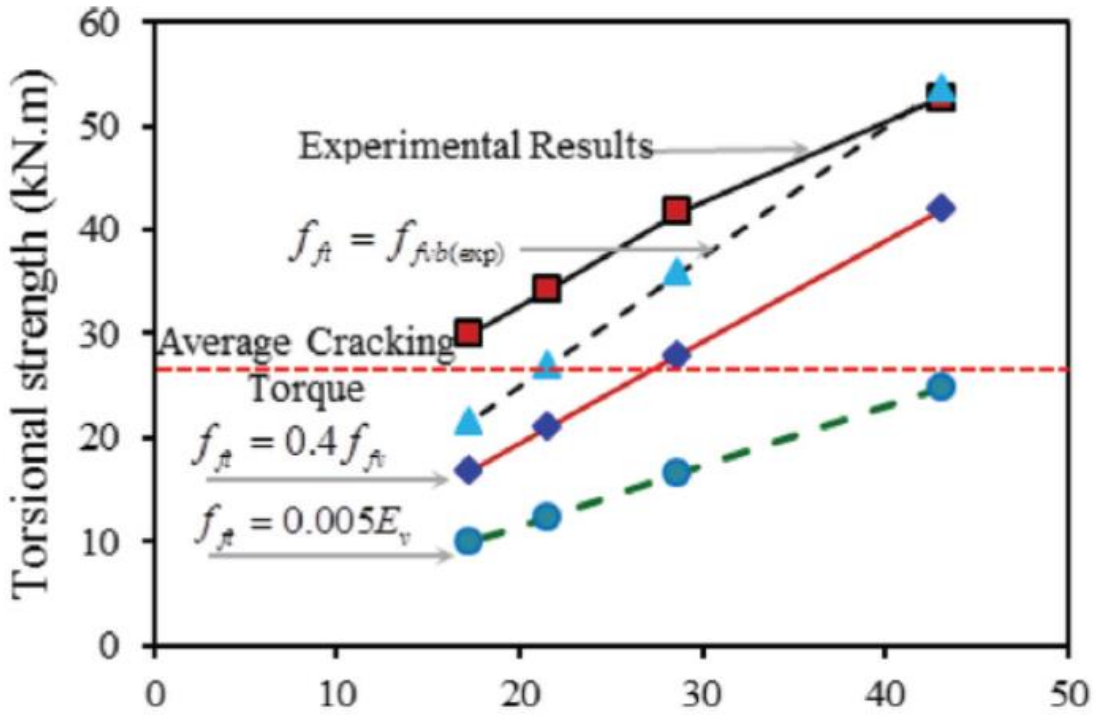

Figure (2-20): Effect of Stirrup Spacing on Predicted Torsion Strength **[29]**

Jikai Zhou , Wei Shen, Shifu Wang [30] examined eight GFRP bars reinforced concrete beams with different fiber contents were tested under pure torsion to study the influence of fibers on the torsional behavior of GFRP reinforced concrete beams (bars and stirrups). The beams were made from ordinary concrete, fiber reinforced concrete (FRC) and cementitious composite (ECC). In the experiment the polypropylene fiber (PP) was used to improve the mechanical properties of the beams. Effectively, The PP fibers could prohibit the crack propagations by decreasing the spacing and width of the cracks. As a result, the torsional moment of the fiber reinforced concrete (FRC) beams and engineered cementitious composite (ECC) beams were 10% and 40% greater than ordinary concrete beams respectively, Under the allowable crack width of 0.7 mm. By increasing fiber ratio, the greater the torsional strength and the toughness of the beams were improved. Within the fiber contents of 1.5%, the utilization intensity of the stirrups was enhanced by the fibers. The fibers improved the torsional

toughness of the tested beams significantly. An empirical formula for predicting the ultimate torsional moment of the beams was proposed, the contribution of the concrete, the PP fibers and the GFRP bars to the torsional strength were considered separately, the predicted values had good agreements with the experimental results.

With using experimental properties for GFRP, steel reinforcements and concrete strength **A. Prabaghar and G. Kumaran** Presented a theoretical model for rectangular GFRP reinforced rectangular concrete beams under pure torsion **[31]**. The main parameters in the study were longitudinal, transverse reinforcement ratio and concrete grade. By using elastic and plastic theories of torsion the theoretical torque verses twist relationship is established for various values of torque and twist. Finally, the ultimate torque is determined using space truss analogy and softening truss model for different parameters and based on this study, a good agreement is made between the theoretical behavior GFRP reinforced and conventionally reinforced beams. The more reliable to predict the torsional behavior according to study was the space truss analogy and softening truss model. By replacing the conventional steel reinforcement ratio by the same GFRP reinforcement ratio for bars and stirrups the ultimate torsional strength reduced but the greater effect was the stirrups spacing. The increase of concrete grade and reinforcement ratio have been increased the ultimate torsional strength. Lower tensile strain values for steel than the GFRP reinforcements made the angle of twist of steel reinforcement concrete beams was lower than GFRP reinforcement concrete beams and the ductility of the beams in the post cracking stages increased for lower percentage of steel however these variations much higher for beams reinforced with GFRP. The Indian Standards controlled the minimum stirrups spacing.

CHAPTER THREE
EXPERIMENTAL WORK

3.1 Introduction

In this Chapter, the details of the experimental work including materials, preparation of concrete, used mixing procedure, tested specimens and the test procedure will be discussed.

The experimental study includes testing of nine renforced concrete beams which were tested under torsion. One beam was tested as control beams by using longitudinal and transverse steel reinforcement with normal concrete strength and the distance between stirrups was 150 mm. Second beam constructed by changing the longitudinal and transverse reinforcement from steel to GFRP with the same normal concrete strength and the distance between stirrups. Third beam constructed similar to 2nd beam by changing the distance between stirrups to be 100 mm.

Fourth beam constructed similar to 2th beam by addition one GFRP longitudinal bars to the two sides of beam with 8 mm. Fifth beam constructed similar to the 2nd beam but it was tested under bending and torsional moments. Sixth beam constructed with inclined stirrups 45^{o} with 150mm spacing and ordinary concrete. seventh beam constructed similar to the 2nd beam with concrete strength 50 MPa. Eighth beam was constructed with steel reinforced longitudinal bars without stirrups and ordinary concrete strength. Nineth constructed similar to the 8nd beam but it was tested under bending and torsional moments.

The torsional strength, peck crack and deflection, the first and failure crack of the reinforced concrete beams were obtained. The GFRP, steel with high strength type, normal concrete strength with normal aggregate type, which used commonly for wide range of buildings in Egypt was used, also were

used. The study of the behavior GFRP reinforced concrete beams under torsion, shape of failure, deflection and strain in concrete are the main objectives of the present research.

3.2 Experimental Program

To achieve the goals of this research work, the specimens were tested in the laboratory and loaded torsional moment, and measuring deflections, strain in concrete surface in shear failure zone and failure of the beam specimens will be obtained.

3.2.1 Test Parameters

The effects of the following parameters were studied:

- Behavior of GFRP reinforcement under torsion, by compare the same beam with the same conditions and dimensions with change of reinforcement from steel to GFRP.
- Configuration of stirrups, by change the angle of stirrups from 90^{o} to 45^{o} and 135^{o}.
- Changing of stirrups spacing, by decrease the spacing between stirrps for GFRP beam.
- The difference loading, by add bending moment and shear loads with torsional moment for specimen.
- Changing of concrete strength, by change the concrete strength from 30 MPa to 50 MPa.
- Influence of lack or absent stirrups, by testing specimens without stirrups only longitudinal reinforcement.

Each parameter was individually studied to achieve its particular effect on the behaviour of the tested R.C beams.

All specimens of the experimental program were tested in laboratory of the Faculty of Engineering, El-Mataria, Helwan University. Details of the

specimens' materials, geometry, casting and testing methodology will be described. The measurement devices and test setup were used in the experiments will be described.

3.2.2 Specimens Details

The experimental program consisted of nine R.C. beams, the details of the R.C. beams are listed in Table (3-1). All the beams had a typical geometry. The beam length was 2000×300×150 mm. with beam volume 0.09 m^3 and the beam weight was 2.25 KN.

All the tested specimens were reinforced typically torsion. For all beams the bottom longitudinal reinforcement was two bars of nominal diameter 12 mm. The top longitudinal reinforcement was two bars of nominal diameter 10 mm. The concrete cover was 15 mm. These stirrups had a nominal diameter of 8 mm, and as shaped closed stirrups. These stirrups were arranged uniformly along the beam length with internal spacing of 150 mm, with the concrete strength was 30 N/mm^2. Fourth beam had additional two GFRP longitudinal reinforced, third beam stirrups were arranged uniformly along the beam length with internal spacing of 100 mm. sixth beam had inclined stirrups 45^o and 135^o, seventh beam constructed with concrete strength 50 N/mm^2, eighth and nineth beams had been without stirrups. Reinforcement of specimens are shown in Figure (3-1).

T able (3-1): Details of Tested Specimens.

Specimen Name	F_{cu} N/mm²	Reinforcement					Additional side Longitudinal RFT	Loading
		Configuration	Spacing (mm)	longitudinal RFT Type	Top	Bottom		
B1-S	30	Closed-Vertical	150	Steel	2Ø10	2Ø12	- - - - -	Torsion
B2-G	30	Closed-Vertical	150	GFRP	2Ø10	2Ø12	- - - - -	Torsion
B3-G	30	Closed-Vertical	100	GFRP	2Ø10	2Ø12	- - - - -	Torsion
B4-G	30	Closed-Vertical	150	GFRP	2Ø10	2Ø12	2Ø8	Torsion
B5-G	30	Closed-Vertical	150	GFRP	2Ø10	2Ø12	- - - - -	Torsion & Moment
B6-G	30	Closed-Inclined 45°	150	GFRP	2Ø10	2Ø12	- - - - -	Torsion
B7-G	50	Closed-Vertical	150	GFRP	2Ø10	2Ø12	- - - - -	Torsion
B8-S	30	Without stirrups	- - - - -	Steel	2Ø10	2Ø12	- - - - -	Torsion
B9-S	30	Without stirrups	- - - - -	Steel	2Ø10	2Ø12	- - - - -	Torsion & moment

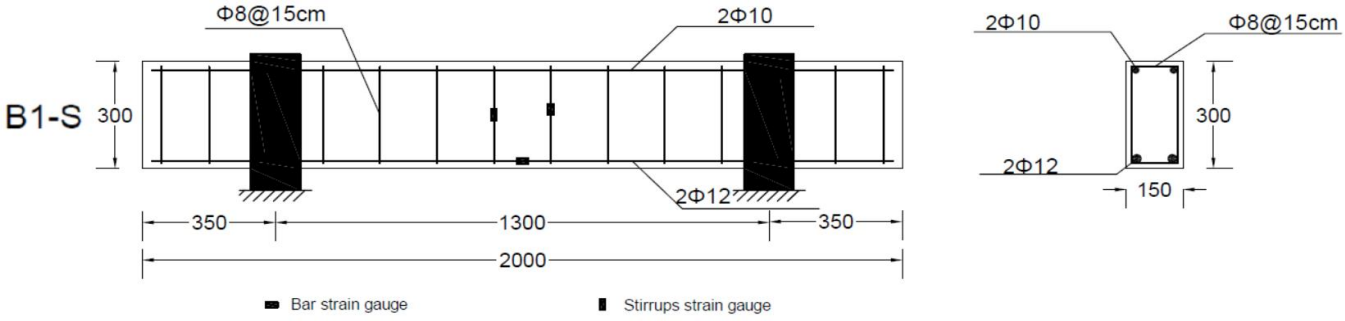

(a) Control Beam

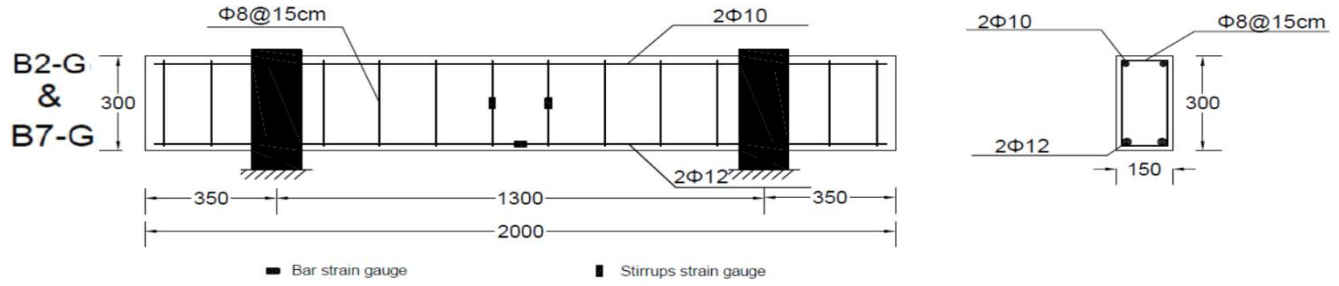

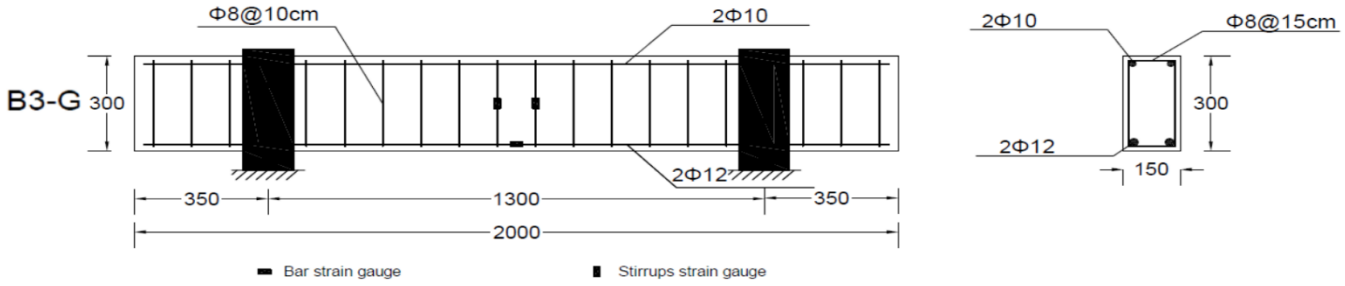

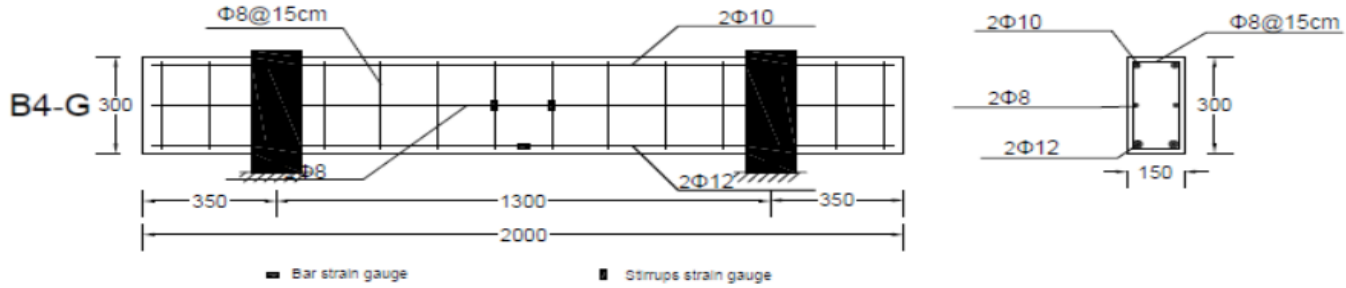

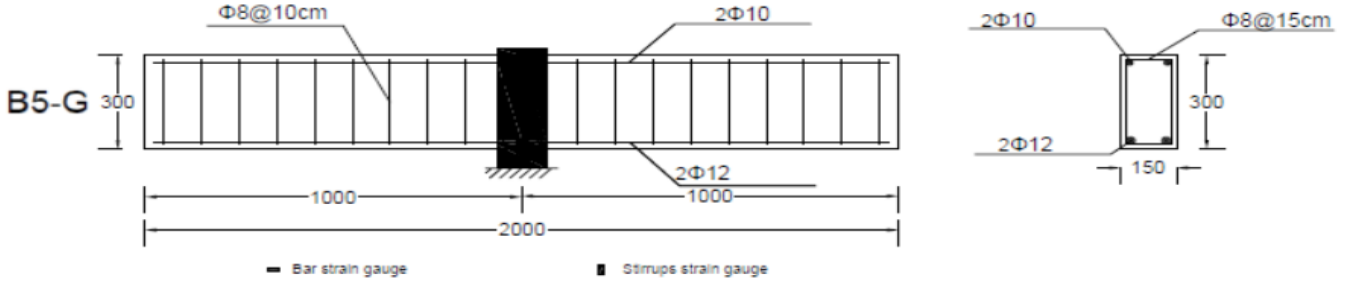

(b) GFRP Reinforced Concrete Beam

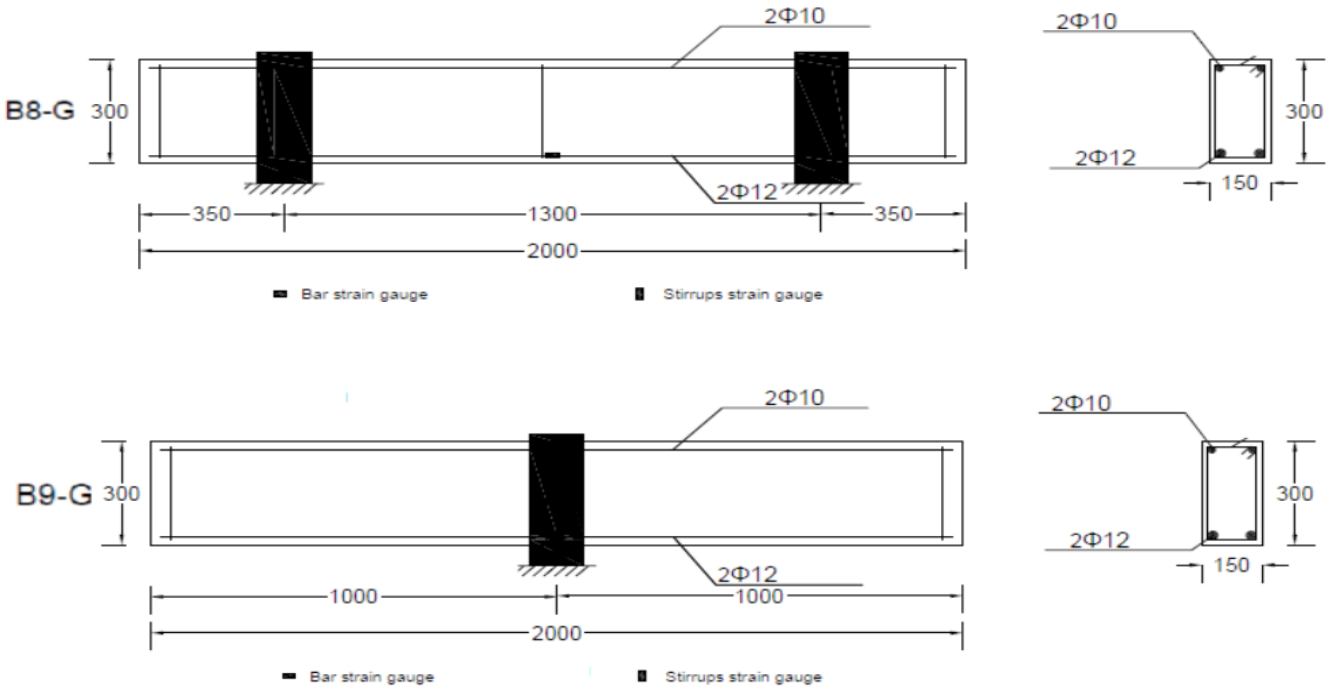

(c) Steel Reinforced Concrete Beam Without Stirrups

Figure (3-1): Details of Beams Reinforcement

3.3 Materials Properties

The Materials used in casting and reinforcement of the tested beams were aggregates, cement, water, reinforced steel, GFRP bars and stirrups, silica fume and superplasticizer. The process of manufacturing was simulated as closely as the common way of practice of concrete construction. The obtained results were compared with the limits recommended by the local specifications or codes of practice. The characteristics of the materials used in this research were discussed in the following sub-sections.

3.3.1 Coarse Aggregate

Coarse aggregates are the crushed stone used for making concrete. The commercial stone is quarried, crushed, and graded. Much of the crushed stone used is granite, limestone, and trap rock. The used coarse aggregates had a nominal maximum size of 20mm. This nominal size was chosen taking into consideration the dimensions of the tested beams as well as the spacing between the reinforcing bars. It was clean and free from organic material.

3.3.2 Fine Aggregates

Fine aggregate (sand) is an accumulation of grains of mineral matter derived from disintegration of rocks. It is distinguished from gravel only by the size of the grains or particles but is distinct from clays which contain organic material. Sand is used for making mortar and concrete and for polishing and sandblasting. Clear sands are employed for filtering water. Here, the fine aggregate/sand is passing through 4.75 mm sieve.

3.3.3 Cement

Ordinary Portland cement was used provided from Suez factory in Katameya in Cairo as shown in Figure (3-2). The usual chemical analysis as well as the physical properties of the Torah cement batches in this work as determined by laboratory tests, showed its suitability for concrete works.

There are some conditions before using cement.

1. Cement must be stored under cover.
2. Cement must not get damp or wet.
3. Cement bags must not be stacked higher than seven bags and must not be in contact with the floor or walls.
4. Doors must be opened as infrequently as possible and windows must be kept closed.
5. Cement should not be kept in storage for longer than eight weeks from production date.
6. Cement should be used before its expired date.

Figure (3-2): Cement

3.3.4 Mixing Water

Clean fresh drinking water was used free from acids, alkalis, oils or other organic impurities for mixing and curing all concrete specimens in this work. A water cement ratio was according to mix design to ensure required strength and adequate workability for casting. The water was valid to drink.

3.3.5 Steel Reinforcement

Different reinforcement diameters and types were used in this study. High tensile ribbed steel bars of 12 mm diameter were used as main steel of beams. and 10 diameter was used as compression steel in all beams. Mild smooth steel 8 mm diameter was used as stirrups in all beams. The properties of reinforcing steel bars are in Table (3-2).

Table (3-2): Factory Data of Steel used in the Experimental Work

Reinforcement	**Yield Strength N/mm^2**	**Ultimate Strength N/mm^2**	**Young's Modulus kN/mm^2**
Mild Steel	240	350	200
High Tensile Steel	360	520	200

3.3.6 GFRP Fiber

High tensile ribbed GFRP bars of 12 mm diameter were used as main reinforcement of beams and have a rough surface to get more bonds between GFRP bars and concrete. The top reinforcement of beams was 2 GFRP bars with 10 mm diameter for the beams reinforced by GFRP bars and steel in the other beams with the same dimeters and amount.

3.3.6.1 Tensile Strength

Because of the brittle nature of the FRP bars, they usually fail in the gripped zones when tested in tension leading to inaccurate results. Therefore, the design and development of the test specimens should include suitable gripping mechanism to assure that the failure takes place away from the gripped zones. In this research the special precautions mentioned in ACI-440, were applied. The precautions are to use steel tube end anchors on both ends of the tested bars to allow for uniform distribution of the load applied from the testing machine to the test specimen. The anchorage system is composed of a steel tube of 28 mm and 20 mm external and internal diameter, respectively. The steel tube was filled with a high-performance resin grout to assure good bond between the bar and the steel tube. Figure (3-3) shows a schematic diagram of the details of the used anchorage system. Figure (3-4) shows the test setup, and the test results were presented in Figures from (3-5). The modulus of Elasticity Ef was determined as the average value of the ratio between the difference between two successive readings of stress and the difference between the corresponding reading of strains for each two successive reading.

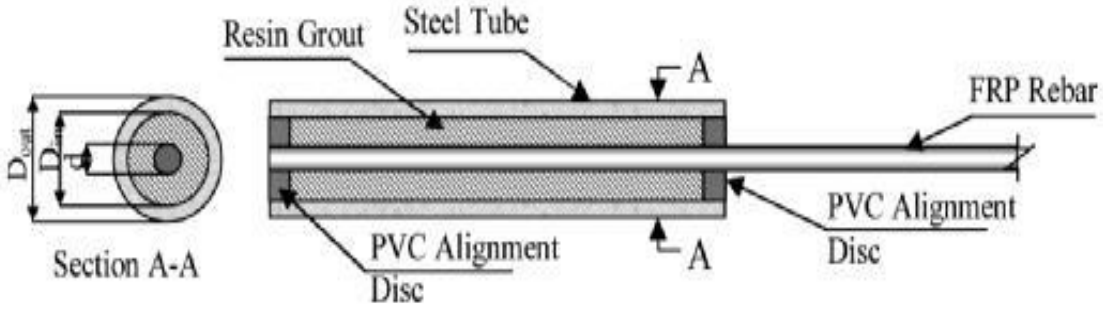

Figure (3-3): A schematic Diagram of the Details of the Used Anchorage System.

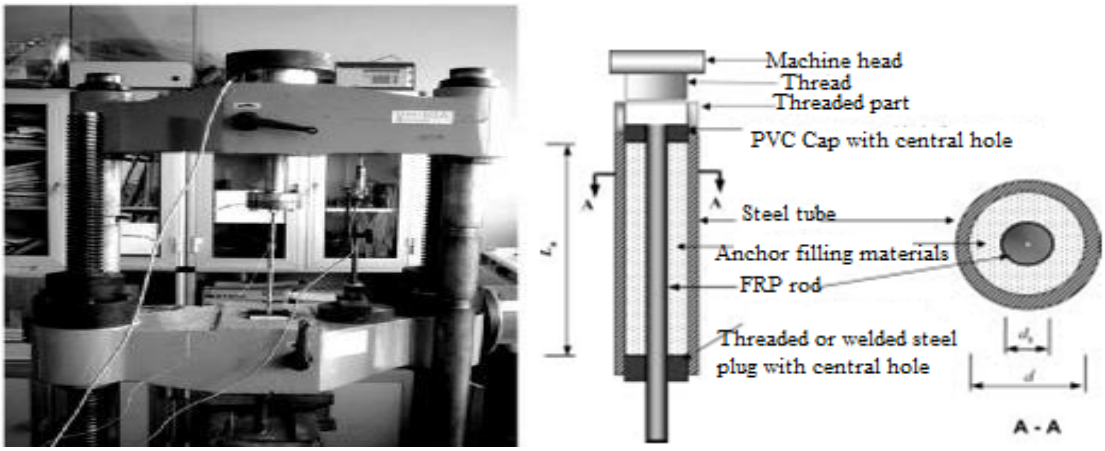

Figure (3-4): The Test Setup

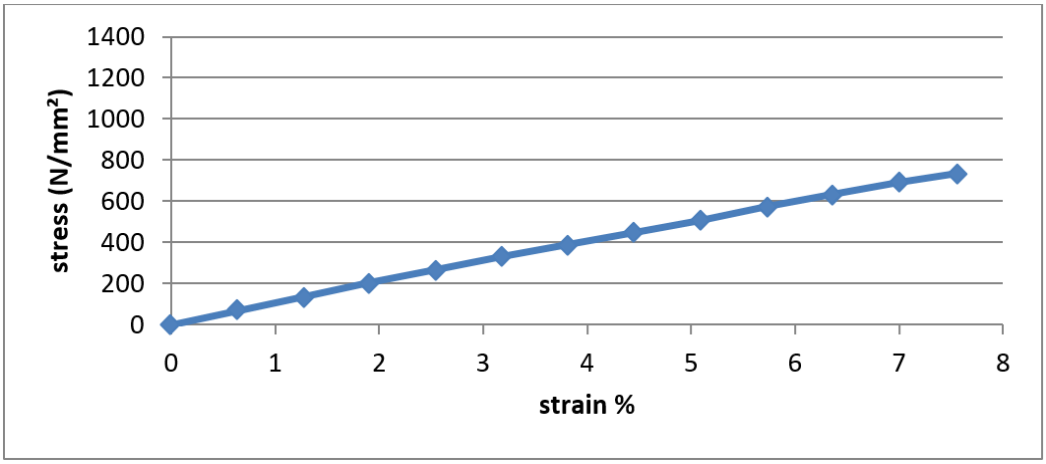

Figure (3-5): Stress Strain Curve for Fiber Glass Bars.

3.3.7 Silica Fume

Silica Fume was used in this investigation was Sika Fume which is a product of Sika. The mechanical properties of used silica fume are given in Table (3-3).

Table (3-3): Mechanical Properties of Sikadur-330.

Composition	A latently hydraulic blend of active ingredients
Appearance / Colour	Grey powder
Bulk Density	300 kg/m^3

3.3.8 Superplasticizer

Superplasticizer was manufactured by Chemicals for Modern Building International (CMB) Company under trade name Addicrete BVF1 is used in this research work. Addicrete BVF1 is added to concrete during the mixing process or to the water prior to concrete mixing. Table (3-4) gives the characteristics of Superplasticizer.

Table (3-4): Mechanical Properties of Addicrete BVF1.

Base	Selective synthetic polymer
Appearance	Brown liquid
Density	1.18 ± 0.01 kg/1
Chloride content	Nil
Compatibility with cement	All types of Portland cement

3.4 Preparation of Test Specimens

3.4.1 Formwork

Nine wood forms were prepared for casting concrete of the tested beams specimens with clear dimensions of 150 mm width, 300 mm height and 1650

mm length. Therefore, the formwork should be rigid and strong to hold the weight of wet concrete without bulging anywhere. The joints of the formwork are sealed to avoid leakage of cement slurry. Water was then applied to the inner faces of formwork. Formwork as shown in Figures (3-6) and the steel and GFRP reinforcements details of beams as shown in Figures (3-7) and (3-8).

Figure (3-6): Wood Forms of Specimens.

Figure (3-7): Steel Reinforcement Details of Beams.

Figure (3-8): GFRP Reinforcement Details of Beams.

3.4.2 Concrete Mix Design

A concrete mix 30 MPa concrete mixture was used to cast all the tested concrete beams except B7 was casted with concrete mix 70 MPa. Coarse aggregate and fine aggregate were mixed together, the grading of this mix obtained from the sieve analysis test according to the Egyptian Standard

Specifications (ECP 203-2019). The mix proportions of the concrete used are given in Table (3-5).

Table (3-5): Concrete Mix Design Proportions (Kg/m^3).

F_{cu} N/mm^2	**Cement**	**Coarse Aggregate**	**Fine Aggregate**	**Silica Fume**	**Water Liter/m^3**	**Superplasticizer Liter/m^3**
30	382	1196	563	-------	210	--------
50	500	1050	677	55	`160	11

The coarse aggregate used was of 20 mm maximum nominal aggregate size. and natural sand was used as fine aggregate.

Concrete constitutes were added separately, while water was added by volume. Mixing was performed using a concrete drum mixer. First, sand, aggregate and cement were dry mixed for about one minute until a homogeneous colour was observed, then the water was gradually added and mixed thoroughly. Mixing operation continued for a period of about 3-minutes after adding water until a uniform colour obtained.

3.4.3 Casting and Compaction

The formworks were sprayed with water before casting of concrete, and then reinforcements were placed in their right position in the forms. Just after mixing, the concrete was cast in the wood molds. The concrete was compacted using vibrator machine for 1 minute for good compaction of concrete as shown in Figure (3-9).

Figure (3-9): Compaction of Concrete

3.4.4 Quality Control Tests

Cubes with dimension 150 × 150 × 150 mm were taken during casting all beams. The quantity of concrete in each batch was enough for casting Nine beams. Three cubes were taken from each mixture. Cubes were prepared and coated with oil before casting and then concrete was placed after mixing in three layers each layer compacted by 25 blows with standard rods according to the Egyptian Standard Specifications (ECP 203-2019) to determine the compressive strength of concrete after 28 days from casting. The cubes were submerged in water during the curing duration.

Table (3-6): Cube Strength After 28 Day.

Cube no.	1	2	3	Average (N/mm^2)
NSC C30 (N/mm^2)	55.01	44.6	52.93	50.85
HSC C50 (N/mm^2)	38.02	26.90	27.60	30.84

Average strengths are 50.85 N/mm^2 (HSC) and 30.84 N/mm^2 (NSC).

3.4.5 Curing

Curing is done to prevent the loss of water, which is essential for the process of hydration and hence for hardening. After the molds and forms were compacted, the specimens were covered with wet burlap for 24 hours. After 48 hours, the sides of the form were stripped away, the specimens were covered completely with wet burlap to complete the curing and the concrete cubes were totally submerged in water for 28 days.

3.5 Test Set-up

The present research investigates the behavior of GFRP reinforced concrete beams under torsion. To achieve that, the torsional setup was prepared, as shown in Figure (3-10). The test setup was designed and fabricated in the Concrete Laboratory of Civil Engineering at the Faculty of Engineering, El-Mataria, Helwan University. A very rigid steel frame consisting of I-sections was used as a base to support a beam specimen. The support of beams was roller to make the specimen able to rotate around the axis of beam during the test, as shown in Figure (3-11). To present torsion, the two sections edges of beams were fixed with arm (a wing steel spreader resting on two rigid steel arms), as shown in Figure (3-12). The arms were loaded with beam (I-section) to introduce torsional moment and the beam roller around the axises of beam. The load was applied vertically using a hydraulic jack with 250 KN capacity in the middle of a distribution beam (I-section). The distribution beam was supported on the tip of two arms. To enable tracing of the crack propagation easily during testing all beams specimens were painted white with lime. The jack was connected to S.I.B. 360 to keep it in a vertical position. A load cell was directly located underneath the jack to measure the load equal increments. The loading was increased by 150 KN.

Figure (3-10): Specimen Shape.

Figure (3-11): Torsional Roller Support.

Figure (3-12): The Wing Steel with Arm.

3.6 Instrumentation

3.6.1 Load Measurement

Sensitive electrical load cell was used to measure the applied load on the specimen during the test, as shown in Figure (3-13), (3-14) and (3-15).

Figure (3-13): Measurement Device.

Figure (3-14): Electrical Instrumentation Reading.

Figure (3-15): Loading Machine.

3.7 Measuring Devices

3.7.1 Deflection Measurements

To measure the deflection of beams, three aluminum frames were located to measure the relative rotation of the specimens' cross sections. Two aluminum frames were located at the right of specimen with distance 30 mm from the section edges of beams (50 mm from the wing steel), and the other one in the opposite edge at left side with the same distance. Deflection was obtained as mentioned before by the load-deflection curves.

3.7.2 Steel Strain Measurements

Before casting the specimens, electrical resistance stain (ERS) gauges were prepared and fixed on the longitudinal bars and stirrups by epoxy. The proportions of electrical resistance stain (ERS) gauges are shown in Table (3-6). The reinforcement strain was measured and recorded using a digital strain indicator connected to the data acquisition system. It is located as shown in Figure (3-1) & (3-16).

Table (3-7): Proportions of Reinforcement Electrical Resistance Stain (ERS) Gauges.

Model	KFGS-10-120-C1-11 L1M2R
Gage factor	2.12±1.0%
Gage Length	10 mm
Gage Resistance	120.4 Ω±0.4
Transverse Sensitivity Ratio	(0.2±0.2)%
Adoptable Thermal Expansion	$11.7*10^{-6}/^{o}C$

Figure (3-16): Reinforcement Electrical Resistance Strain

3.7.3 Concrete Strain Measurements

Before testing the beams, electrical resistance stain (ERS) gauges were prepared and fixed on the tested beams by epoxy. One strain gauge with a gauge length of 60 mm (2.36 in.) was mounted onto the concrete front surface at 135 degrees to the beam axis in the quarter distance from the support to support in the left side of tested beam for measuring the surface strains. The proportions of electrical resistance stain (ERS) gauges are shown in Table (3-7). The concrete strain was measured and recorded using a digital strain indicator connected to a data acquisition system. It is located as shown in Figure (3-17).

Table (3-8): Proportions of Steel Electrical Resistance Stain (ERS) Gauges.

PL-60-11-1LJC-F
2.10±1.0%
60 mm
120 Ω±0.5
1.1%
10/0.12 2W 1m r=0.32(Ω/m)
$11*10^{-6}/^{o}c$

Figure (3-17): Concrete Electrical Resistance Strain.

CHAPTER FOUR
EXPERIMENTAL TEST RESULTS

4.1 Introduction

This Chapter introduces the results of the experimental program, which was obtained to study the behavior of GFRP-reinforced concrete beams under torsion. The experimental parameters were the using variable concrete types, existence and absence stirrups, reinforcement types (steel, GFRP), stirrups configuration, stirrups spacing 150,100 mm, load types and shrinkage bars. Experimental program consisted of nine beams.

Beam (1): Control specimen, which consists of longitudinal and transverse steel reinforcement with normal concrete strength 30 MPa and the distance between stirrups was 150 mm, it was tested under torsional moment.

Beam (2): Consists of longitudinal and transverse GFRP reinforcement with normal concrete strength 30 MPa and the distance between stirrups was 150 mm, it was tested under torsional moment.

Beam (3): Consists of longitudinal and transverse GFRP reinforcement with normal concrete strength 30 MPa and the distance between stirrups was 100 mm, it was tested under torsional moment.

Beam (4): Constructed similar to 2^{th} beam by addition one GFRP longitudinal bars to the two sides of beam with 8 mm, it was tested under torsional moments with concrete strength 30 MPa.

Beam (5): Constructed similar to the 2^{nd} beam but it was tested under bending and torsional moments with concrete strength 30 MPa.

Beam (6): Constructed with inclined stirrups 45^{o} and 135^{o} with 150mm spacing and ordinary concrete 30 MPa, it was tested under torsional moment.

Beam (7): Constructed similar to the 2nd beam with concrete strength 50 MPa, it was tested under torsional moment.

Beam (8): Constructed with steel reinforced longitudinal bars without stirrups and ordinary concrete strength 30 MPa, it was tested under torsional moment.

Beam (9): Constructed similar to the 8th beam but it was tested under bending and torsional moments with concrete strength 30 MPa.

4.2 Experimental Results

All beams were tested under torsional moments with recording the maximum and failure torsional capacities, the results are shown in Table (4-1).

4.2.1 Results of Tested Beam (B1)

- **Specimen Description**

This beam is reinforced by steel in longitude and transverse directions with stirrups spacing 150 mm and 2 φ 10 as a compression steel and 2 φ 12 as a tensile steel with section 150*300 mm and concrete cover 20 mm.

- **Crack Pattern**

Figure (4-1) shows the cracking pattern for control test beam (B1). In the Figure, each crack is marked by a line representing the direction of cracking. The crack patterns at both faces of all beams were recorded at several load stages up to failure. The effect of steel reinforcement made the cracks over all the beams. Torsional cracking (continuous diagonal cracks) at first took place at mid and left span of the tested beams then extended over the beam. Both patterns are largely reversed in direction and similar in width. The specimen remained with no visible cracks until torsional cracks took place. The first crack occurred at torsional moment of 8.008 KN.m.

Table (4-1): Results and Details of Tested Specimens

Specimen Name	F_{cu} (N/mm^2)	Reinforcement					Additional side Longitudinal Reinforcement	Loading	Crack Strength (kN.m)	Max Experimental Load (kN.m)
		Configuration	Spacing (mm)	Longitudinal Reinforcement Type	Top	Bottom				
B1-S	30	Closed-Vertical	150	Steel	2Ø10	2Ø12	- - - - -	Torsion	8.008	13.29
B2-G	30	Closed-Vertical	150	GFRP	2Ø10	2Ø12	- - - - -	Torsion	5.94	6.44
B3-G	30	Closed-Vertical	100	GFRP	2Ø10	2Ø12	- - - - -	Torsion	3.74	7.87
B4-G	30	Closed-Vertical	150	GFRP	2Ø10	2Ø12	2Ø8	Torsion	6.93	6.93
B5-G	30	Closed-Vertical	150	GFRP	2Ø10	2Ø12	- - - - -	Torsion & Moment	6.908	11.84
B6-G	30	Closed-Inclined 45°	150	GFRP	2Ø10	2Ø12	- - - - -	Torsion	5.236	5.236
B7-G	50	Closed-Vertical	150	GFRP	2Ø10	2Ø12	- - - - -	Torsion	5.61	7.326
B8-S	30	Without stirrups	- - - - -	Steel	2Ø10	2Ø12	- - - - -	Torsion	5.434	5.478
B9-S	30	Without stirrups	- - - - -	Steel	2Ø10	2Ø12	- - - - -	Torsion & moment	11.13	10.87

All beams are 150mm X 300 mm

All beams are reinforced by (2Ø10 comp. and 2Ø12 main)

The first torsional cracks took place at mid, and lift-span of the tested beam (B1) then torsional cracking extended over the beam. As loading increased, more torsional cracks were formed in four faces continuously and cracks became wider. The maximum torsional moment was 13.29 KN.m and after that the cracks weakened the beam which caused decreasing in capacity of beam and its stiffness. The capacity of beam decreased until the failure with torsional moment 8.536 KN.m. As clearly, the failure was torsional failure and the main crack sloped with angle from 40 to 45 degrees and the crack width reached to 5.5 mm at the main torsional cracking in the middle. It was noticed that the beam had twist in the main bottom bars as a result of applied torsional moment as shown in Figure (4-2).

- **Twist of the Beam Section**

The relation between the twist of beam section and the torsional moment is shown in Figure (4-3). Three points of deflection (LVDT) for each specimen were measured, the first one at far 5 cm from the first torsional arm in one side of section 3 cm away, second point for measuring deflection in the same section in second side of section with the same dimensions and the third point in the second torsional arm with 5 cm from the torsional arm and 3 cm from the section side. The three-measure deflection would provide us by the same result but the reason for using 3 deflection measure to sure the result and to avoid any defect with them. The maximum twist was $5.85*10^{-2}$ rad/m for the left torsional beam section and 11.5*10-2 for the right torsional beam section with torsional moment 8.536 KN.m. It was observed that the first crack at 8.008 KN.m with $1.52*10^{-2}$ rad/m without voice and the maximum capacity was 13.288 KN.m with twist $5.24*10^{-2}$ rad/m. The twist increased with decreasing in torsional moment, twist and torsional moment at three phases is shown in Figures (4-4a) and (4-4b).

Figure (4-1): Cracks Pattern for Specimen B1.

Figure (4- 2): Twist of Main Bottom Bars for Specimen B1.

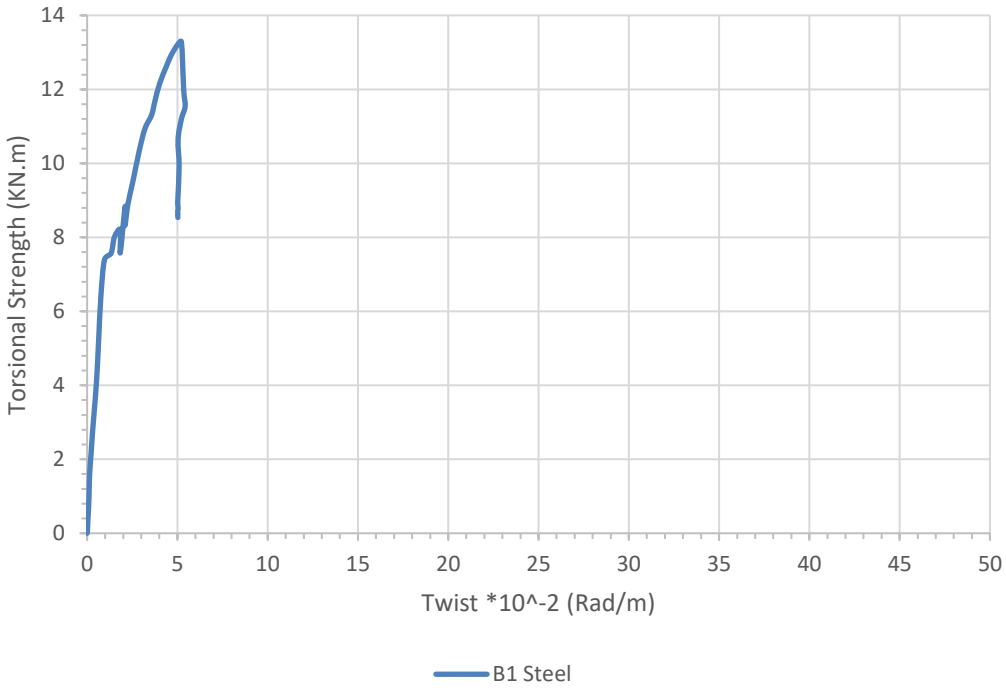

Figure (4-3): Torsional Moment-Twist Curve for Specimen B1.

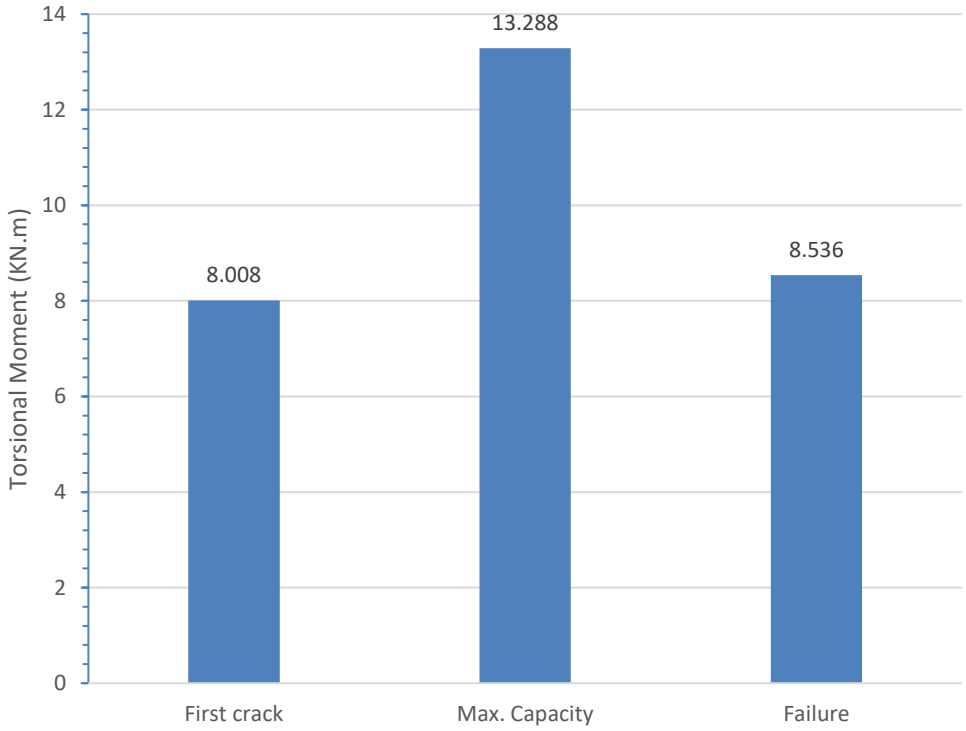

Figure (4-4a): Torsional Moment at Three Phases for B1.

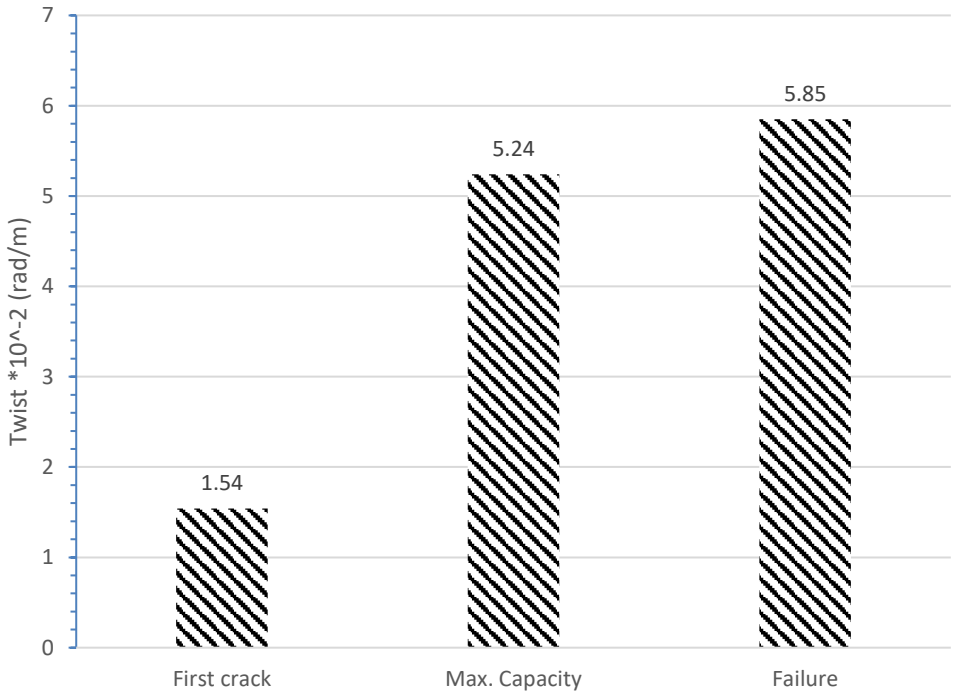

Figure (4-4b): Twist at Three Phases for B1.

- **Strain of GFRP Bars**

The relation between the strain of GFRP Bars and the applied torsional moment is shown in Figure (4-5). The strain gauge is located at the mid span of the beam with the bottom reinforcement. Strain of steel bars of beam didn't reach to yielding point.

The strain gauge was fixed on the center of the middle bar. From this result it is observed that B1 didn't reach the yield value stress. By comparing the strain distribution of the beam, it can be noticed that B1 failure torsional moment occurred without steel carry a large amount of stress. Strain of maximum capacity increased 75.4% from the strain at first cracking with increasing in torsional moment 66% from torsional moment at first crack. The first crack strain was $0.912*10^{-3}$ and $1.6*10^{-3}$ at maximum capacity. With accident the stain gauge stopped to measure, so we couldn't provide the bar strain at failure as shown in Figure (4-6).

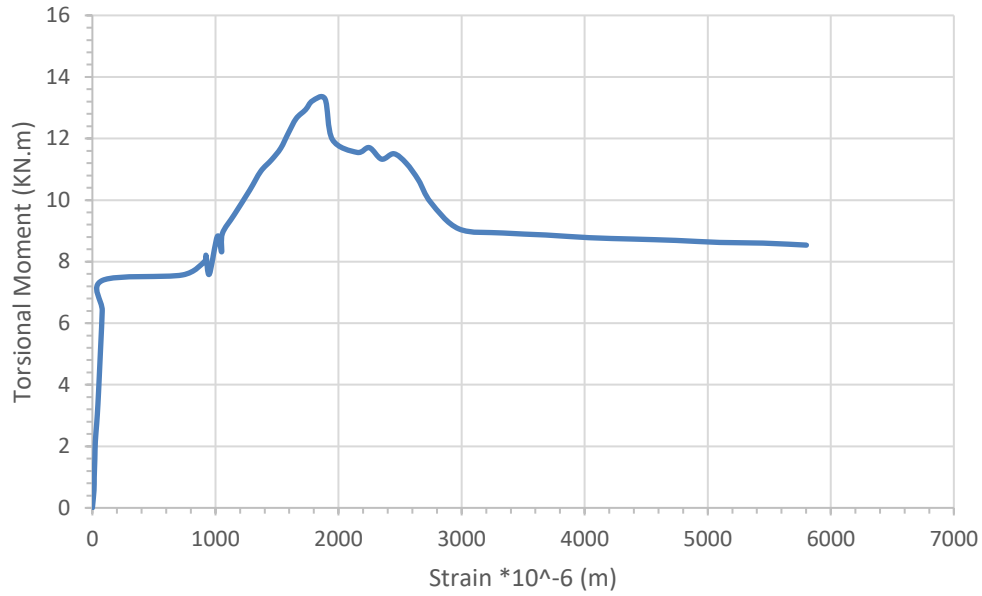

Figure (4-5): Torsional Moment-Strain Curve for Steel Bars for Specimen B1

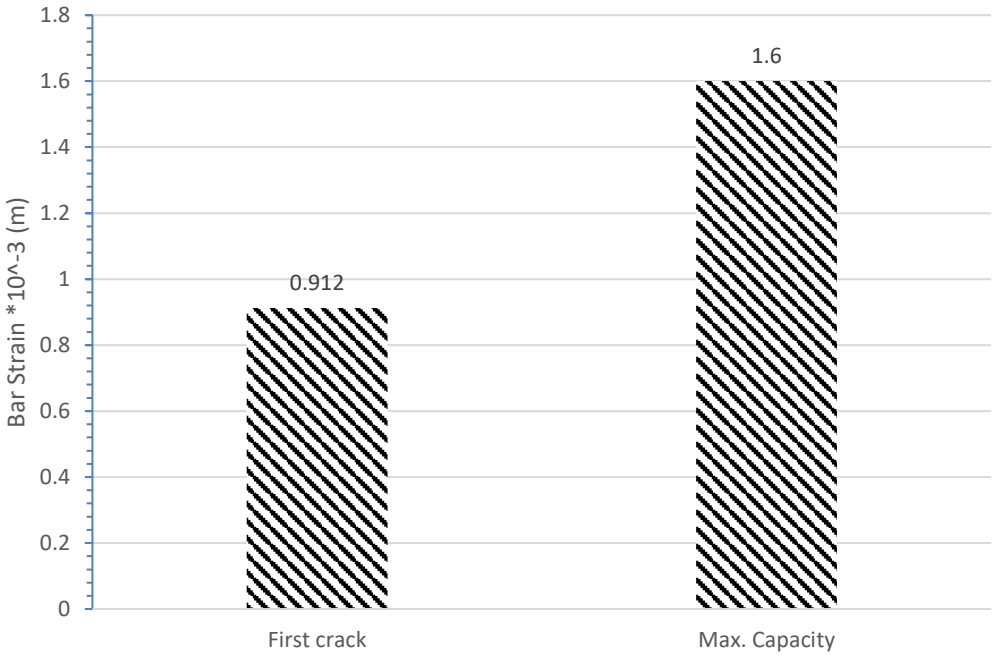

Figure (4-6): Bar strain at two phases for B1.

- **Strain of Concrete**

The relation between the concrete strain and torsional moment as shown in Figure (4-5). The strain gauge was located at quarter of beam span with angle 135º in the front face. Figure (4-7) shows torsional moment-strain relationship for the concrete. Concrete strain gauge 60 mm was mounted on

the concrete front at 135˚ in the middle distance between the middle span and the left torsional arm. By comparing the strain distribution of the beam, it can be noticed that B1 failure torsional moment occurred with concrete carry a large amount of stress. Strain of maximum capacity increased 63.6% from the strain at first cracking, the pick of strain was in maximum capacity with $5.43*10^{-4}$ and decreased 37.7% from the strain at failure as shown in Figure (4-8).

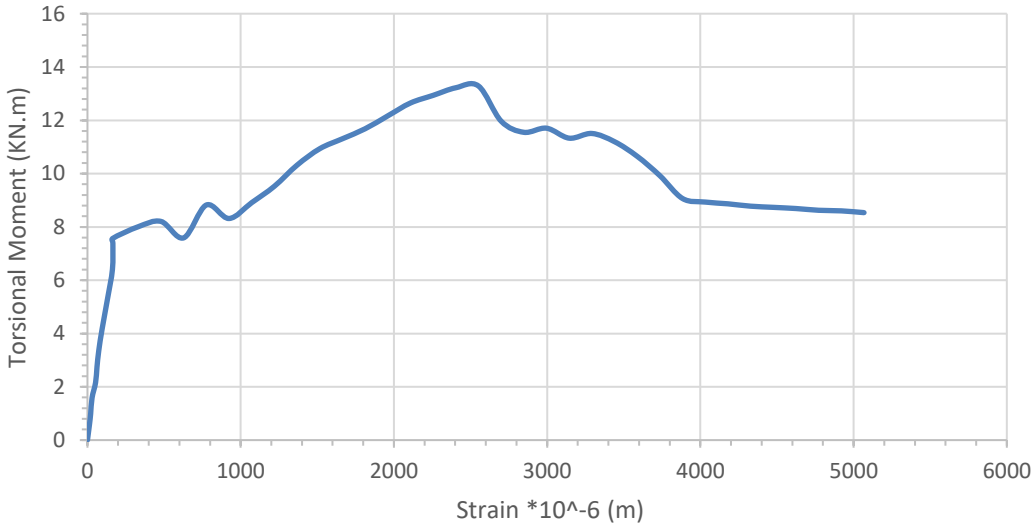

Figure (4-7): Torsional Moment-Strain Curve for the Concrete at Quarter of Span Zone for Specimen B1.

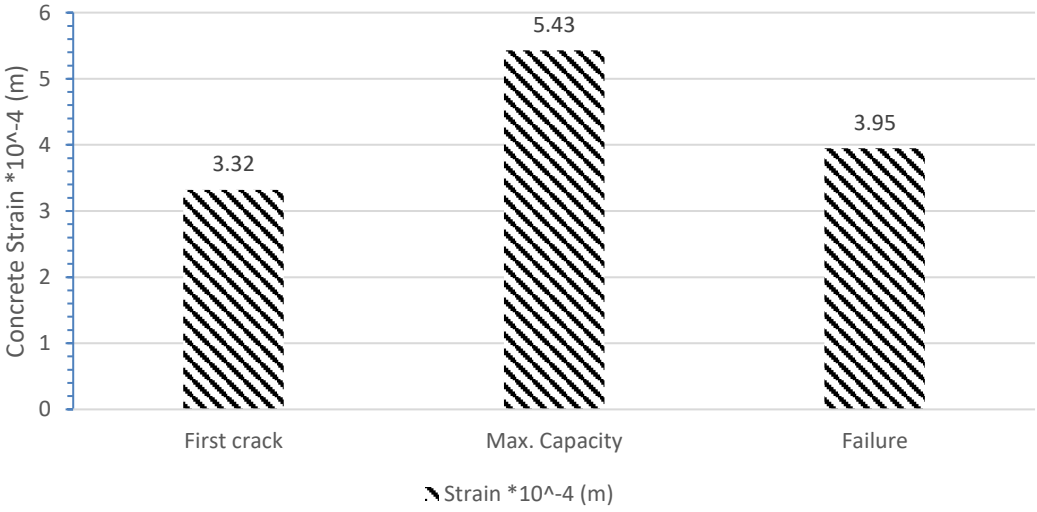

Figure (4-8): Concrete Strain and Torsional Moment at Three Phases for B1.

- **Strain of Stirrups**

The relation between the stirrups strain and torsional moment as shown in Figure (4-9-a) and (4-9-b). The strain gauge was located at two separated stirrups in the middle beam span with length of stirrups. Stirrup strain gauge was fixed on stirrup at the middle of span with two stirrups. Figure (4-10-a) shows the difference between the right stirrup strain and the torsional moment in three phases. For right stirrup, the maximum strain was $1.944*10^{-3}$ m with torsional moment 8.008 KN.m at the failure and the maximum torsional moment was 13.29 KN.m with strain $13.29*10^{-3}$ m and the first crack was strain $2.82*10^{-4}$ m with torsional moment 8.008 KN.m, the strain at first crack was 6.89% from the maximum strain by decreasing in capacity 6% from the capacity at failure and the strain at maximum capacity was 62.7% from the maximum strain by decreasing in capacity 56.4% from the capacity at failure.

For left stirrup, strain of first crack was $0.635*10^{-3}$ and strain of maximum capacity was $1.19*10^{-3}$. Capacity strain of maximum capacity increased 18.7% from the strain at first cracking with increasing in torsional moment 66% from torsional moment at first crack. With accident the stain gauge stopped to measure, so we couldn't provide the bar strain at failure as shown in Figure (4-10-b).

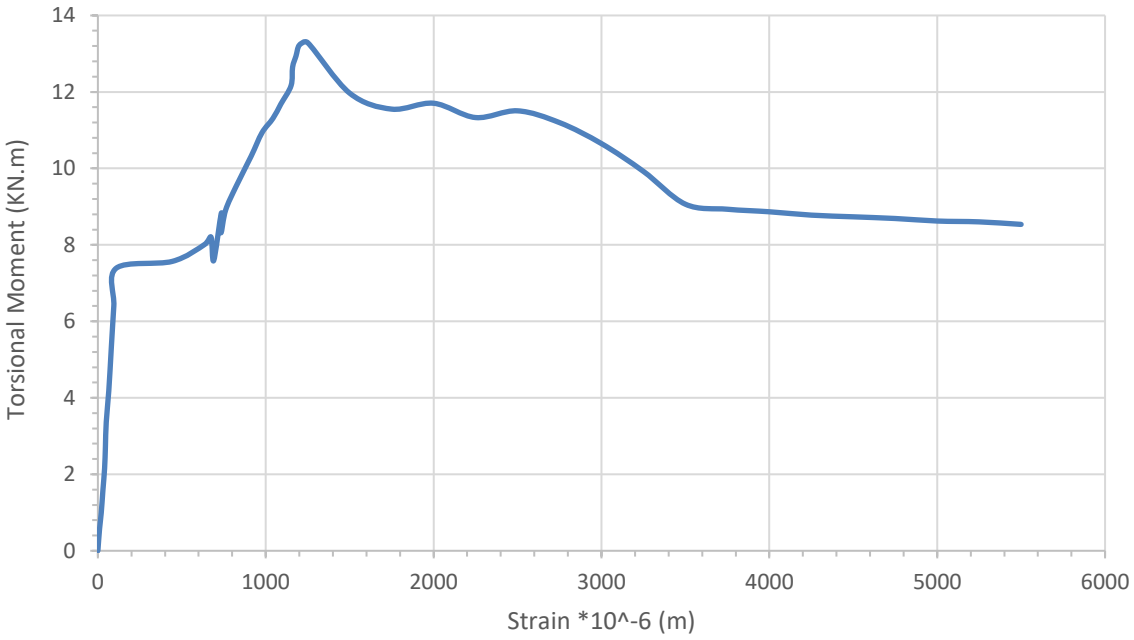

Figure (4-9-a): Torsional Moment-Strain Curve for the Left Stirrup at the Middle Span for Specimen B1.

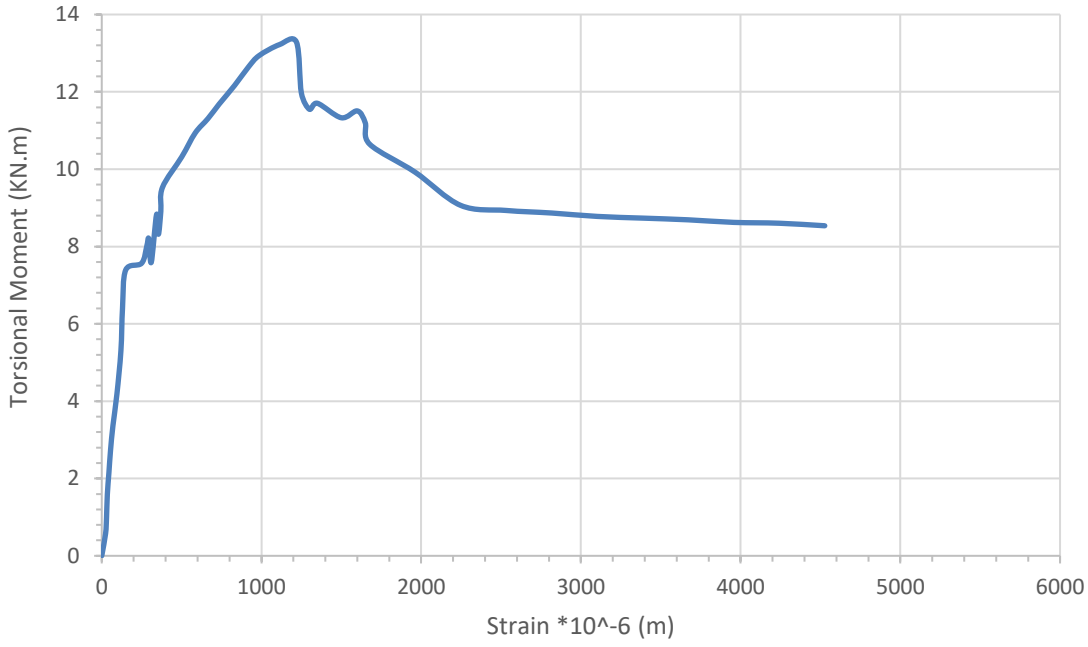

Figure (4-9-b): Torsional Moment-Strain Curve for the Right Stirrup at the Middle Span for Specimen B1.

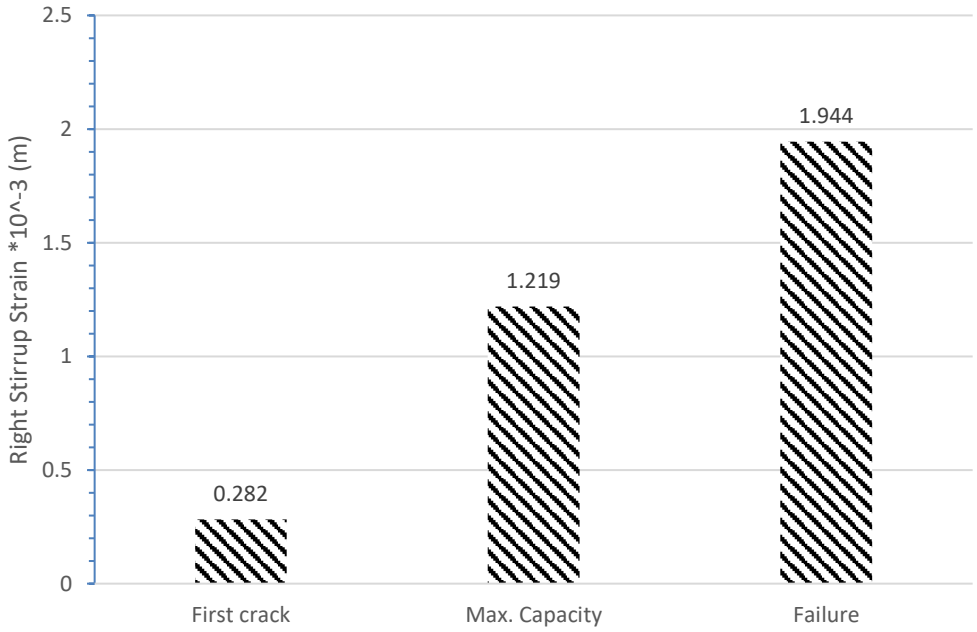

Figure (5-10-a) Right Stirrup Strain at Three Phases for B1.

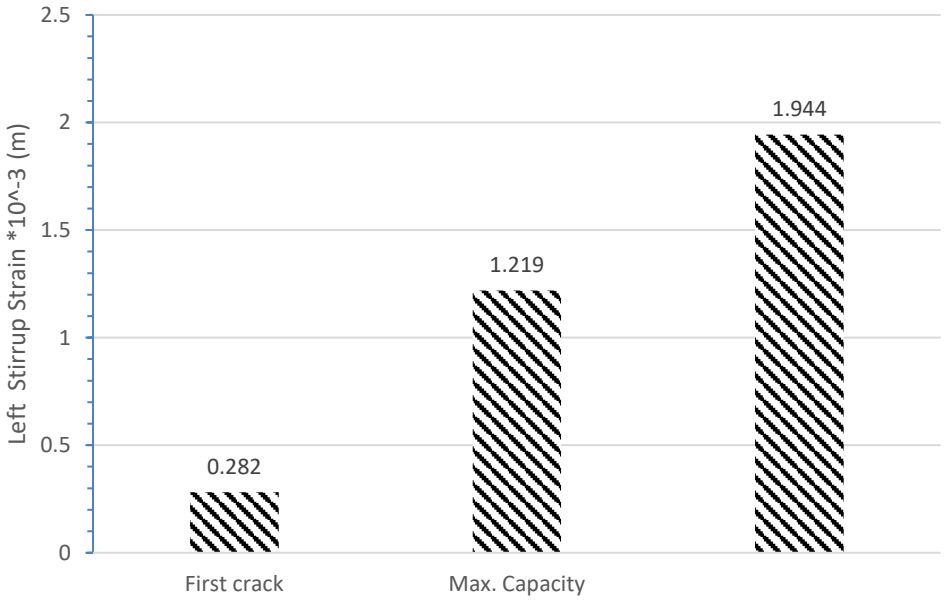

Figure (5-10-b): Left Stirrup Strain at Three Phases for B1.

4.2.2 Results of Tested Beam (B2)

- **Specimen Description**

This beam is reinforced by GFRP in longitude and transverse directions with stirrups spacing 150 mm and 2 φ 10 as a compression GFRP reinforcement

and 2 φ 12 as a tensile GFRP reinforcement with section 150*300 mm and concrete cover 20 mm. This beam is similar to a control beam by changing the steel by GFRP.

- **Crack Pattern**

Figure (4-12-a) and (4-12-b) show the cracking pattern for tested beam (B2). In the Figure, each crack is marked by a line representing the direction of cracking. The crack patterns at both faces of all beams were recorded at several load stages up to failure. The cracks started in the left side of beam near the torsional arm in the shear zone and continued to wide in the same location until the failure. The specimen remained with no visible cracks until torsional cracks took place cracking (continuous diagonal cracks) at left-span of the tested beams then extended in the same location of the beam near the torsional arm in the shear zone of the tested beam (B2). The first crack occurred at the torsional moment of 5.94 KN.m and continued to reach the max capacity 6.44 KN.m after few seconds than it went down and after that the capacity of beam decreased until the failure with torsional moment 3.43 KN.m. As clearly, the failure was torsional failure that clear in the rupture of stirrup and the main crack sloped with angle from 40 to 45 degrees. It was noticed that the beam ruptured in the edge of stirrup as a result for applied torsional moment as shown in Figure (4-13). It has been noticed that with increasing loading, cracks became wider, and cracks took place at the top and bottom of beam in the same crack location. The cracks weakened the beam which caused a decrease in capacity of beam and its stiffness. Because of the non-homogenousty and the natural of GFRP made the once the crack happened decreased the stiffness and the load traded to the weakest point which has impacted on the torsional strength and after the first crack the increase in capacity was little and in one place. The spacing between stirrups has helped to observe the impact GFRP cracks and propagation of cracks patterns.

- **Twist of the Beam Section**

The relation between the twist of beam section and the torsional moment is shown in Figure (4-14). At the final of experiment, the right torsional section beam changed from 0 rad/m to $17.53*10^{-2}$ rad/m and the left torsional beam section from 0 rad/m to $48.8*10^{-2}$ rad/m. Three points of deflection (LVDT) for each specimen were measured, the first one at far 5 cm from the first torsional arm in one side of section 3 cm away, second point for measuring deflection in the same section in second side of section with the same dimensions and the third point in the second torsional arm with 5 cm from the torsional arm and 3 cm from the section side.

Figure (4-12-a): Cracks Pattern First Side for Specimen B2.

Figure (4-12-b): Cracks Pattern Second Side for Specimen B2.

Figure (4-13): Rupture of Stirrup for Specimen B2.

The three-measure deflection would provide us with the same result but the reason for using 3 deflection measure to sure the result and to avoid any defect with them. The maximum twist was $48.8*10^{-2}$ rad/m until stop the test but the actual twist was 25.6 KN.m because the torsional resistance was semi constant with increasing only twist with torsional moment 3.43 KN.m with voice and the crack was on back. It was observed that the first crack at 5.94 KN.m with $0.89*10^{-2}$ rad/m without voice and the maximum capacity was 6.446 KN.m with twist $0.97*10^{-2}$ rad/m. The twist increased with decreasing in torsional moment as shown in Figure (5-14). Figures (5-15a) and (5-15b) show the difference between the twist and the torsional moment in three phases. By comparison the first and maximum capacities stages, by increasing in capacity 8.4% from the capacity at first crack the twist increased 9 % from the twist at first crack. On the other side at failure, by decreasing in capacity 42.6 % from the capacity at first crack the twist increased 29 times from the twist at first.

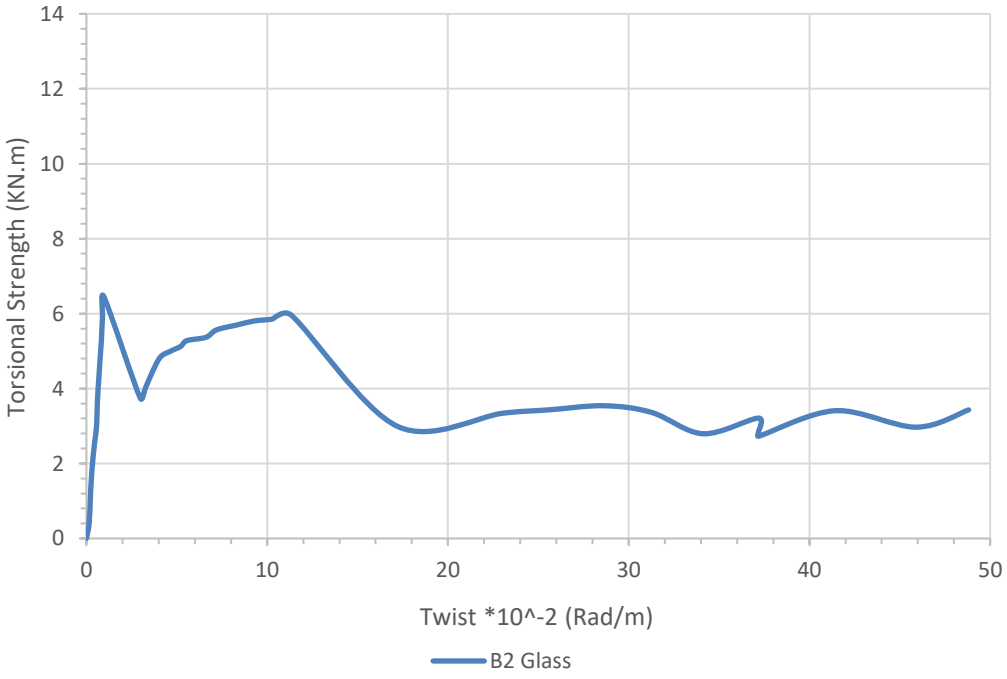

Figure (4-14): Torsional Moment-Twist Curve for Specimen B2.

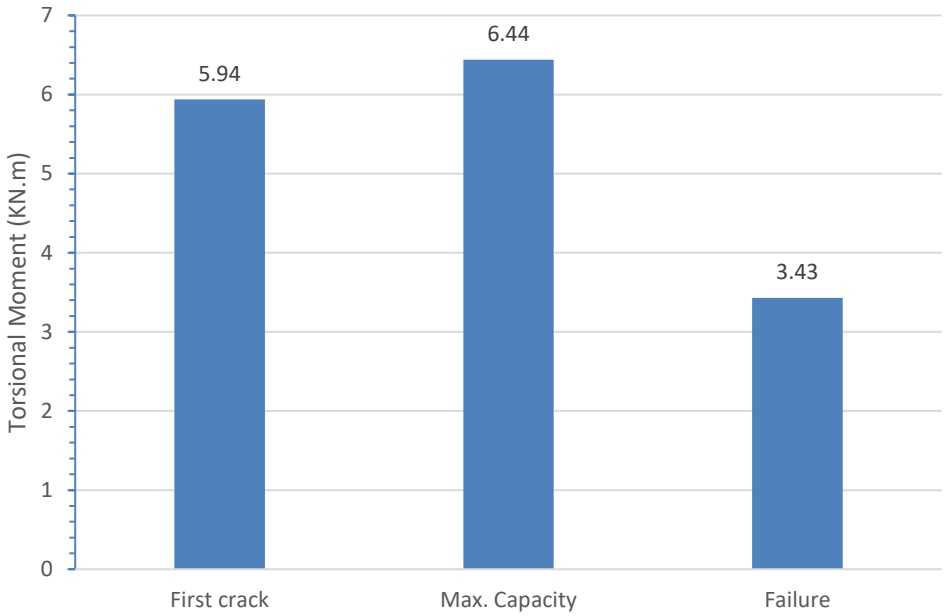

Figure (4-15a): Torsional Moment at Three Phases for B2.

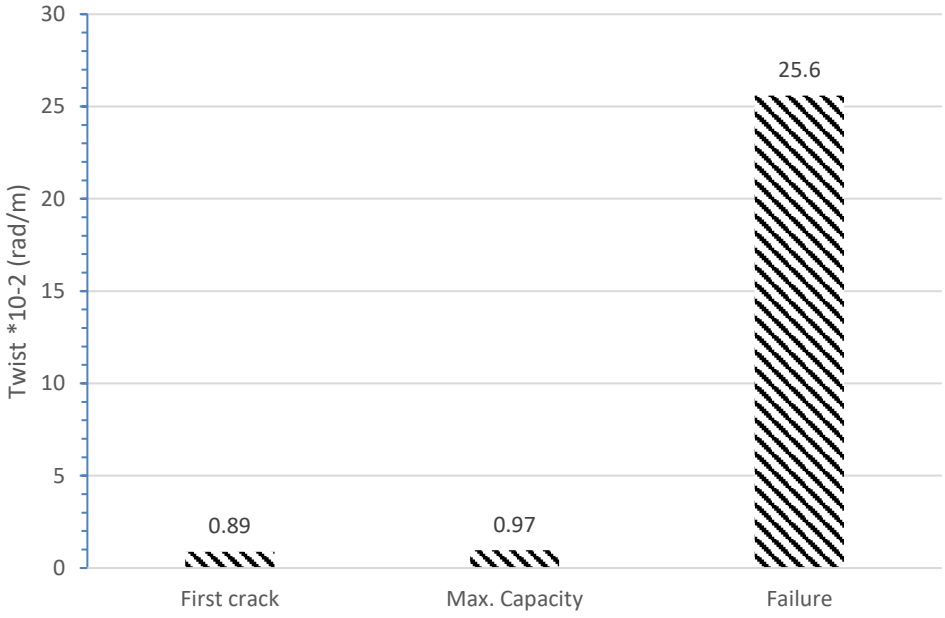

Figure (4-15b): Twist at Three Phases for B2.

- **Strain of GFRP Bars**

The relation between the strain of GFRP Bars and the applied torsional moment is shown in Figure (4-16). The strain gauge was located at the mid span of the beam with the bottom reinforcement. Strain of GFRP Bars of beam didn't reach to yielding point.

The strain gauge was fixed on the center of the middle bar. From this result it is observed that B2 didn't reach the yield value stress for bars. By comparing the strain distribution of the beam, it can be noticed that B2 failure torsional moment occurred without GFRP carried a large amount of stress. Strain of maximum capacity increased 13.16 times from the strain at first cracking with decreasing in torsional moment 45% from torsional moment at first crack. The first crack strain was $0.24*10^{-3}$ m and $3.4*10^{-3}$ m at maximum capacity. The bar strain at maximum capacity stage was $0.26*10^{-3}$ m it noticed that the strain at maximum capacity was closer to the strain at first crack because of the convergence values for first and maximum capacities as shown in Figure (4-17).

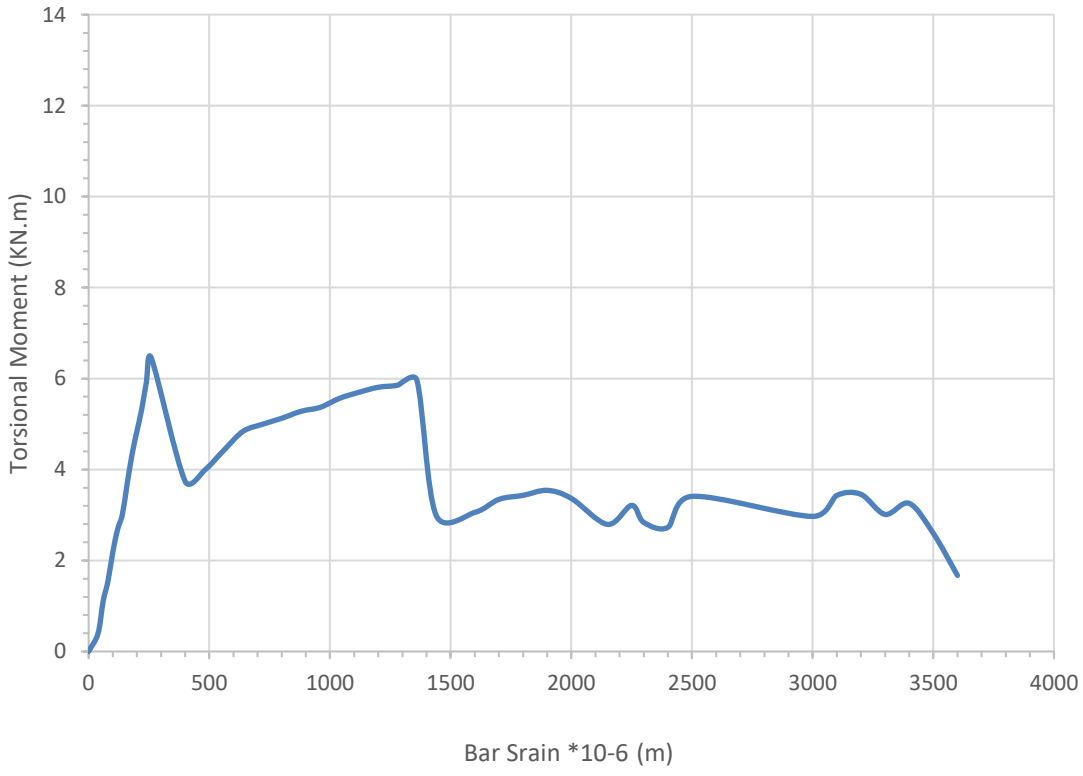

Figure (4-16): Torsional Moment-Strain Curve for GFRP Bars for Specimen B2.

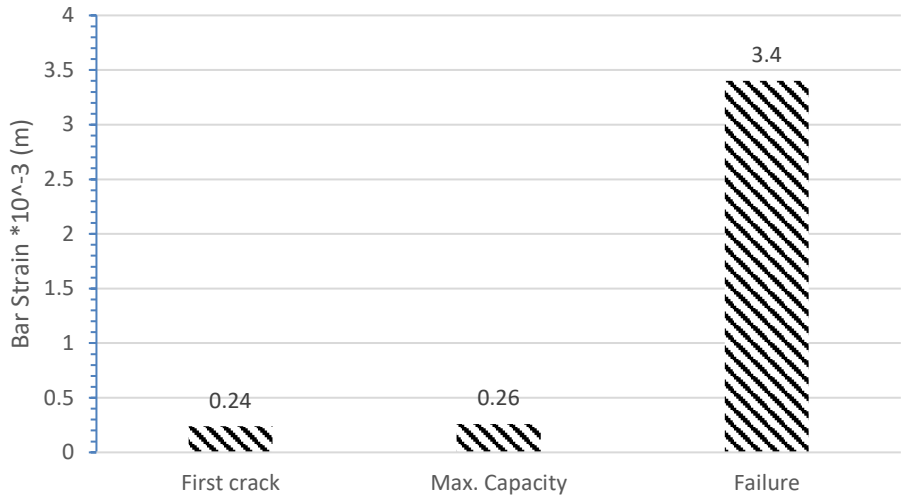

Figure (4-17): Bar Strain at Three Phases for B2.

- **Strain of Concrete**

Figure (4-18) shows torsional moment-strain relationship for the concrete. Concrete strain gauge 60 mm was mounted on the concrete front at 135˚ in the middle distance between the middle span and the left torsional arm. By comparing the strain distribution of the beam, it can be noticed that B1 failure torsional moment occurred with concrete carry a large amount of stress as shown in Figure. Figure (4-19) shows the difference between the concrete strain in three phases. the maximum concrete strain was 9.085*10-3 m with torsional moment 3.256 KN.m and the maximum torsional moment was 6.44 KN.m with concrete strain $1.271*10^{-3}$m and the first crack was concrete strain 2.57*10-4 m with torsional moment 5.94KN.m, the concrete strain at first crack was 2.83% from the maximum concrete strain by increasing in capacity to reach 182% from the capacity at failure and the concrete strain at maximum capacity was 14% from the maximum strain by increasing in capacity to reach 198% from the capacity at failure. The concrete strain increased by 11.17% from the maximum concrete strain with increasing torsional moment 16% from the torsional moment at the failure.

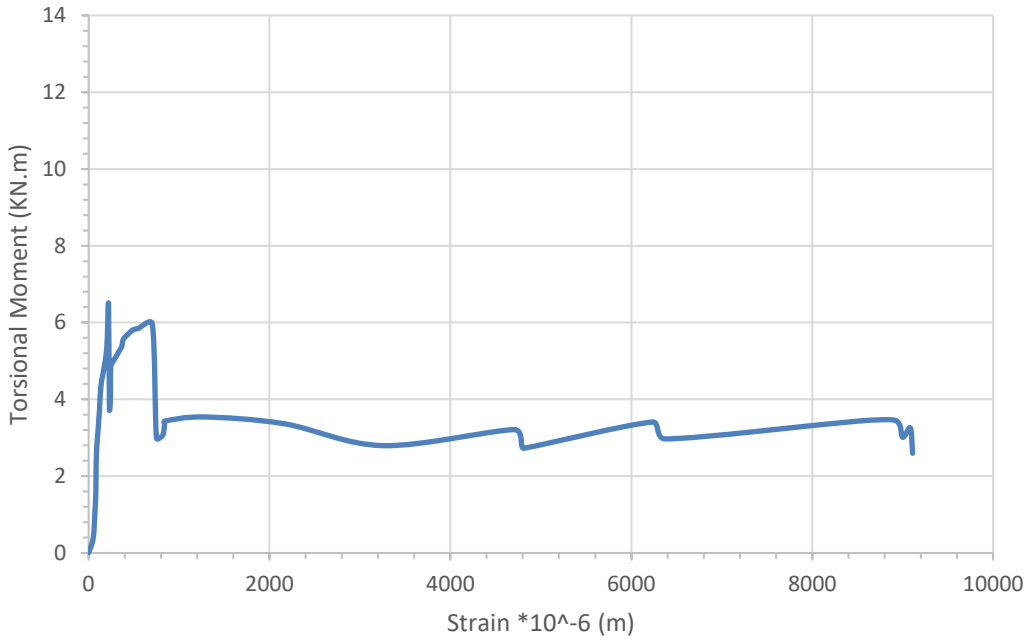

Figure (4- 18): Torsional Moment-Strain Curve for the Concrete at Quarter of Span Zone for Specimen B2

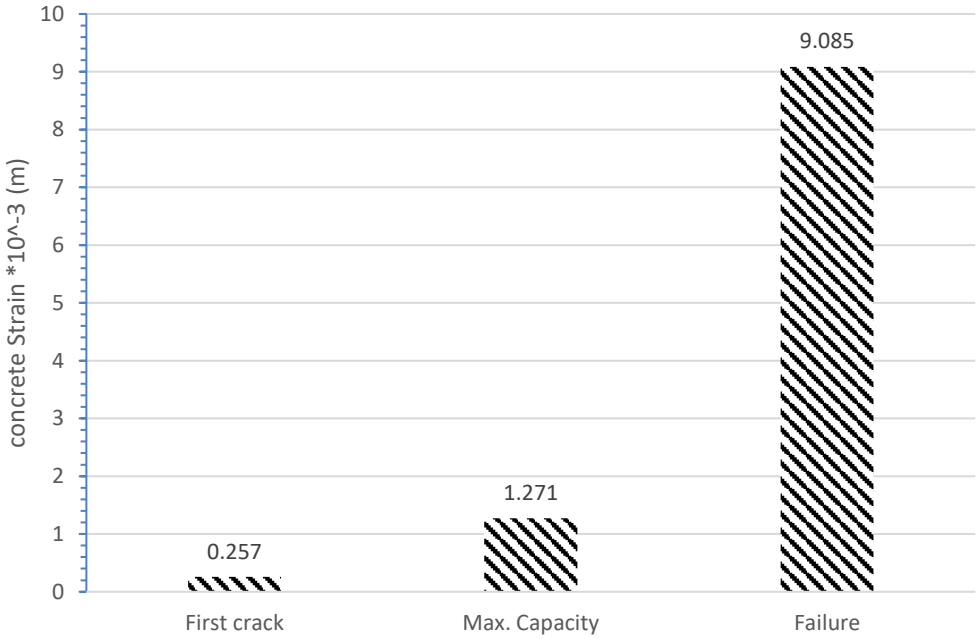

Figure (4-19): Concrete Strain at Three Phases for B2.

- **Strain of Stirrups**

The relation between the stirrups strain and torsional moment as shown in Figure (4-20) for the left stirrup strain. The strain gauge located at two

separated stirrups in the middle beam span with length of stirrups. Stirrup strain gauge was fixed on stirrup at the middle of span with two stirrups. Figure (4-21) shows the difference between the left stirrup strain in three phases. For left stirrup, the maximum strain was $6.75*10^{-3}$ m with torsional moment 3.24 KN.m at the failure and the maximum torsional moment was 6.44 KN.m with strain $0.3*10^{-3}$ m and the first crack was strain $0.25*10^{-3}$ m with torsional moment 5.94 KN.m, the strain at first crack was 3.7% from the maximum strain by decreasing in capacity 83% from the capacity at failure and the strain at maximum capacity was 4.4% from the maximum strain by decreasing in capacity to the half from the capacity at failure, the GFRP stirrups and bars have lost the resistance after maximum capacity and produced strains with little resistance because of the non- homogeneousty made corner cracks for stirrups, the matrix material for stirrup corner cracks quickly and the stirrup fiber is bended and not homogeneous like steel bars make the GFRP stirrup corner is weakest point as shown in Figure (4-12-a).

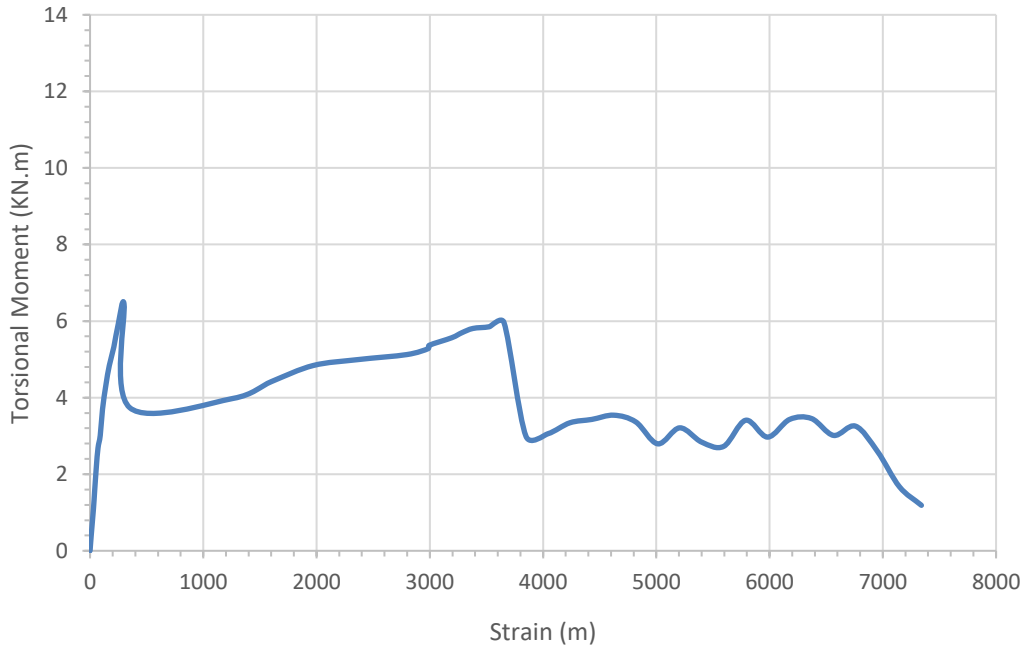

Figure (4-20): Torsional Moment-Strain Curve for the Left Stirrup at the Middle Span for Specimen B1.

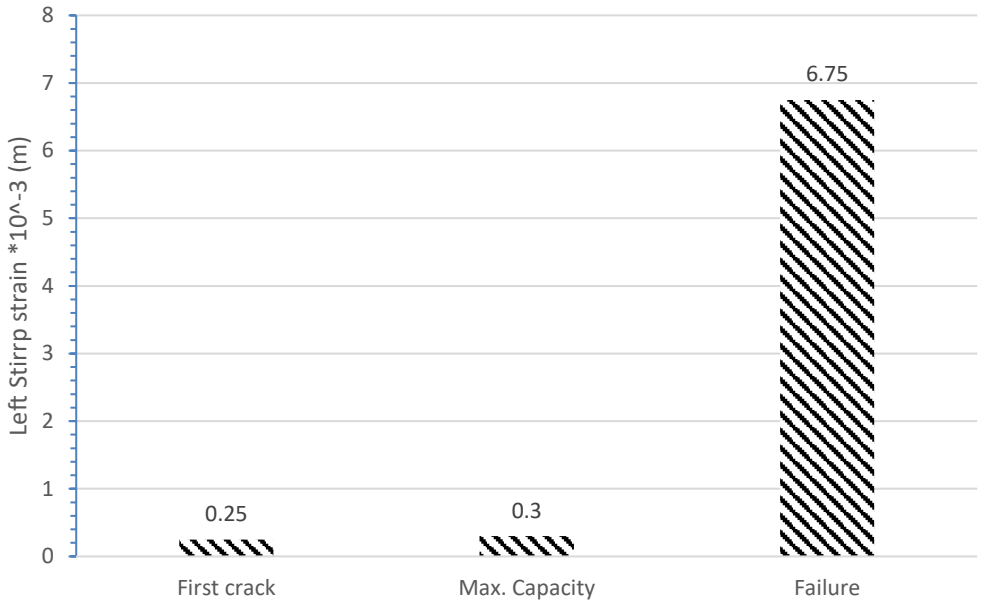

Figure (4- 21): Left Stirrup strain at three phases for B2.

4.2.3 Results of Tested Beam (B3)

- **Specimen Description**

This beam reinforced by GFRP in longitude and transverse directions with stirrups spacing 100 mm and 2 φ 10 as a compression reinforcement and 2 φ 12 as a tensile reinforcement with section 150*300 mm and concrete cover 20 mm.

- **Crack Pattern**

Figure (4-22-a) and (4-22-b) shows the cracking pattern for tested beam (B3). In the Figure, each crack is marked by a line representing the direction of cracking. The crack patterns at both faces of all beams were recorded at several load stages up to failure. The cracks started in the middle of beam span. The first crack started as flexural crack at the torsional moment 3.74 KN.m and continued over all beam except around 30% of beam span in the right beam span with trending the slop with angle 45^{o} and extended as torsional cracks and the cracks wided until the failure. The specimen remained with no visible cracks until torsional cracks took place. As loading increased, the same crack extended continuously and became wider. The

maximum torsional moment was 7.876 KN.m and after that the cracks weakened the beam which caused a decrease in capacity of beam and its stiffness. The capacity of beam decreased until the failure with torsional moment 5.37 KN.m. As clearly, the failure was torsional failure that clearly in the cracks of four faces inclined and continuous cracks and the main crack sloped with angle from 40 to 45 degrees. That noticed that the first crack was at torsional moment 3.74 KN.m and continued to reach the max capacity then it went down. The obversion, after the first crack the increase in capacity was observed, it was 210% from the torsional moment at the first crack. The decrease in stirrups spacing improved the pattern cracks distribution, it made the torsional cracks covered and spreaded well.

Figure (4-22-a): Cracks Pattern for Specimen B3.

Figure (4-22-b): Cracks Pattern of Bottom Side for Specimen B3.

- **Twist of the Beam Section**

Three points of deflection for each specimen were measured, the first one at far 5 cm from the first torsional arm in one side of section 3 cm away, second point for measuring deflection in the same section in second side of section with the same dimensions and the third point in the second torsional arm with 5 cm from the torsional arm and 3 cm from the section side. The three-measures deflection would provide us with the same result but the reason for using 3 deflection measure to sure the result and to avoid any defect with them. The maximum twist was $19.84*10^{-2}$ rad/m with torsional moment 5.37 KN.m. It was observed that the first crack at 3.74 KN.m with $0.54*10^{-2}$ rad/m with voice and the maximum capacity was 7.874 KN.m with twist $1.7*10^{-2}$ rad/m. At the final of experiment, the right torsional beam section changed from 0 rad/m to $15.4*10^{-2}$ rad/m and the left torsional beam section from 0 rad/m to $19.84*10^{-2}$ rad/m. The twist for right beam section increased with decreasing in torsional moment as shown in Figure (4-23).

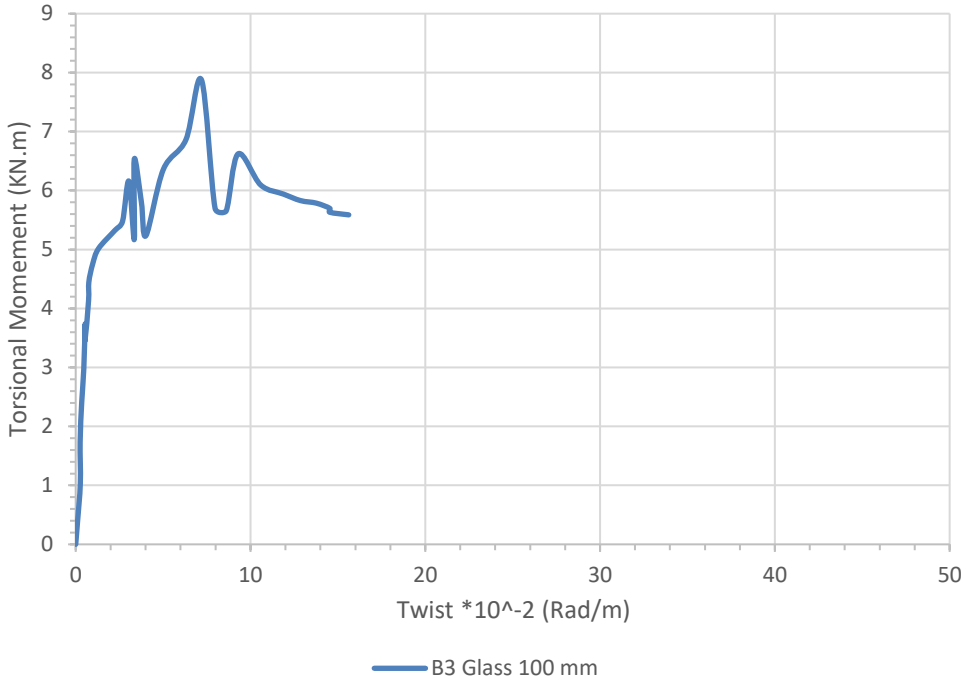

Figure (4-23): Torsional Moment-Twist Curve for Specimen B3.

Figure (4-24-a) and (4-24-b) show the difference between the twist and torsional moment in three phases. The twist at first crack was 2.7% from the maximum twist in capacity 66.9% from the capacity at failure and the twist at maximum capacity was 8.6% from the maximum twist by capacity 140.9% from the capacity at failure. On the other side, it can be considered the beam failed at torsional moment 5.6 KN.m with twist 14.5 rad/m because after that point the beam capacity and reaction were constant.

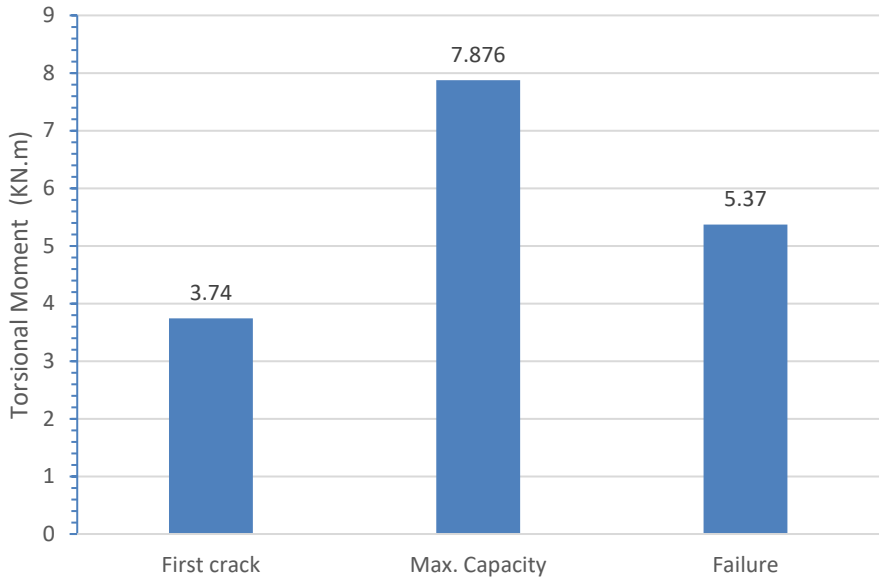

Figure (4-24-a): Torsional Moment at Three Phases for B3.

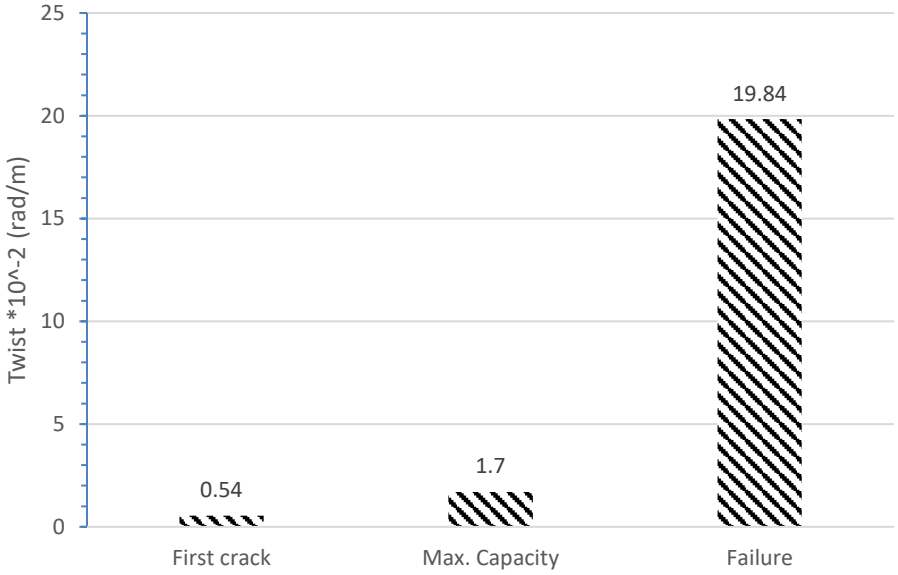

Figure (4-24-b): Twist at Three Phases for B3.

- **Strain of GFRP Bars**

The relation between the strain of GFRP Bars and the applied torsional moment is shown in Figure (4-25). The strain gauge was located at the mid span of the beam with the bottom reinforcement. Strain of GFRP Bars of beam didn't reach to yielding point.

The strain gauge was fixed on the center of the middle bar. From this result it is observed that B2 didn't reach the yield value stress for bars. By

comparing the strain distribution of the beam, it can be noticed that B3 failure torsional moment occurred without GFRP carried a large amount of stress. Strain of maximum capacity increased 8.6 times from the strain at first cracking with decreasing in torsional moment 48.6% from torsional moment at first crack. The first crack strain was $0.376*10^{-3}$ m and $3.6*10^{-3}$ m at maximum capacity. The bar strain at maximum capacity stage was $0.1.78*10^{-3}$ m it noticed that the bar strain was significantly bigger than strain at first stage because of impacting of decreasing stirrups spacing made the beam was able to carry torsional resistance after first crack and grew more than torsional resistance at first crack as shown in Figure (4-26), the bar strain at Three Phases.

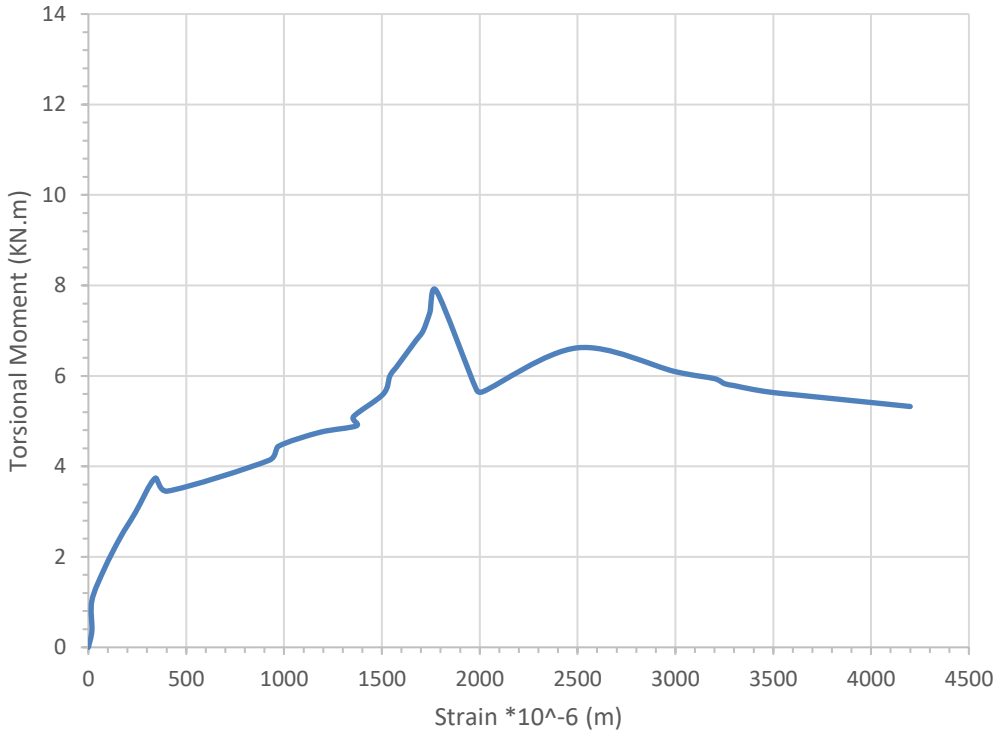

Figure (4-25): Torsional Moment-Strain Curve for GFRP Bars for Specimen B3.

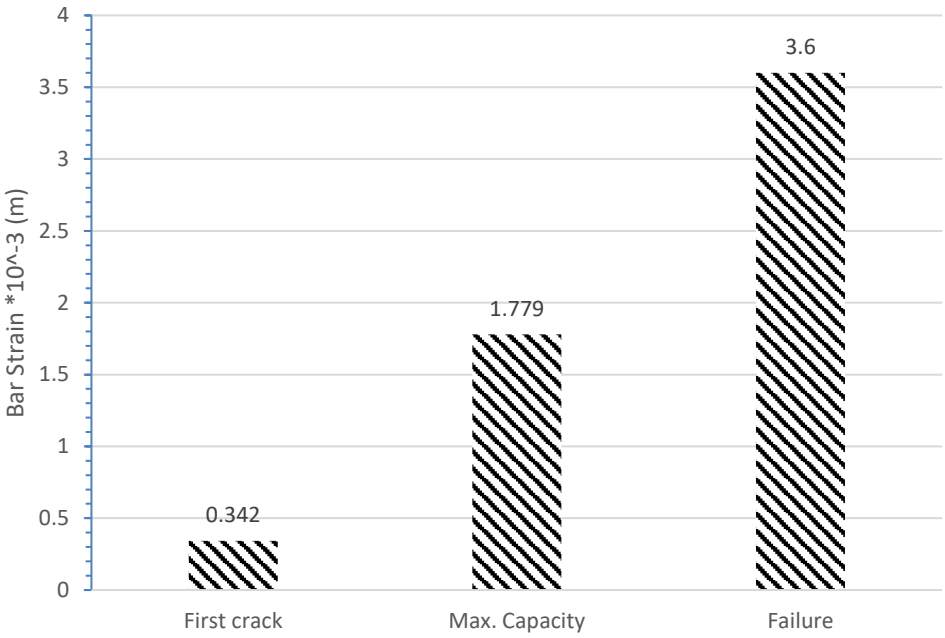

Figure (4-26): Bar Strain at Three Phases for B3.

- **Strain of Concrete**

Figure (4-27) shows torsional moment-strain relationship for the concrete. Concrete strain gauge 60 mm was mounted on the concrete front at 135˚ in the middle distance between the middle span and the left torsional arm. By comparing the strain distribution of the beam, it can be noticed that B3 failure torsional moment occurred with concrete carry a large amount of stress. Figure (4-28) shows the difference between the concrete strain in three phases. the maximum concrete strain was $6.326*10^{-3}$ m with torsional moment 5.588 KN.m and the maximum torsional moment was 7.874 KN.m with concrete strain $5.651*10^{-3}$m and the first crack was concrete strain $0.198*10^{-3}$ m with torsional moment 3.74 KN.m, the concrete strain at first crack was 3.1% from the maximum concrete strain with capacity 66.9% from the capacity at failure and the concrete strain at maximum capacity was 89.3% from the maximum strain with capacity 140.9% from the capacity at failure. The concrete strain increased by 86.2% from the maximum concrete strain with increasing torsional moment 74% from the torsional moment at the failure.

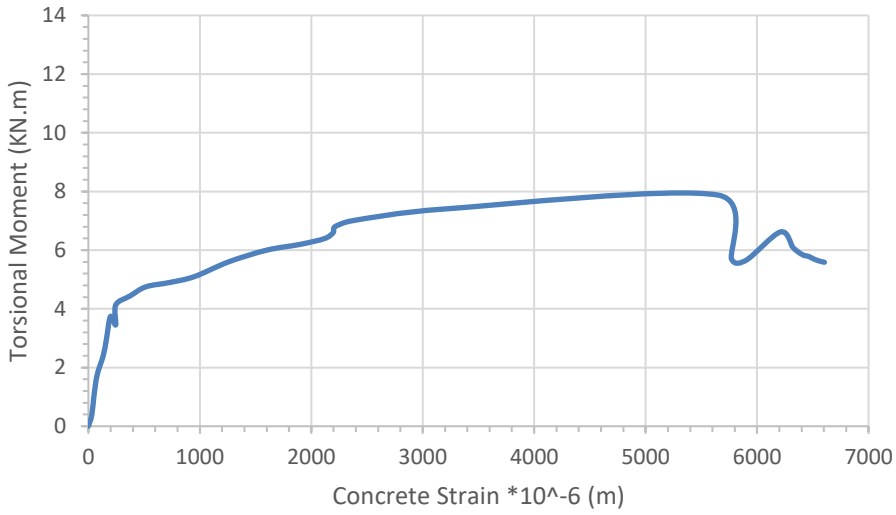

Figure (4-27): Torsional Moment-Strain Relationship for the Concrete in the Concrete Front at 135˚ in the Middle Distance Between the Middle Span and the Left Torsional Arm for B3.

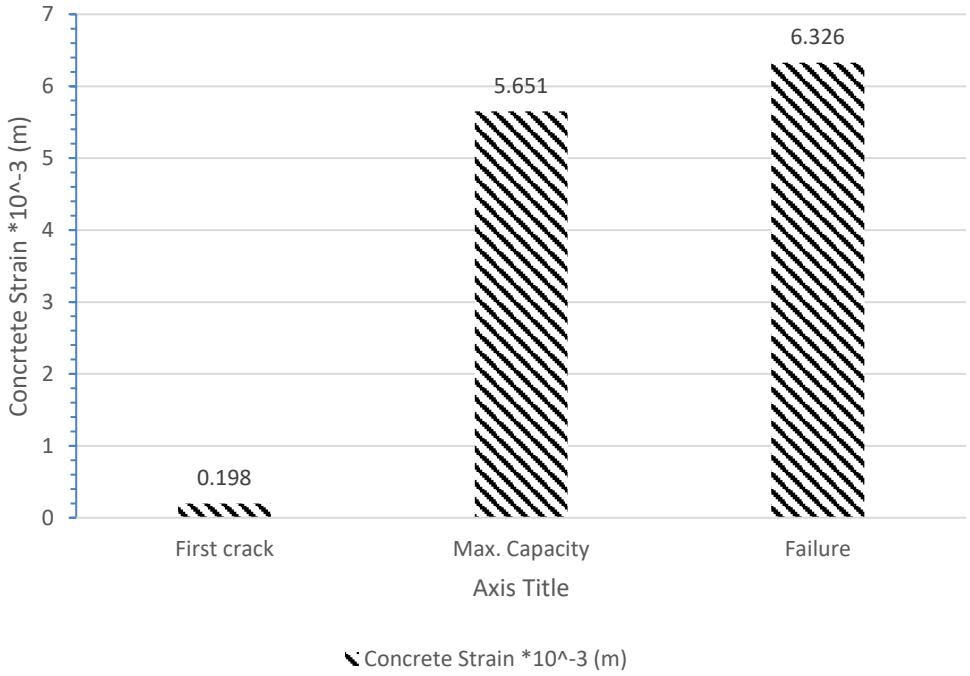

Figure (4-28): Concrete Strain at Three Phases B3

- **Strain of Stirrups**

The relation between the stirrups strain and torsional moment can't show in relation because the damage in strain gauge during the experiment.

4.2.4 Results of Tested Beam (B4)

- **Specimen Description**

This beam was reinforced by GFRP in longitude and transverse directions with stirrups spacing 150 mm and 2 φ 10 as a compression GFRP reinforcement and 2 φ 12 as a tensile GFRP reinforcement with section 150*300 mm and concrete cover 20 mm. This beam is like B2 by adding 1 φ 8 for both sides.

- **Crack Pattern**

Figure (4-29) shows the cracking pattern for tested beam (B4). In the Figure, each crack is marked by a line representing the direction of cracking. The crack patterns at all faces of all beams were recorded at several load stages up to failure. The cracks started in the middle of beam span with inclined by angle 50^{o} and continued to wide in the same location until the failure. The specimen remained with no visible cracks until torsional cracks took place. The first crack took place in the middle of beam span with torsional moment 6.93 KN.m and continued to produce cracks around the first crack zone, around 50% of beam span in the middle beam span. The cracks were clearly torsional cracking (continuous diagonal cracks at the sides, top and bottom of beam). As loading increased, cracks became wider and more numbers. As clearly, the failure was torsional failure. The cracks weakened the beam which caused a decrease in capacity of beam and its stiffness. After the first crack, the load of beam went down and grew again but it didn't reach more than the first load crack. The torsional moment which caused the first crack was at the same time the maximum capacity for beam. That noticed that the maximum torsional moment after first crack was 6.47 KN.m with cracks and sound and the load went down again. As loading increased, the same crack extended continuously and became wider and some cracks appeared, but with capacity less than the first torsional moment crack because the beam lost some of it's loading after the crack to reach the maximum torsional

moment as the same torsional cracking and after that the capacity of beam decreased until the failure with torsional moment 4.2 KN.m. As clearly, the failure was torsional failure that cleared in the inclined cracks in the middle and in other places and the main crack sloped with angle from 40 to 50 degrees. That noticed, after cracks the load was going down and growing again. The adding side bars has improved the torsional capacity and cracks pattern distribution. The beam carried maximum capacity one time after that the torsional resistance didn’t grow back and decreased up to failure.

Figure (4-29): Cracks Pattern for Specimen B4.

- **Twist of the Beam Section**

Three points (LVDT) of deflection for each specimen were measured, the first one at far 5 cm from the first torsional arm in one side of section 3 cm away, second point for measuring deflection in the same section in second side of section with the same dimensions and the third point in the second torsional arm with 5 cm from the torsional arm and 3 cm from the section side. The three-measure deflection would provide us with the same result but the reason for using 3 deflection measure to sure the result and to avoid any defect with them. The maximum twist was $13.5*10^{-2}$ rad/m with torsional moment 4.2 KN.m in the failure phase. It was observed that the first crack was the maximum capacity at the same time 6.93 KN.m with $2.18*10^{-2}$ rad/m with voice. At the final of experiment, the right torsional beam section changed from 0 rad/m to $13.5*10^{-2}$ rad/m and the left torsional beam section from 0 rad/m to $5.7*10^{-2}$ rad/m. The twist for right increased with decreasing in torsional moment as shown in Figure (4-30).

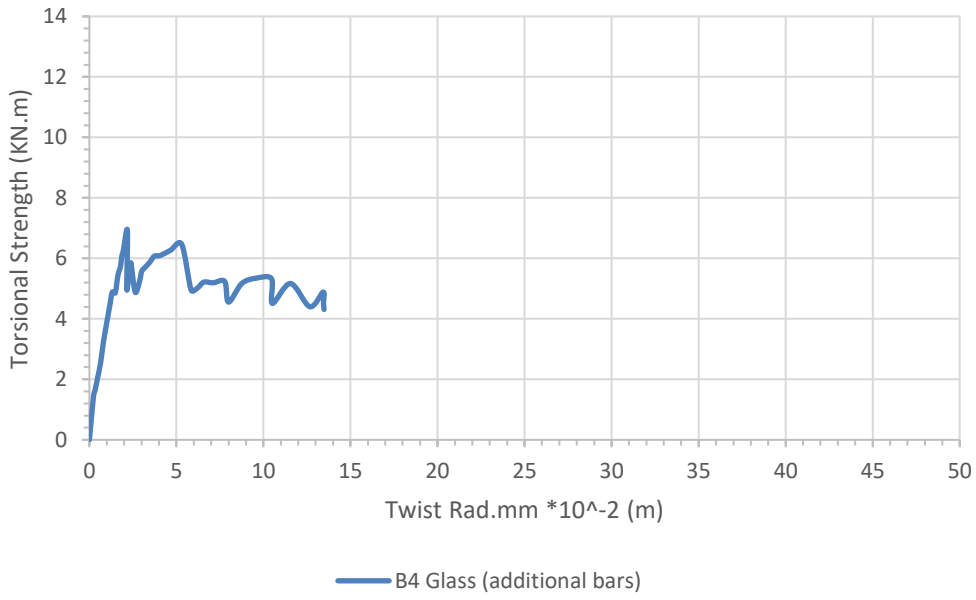

Figure (4-30): Torsional Moment-Twist Curve for Specimen B4.

Figure (4-31-a) and (4-31-b) show the difference between the twist and the torsional moment in two phases. The twist at first crack (the twist at

maximum capacity at the same time) was 16.14% from the maximum twist in load 165% from the capacity at failure. At the failure, the twist increased by 83.86% from the maximum twist with decreasing torsional moment 39.4% from the torsional moment at maximum capacity.

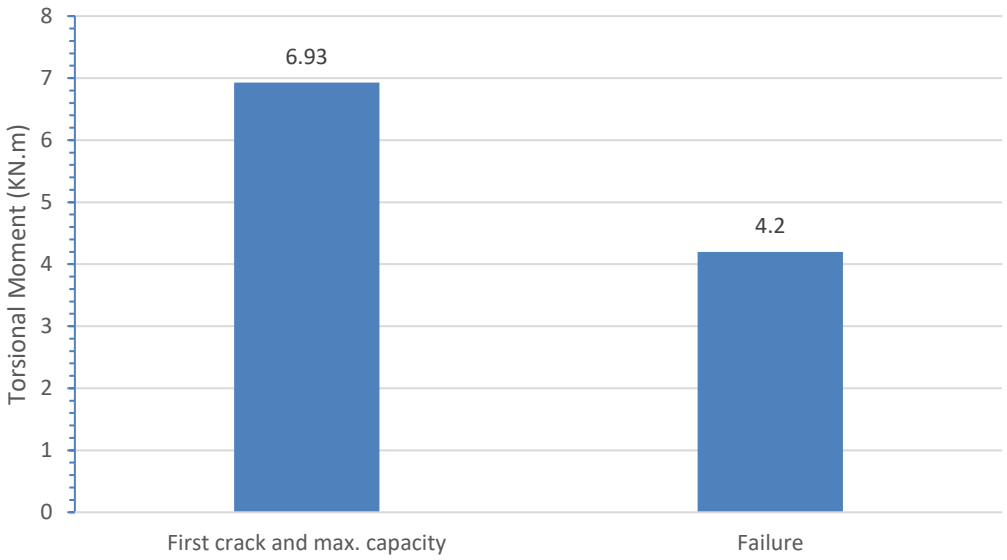

Figure (4-31-a) Twist and Torsional Moment at Two Phases for B4.

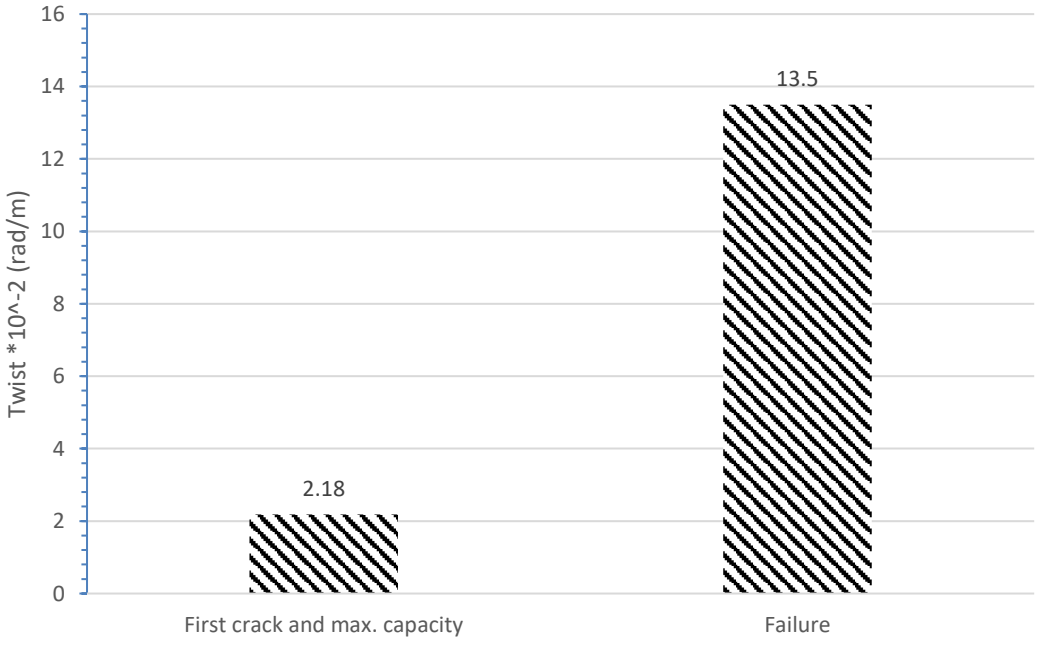

Figure (4-31-b) Twist and Torsional Moment at Two Phases for B4.

- **Strain of GFRP Bars**

The strain gauge was fixed on the center of the middle span bar to provide us with information like torsional moment - strain relationship for the GFRP bars reinforcement and for stirrup strain gauge fixed in two stirrups in middle span. Figure (4-32) show the relation between torsional moment-strain curve for GFRP bars for specimen B4. The bar strain at failure eas $3.349 *10^{-3}$ with torsional moment 4.2 KN.m but the bar strain for first crack and maximum capacity was $1.203*10^{-3}$. The bar strain at failure increased 278.3% from the bar strain at the first crack with decreasing in load as shown in Figure (4-33)

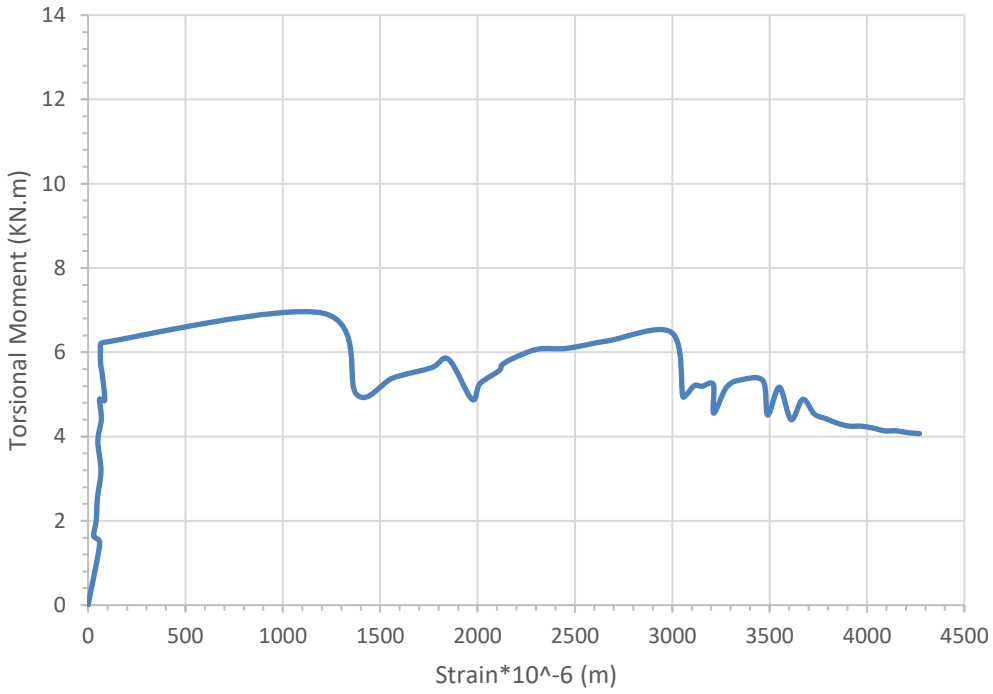

Figure (4-32): Torsional Moment-Strain Curve for GFRP Bars for Specimen B4.

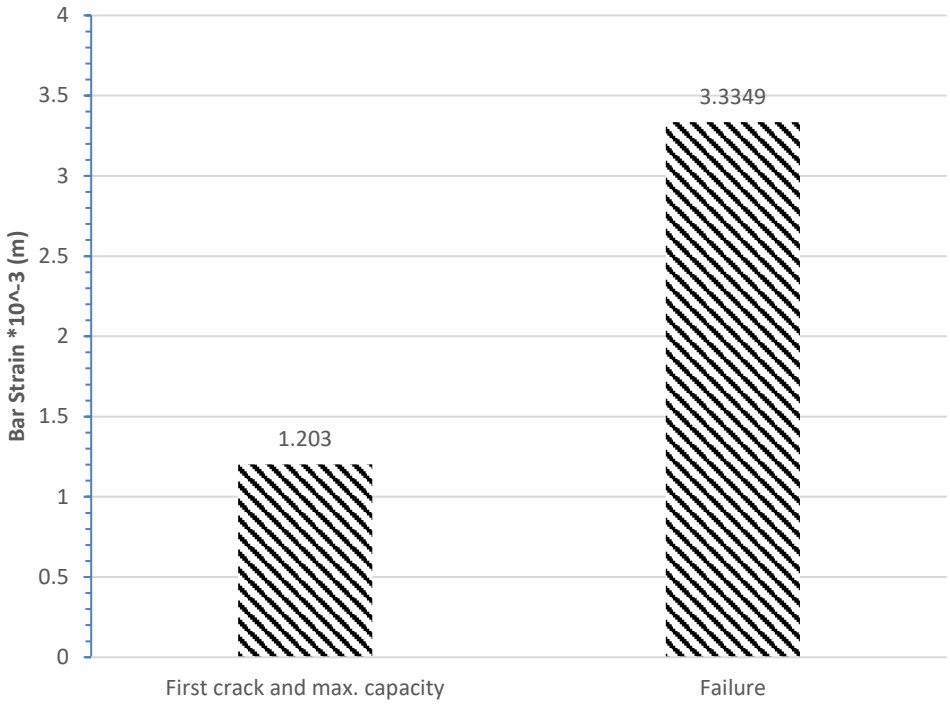

Figure (4-33): Bar Strain and Torsional Moment at Two Phases for B4.

- **Strain of Concrete**

Figure (4-34) shows torsional moment-strain relationship for the concrete. Concrete strain gauge 60 mm was mounted on the concrete front at 135˚ in the middle distance between the middle span and the left torsional arm. By studying the strain distribution of the beam, it can be noticed that B4 failure torsional moment occurred with concrete carry a large amount of stress. Figure (4-35) shows the difference between the concrete strain in three phases, the maximum concrete strain was $3.1*10^{-3}$ m with torsional moment 4.2 KN.m and the maximum torsional moment was 6.93 KN.m with concrete strain $0.28*10^{-3}$m and the first crack was at the same point, the concrete strain at first crack (in the same time it is the maximum torsional resistance) was 9.2% from the maximum concrete strain with capacity 165% from the capacity at failure. At the failure the concrete strain increased by 9.9 times from the concrete strain at maximum torsional resistance with decreasing torsional moment 39% from the maximum torsional moment.

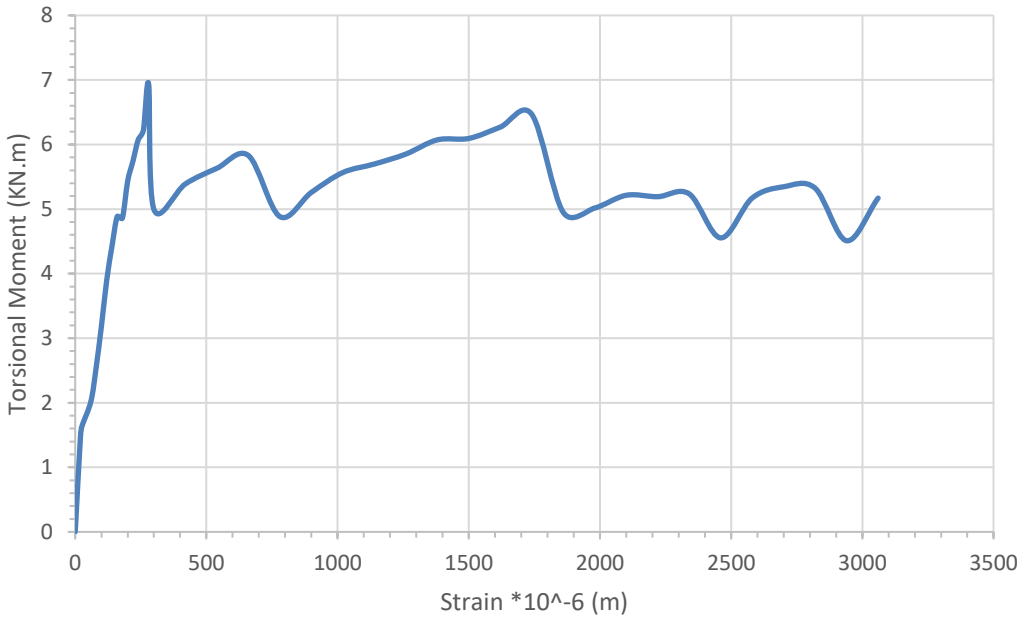

Figure (4-34): Torsional Moment-Strain Curve for the Concrete at Quarter of Span Zone for Specimen B4.

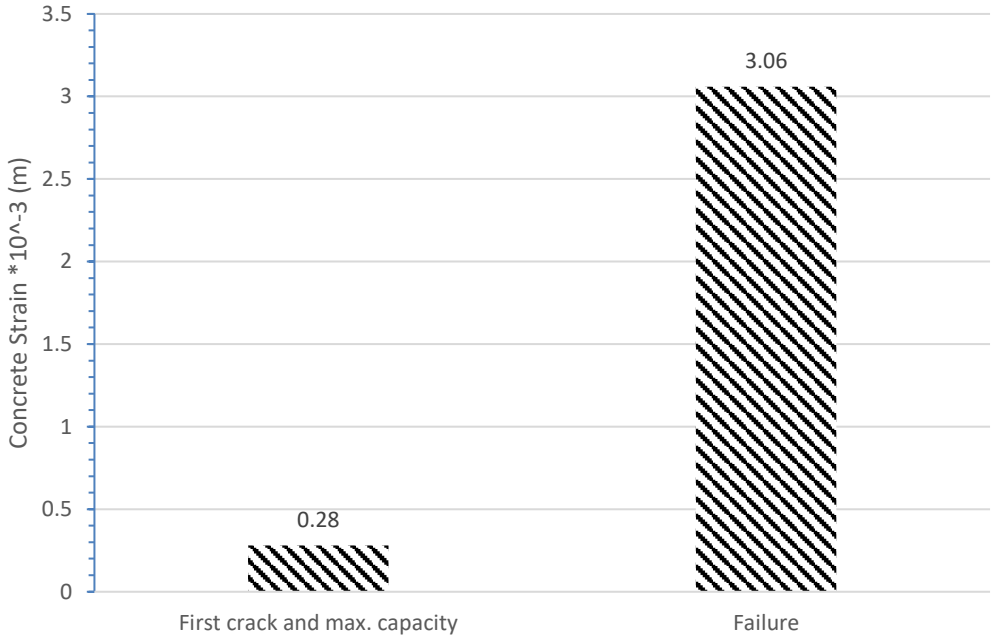

Figure (4-35): Concrete Strain at Two Phases for B4.

- **Strain of Stirrups**

The relation between the stirrups strain and torsional moment as shown in Figure (4-36-a) and (4-36-b). The strain gauge was located at two separated stirrups in the middle beam span with length of stirrups. The capacity of

beam was maximum at 6.93 KN.m with stirrup strain $1.193*10^{-3}$ m for right stirrups and $1.265*10^{-3}$ m for left stirrup. On the other side, the failure torsional capacity was 1.75 KN.m with strains for right and left stirrups 8.75*10-3 m and 7.55*10-3 m, respectively.

The stirrups strain and the torsional moment at the max. capacity (first crack in same time) and the failure, for right stirrup, the strain was 68.5% from the strain at failure with decreasing 65% torsional moment from moment at failure, for left stirrup, the strain was 34.1% from the strain at failure with decreasing 65% torsional moment from moment at failure. That noticed, the two stirrups were maximum strain at 4.2 KN.m after the maximum capacity with $1.75*10^{-3}$ and $3.7*10^{-3}$ for right and left stirrups as shown in Figure (4-37-a) and (4-37-b).

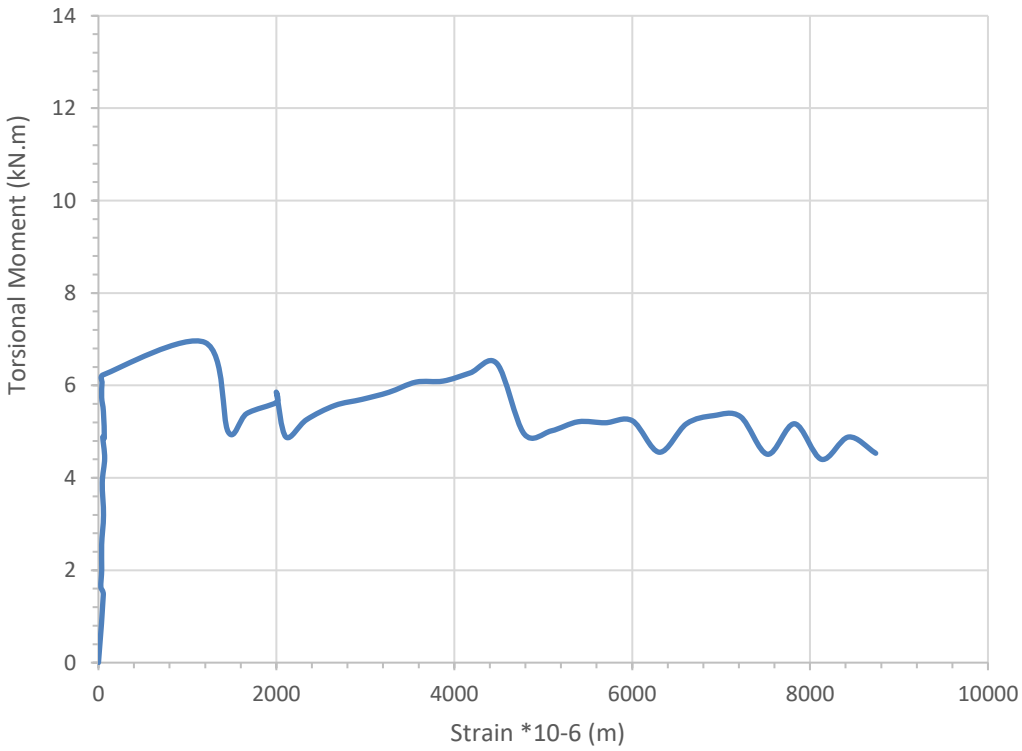

Figure (4-36-a) Torsional Moment-Strain Curve for the Right Stirrup at the Middle Span for Specimen B4.

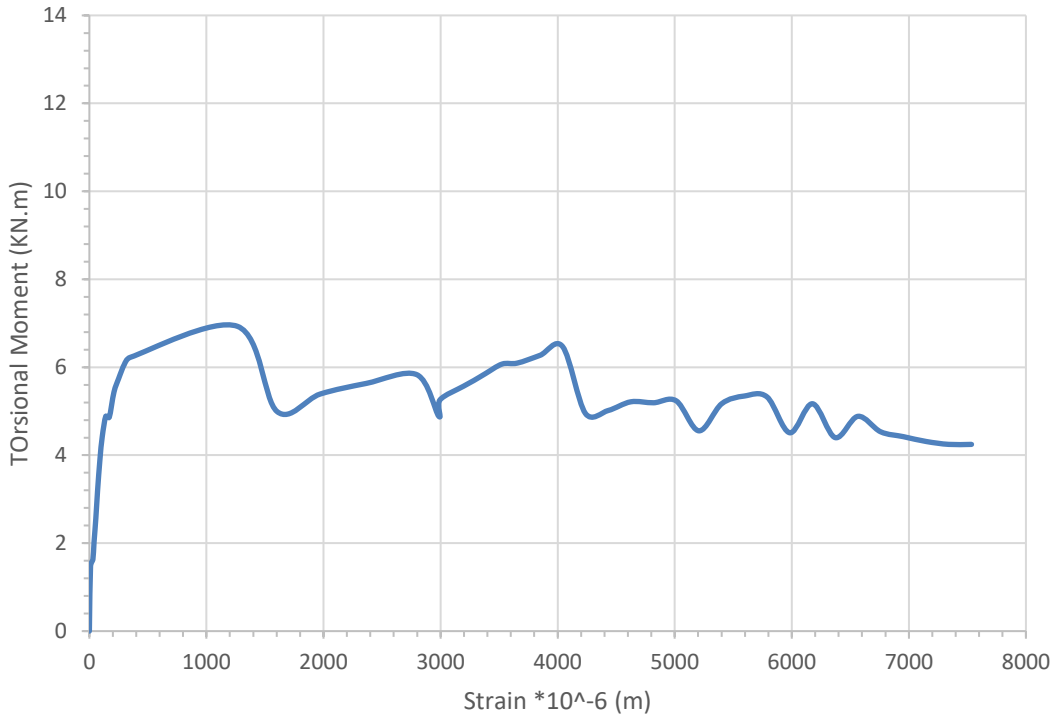

Figure (4-36-b) Torsional Moment-Strain Curve for the Left Stirrup at the Middle Span for Specimen B4.

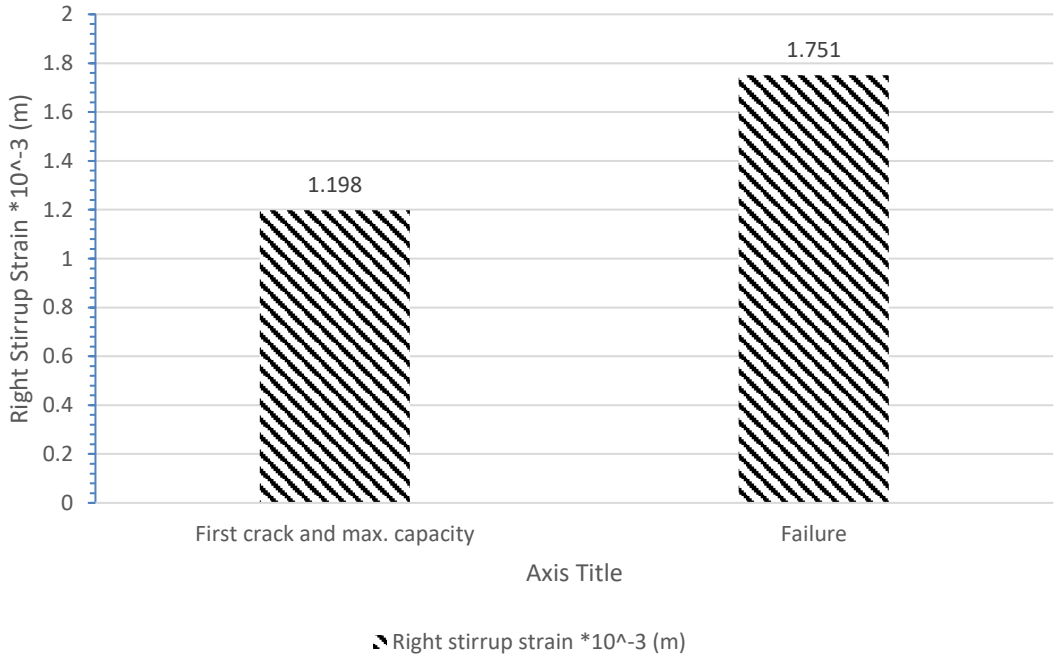

Figure (4-37-a): Right Stirrup Strain and Torsional Moment at Two Phases for B4.

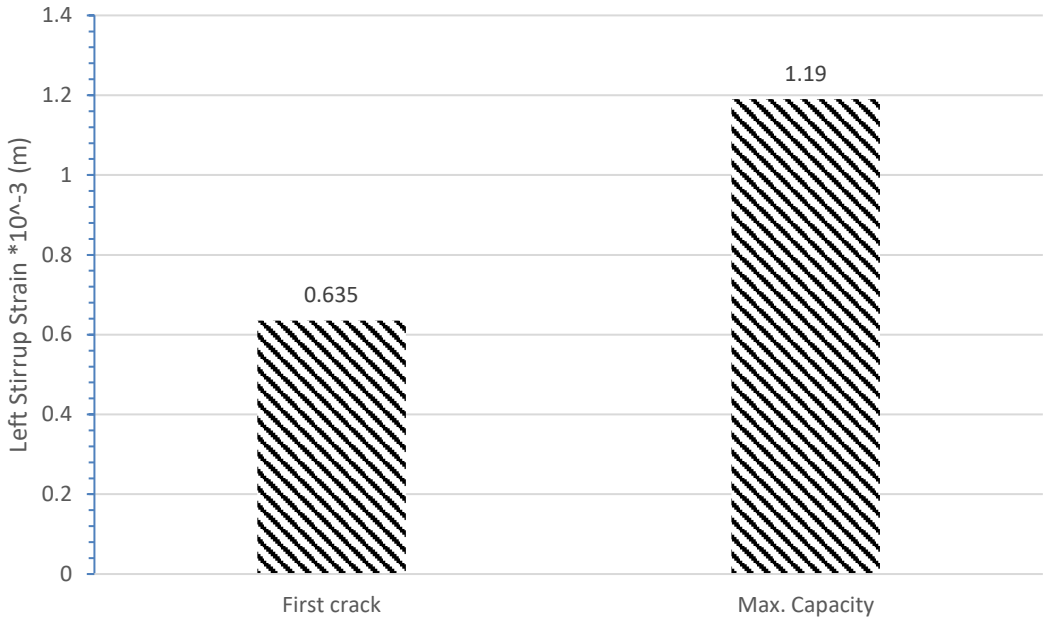

Figure (4-37-b): Left Stirrup Strain and Torsional Moment at Two Phases for B4.

4.2.5 Results of Tested Beam (B5)

- **Specimen Description**

This beam reinforced by GFRP in longitude and transverse directions with stirrups spacing 150 mm and 2 φ 10 as a compression reinforcement and 2 φ 12 as a tensile reinforcement with section 150*300 mm and concrete cover 20 mm. This beam is similar to B2 beam by changing the load type to test the beam under torsional and bending moment. The torsional arm was only one in the middle of span as shown in Figure (4-37a) and (4-37b).

- **Crack Pattern**

Figures (4-38-a), (4-38-b) and (4-38-c) show the cracking pattern for tested beam (B5). In the Figure, each crack is marked by a line representing the direction of cracking. The crack patterns at all faces of beams were recorded at several load stages up to failure. The first crack took place in the back middle of beam span around the torsional arm (in the right side of beam span near the torsional arm) as shear crack at the torsional moment 6.9 KN.m in back side from the torsional arm with angle 135^{o} and extended as torsional

cracks and appeared cracks in the other side with angle 45^{o} and continued to produce cracks around the first crack zone, around 50% of beam span in the middle beam span. The first crack started the specimen remained with no visible cracks until torsional cracks took place. As loading increased, the same crack extended continuously and became wider. The maximum torsional moment was 11.84 KN.m was sound and after that the capacity of beam decreased until the failure with torsional moment 5.4 KN.m. clearly, the failure was torsional failure that clear in the cracks of four faces inclined and continuous cracks and the main crack sloped with angle from 40 to 45 degrees and the rupture of corner stirrup as a result for torsion as shown in Figure (4-38-d). The rupture was in a stirrup near torsional arm in the cracking zone. The cracks were almost around the torsional arm. The cracks weakened the beam which caused a decrease in capacity of beam and its stiffness. After the first crack, the load of beam went down and grew again. That noticed, after cracks the load was going down and growing again. Shear force with torsional stress helped the beam to failed in shear critical section around the torsional arm (concentrated load area), and the loads traded to the weakest point at stirrups corner to form at the end rupture for the stirrups in the corner zone.

Figure (4-38-a): Cracks Pattern for the First Side of Specimen B5.

Figure (4-38-b): Cracks Pattern for the second side of Specimen B5.

Figure (4-38-c): Cracks Pattern for the Bottom of Specimen B5.

Figure (4-38-d) Rupture of Stirrup of Specimen B5.

- **Twist of the beam section**

Three points of deflection for each specimen were measured, the first one at far 5 cm from the first torsional arm in one side of section 3 cm away, second point for measuring deflection in the same section in second side of section with the same dimensions and the third point in the second torsional arm with 5 cm from the torsional arm and 3 cm from the section side. The three-measure deflection would provide us by the same result but the reason for using 3 deflection measure to sure the result and to avoid any defect with them. The maximum twist was $21.7*10^{-2}$ rad/m with torsional moment 5.37 KN.m in the failure phase. It was observed that the first crack was 6.9 KN.m with $4.82*10^{-2}$ rad/m with voice, but the maximum capacity was 11.84 KN.m with twist $1.42*10^{-2}$ The twist increased with decreasing in torsional moment as shown in Figure (4-39).

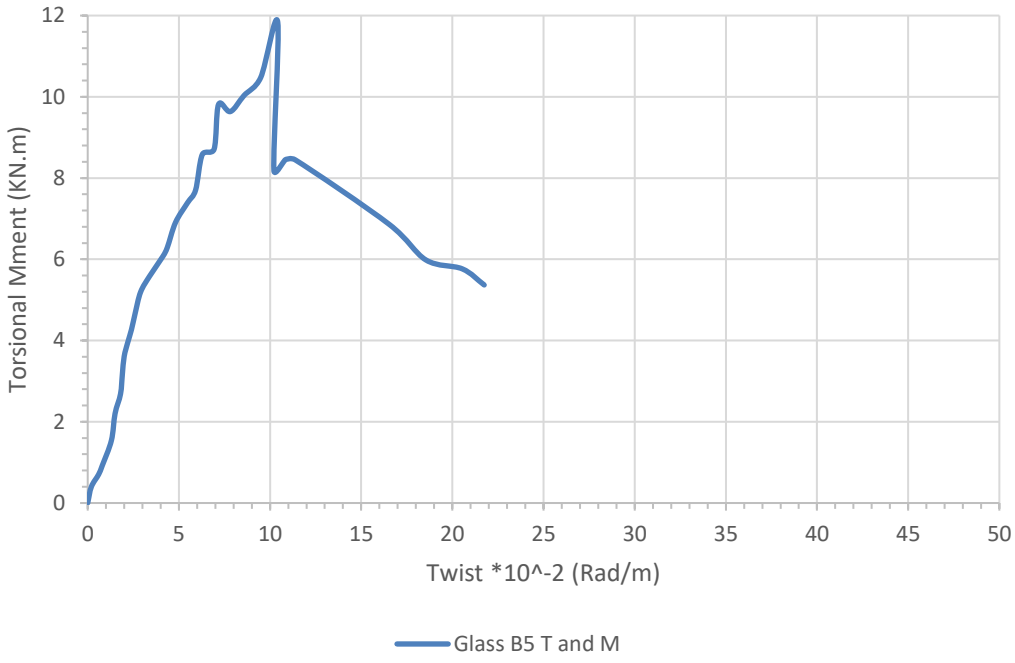

Figure (4-39): Torsional Moment-Twist Curve for Specimen B5.

Figure (4-40-a) and (4-40-b) show the difference between the twist and the torsional moment in three phases. The twist at first crack was 22.2% from the maximum twist in load 128.5% from the capacity at failure. At the

failure, the twist increased by 108.25% from the twist at maximum capacity with decreasing torsional moment 120.3.

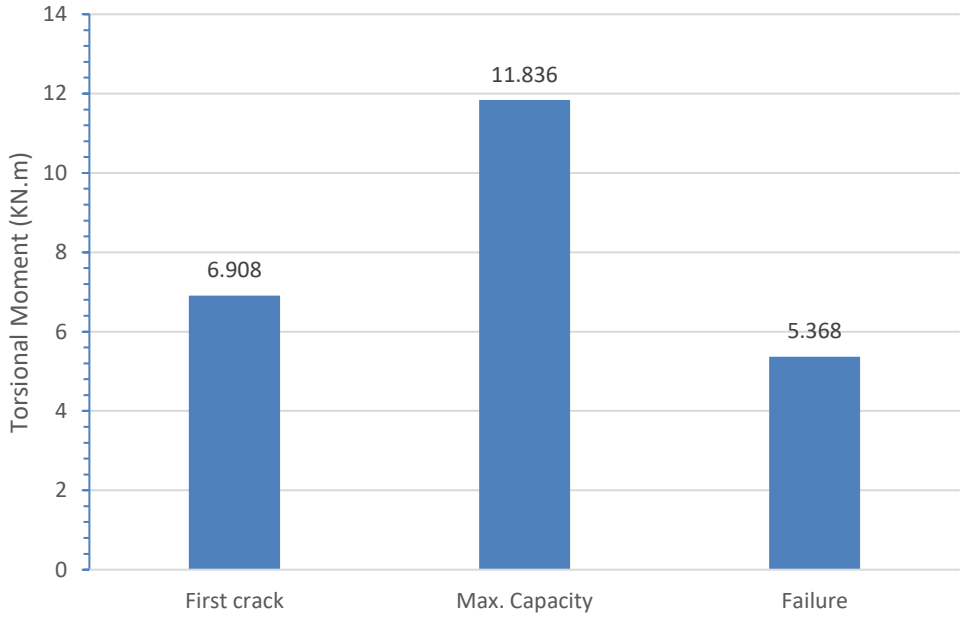

Figure (4-40-a): Torsional Moment at Three Phases for B5.

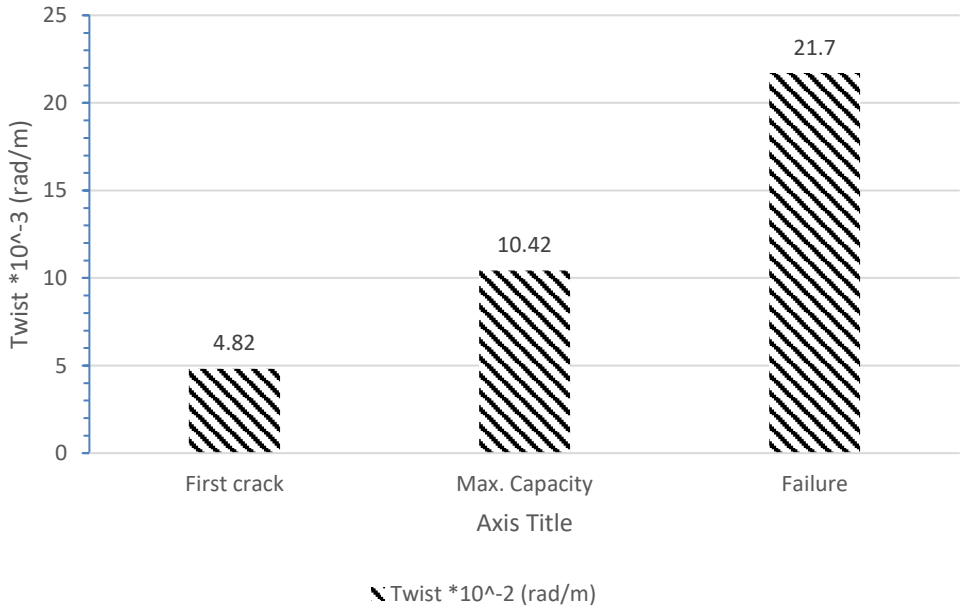

Figure (4-40-b): Twist at Three Phases for B5.

- **Strain of GFRP Bars**

The relation between the bar strain and torsional moment as shown in Figure (4-41). The strain gauge was fixed on the center of the middle span bar to provide us with information like torsional moment - strain relationship for

the GFRP bars reinforcement. The bar strain was $1.97*10^{-3}$ m with first visible crack at 6.9 KN.m torsional capacity than the cracks continued with increasing in torsional resistance to reach to maximum torsional capacity 11.836 KN.m with bar strain $3.077*10^{-3}$ m then the resistance decreased with more bar strain to fail the beam with torsional load 5.37 KN.m as shown in Figure (4-42).

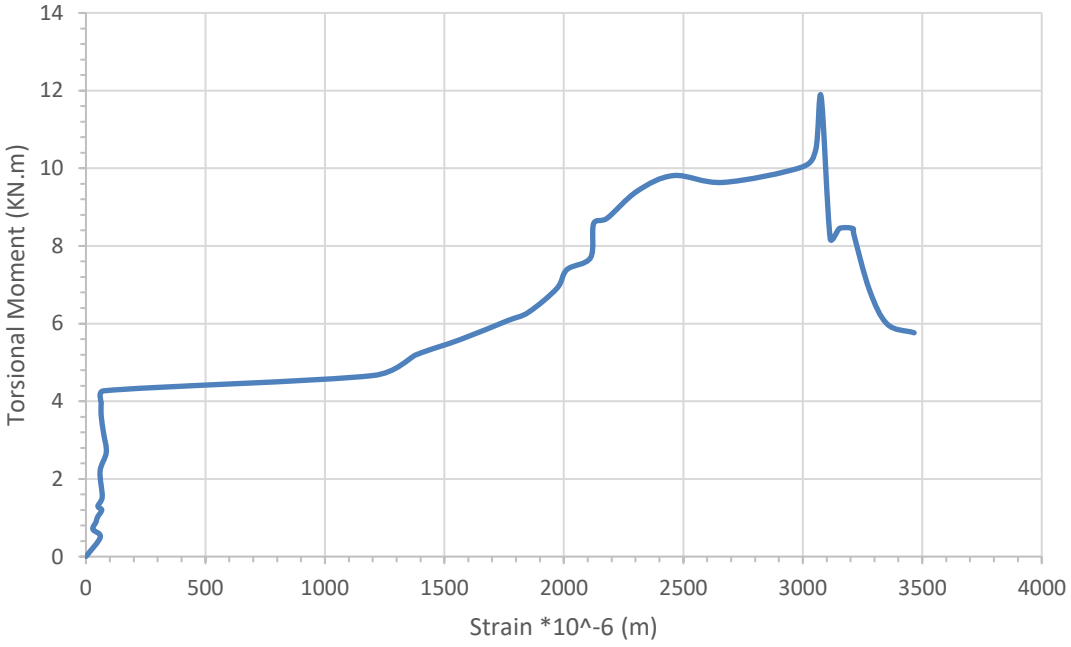

Figure (4-41): Torsional Moment-Strain Curve for GFRP Bars for Specimen B3.

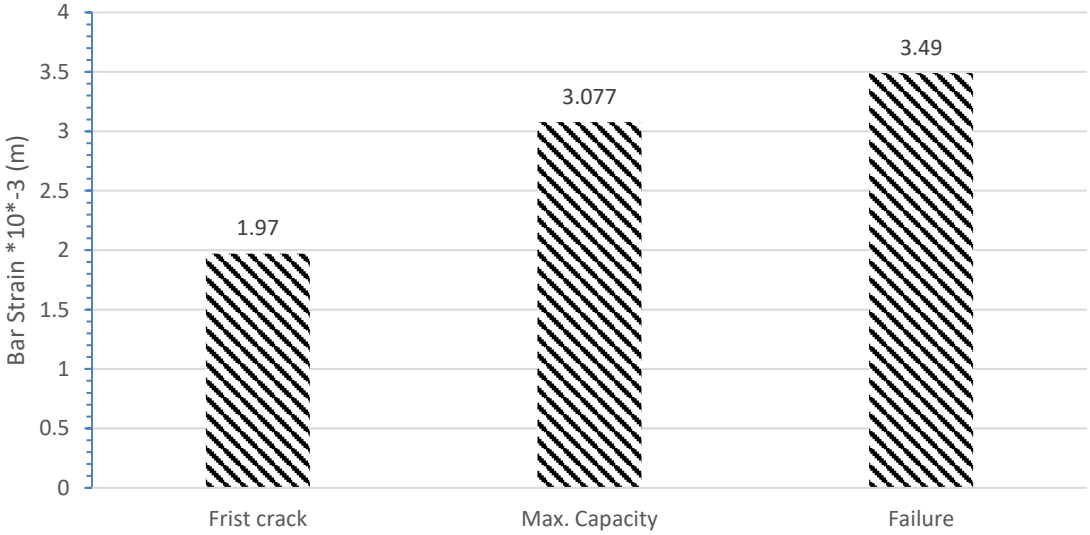

Figure (4-42): Bar Strain at Three Phases for B5.

- **Strain of Concrete**

Figure (4-43) shows torsional moment-strain relationship for the concrete. Concrete strain gauge 60 mm was mounted on the concrete front at 135˚ in the middle distance between the middle span and the left torsional arm. Figure (4-44) shows the difference between the concrete strain and the torsional moment in three phases. the maximum concrete strain was $8.92*10^{-3}$ m with torsional moment 5.37 KN.m and the maximum torsional moment was 11.836 KN.m with concrete strain $0.84*10^{-3}$m and the first crack was $6.93*10^{-3}$ m with concrete strain $0.342*10^{-3}$ m, the concrete strain at first crack was 4.17% from the maximum concrete strain with torsional capacity 129% from the capacity at failure. At the failure the concrete strain increased by 9.6 times from the concrete strain at maximum torsional resistance with decreasing torsional moment 55% from the maximum torsional moment as shown in Figure (4-44).

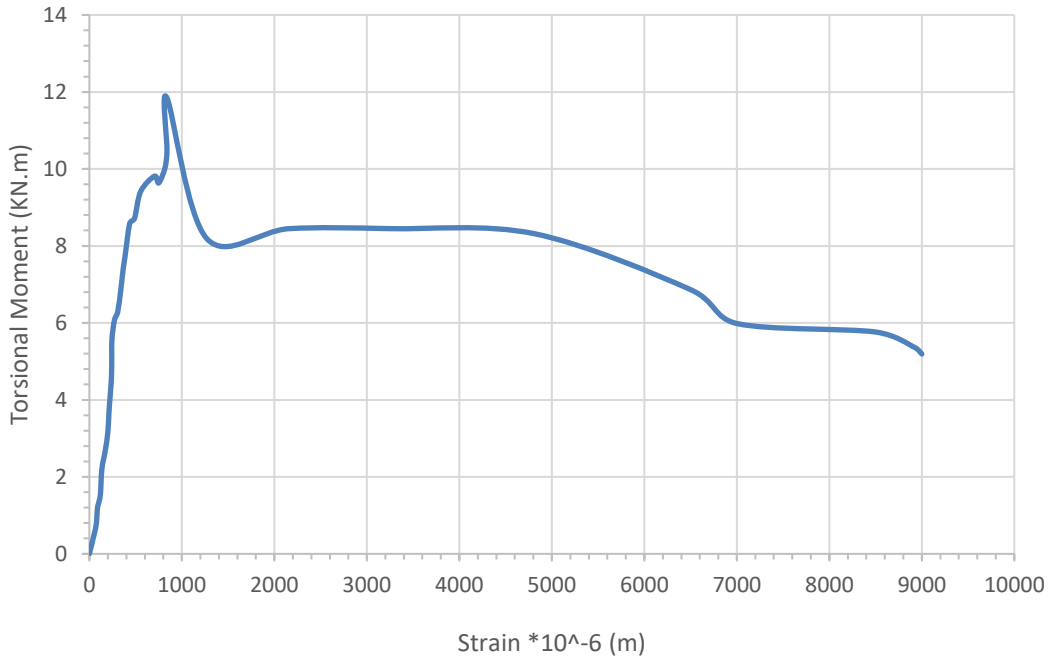

Figure (4-43): Torsional Moment-Strain Curve for the Concrete at Quarter of Span Zone for Specimen B5.

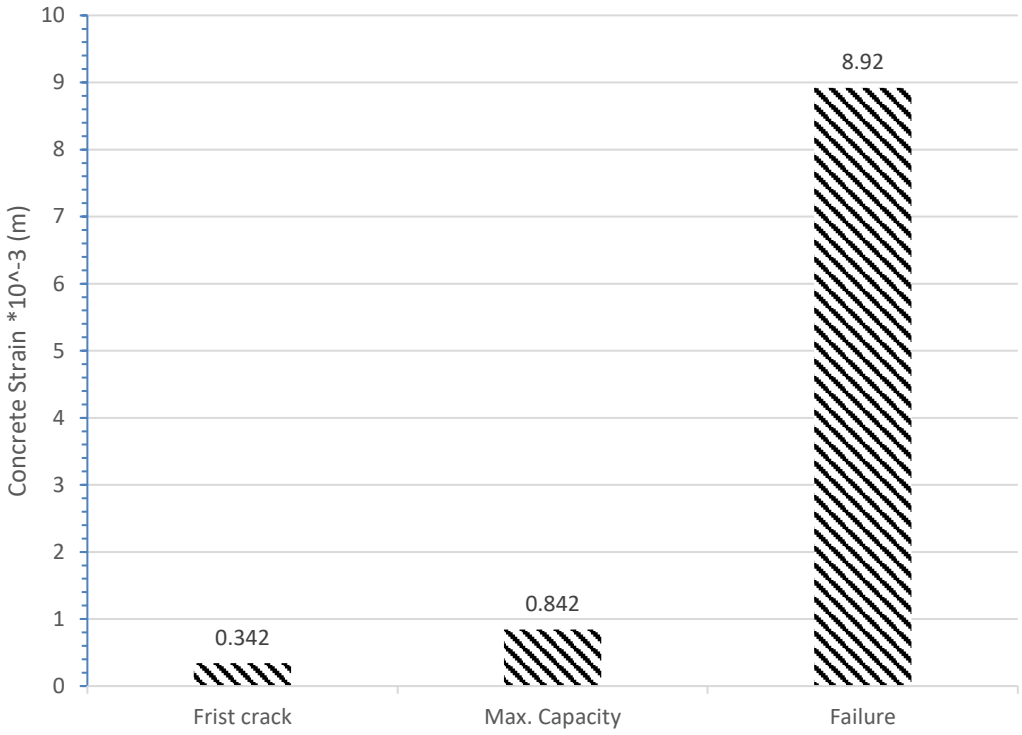

Figure (4-44): Concrete Strain at Three Phases for B5.

- **Strain of Stirrups**

The strain gauge was located at two separated stirrups in the middle beam span with length of stirrups near torsional arm but damaged during test.

4.2.6 Results of Tested Beam (B6)

- **Specimen Description**

This beam reinforced by GFRP in longitude and transverse directions with stirrups spacing 150 mm and 2 φ 10 as a compression reinforcement and 2 φ 12 as a tensile reinforcement with section 150*300 mm and concrete cover 20 mm, the stirrups was inclined. This beam is similar to B2 beam by changing the stirrups configuration.

- **Crack Pattern**

Figure (4-45-a) and (4-45-b) shows the cracking pattern for tested beam (B6). In the Figure, each crack is marked by a line representing the direction of cracking. The crack patterns at all faces of beams were recorded at several load stages up to failure. The cracks started in the middle of beam span. The

first visible crack started as flexural crack at the torsional moment 5.236 KN.m (the torsional moment was at the same time the maximum capacity) and extended as torsional cracks and appeared cracks in the other side with angle 45^{o} and the cracks expanded until the failure. The specimen remained with no visible cracks until torsional cracks took place. As loading increased, the same crack extended continuously and became wider. The capacity of beam decreased after cracking and the started to appear torsional moment but didn't reach back to the first torsional moment capacity, the cracks weakened the beam which caused a decrease in capacity of beam and its stiffness. Because of the stirrups were formed inclined 45^{o} and 135^{o} and the torsional cracks is spiral and continues so the cracks met the stirrups with the same angle (cracks were parallel to stirrups) and the torsional in this moment resisted by concrete only and torsional capacity didn't increase more than the capacity at first visible crack. The maximum torsional moment was the same first torsional moment crack 5.236 KN.m. After cracking the capacity of beam decreased until the failure with torsional moment 2.97 KN.m. As clearly, the failure was torsional failure that cleared in the cracks of four faces inclined and continuous cracks and the main crack sloped with angle from 40 to 45 degrees.

Figure (4-45-a): Cracks Pattern for the first side of Specimen B6.

Figure (5-45-b): Cracks Pattern for the Top Side of Specimen B6.

- **Twist of the Beam Section**

Three points of deflection for each specimen were measured, the first one at far 5 cm from the first torsional arm in one side of section 3 cm away, second point for measuring deflection in the same section in second side of section with the same dimensions and the third point in the second torsional arm

with 5 cm from the torsional arm and 3 cm from the section side. The three-measure deflection would provide us with the same result but the reason for using 3 deflection measure to sure the result and to avoid any defect with them. The maximum twist was $13.1*10^{-2}$ rad/m with torsional moment 2.926 KN.m in the failure phase. It was observed that the first crack was the maximum capacity at the same time 5.239 KN.m with $1.3*10^{-5}$ rad/m with sound. The twist increased with decreasing in torsional moment as shown in Figure (4-46). At the final of experiment, the right torsional beam section changed from 0 rad/m to $13.1*10^{-2}$ rad/m mm and the left torsional beam section from 0 rad/m to $3.5*10^{-2}$ rad/m.

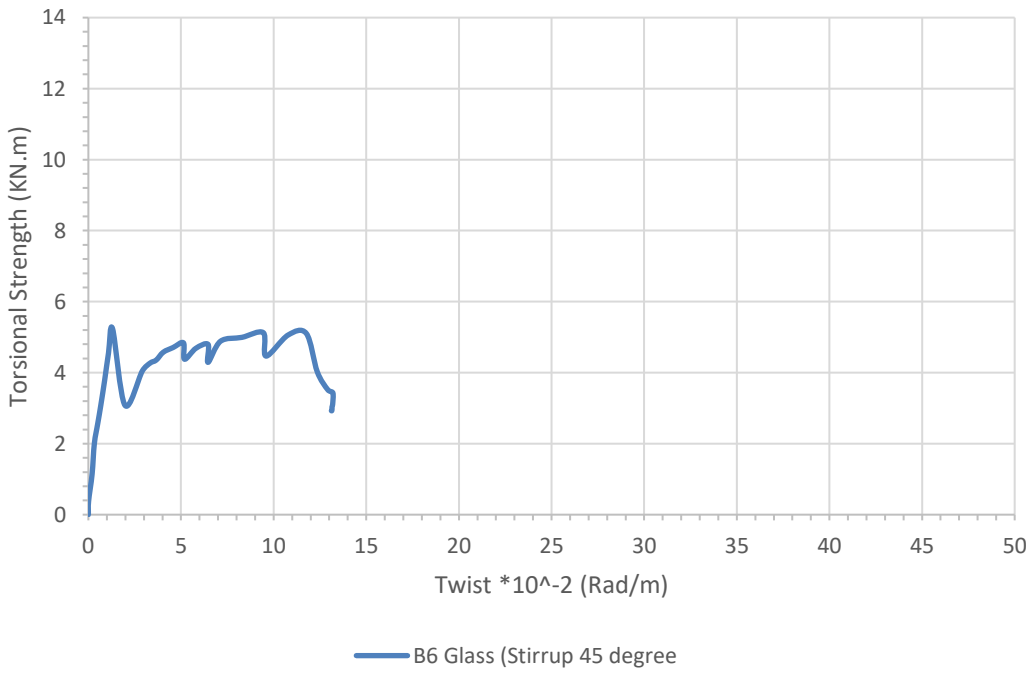

Figure (4-46): Torsional Moment-Twist Curve for Specimen B6.

Figure (4-47-a) and (4-47-b) show the difference between the twist and the torsional moment in two phases. The twist at first crack (the twist at maximum capacity) was 10% from the maximum twist in load 178.94% from the capacity at failure. The twist increased by 902% from the maximum twist with decreasing torsional moment 78.94% from the torsional moment at the failure.

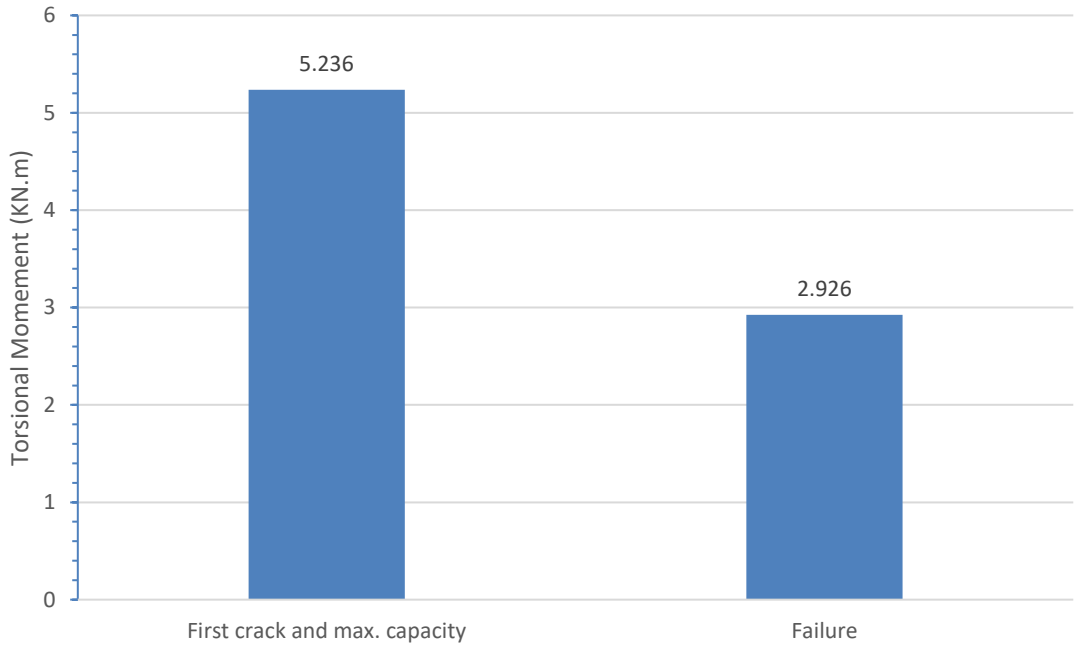

Figure (4-47-a): Torsional Moment at Two Phases for B6.

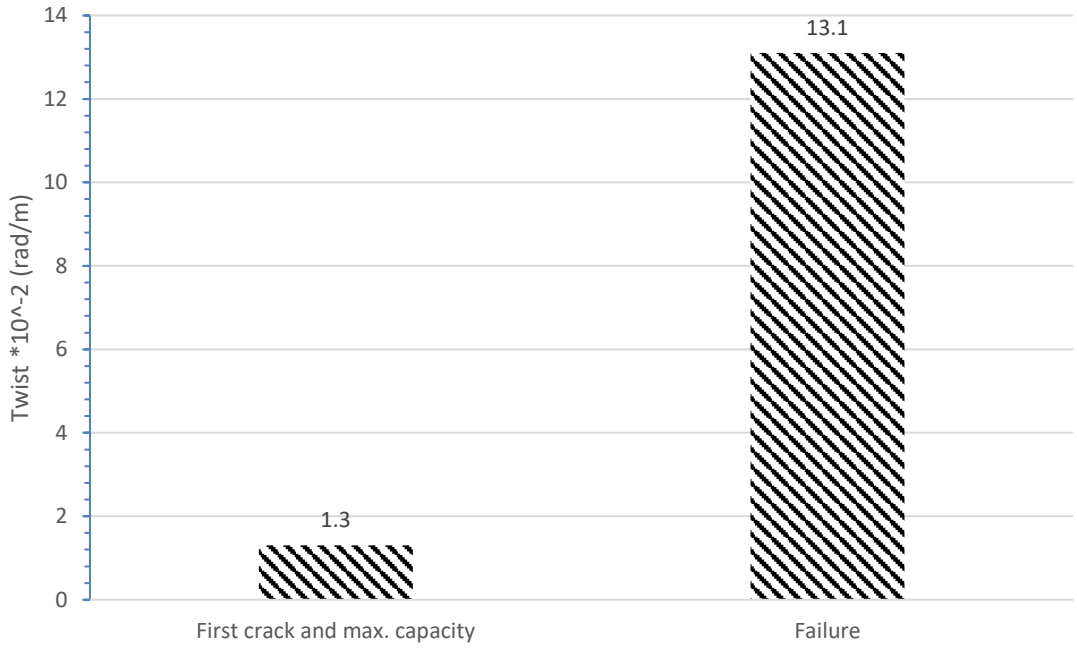

Figure (4-47-b): Twist at Two Phases for B6.

- **Strain of GFRP Bars**

The strain gauge was fixed on the center of the middle span bar to provide us by information like torsional moment - strain relationship for the GFRP bars reinforcement and for stirrup strain gauge fixed in two stirrups in middle span. Figure (4-48) show the relation between torsional moment-

strain curve for GFRP bars for specimen B6. The bar strain at failure was 2.441 *10-3 with torsional moment 2.926 KN.m but the bar strain for first crack and maximum capacity was 0.375*10-3. The bar strain at failure increased 551% from the bar strain at the first crack with decrease in torsional moment 88.7% from the failure moment as shown in Figure (4-49).

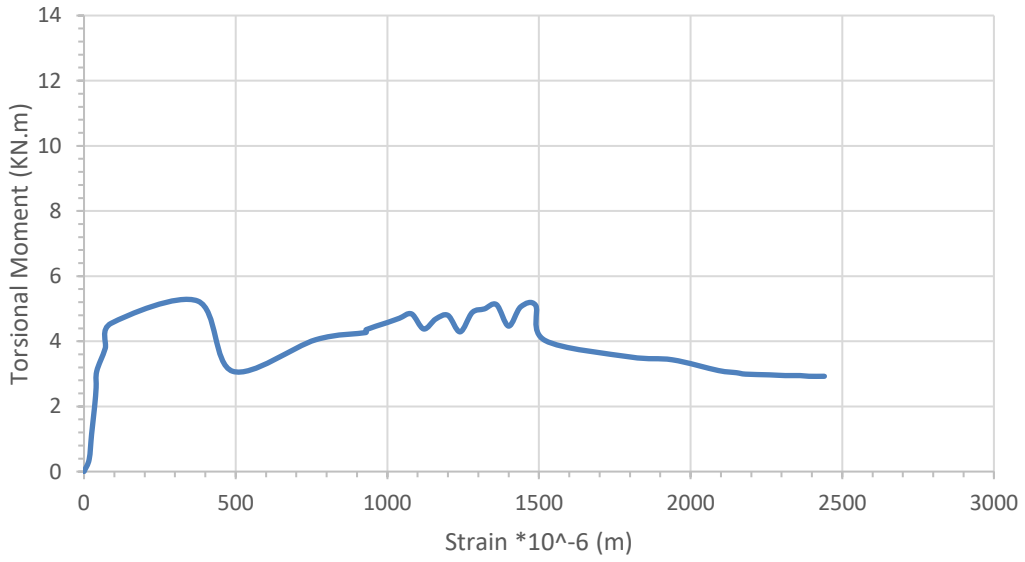

Figure (4-48): Torsional Moment-Strain Curve for GFRP Bars for Specimen B6.

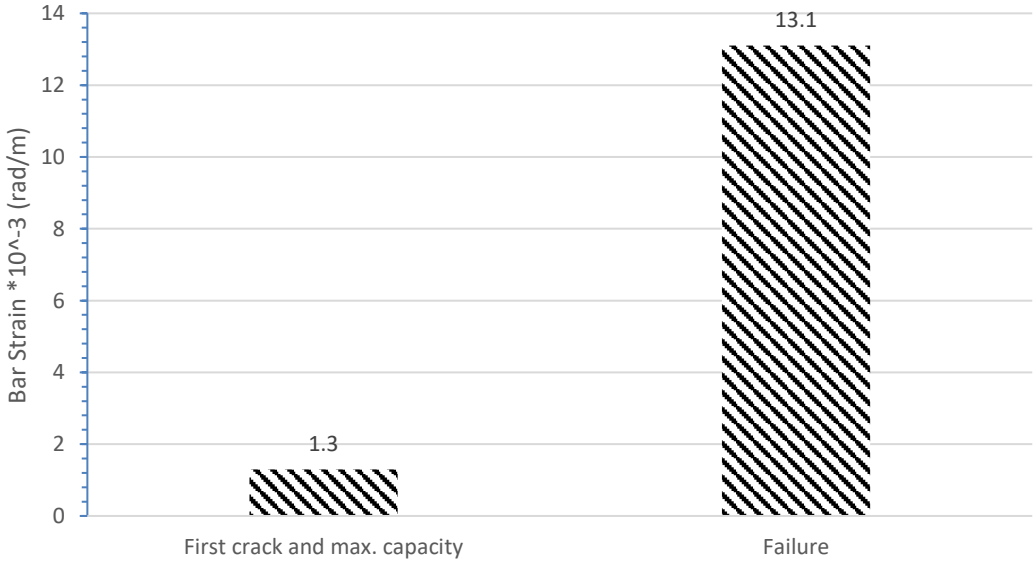

Figure (4-49): Bar Strain at Two Phases for B6.

- **Strain of Concrete**

Figure (4-50) shows torsional moment-strain relationship for the concrete. Concrete strain gauge 60 mm was mounted on the concrete front at 135˚ in the middle distance between the middle span and the left torsional arm. By studying the strain distribution of the beam, it can be noticed that B6 failure torsional moment occurred with concrete carry a large amount of stress. Figure (4-51) shows the difference between the concrete strain and the torsional moment in three phases. the maximum concrete strain was $6.40*10^{-3}$ m with torsional moment 2.926 KN.m and the maximum torsional moment was 5.536 KN.m with concrete strain $0.303*10^{-3}$ m and the first crack was at the same point, the concrete strain at first crack (in the same time it is the maximum torsional resistance) was 4.73% from the maximum concrete strain with capacity 189% from the capacity at failure. At the failure the concrete strain increased by 21 times from the concrete strain at maximum torsional resistance (torsional moment of resistance of first crack) with decreasing torsional moment to around half from the maximum torsional moment as shown in Figure (4-51).

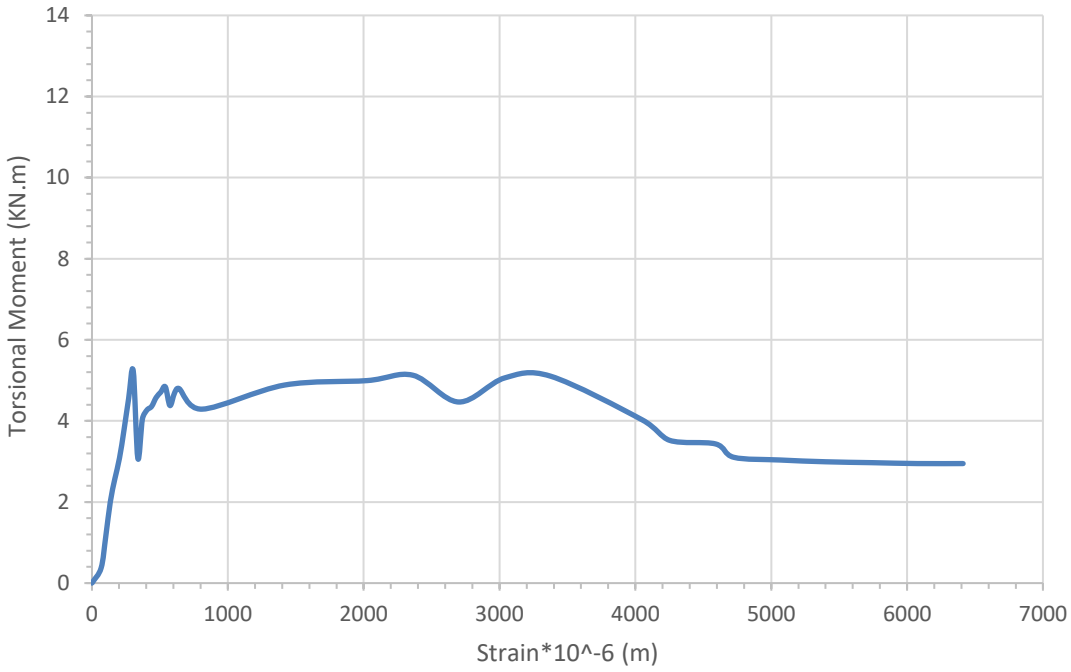

Figure (4-50): Torsional Moment-Strain Curve for the Concrete at Quarter of Span Zone for Specimen B6.

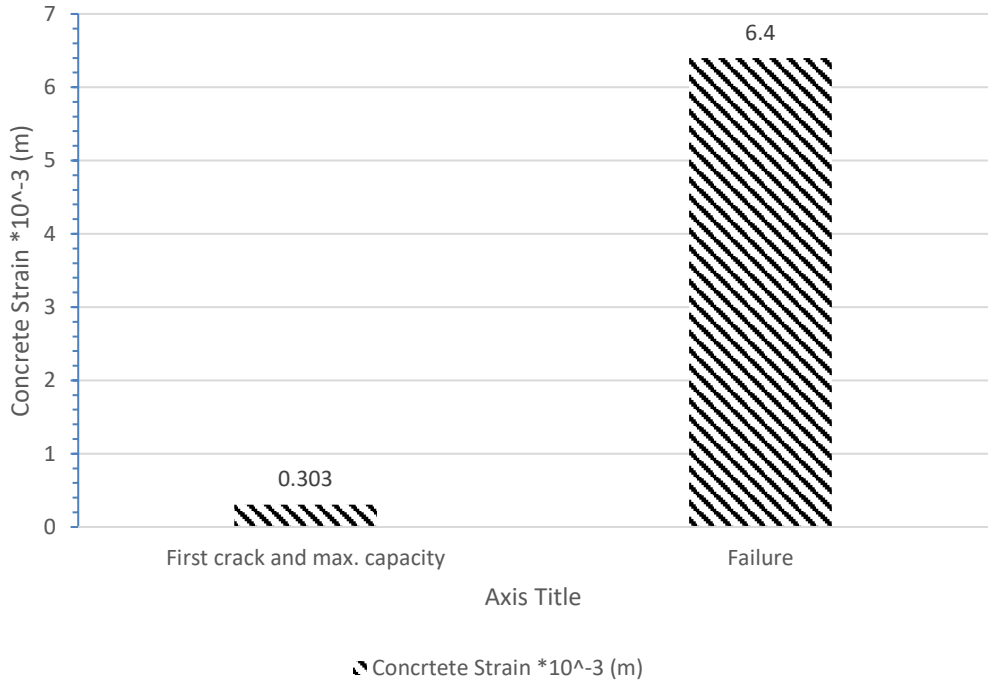

Figure (4-51): Concrete Strain at Two Phases for B6.

- **Strain of Stirrups**

The strain gauge is located at two separated stirrups in the middle beam span with length of stirrups. The relation between the stirrups strain and torsional

moment as shown in Figure (4-52). The first visible crack was at torsional capacity 5.536 KN.m met stirrup strain $0.131*10^{-3}$ m and 2.926 KN.m for torsional capacity at failure met $8.941*10^{-3}$ m stirrup strain. Figure (4-53) the stirrups strain at the maximum capacity (first crack in same time) and the failure. Right stirrup strain damaged during the casting and transport however extreme care. For left stirrup, the strain was 1.5% from the strain at failure with decreasing around twice torsional moment at failure. That noticed that the cracks and capacity of beam were wobbling, the torsional moment resistance didn't raise back up after visible first crack.

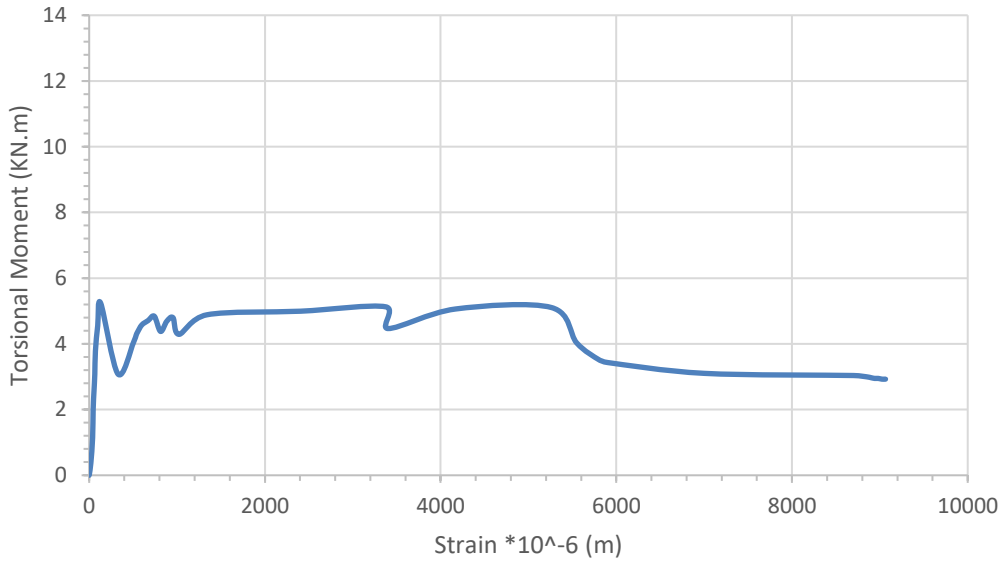

Figure (4-52): Torsional Moment-Strain Curve for the Left Stirrup at the Middle Span for Specimen B6.

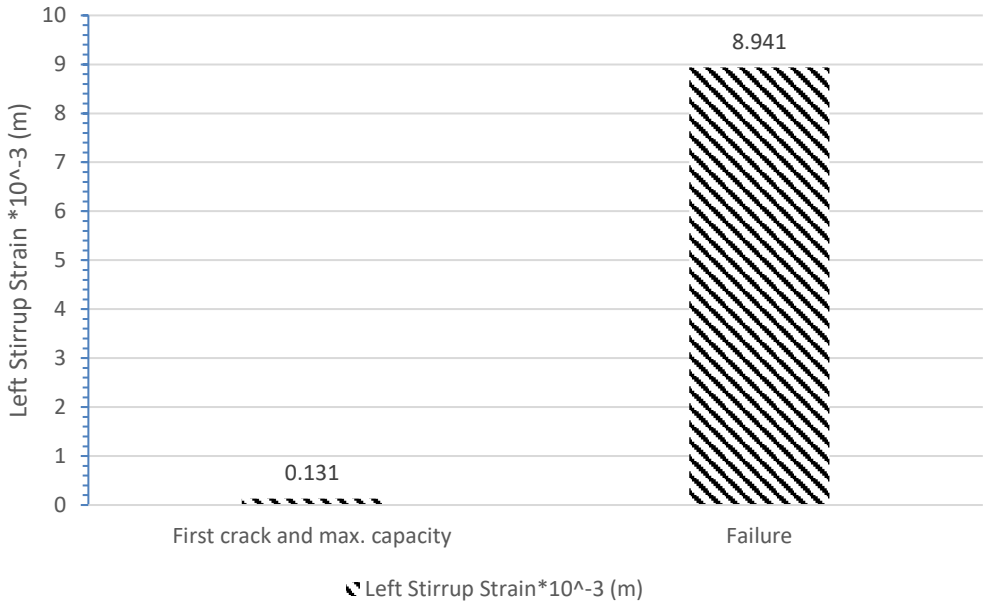

Figure (5-53): Left Stirrup Strain at Two Phases for B6.

4.2.7 Results of Tested Beam (B7)

- **Specimen Description**

This beam reinforced by GFRP in longitude and transverse directions with stirrups spacing 150 mm and 2 φ 10 as a compression reinforcement and 2 φ 12 as a tensile reinforcement with section 150*300 mm and concrete cover 20 mm. This beam is like B2 beam F_{cu}=50 MPa, all beams had F_{cu}=30 MPa except this beam.

- **Crack Pattern**

Figure (4-54-a), (4-54-b) and (4-54-c) shows the cracking pattern for tested beam (B7). In the Figure, each crack is marked by a line representing the direction of cracking. The crack patterns at all faces of beams were recorded at several load stages up to failure. The specimen remained with no visible cracks until torsional cracks took place. The first crack started as flexural crack in the first quarter from the right span and in the compression zone in the same area at the torsional moment 5.61 KN.m and continued to produce cracks around the first crack zone, the cracks continued in the same crack has been wider and small crack produced around the first crack until the

failure, the cracks were accompanied by cracking sound. As loading increased, the same crack extended continuously and became wider. The capacity of the torsional moment increased to reach to maximum torsional moment 7.326 KN.m. After cracking the capacity of beam decreased until the failure with torsional moment 2.66 KN.m. The cracks were clearly torsional cracking (continuous diagonal cracks at the sides, top and bottom of beam). As clearly, the failure was torsional failure, the GFRP reinforcement with the high concrete strength made the beam stiff and the crack continued in the same crack and took place rupture in the stirrup. The cracks weakened the beam which caused a decrease in capacity of beam and its stiffness. After the first crack, the load of beam went down and grow again but it didn't reach more than the first load crack. The torsional moment which caused the first crack was at the same time the maximum capacity for beam. That noticed, after any cracks the load was going down and growing again after cracking. In the cracking zone, the stirrup ruptured as shown in Figure (4-55) and the cracks were inclined in one face and continuous by the top as shown in Figure (4-54-b).

Figure (4-54-a): Cracks Pattern for the First Side of Specimen B7.

Figure (4-54-b): Cracks Pattern for the Second Side of Specimen B7.

Figure (4-54-c): Cracks Pattern for the top side of Specimen B7.

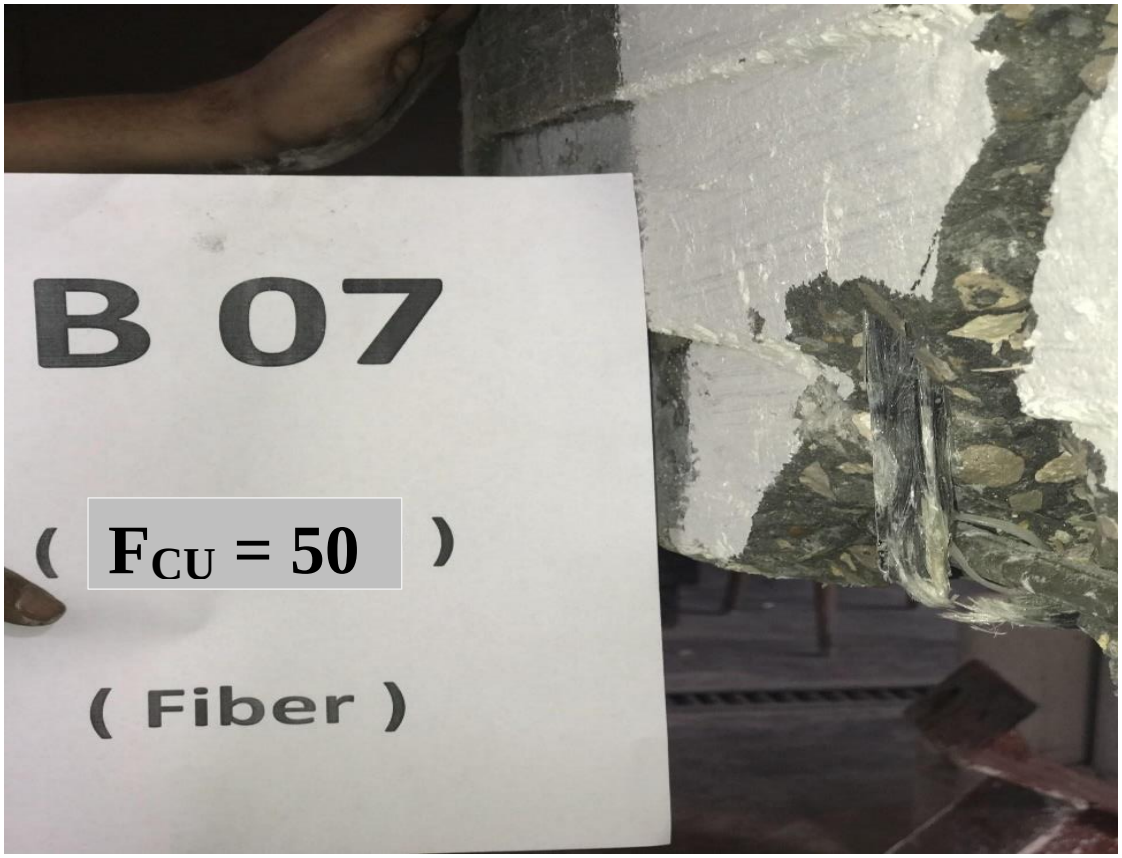

Figure (4-55): Rupture of stirrup for Specimen B7.

- **Twist of the Beam Section**

The relation between the twist of beam section and the torsional moment is shown in Figure (4-56). LVDT was located 5 cm from the torsional arm and 3 cm from the edge of beam. At the final of experiment, the right torsional beam section changed from 0 rad/m to $14.4*10^{-2}$ rad/m and the left torsional arm from 0 rad/m to $8.1*10^{-2}$ rad/m.

Three points of deflection for each specimen were measured, the first one at far 5 cm from the first torsional arm in one side of section 3 cm away, second point for measuring deflection in the same section in second side of section with the same dimensions and the third point in the second torsional arm with 5 cm from the torsional arm and 3 cm from the section side. The three-measure deflection would provide us with the same result but the reason for using 3 deflection measure to sure the result and to avoid any defect with them. The maximum twist was $14.4*10^{-2}$ rad/m with torsional moment 2.662 KN.m in the failure phase. It was observed that the first crack was 5.61 KN.m with $1.68*10^{-2}$ rad/m with voice and stilled resisted up to maximum torsional resistance 7.326 KN.m with twist $2*10^{-2}$ rad/m to get more twist with loading to fail at 2.664 KN.m torsional moment resistance with twist $14.4*10^{-2}$ rad/m as shown in Figure (4-57).

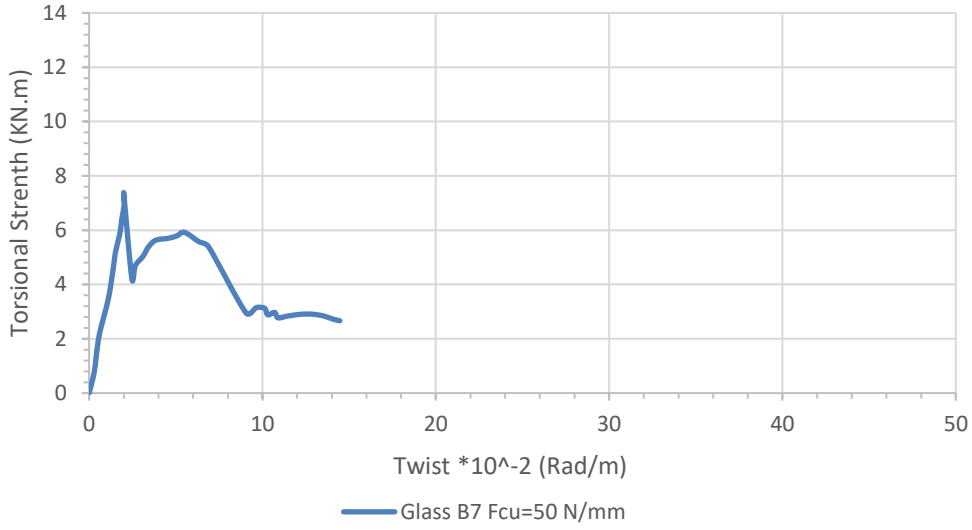

Figure (4-56): Torsional Moment-Twist Curve for Specimen B7.

Figure (5-57-a) and (5-57-b) shows the difference between the twist and the torsional moment in three phases. The twist at first crack was 11.6% from the maximum twist in load 210% from the capacity at failure. The twist increased at maximum resistance to reach to 13.8% from the maximum twist in load 275% from the capacity at failure. the twist increased little with more torsional resistance to reach to the maximum then the resistance decreased with more increasing of twist.

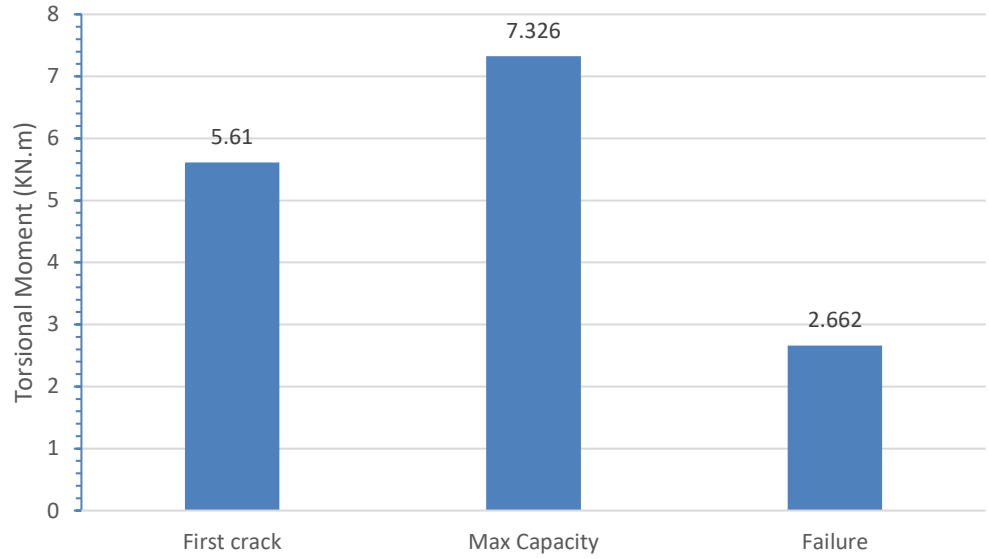

Figure (4-57-a): Torsional Moment at Three Phases for B7.

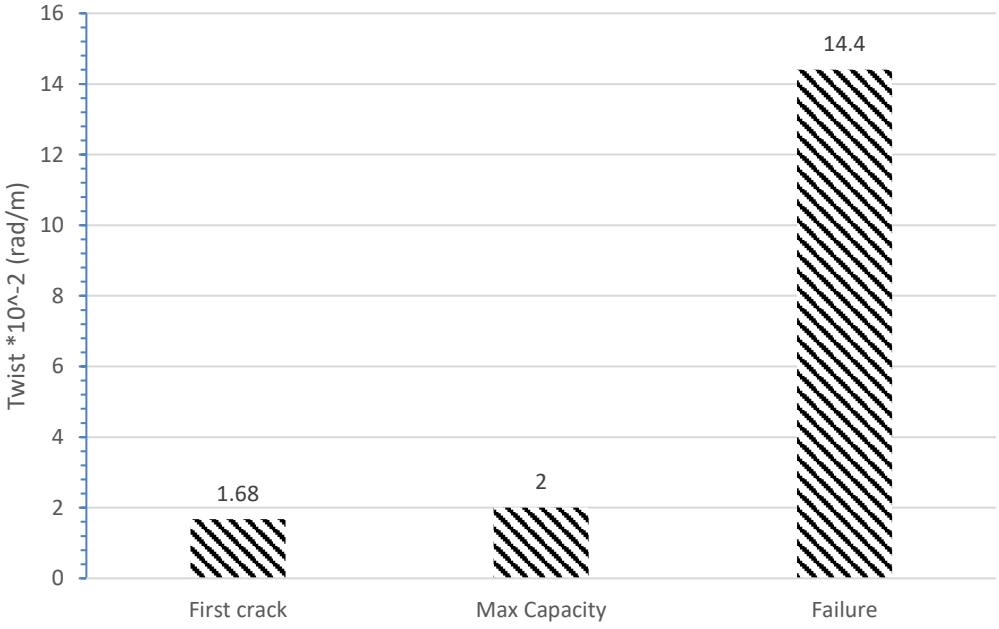

Figure (4-57-b): Twist at Three Phases for B7.

- **Strain of GFRP Bars**

The relation between the bar strain and torsional moment as shown in Figure (4-58). The strain gauge was fixed on the center of the middle span bar to provide us with information like torsional moment - strain relationship for the GFRP bars reinforcement. The bar strain was $0.924*10^{-3}$ m with first visible crack at 5.61 KN.m torsional capacity then the cracks continued with increasing in torsional resistance to reach to maximum torsional capacity 7.326 KN.m with bar strain $1.355*10^{-3}$ m then the resistance decreased with more bar strain to fail the beam with torsional load 2.66 KN.m with bar strain $3.9*10^{-3}$ m as shown in Figure (5-59).

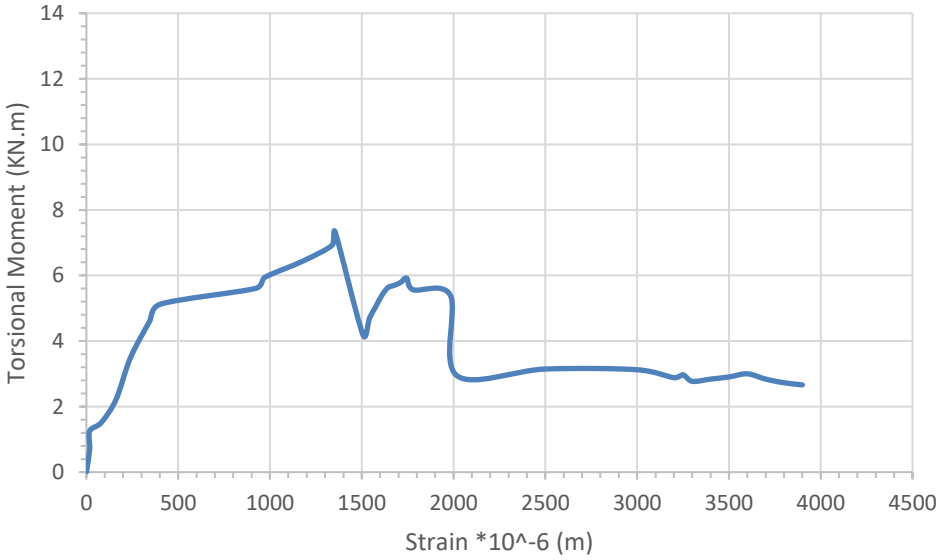

Figure (4-58): Torsional Moment-Strain Curve for GFRP Bars for Specimen B7.

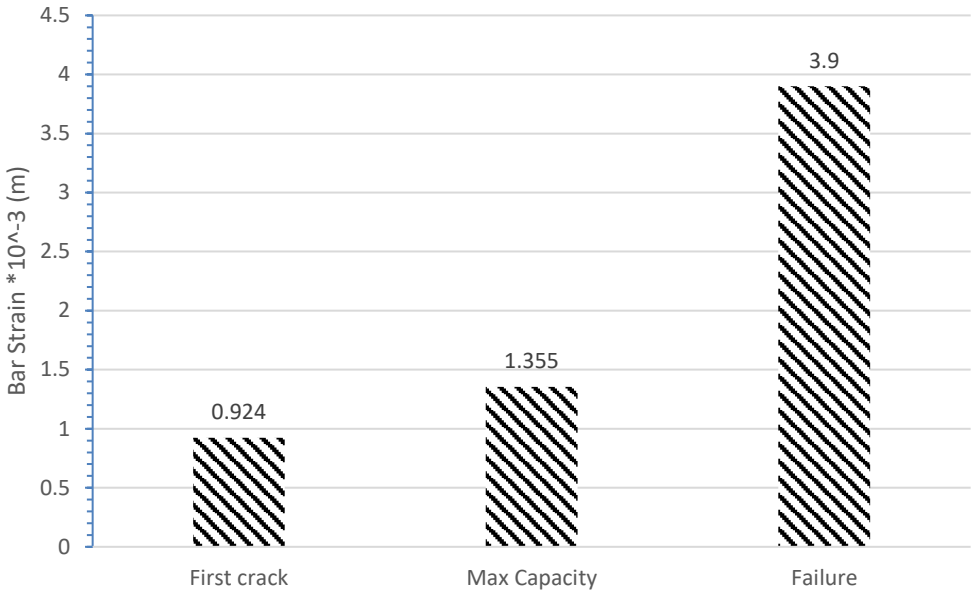

Figure (4-59): Bar Strain at Three Phases for B7.

- **Strain of Concrete**

Figure (4-60) shows torsional moment-strain relationship for the concrete. Concrete strain gauge 60 mm was mounted on the concrete front at 135˚ in the middle distance between the middle span and the left torsional arm. Figure (4-61) shows the difference between the concrete strain and the torsional moment in three phases. the maximum concrete strain was $3.1*10^{-3}$ m with torsional moment 2.66 KN.m and the maximum torsional moment was 7.326 KN.m with concrete strain $1.355*10^{-3}$ m and the first crack was 5.61 KN.m with concrete strain $0.342*10^{-3}$ m, the concrete strain at first crack was 10.45% from the maximum concrete strain with torsional capacity 210% from the capacity at failure. At the failure the concrete strain increased by 5.87 times from the concrete strain at maximum torsional resistance with decreasing torsional moment 1.75% from the maximum torsional moment as shown in Figure (5-61).

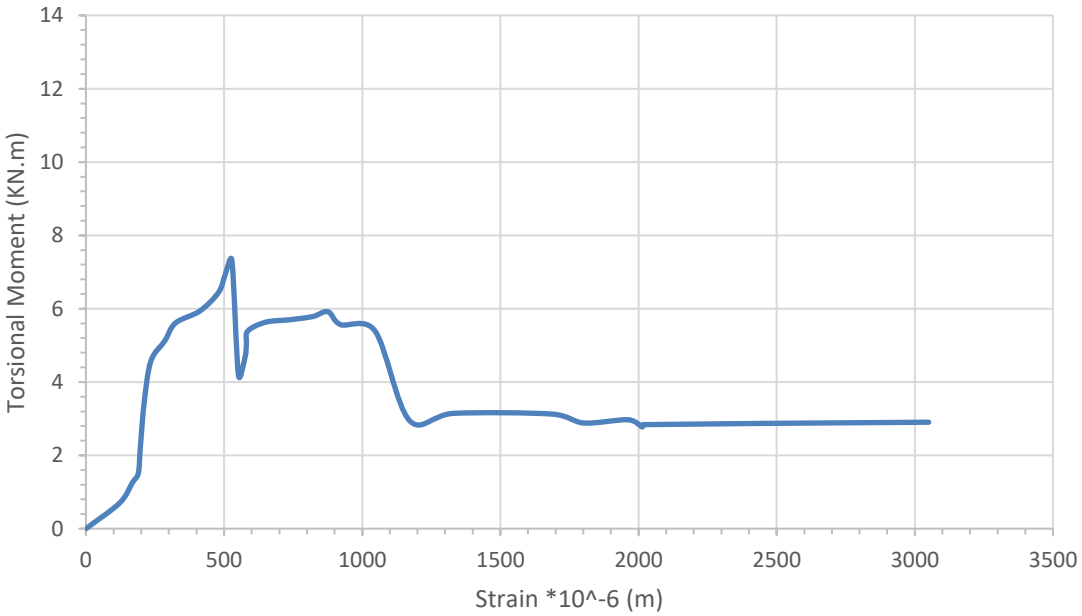

Figure (4-60): Torsional Moment-Strain Curve for the Concrete at Quarter of Span Zone for Specimen B7.

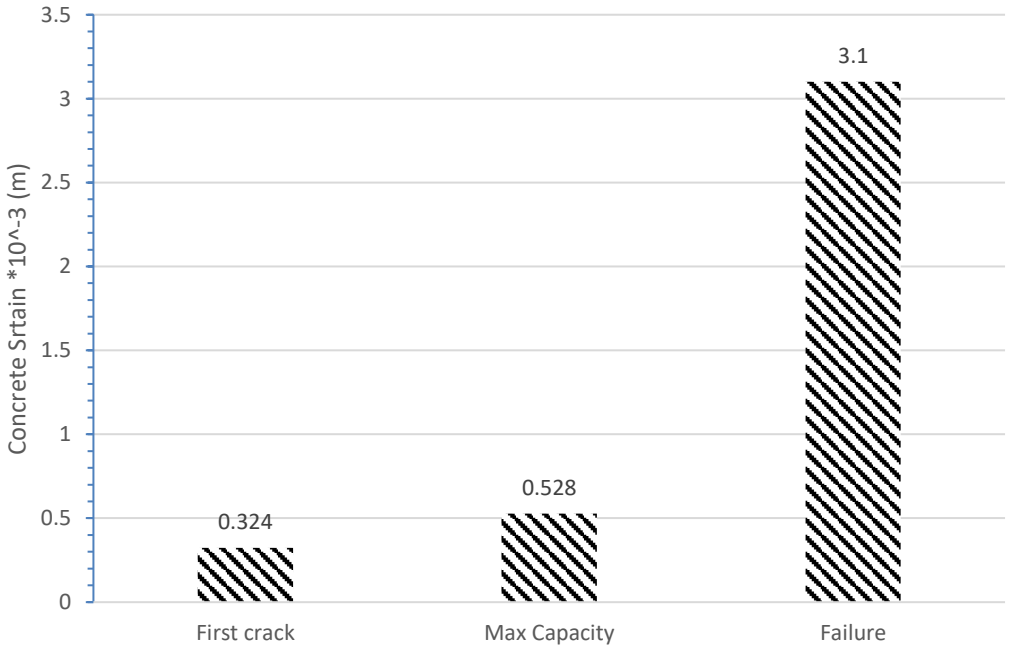

Figure (4-61): Concrete Strain at Three Phases for B7.

- **Strain of Stirrups**

The relation between the stirrups strain and torsional moment as shown in Figure (4-62) for the right stirrup strain. The strain gauges were located at two separated stirrups in the middle beam span with length of stirrups.

Stirrup strain gauge was fixed on stirrup at the middle of span with two stirrups. Figure (4-63) shows the difference between the right stirrup strain in three phases. For right stirrup, the maximum strain was $6.83*10^{-3}$ m with torsional moment 2.66 KN.m at the failure and the maximum torsional moment was 7.326 KN.m with strain $1.669*10^{-3}$ m and the first crack was strain $1.124*10^{-3}$ m with torsional moment 5.61 KN.m, the strain at first crack was 16.4% from the maximum strain by decreasing in capacity 110% comparing the capacity at failure and the strain at maximum capacity was 24.4% from the maximum strain by decreasing in capacity to the 175% from the capacity at failure, the GFRP stirrups and bars have lost the resistance after maximum capacity and produced strains with little resistance because of the non-homogeneousty plus the increasing in concrete strength the made the beam more rigid and the cracks started with corner cracks for stirrups, the matrix material for stirrup corner cracks quickly and the stirrup fiber is bended and not homogeneous like steel bars make the GFRP stirrup corner is weakest point as shown in Figure (4-55).

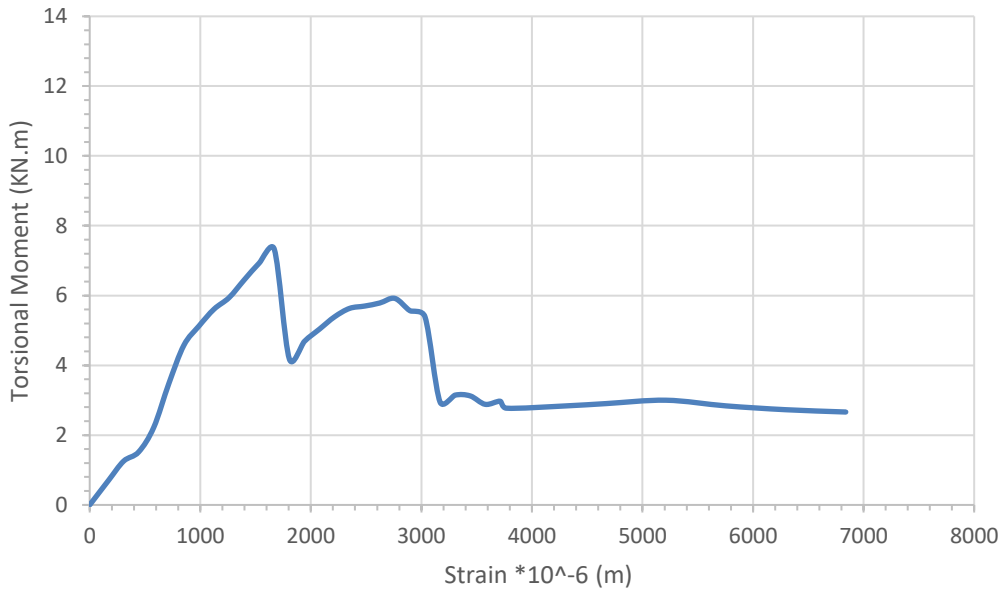

Figure (4-62): Torsional Moment-Strain Curve for the Right Stirrup at the Middle Span for Specimen B7.

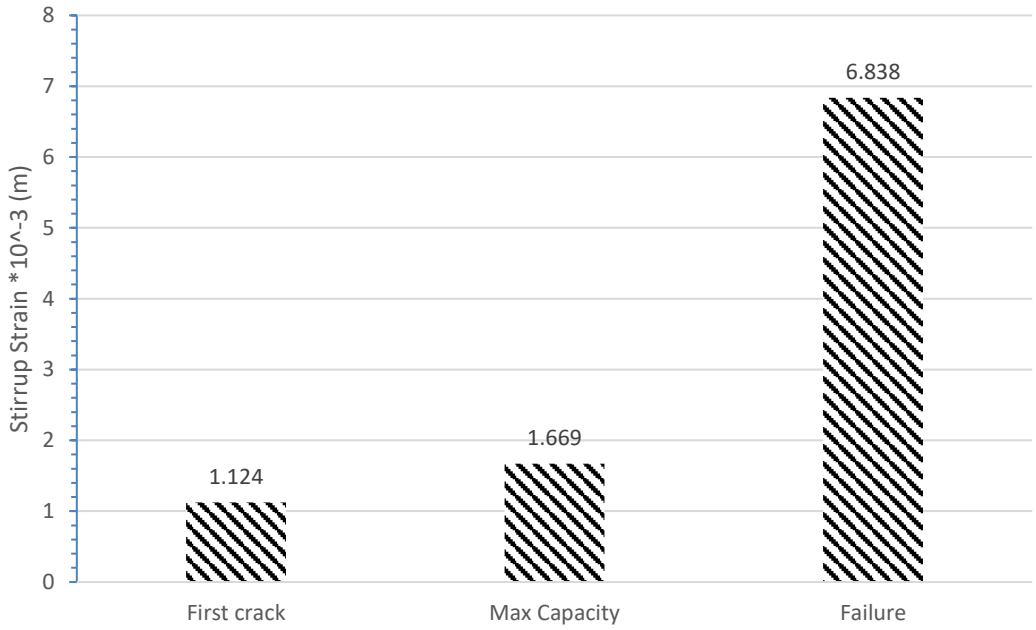

Figure (4-63): Stirrup Strain at Three Phases for B7.

4.2.8 Results of Tested Beam (B8)

- **Specimen Description**

This beam reinforced by steel in longitude direction without, 2 φ 10 as a compression reinforcement and 2 φ 12 as a tensile reinforcement with section 150*300 mm and concrete cover 20 mm. This beam is similar to B1 but without stirrups.

- **Crack Pattern**

Figures (4-64-a) and (4-64-b) show the crack pattern for tested beam (B8). In the Figure, each crack is marked by a line representing the direction of cracking. The crack patterns at all faces of beams were recorded at several load stages up to failure. The cracks started in the middle of beam span. The cracks were accompanied by crackling sound. The specimen remained with no visible cracks until torsional cracks took place. The visible first crack took place in the 4 sides of middle beam span with torsional moment 5.434 KN.m and continued to produce cracks around the first crack zone, the cracks continued and made another wider crack with sound. The cracks were clearly torsional cracking (continuous diagonal cracks at the sides, top and

bottom of beam) and the cracks were inclined with angle 40° to 50°. As clearly, the failure was torsional failure, the stirrup absent (traverse reinforcement) made the beam cracked continued in the same first crack zone because it was the weaker area and no had traverse reinforcement to distribute the load. The cracks weakened the beam which caused decreasing in capacity of beam and its stiffness. After the first crack, the load of beam went down and grow again, and it reached little more capacity 5.478 KN.m (maximum capacity). That noticed that the beam failed with load 2.178 KN.m. that noticed, after any cracks the load was going down and growing again.

Figure (4-64-a): Cracks Pattern for the First Side of Specimen B8.

Figure (4-64-b): Cracks Pattern for the Second Side of Specimen B8.

- **Twist of the Beam Section**

Three points of deflection for each specimen were measured, the first one at far 5 cm from the first torsional arm in one side of section 3 cm away, second point for measuring deflection in the same section in second side of section with the same dimensions and the third point in the second torsional arm with 5 cm from the torsional arm and 3 cm from the section side. The three-measure deflection would provide us by the same result but the reason for using 3 deflection measure to sure the result and to avoid any defect with them. The maximum twist was $7.8*10^{-2}$ rad/m with torsional moment 2.178 KN.m for the left torsional arm in the failure phase. It was observed that the first crack was 5.434 KN.m with $1.44*10^{-2}$ rad/m with voice and the maximum capacity was 5.478 with twist $4.2*10^{-2}$ rad/m. At the final of experiment, the right torsional beam section changed from 0 rad/m to

$3.1*10^{-2}$ rad/m and the left torsional arm from 0 rad/m to $7.8*10^{-2}$ rad/m as shown in Figure (4-65) for the left torsional arm.

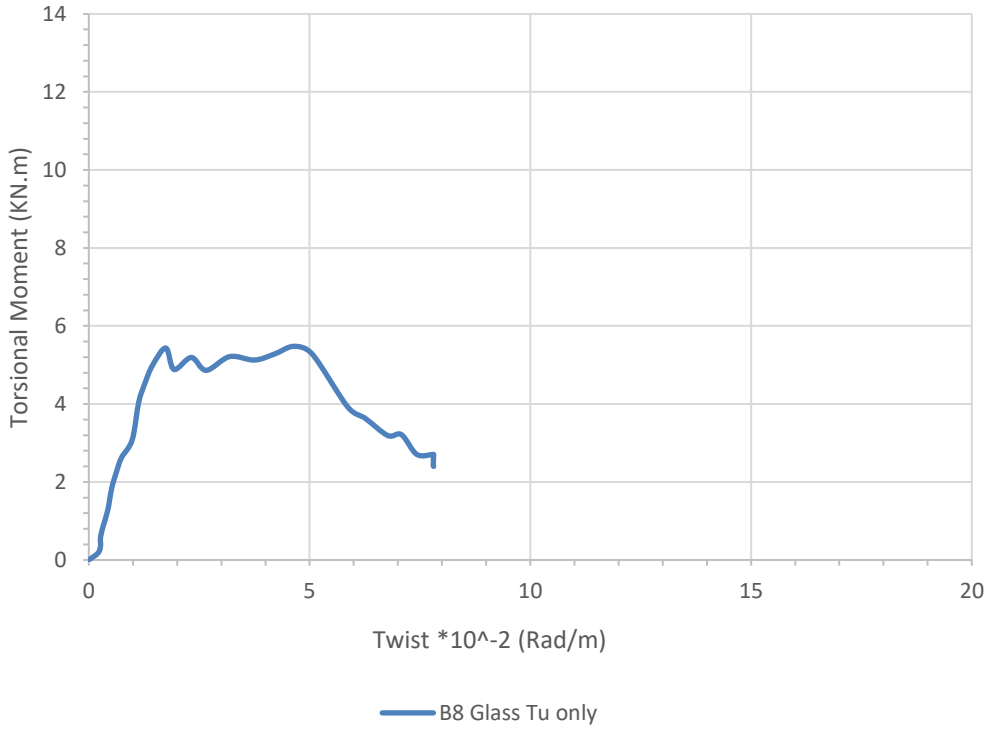

Figure (4-65): Torsional Moment-Twist Curve for Specimen B8.

Figure (4-66-a) and (4-66-b) shows the difference between the twist and the torsional moment in three phases. The twist at first crack was 18.5% from the maximum twist in load 249.5% from the capacity at failure. The twist increased by 439.5% with decreasing torsional moment 149.5% compering the first and failure stages, and the twist increased by 85.5% with decreasing torsional moment 151% by compression the maximum capacity with the maximum twist phases.

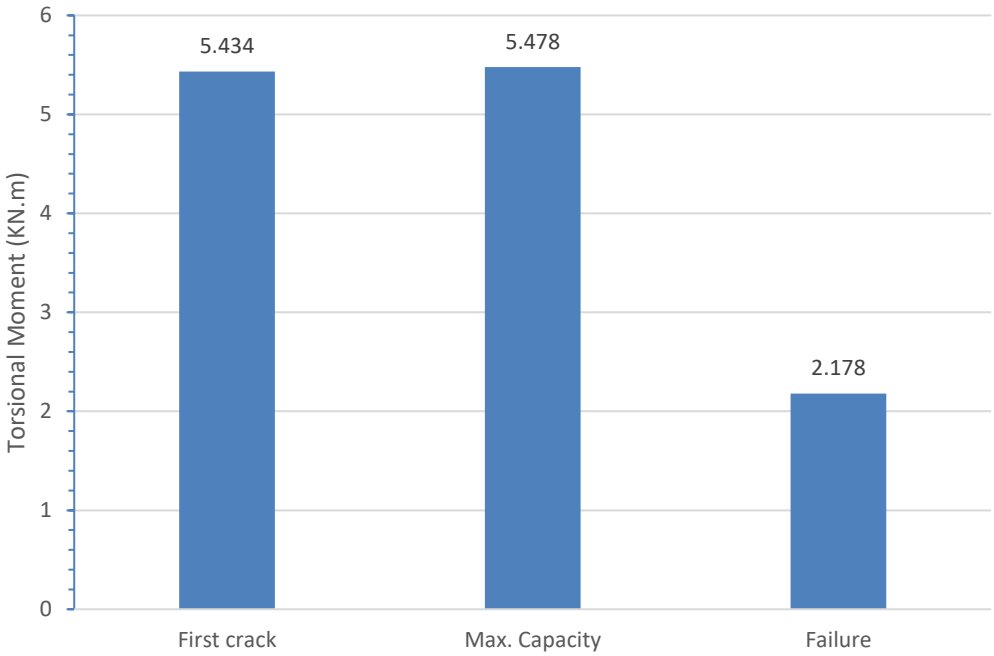

Figure (4-66-a): Torsional Moment at Three Phases for B8.

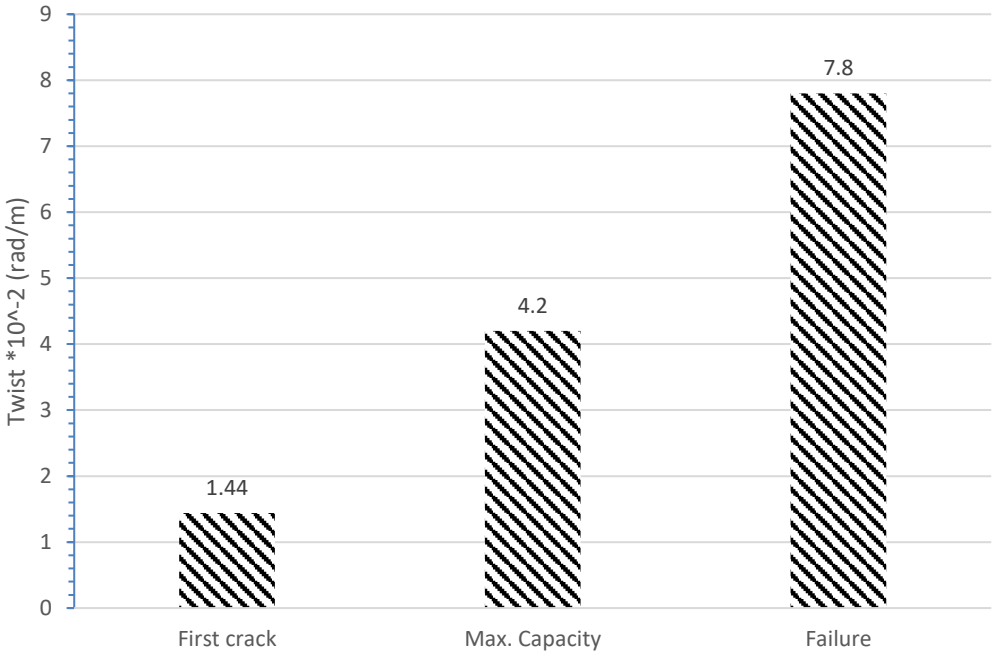

Figure (4-66-b): Twist at Three Phases for B8.

- **Strain of GFRP Bars**

The relation between the bar strain and torsional moment as shown in Figure (4-67). The strain gauge was fixed on the center of the middle span bar to provide us with information like torsional moment - strain relationship for

the steel bars reinforcement. The bar strain was $0.06*10^{-3}$ m with first visible crack at 5.434 KN.m torsional capacity then the cracks continued with too little increasing in torsional resistance to reach to maximum torsional capacity 5.478 KN.m with bar strain $0.613*10^{-3}$ m then the resistance decreased with more bar strain to fail the beam with torsional load 2.178 KN.m with bar strain $1.416*10^{-3}$ m as shown in Figure (4-68).

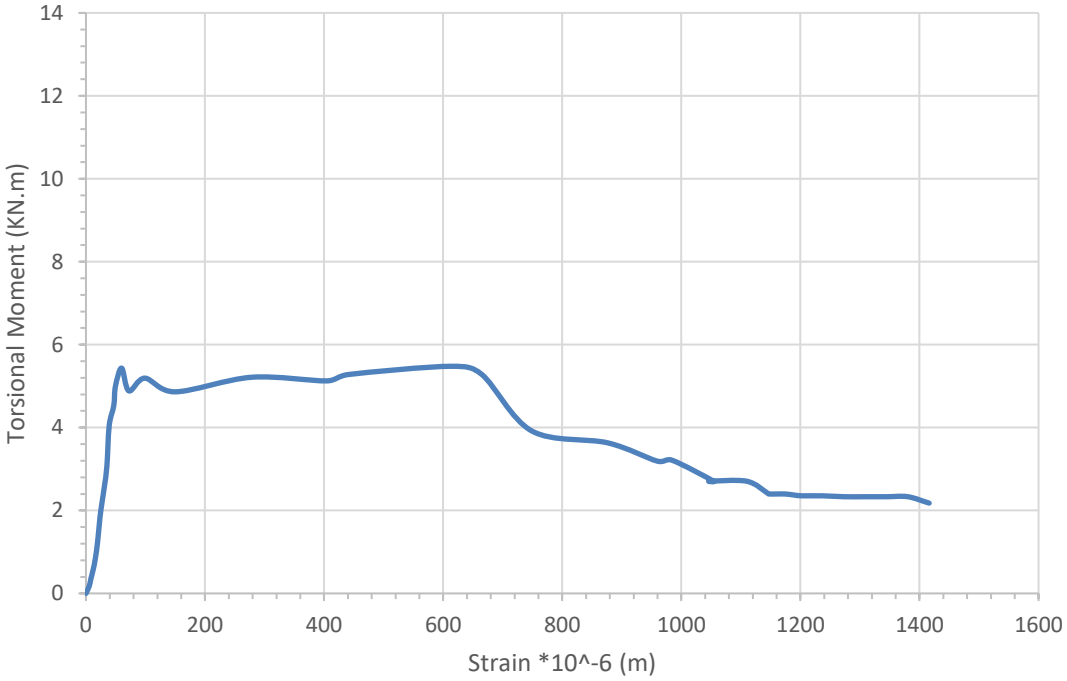

Figure (4-67): Torsional Moment-Strain Curve for GFRP Bars for Specimen B8.

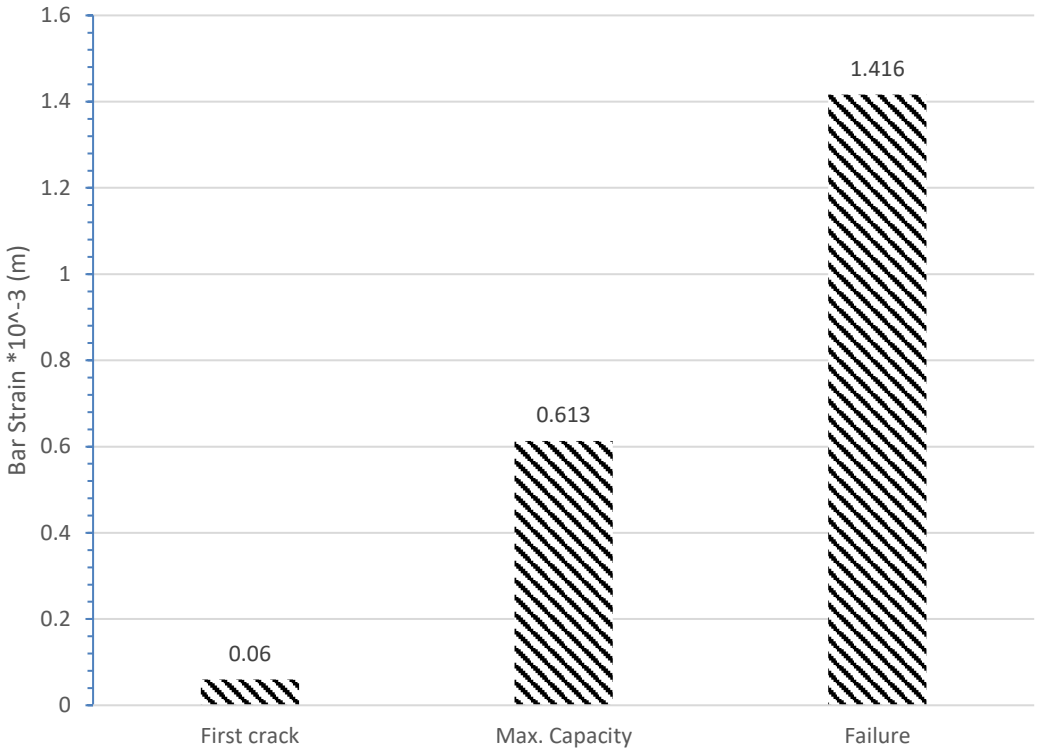

Figure (4-68): Bar Strain and Torsional Moment at Three Phases for B8.

- **Strain of Concrete**

Figure (4-69) shows torsional moment-strain relationship for the concrete. Concrete strain gauge 60 mm was mounted on the concrete front at 135˚ in the middle distance between the middle span and the left torsional arm. Figure (4-70) shows the difference between the concrete strain and the torsional moment in three phases. the maximum concrete strain was $1.687*10^{-3}$ m with torsional moment 2.178 KN.m and the maximum torsional moment was 5.478 KN.m with concrete strain $0.283*10^{-3}$ m and the first crack was 5.434 KN.m with concrete strain $0.094*10^{-3}$ m, the concrete strain at first crack was 5.5% from the maximum concrete strain with torsional capacity 250% from the capacity at failure. At the failure the concrete strain increased by 5 times from the concrete strain at maximum torsional resistance with decreasing torsional moment 150% from the maximum torsional moment as shown in Figure (4-70).

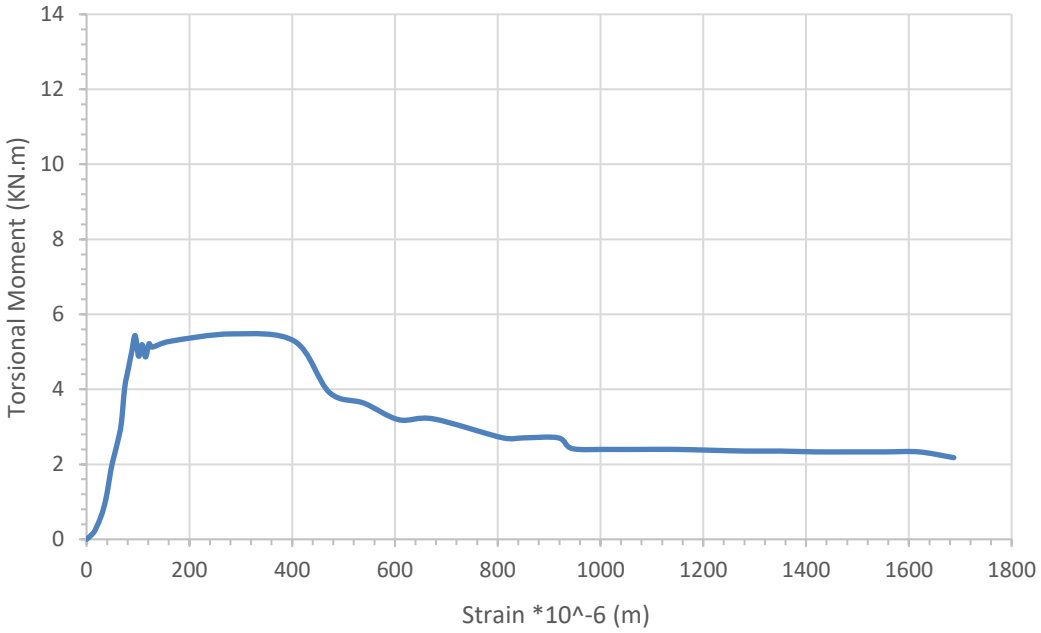

Figure (4-69): Torsional Moment-Strain Curve for the Concrete at Quarter of Span Zone for Specimen B8.

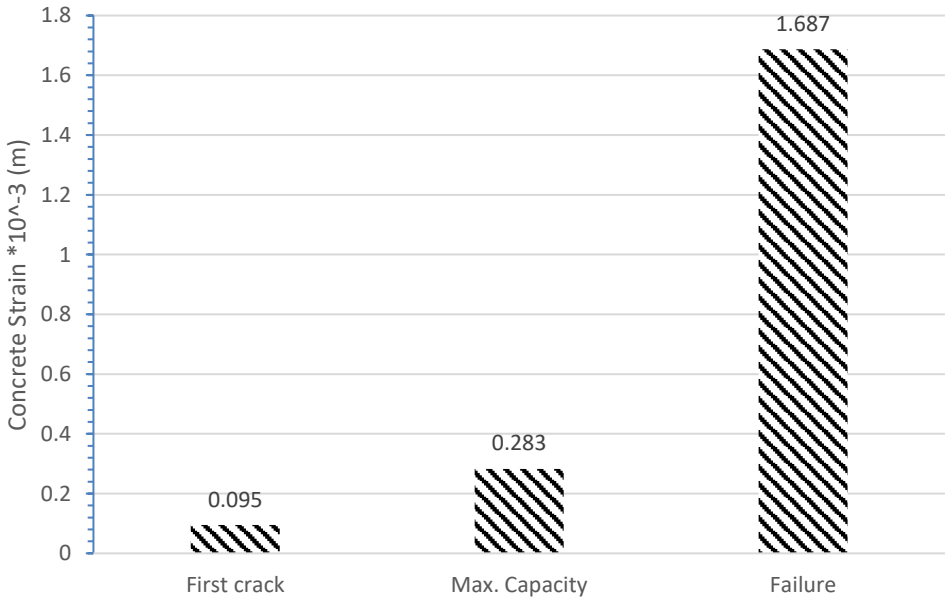

Figure (4-70): Concrete Strain at Three Phases for B8.

4.2.9 Results of Tested Beam (B9)

- **Specimen Description**

This beam reinforced by steel in longitude direction without, 2 φ 10 as a compression reinforcement and 2 φ 12 as a tensile reinforcement with

section 150*300 mm and concrete cover 20 mm. This beam is similar to B1 but without stirrups and tested under torsional and bending moments.

- **Crack Pattern**

Figure (4-71-a) and (4-71-b) show the cracking pattern for tested beam (B9). In the Figure, each crack is marked by a line representing the direction of cracking. The crack patterns at all faces of beams were recorded at several load stages up to failure. The cracks started in the middle of beam span in the left near the torsional arm. The first crack started as shear crack at the torsional moment 11.13 KN.m and other cracks were created and extended; the cracks expanded until the failure. The specimen remained with no visible cracks until torsional cracks took place. As loading increased, the same cracks extended continuously and became wider. The capacity of the torsional moment increased to reach a maximum torsional moment 11.97 KN.m. After cracking the capacity of beam decreased until the failure with torsional moment 5.32 KN.m. It was clear, that the failure was torsional failure, and the cracks were inclined with angle 40^{o} to 50^{o}. As clearly, the failure was torsional and shear failures, the stirrup absent (traverse reinforcement) made the beam weaker and no had traverse reinforcement to distribute the load. The cracks weakened the beam which caused decreasing in capacity of beam and its stiffness.

Figure (4-71-a): Cracks Pattern for Specimen B9.

Figure (4-71-b): Cracks Pattern for Specimen B9.

- **Twist of the Beam Section**

Three points of deflection for each specimen were measured, the first one at far 5 cm from the first torsional arm in one side of section 3 cm away, second point for measuring deflection in the same section in second side of section with the same dimensions and the third point in the second torsional arm with 5 cm from the torsional arm and 3 cm from the section side. The three-measure deflection would provide us by the same result but the reason for using 3 deflection measure to sure the result and to avoid any defect with them. The maximum twist was $18.1*10^{-2}$ rad/m with torsional moment 5.32 KN.m in the failure phase. It was observed that the first crack was 11.13 KN.m with $9.5*10^{-2}$ rad/m and the maximum capacity was 11.97 KN.m with twist $13.57*10^{-2}$ rad/m as shown in Figure (4-72).

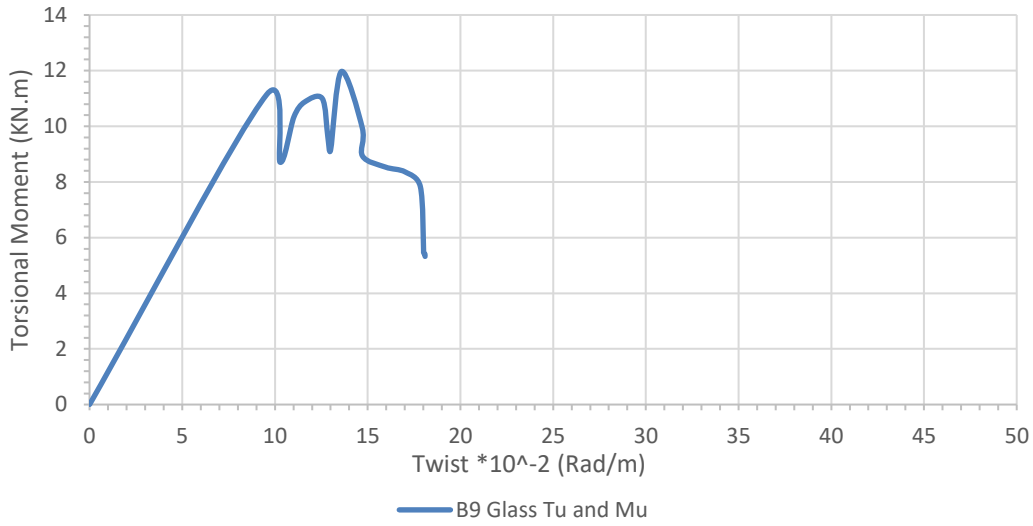

Figure (4-72): Torsional Moment-Twist Curve for Specimen B9.

Figure (4-73-a) and (4-73-b) show the difference between the twist and the torsional moment in three phases. The twist at first crack was 52.5% from the maximum twist in load 209% from the capacity at failure. The twist increased around double with decreasing torsional moment to half by compression first crack and failure phase. The twist increased by one third with decreasing torsional moment half capacity by compression the maximum capacity and failure phases.

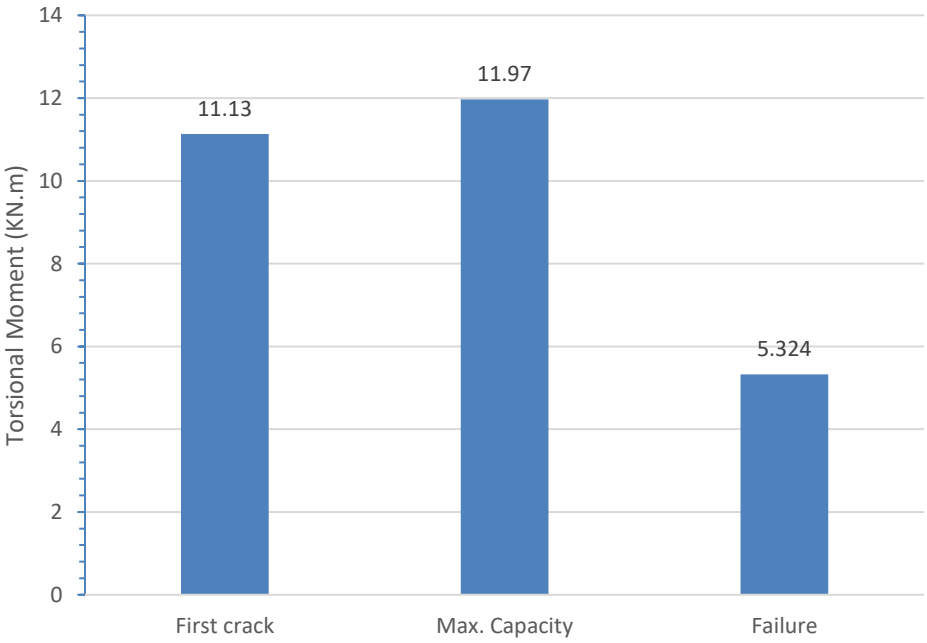

Figure (4-73-a): Torsional Moment at Three Phases for B9.

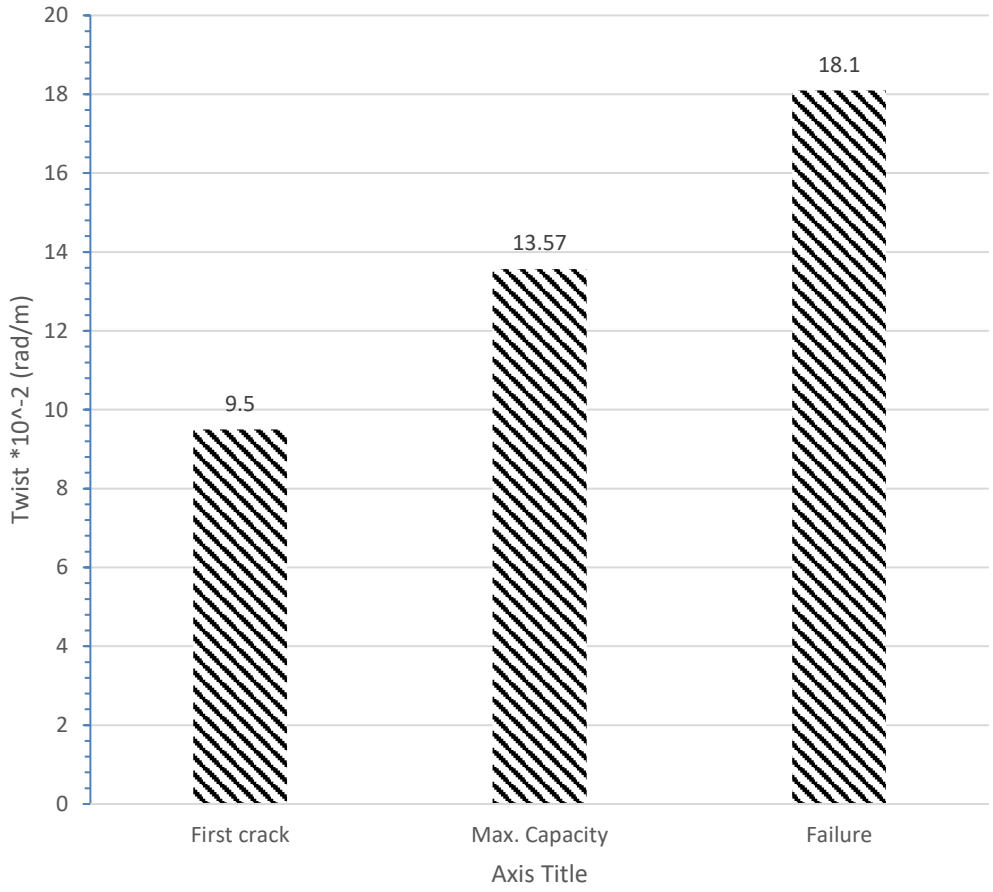

Figure (4-73-b): Twist at Three Phases for B9.

- **Strain of GFRP Bars**

The relation between the strain of GFRP Bars and the applied torsional moment is shown in Figure (4-74). The strain gauge was fixed on the center of the middle span bar to provide us by information like torsional moment - strain relationship for the steel bars reinforcement. The bar strain at first crack was 76.7% from the maximum bar strain in load 209% (double capacity) from the capacity at failure. The bar strain increased quarter with decreasing torsional moment to more than the half capacity at maximum capacity by compression the maximum capacity with the failure phases as shown in Figure (4-75).

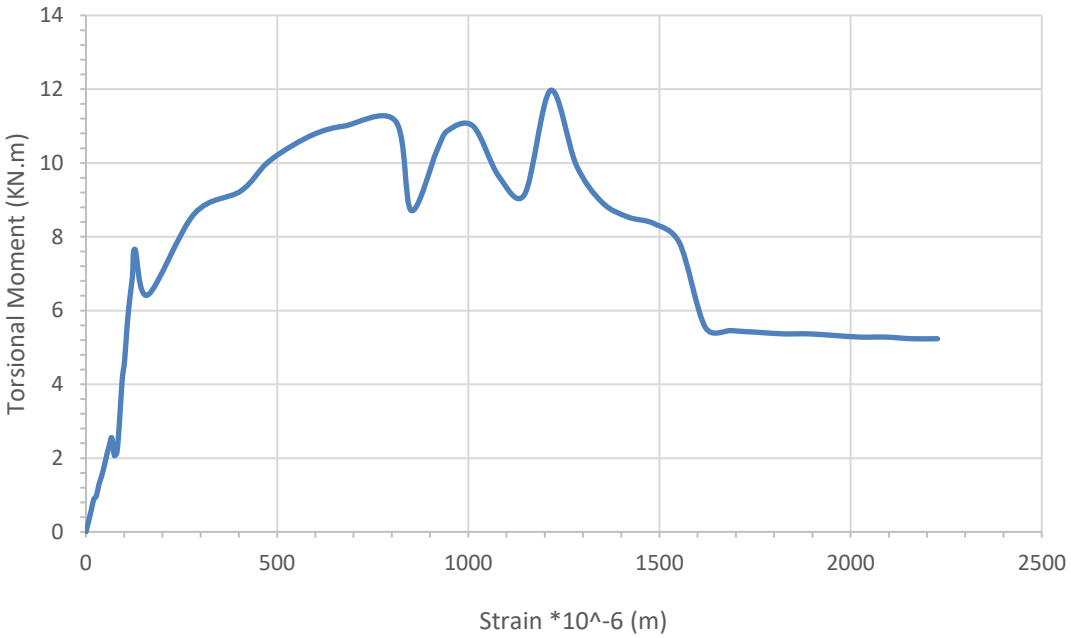

Figure (4-74): Torsional Moment-Strain Curve for GFRP Bars for Specimen B9.

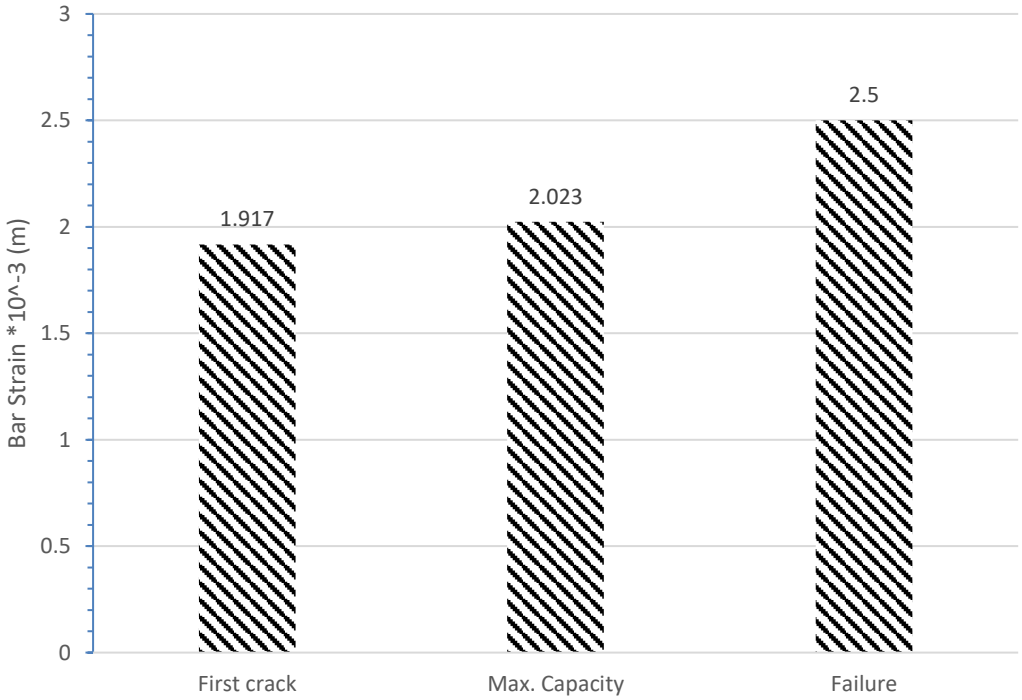

Figure (4-75): Bar Strain at Three Phases for B9.

- **Strain of Concrete**

Figure (4-76) shows torsional moment-strain relationship for the concrete. Concrete strain gauge 60 mm was mounted on the concrete front at 135˚ in

the middle distance between the middle span and the left torsional arm. Figure (4-77) shows the difference between the concrete strain and the torsional moment in three phases. The maximum concrete strain was $2.25*10^{-3}$ m with torsional moment 5.324 KN.m and the maximum torsional moment was 11.97 KN.m with concrete strain $1.215*10^{-3}$ m and the first crack was 11.13 KN.m with concrete strain $0.811*10^{-3}$ m, the concrete strain at first crack was 36% from the maximum concrete strain with torsional capacity 209% from the capacity at failure. At the failure the concrete strain increased by 1.85 times from the concrete strain at maximum torsional resistance with decreasing torsional moment 125% from the maximum torsional moment as shown in Figure (4-77).

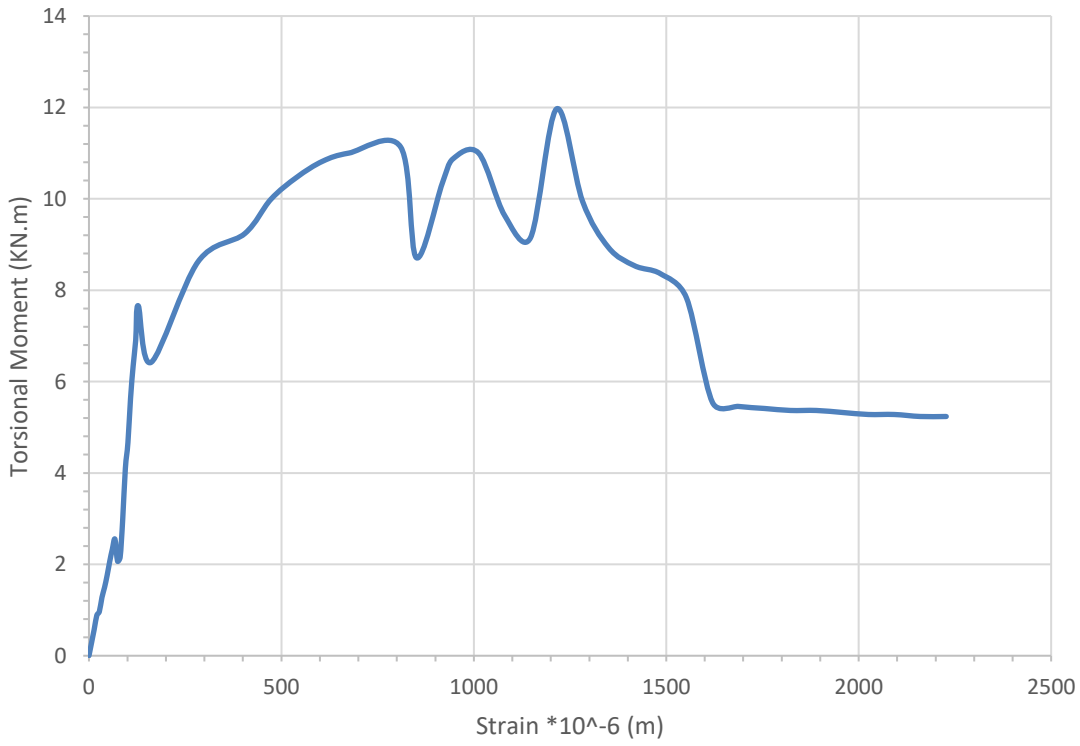

Figure (4- 76): Torsional Moment-Strain Curve for the Concrete at Quarter of Span Zone for Specimen B9.

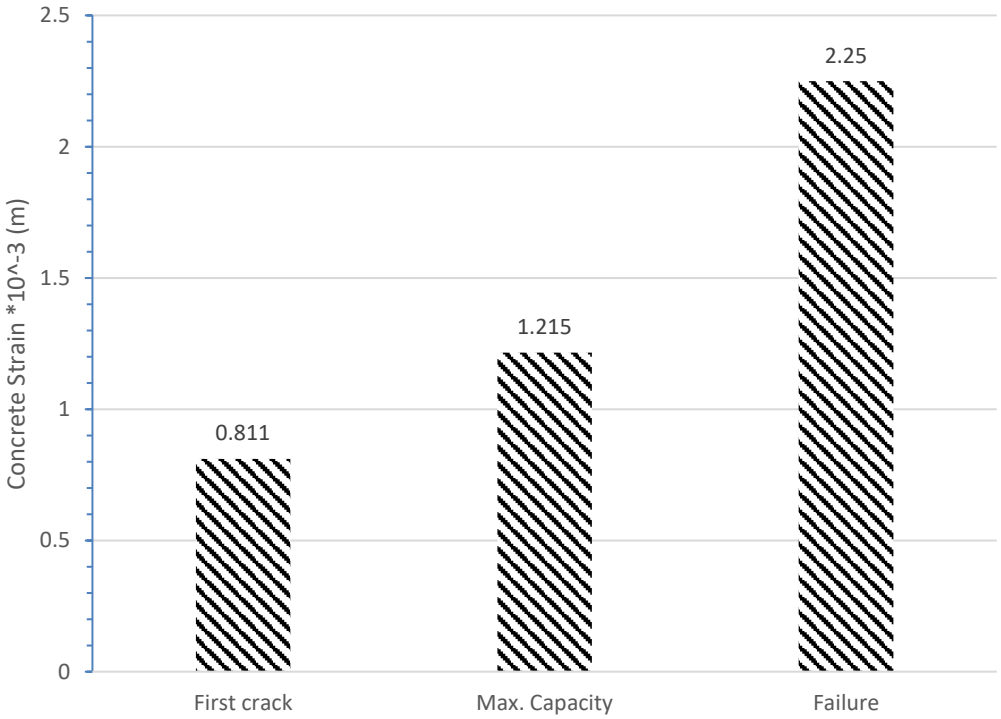

Figure (4-77): Concrete Strain at Three Phases for B9.

CHAPTER FIVE
DISCUSSION AND ANALYSIS OF EXPERIMENTAL RESULTS

5.1 Introduction

In this chapter, a detailed description will give to the experimental program; carried out on the present work, for testing of concrete beams reinforced by GFRP under torsion. Nine beams were loaded by torsion up to failure. Three measurements of the deflection, one near the first torsional arm in the right of section side, second in the left of the same section and third near the second torsional arm near the section side, electrical concrete strain in the compression and shear zone and ultimate torsion loads were recorded. The initiation and propagation of cracks up to failure were noticed and detected.

The aim of this chapter is to discuss the experimental results. The analysis of these results is important to study the torsional failure mechanisms with the static loading of concrete beams reinforced GFRP.

5.2 Discussion of Test Results

5.2.1 Effect Reinforcement on Torsion

This compression between B1 and B2, the two beams were had the same reinforcement by change the type of reinforcement. B1 reinforced by steel in longitude and transvers directions and B2 reinforced by GFRP in longitude and transvers directions, 2 φ 10 as a compression reinforcement and 2 φ 12 as a tensile reinforcement with spacing 150mm between stirrups with section 150*300 mm and concrete cover 20 mm. B1 and B2 had F_{cu} = 30.84 N/mm^2.

5.2.1.1 General Behavior and Cracking Patterns

Figure (5-1) shows the cracking patterns for both beams B1 and B2 tested beam after failure. In the Figure, each crack is marked by a line representing the direction of cracking.

Comparing the crack patterns between specimens revealed that they were variable. By checking B2 the crack took place in the left span near the torsional arm and continued to wide and few cracks only created around the same crack. The cracks for B2 were mainly in one crack and ruptured the stirrup, because of GFRP reinforcement the cracks continued in one place and the load distribution was difficult, but for B1, the cracks took place in the middle and continued over all the beam and the cracks came wider as shown in Figure (5-1). The main advantage fo using steel as a reinforcement was the distribution for cracks over all the beam for B1.

The experimental torsional moments are shown in Figure (5-2). Maximum capacity for beam (B1) was 13.29 KN.m, while maximum capacity for beam (B2) was 6.44 KN.m. By comparing results, it was clear that change of reinforcement types had big effect on the maximum capacity, the torsional moment which caused the first crack was bigger 34.8% for B1 torsional moment compression by torsional moment for B2, the maximum capacity for B1 increased 106.3% more than the maximum torsional moment for B2 and failure torsional moment for B1 increased 162.2% more than the failure torsional moment for B2. That clear that B1 had big torsional moment capacity in all phases. Steel reinforcement was effective than GFRP.

Figure (5-1): Cracks Pattern for Specimens B1 and B2.

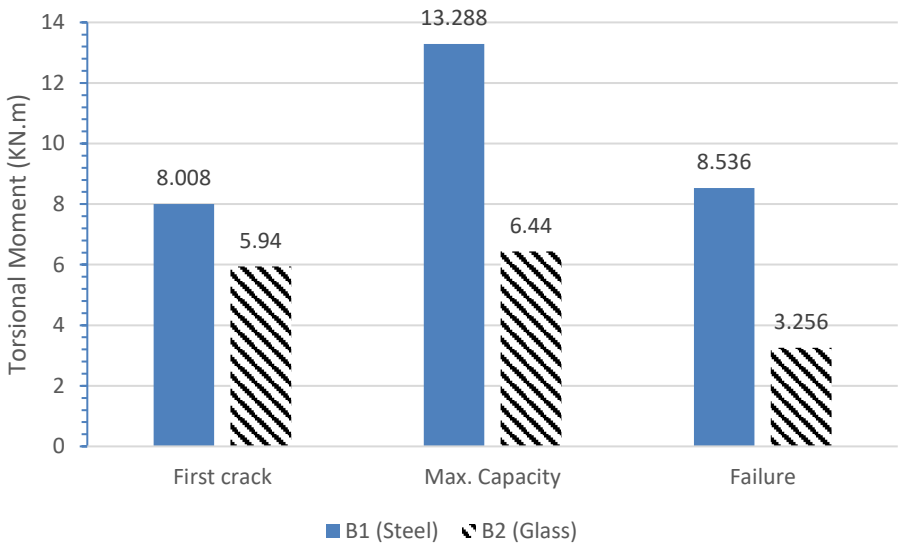

Figure (5-2): Experimental Torsional Moment for Specimens (B1 and B2).

5.2.1.2 Twist-torsional moment

Figure (5-3) and (5-4) show the twist-torsional moment for B1 and B2. The maximum twist for beam (B1) was $5.85*10^{-2}$ rad/m, while maximum twist for beam (B2) was $25.6*10^{-2}$ rad/m (the reason for making the twist of B2 was bigger was the loading with continuity to take measurements, graph was semi constant from $25.6*10^{-2}$ rad/m and the rigidity of steel and bond between steel and concrete had big effect on twist). By comparing results, the curve at the beginning had the same slope the indicated that the load at the beginning resisted by concrete beam section and after that the influence of reinforcement appeared, it was clear that change of reinforcement types had effect on the twist, the twist for B1 increased more than B2 in first crack and maximum capacities stages but for failure phase and the twist for B2 increased more than B1 by 4.4 times, the effect of bond between concrete and steel reinforcement in addition to rigidity of steel made the twist was more on beginning loading and incredible in failure on the other hand the weak bond of GFRP reinforcement and concrete (less bond than steel reinforcement and concrete) made the crack happened with less twist.

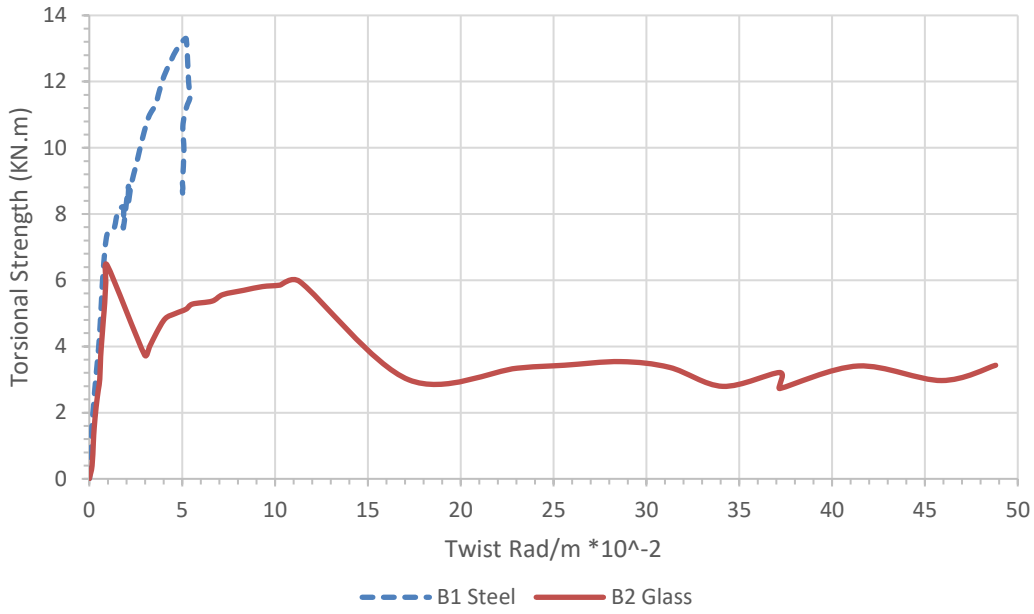

Figure (5-3): Twist-Torsional Moment Curve for B1 and B2.

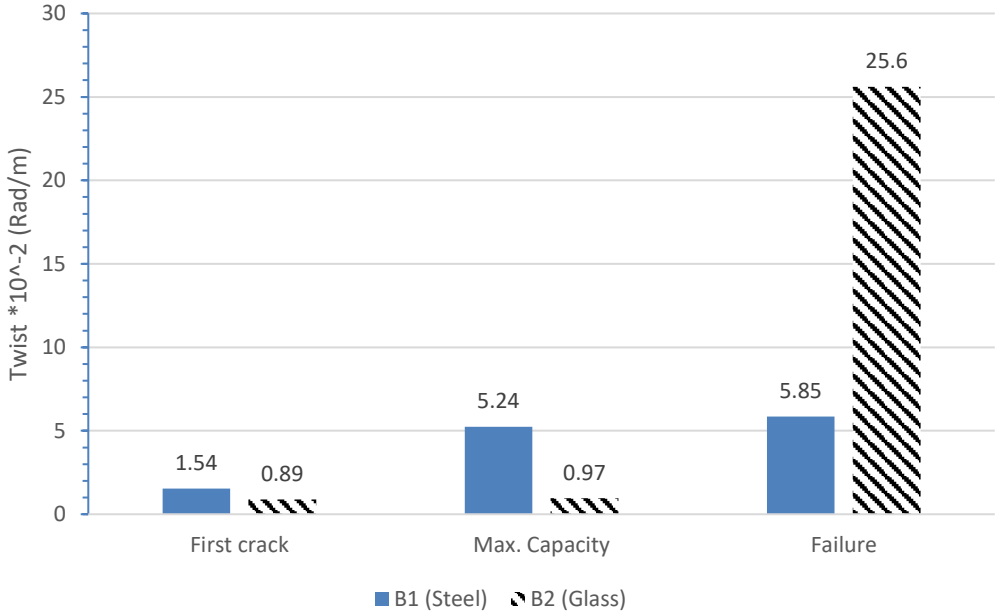

Figure (5-4): Twist for B1 and B2 at Three Phases.

5.2.2 Stirrups Effect on Torsion

This compression between B1 and B8, the two beams were had the same reinforcement in longitude direction by test B8 without stirrups. B1 reinforced by steel in longitude and transvers directions, 2 φ 10 as a

compression reinforcement and 2 φ 12 as a tensile reinforcement with spacing 150mm between stirrups with section 150*300 mm and concrete cover 20 mm. B1 and B8 had F_{cu} = 30 N/mm. B8 had the same reinforcement but without stirrups.

5.2.2.1 General Behavior and Cracking Patterns

Figure (5-5) shows the cracking patterns for both beams B1 and B8 (without stirrups) tested beam after failure. In the Figure, each crack is marked by a line representing the direction of cracking.

Comparing the crack patterns between specimens revealed that they were variable. By check B1, the cracks took place in the middle and continued over all the beam and the cracks came wider. Using steel as a reinforcement was the distribution for cracks over all the beam for B1. The cracks for B8 were mainly in few cracks, the first crack took place in middle and created another one near the first one in the same area and continued to be wider. After the first crack, the capacity grows little up and went down until failure. The main notice for B1, the torsion is over all of beam and continues.

The experimental torsional moments are shown in Figure (5-6). Maximum capacity for beam (B1) was 13.29 KN.m, while maximum capacity for beam (B8) was 5.478 KN.m. By comparing results, it was clear that using steel stirrups had big effect on the maximum capacity, the torsional moment which caused the first crack was smaller 47.4% for B8 torsional moment compression by torsional moment for B1, the maximum capacity for B8 decreased 142.6% from maximum torsional moment for B8 and failure torsional moment for B8 decreased 291.9% from failure torsional moment for B1. That clear that absent of steel stirrups decreased the capacity overall at all phases.

Figure (5-5): Cracks Pattern for Specimens B1 and B8

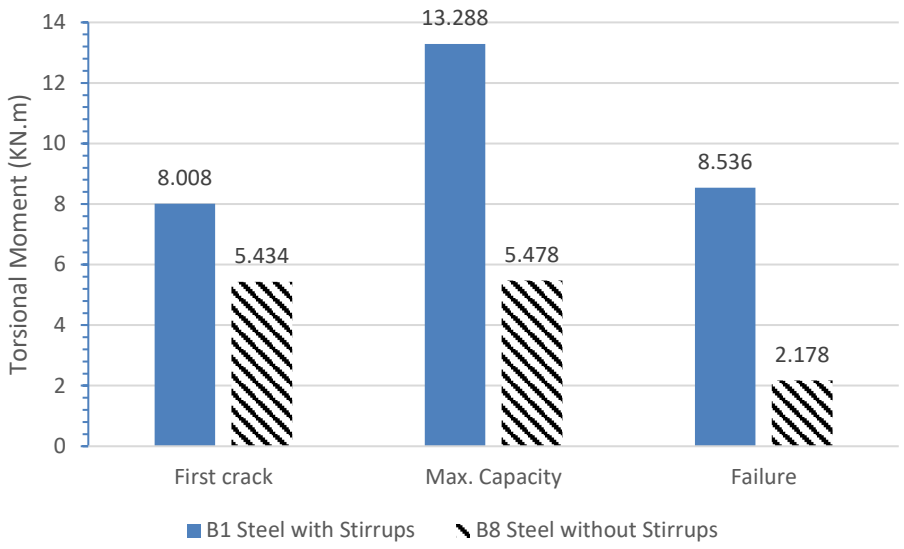

Figure (5-6): Experimental Torsional Moment for Specimens (B1 and B8).

5.2.2.2 Twist-Torsional Moment

Figure (5-7) shows the twist-torsional moment for B1 and B8. The maximum twist for beam (B1) was $5.85*10^{-2}$ rad/m, while maximum twist for beam (B8) was $7.8*10^{-2}$ rad/m. But the twist for the first crack was close. By comparing the results, it was clear that the effect of steel stirrups presents after the first crack and strict the grow of twist as shown in Figure (5-8) and (5-8).

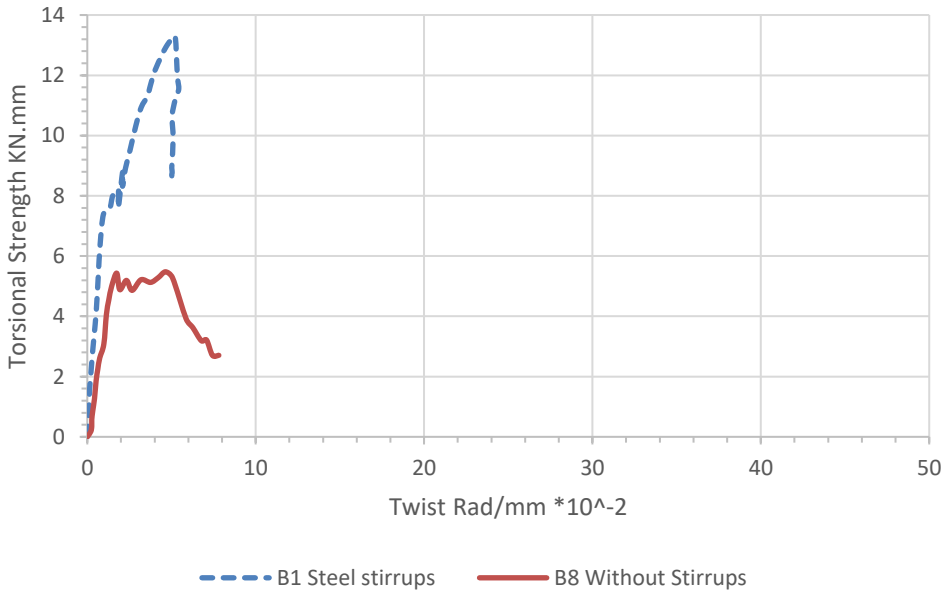

Figure (5-7): Twist-Torsional Moment Curve for B1 and B8.

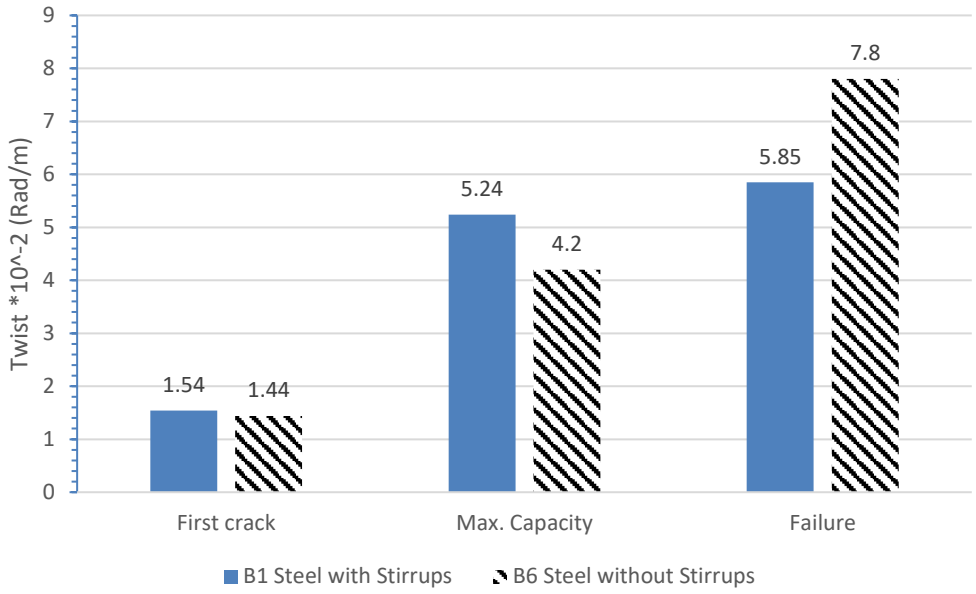

Figure (5-8): Twist for B1 and B8 at Three Phases.

5.2.3 Effect of Stirrups Spacing on Torsion

This compression between B2 and B3, the two beams were had the same reinforcement in longitude and transvers directions. B2 and B3 reinforced by GFRP in longitude and transvers directions, 2 φ 10 as a compression reinforcement and 2 φ 12 as a tensile reinforcement with spacing 150mm for B2 and 100mm for B3 between stirrups with section 150*300 mm and concrete cover 20 mm. B2 and B3 had F_{cu} = 30 N/mm.

5.2.3.1 General Behavior and Cracking Patterns

Figure (5-9) shows the cracking patterns for both beams B2 and B3 tested beam after failure. In the Figure, each crack is marked by a line representing the direction of cracking.

Comparing the crack patterns between specimens revealed that they were variable. By check B2, the crack took place in the left span near the torsional arm and continued to wide and few cracks only created around the same crack. The cracks for B2 were mainly in one crack and ruptured the stirrup, because of GFRP reinforcement the cracks continued in one

place and the load distribution was difficult. For B3 the cracks took place in the middle and continued around most of the beam (more than 70% of span) and the cracks became wider. Decreasing the spacing between stirrups made the distribution for cracks petter for B3. The cracks for B2 were mainly in few cracks (one main crack).

The experimental torsional moments are shown in Figure (5-10). Maximum capacity for beam (B2) was 6.44 KN.m, while maximum capacity for beam (B3) was 7.88 KN.m. By comparing results, it was clear that decreasing the spacing had good effect on the maximum capacity. The torsional moment which caused the first crack for B3 was 63% from torsional moment for B2, the maximum capacity for B3 increased 20.9% from maximum torsional moment of B3 and failure torsional moment for B3 increased 71.65% from failure torsional moment of B2. That clear decrease spacing of stirrups increases the maximum and failure capacities.

5.2.3.2 Twist-Torsional Moment

Figure (5-11) shows the twist-torsional moment for B2 and B3. The maximum twist for beam (B2) was $48.8*10^{-2}$ rad/m but was semi constant from $25.6*10^{-2}$ rad/m so can consider maximum twist $25.6*10^{-2}$ rad/m, while maximum twist for beam (B3) was $19.8*10^{-2}$ rad/m. The twist at maximum capacity for B3 had noted difference than twist at first crack stage but for twist of B2 both stages were semi the same the decreasing in stirrups spacing improve the twist behavior and made B3 carried more capacity and twist after first crack. At failure case, the twist of B2 and B3 didn't have more difference. It is clear good effect for increasing transverse reinforcement, made a good behavior for twist as shown in Figure (5-12).

Figure (5-9): Cracks Pattern for Specimens B2 and B3.

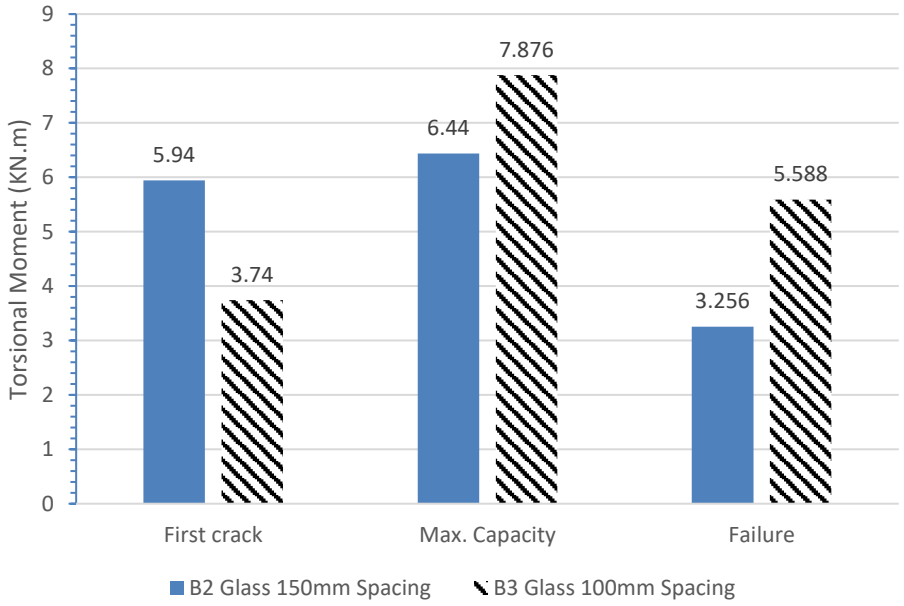

Figure (5-10): Experimental Torsional Moment for Specimens (B2 and B3).

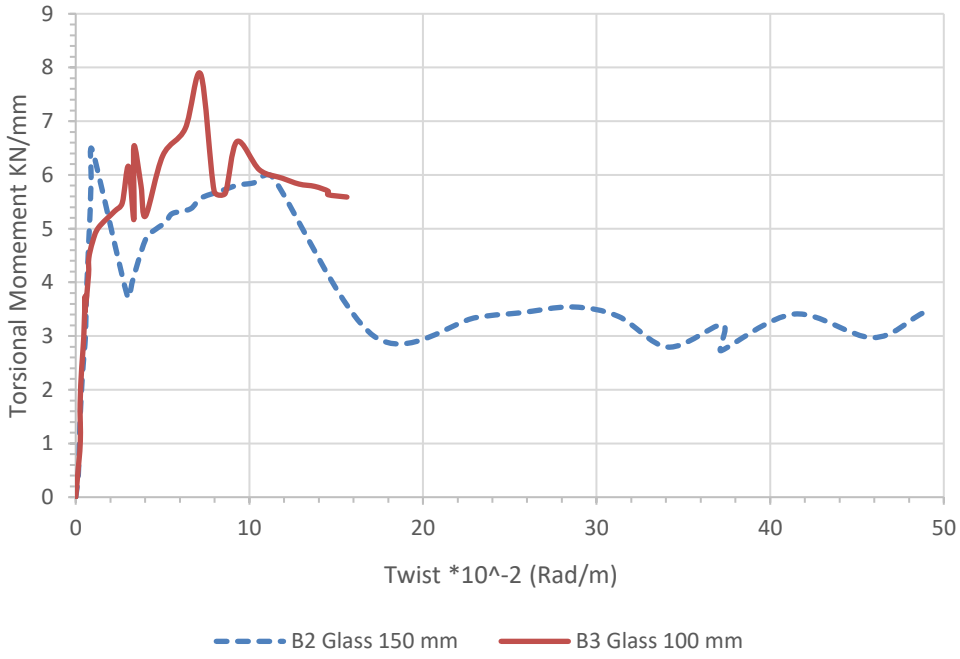

Figure (5-11): Twist-Torsional Moment Curve for B2 and B3.

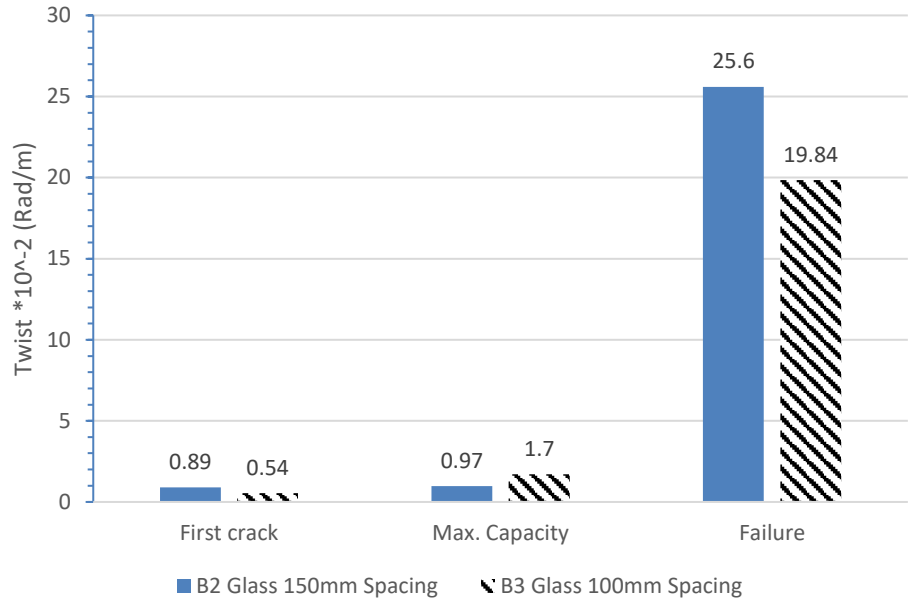

Figure (5-12): Twist for B2 and B3 at Three Phase.

5.2.4 Effect Adding Side Reinforcement Effect on Torsion

This compression between B2 and B4, the two beams were had the same reinforcement by adding 1 φ 8 GFRP bar for each side for B4. B2 and B4 reinforced by GFRP in longitude and transvers directions, 2 φ 10 as a compression reinforcement and 2 φ 12 as a tensile reinforcement with spacing 150mm between stirrups with section 150*300 mm and concrete cover 20 mm. B2 and B4 had F_{cu} = 30 N/mm.

5.2.4.1 General Behavior and Cracking Patterns

Figure (5-13) shows the cracking patterns for both beams B2 and B4 tested beam after failure. In the Figure, each crack is marked by a line representing the direction of cracking. Comparing the crack patterns between specimens revealed that they were variable. By check B2 the crack took place in the left span near the torsional arm and continued to wide and few cracks only created around the same crack. The cracks for B2 were mainly in one crack and ruptured the stirrup, because of GFRP reinforcement the cracks continued in one place and the load distribution was difficult, but for B4, the cracks took place in the middle and continued

over big area of the beam and the cracks came wider as shown in Figure (5-13). The main advantage for adding 1 φ 8 GFRP bar as a side reinforcement made decreased the distance between bars which improved the distribution for cracks for B4.

The experimental torsional moments are shown in Figure (5-14). Maximum capacity for beam (B2) was 6.44 KN.m, while maximum capacity for beam (B4) was 6.93 KN.m. By comparing results, it was clear that adding 1 φ 8 GFRP bar as a side reinforcement for both sides had little effect on the maximum capacity, the torsional moment which caused the first crack was bigger 16.7% for B4 torsional moment compression by torsional moment for B2, the maximum capacity for B4 increased 7.6% from maximum torsional moment for B2 and failure torsional moment for B4 increased 28.8% from failure torsional moment for B2. That clear that B4 had a big torsional moment capacity in all phases. Adding 1 φ 8 GFRP bar as a side reinforcement was effective, it made a good crack distribution and made the beam carry little more capacity. By comparing the difference between the values in Figure (5-14), the effect of adding side bars didn't affect torsional strength but improved the cracks distributions.

5.2.4.2 Twist-Torsional Moment

Figure (5-15) shows the twist-torsional moment for B2 and B4. The twist for beam (B2) was $0.89*10^{-2}$ rad/m and $0.97*10^{-2}$ rad/m, while twist for beam (B4) was $2.18*10^{-2}$ rad/m, respectively, with visible first crack and maximum stages, which clearly the adding 1 φ 8 GFRP bar as a side reinforcement had effect on the twist by improving the twist and made the specimen more unity, the twist for B4 increased more than B2 in first crack and maximum capacities phases and at the end the twist of B2 was more than B4 around one time as shown in Figure (5-16).

Figure (5-13): Cracks Pattern for Specimens B2 and B4.

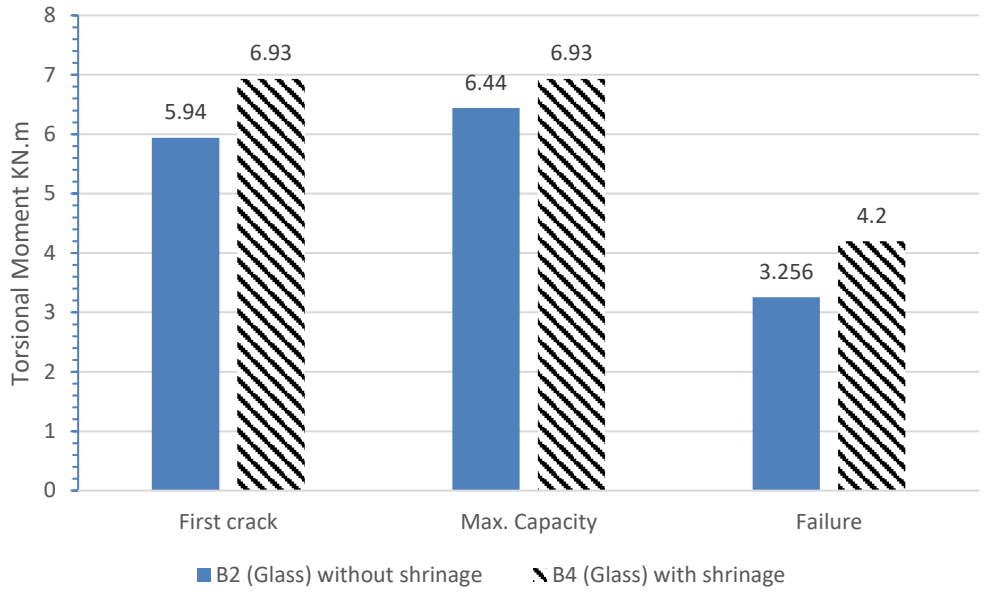

Figure (5-14): Experimental Torsional Moment for Specimens (B2 and B4)

Figure (5-15): Twist-Torsional Moment Curve for B2 and B4.

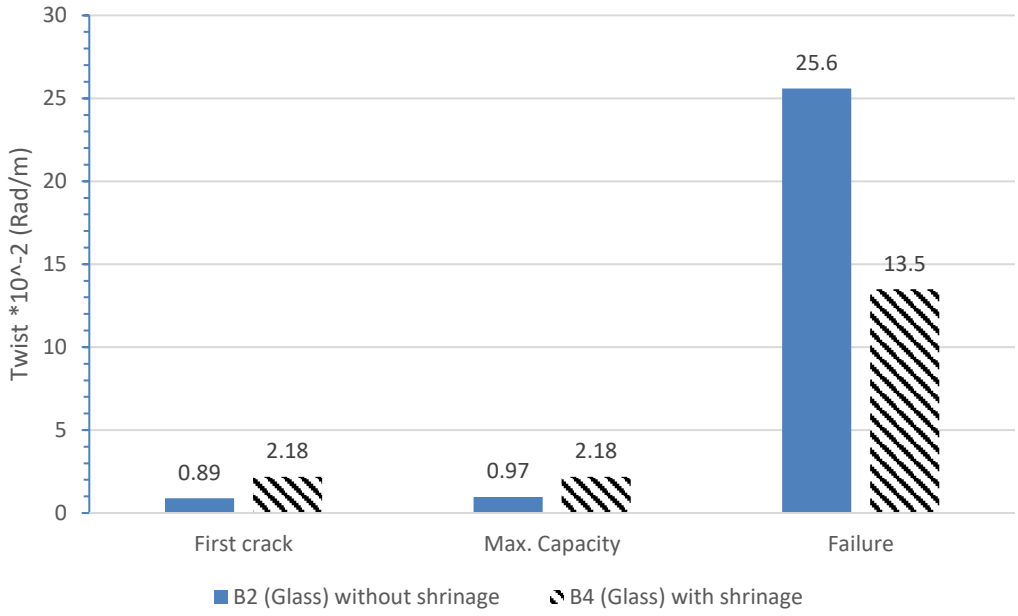

Figure (5-16): Twist for B2 and B4 at Three Phases.

5.2.5 The Load Effect in The Beams with GFRP Stirrups

This compression between B2 and B5, the two beams had the same reinforcement. The beams reinforced by GFRP in longitude and transvers directions, 2 φ 10 as a compression reinforcement and 2 φ 12 as a tensile reinforcement with spacing 150mm between stirrups with section 150*300 mm and concrete cover 20 mm. B2 and B5 had F_{cu} = 30 N/mm but B2 tested under torsion only and B5 tested under torsional and bending moments.

5.2.5.1 General Behavior and Cracking Patterns

Figure (5-17) shows the cracking patterns for both beams B2 and B5 tested beam after failure, the boundary conditions were different as shown which create change in the expected and logical results. In the Figure, each crack is marked by a line representing the direction of cracking. Comparing the crack patterns between specimens revealed that they were variable. By checking B2 the crack took place in the left span near the torsional arm and continued to wide and few cracks only created around the same crack.

The cracks for B2 were mainly in one crack and ruptured the stirrup, because of GFRP reinforcement the cracks continued in one place and the load distribution was difficult, this happened because of the non-homogenousty and the natural of GFRP made the once the crack happened decreased the stiffness and the load traded to the weakest point in the stirrups corner and didn't distribute for the same reason, on the other side B5, the cracks took place around the torsional arm and continued in the same cracks and came wider and few cracks only created around the same cracks and in back side because the accumulation of three forces (shear force, torsional and bending moment) in one location mad the cracks happened in this location and main two cracks because the arm held the beam from two sides as shown in Figure (5-17).

The experimental torsional moments are shown in Figure (5-18). Maximum capacity for beam (B2) was 6.44 KN.m, while maximum capacity for beam (B5) was 11.836 KN.m. By comparing results, it was clear that change of load types had little effect on the capacity, the torsional moment which caused the first crack was bigger 16.2% for B5 torsional moment compression by torsional moment for B2, but the maximum capacity and failure torsional moment for B5 was bigger than B2 which is against the expected and logical results due to change in the boundary conditions.

5.2.5.2 Twist-Torsional Moment

Figures (5-19) and (5-20) show the twist-torsional moment and twist chart for B2 and B5.

Figure (5-17): Cracks Pattern for Specimens B2 and B5

The maximum twist for beam (B2) was $48.4*10^{-2}$ rad/m, while maximum twist for beam (B5) was $21.7*10^{-2}$ rad/m the reason for making the twist of B2 was bigger was the loading with continuity to take measurements, the graph was semi constant after $25.6*10^{-2}$ rad/m but for B5 with more loading might be the specimen would fail but not semi constant like B2, the graph would go sharp to down that because B2 had one load type (torsional moment) but B5 had accumulation of forces (shear force, torsional and bending moments) which will rapid the twist rate with loading, the twist for first crack stage for B5 was 5.4 times B2 and 10.7 times for maximum capacity stage. By comparing results, it was clear that change of load types and boundary conditions had effect on the twist, the twist for B5 increased more than B2 in first crack, maximum capacity and failure phases. The effects for adding bending moment and shear force were clear, increased the twist too much.

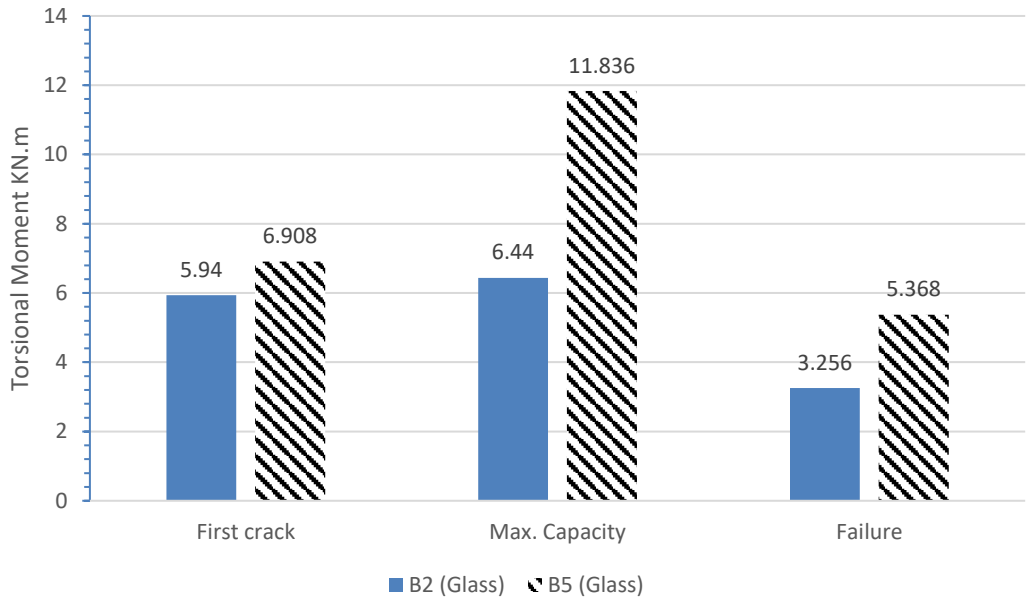

Figure (5-18): Experimental Torsional Moment for Specimens (B2 and B5).

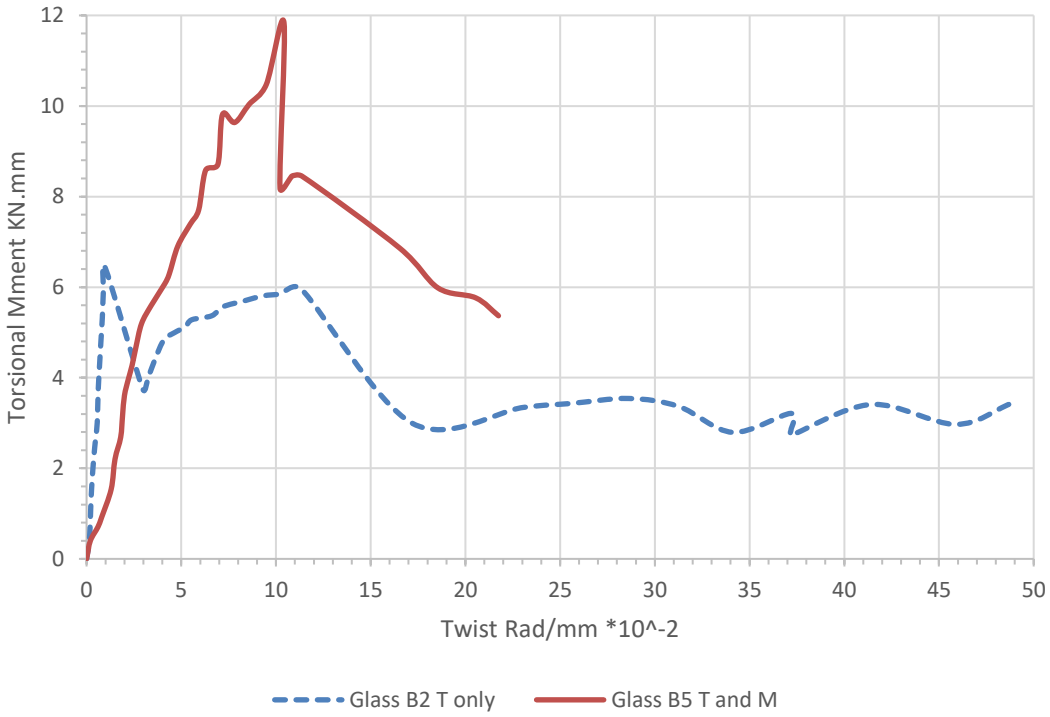

Figure (5-19): Twist-Torsional Moment Curve for B2 and B5.

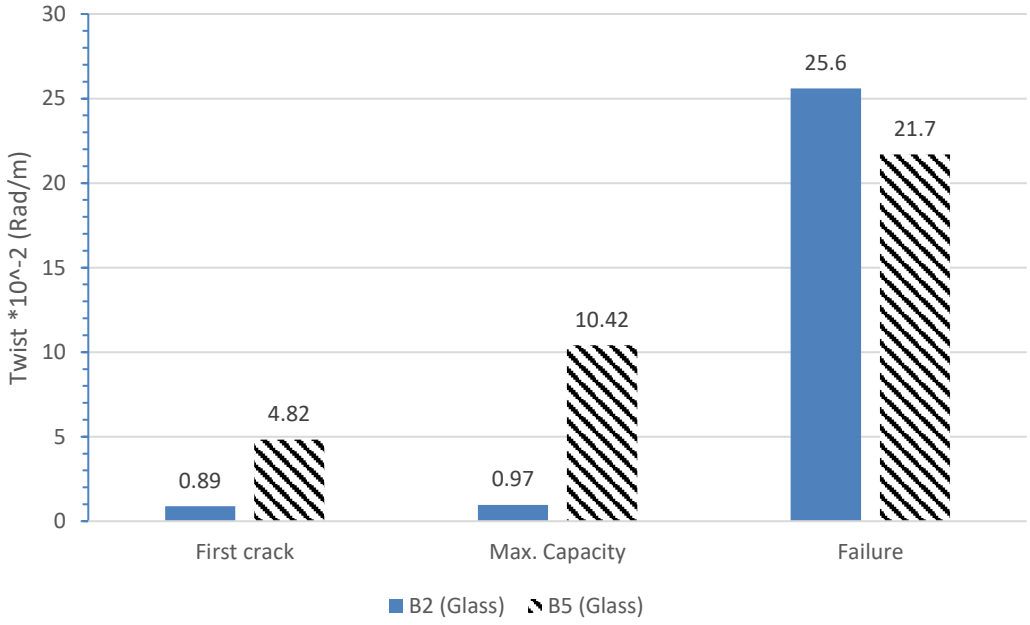

Figure (5-20): Twist for B2 and B5 at Three Phases.

5.2.6 Effect of Stirrup Configurations on Torsion

This compression between B2 and B6, the two beams were had the same reinforcement by change inclined the stirrup of B6. B2 and B6 reinforced

by GFRP in longitude and transvers directions, 2 φ 10 as a compression reinforcement and 2 φ 12 as a tensile reinforcement with spacing 150mm between stirrups with section 150*300 mm and concrete cover 20 mm. B2 and B6 had F_{cu} = 30 N/mm.

5.2.6.1 General Behavior and Cracking Patterns

Figure (5-21) shows the cracking patterns for both beams B2 and B6 tested beam after failure. In the Figure, each crack is marked by a line representing the direction of cracking. Comparing the crack patterns between specimens revealed that they were variable. By check B2 the crack took place in the left span near the torsional arm and continued to wide and few cracks only created around the same crack. The cracks for B2 were mainly in one crack and ruptured the stirrup, because of GFRP reinforcement the cracks continued in one place and the load distribution was difficult, but for B6, the cracks took place in the middle off span parallel to incline of stirrups but in half of beams and continued in the same area and the cracks came wider as shown in Figure (5-21). The main notice, the torsion is over all of beam and continues so it petter to make the stirrups vertical.

The experimental torsional moments are shown in Figure (5-22). Maximum capacity for beam (B2) was 6.44 KN.m, while maximum capacity for beam (B6) was 5.236 KN.m. By comparing results, it was clear that making inclined stirrups had slight effect on the maximum capacity, the torsional moment which caused the first crack was smaller 16.4% for B6 torsional moment compression by torsional moment for B2, the maximum capacity for B6 decreased 23% from maximum torsional moment for B2 and failure torsional moment for B6 decreased 11.3% from failure torsional moment for B2. That clear that B6 had small torsional moment capacity in all phases. Inclining of stirrups was slighted effective,

it made the beam carried less capacity because same cracks is parallel to the transvers reinforcement.

Figure (5-21): Cracks Pattern for Specimens B2 and B6.

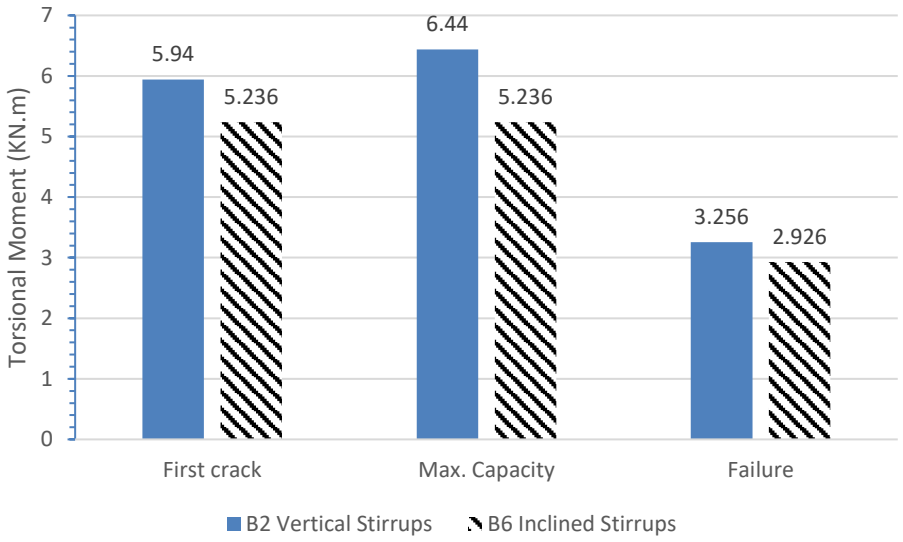

Figure (5-22): Experimental Torsional Moment for Specimens (B2 and B6).

5.2.6.2 Twist-Torsional Moment

Figure (5-23) shows the twist-torsional moment for B2 and B6. The maximum twist for beam (B2) was $25.6*10^{-2}$ rad/m, while maximum twist for beam (B6) was $13.1*10^{-2}$ rad/m, the twist of B2 and B6 were semi the same with first crack, $0.89*10^{-2}$ rad/m and $1.3*10^{-2}$ rad/m, and also for maximum capacity stage,$0.97*10^{-2}$ rad/m and $1.3*10^{-2}$ rad/m, in addition to B6 didn't carry more torsional load after first crack that is because the torsional moment was hold by beam section properties; the inclining stirrups made the spiral torsional crack met the stirrups in the same angle so the stirrups was useless as shown in Figure (5-24).

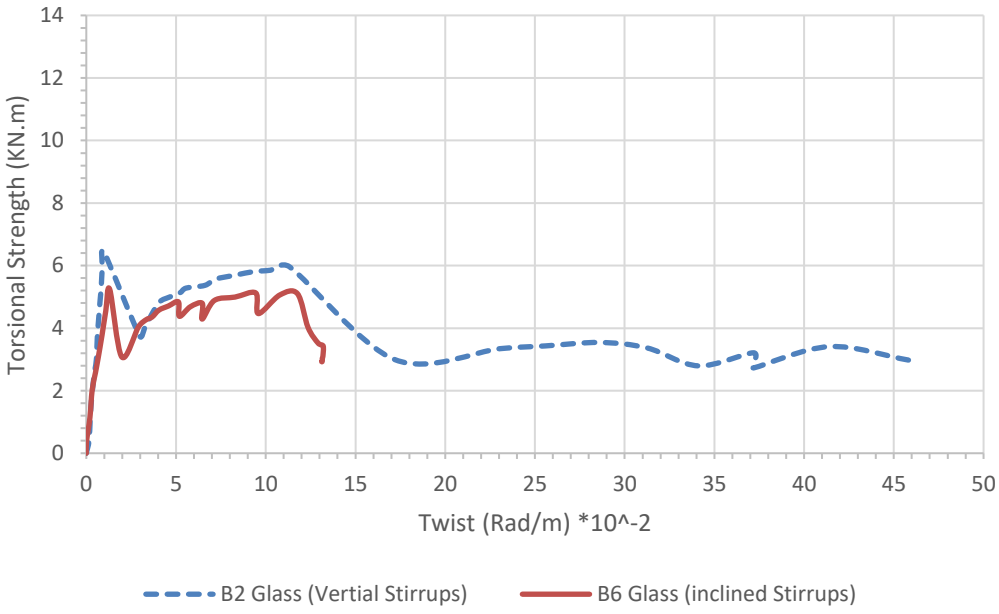

Figure (5-23): Twist-Torsional Moment Curve for B2 and B6.

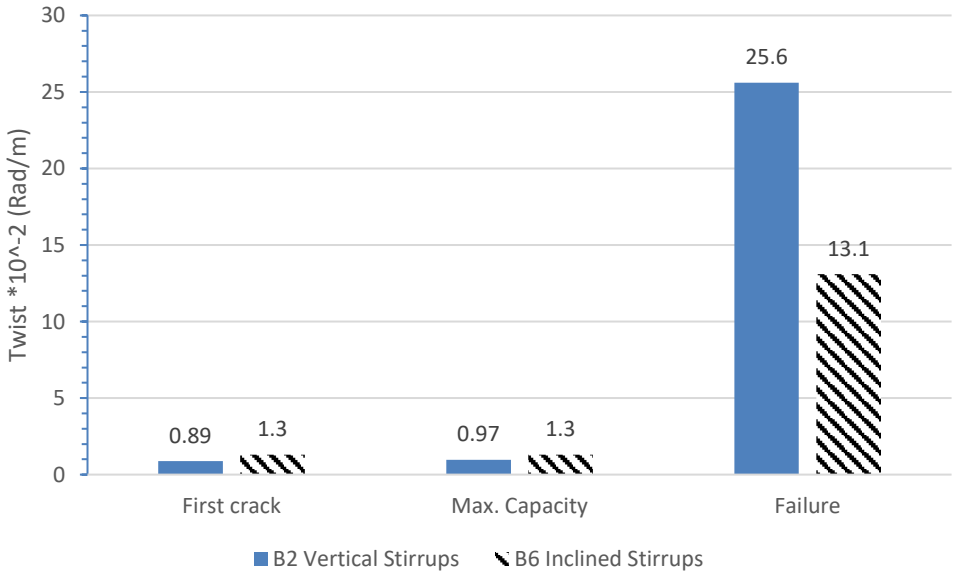

Figure (5-24): Twist for B2 and B6 at Three Phases.

5.2.7 The Effect of Concrete Strength

This compression between B2 and B7, the two beams had the same reinforcement. The beams reinforced by GFRP in longitude and transvers directions with 2 φ 10 as a compression reinforcement and 2 φ 12 as a tensile reinforcement with section 150*300 mm and concrete cover 20 mm. B2 had F_{cu} = 30 MPa but B7 had F_{cu} = 50 MPa.

5.2.7.1 General Behavior and Cracking Patterns

Figure (5-25) shows the cracking patterns for both beams B2 and B7 test beam after failure. In the Figure, each crack is marked by a line representing the direction of cracking. Comparing the crack patterns between specimens revealed that they were close. By check B2 the crack took place in the left side span near the torsional arm and continued in the same crack and came wider and few cracks only created around the same crack, but for B7 the crack took place in the right side of span near the torsional arm and continued in the same crack and came wider and few cracks only created around the same crack but more numbers than B2. Both beams had ruptured in one stirrup which had crack, GFRP stirrups ruptured in the corner of stirrups as took place in the beams as shown in Figure (5-26-a) and (5-26-b).

The experimental maximum torsional moment is shown in Figure (5-27). Maximum capacity for beam (B2) was 6.44 KN.m, while maximum capacity for beam (B6) was 7.326 KN.m. By comparing results, it was clear that concrete strength had little effect on the capacity, the torsional moment increased 13.8% from B2 torsional moment by increasing 66.7% concrete strength. Also, the torsional moment which caused first visible crack for B7 was bigger than B2 by 23.3% from B2 torsional moment. But noticed that B7 after first crack the capacity went down without reach to the same capacity again may be that because of the more strength for B7. For the load failure it couldn’t been study well, because we removed the laboratory instruments (LVDT) as it might be happening unexpected failure that might be damage LVDT, it may be taking more time to fail B2 but that would take more risk for laboratory instruments.

Figure (5-25): Cracks Pattern for Specimens B2 and B7.

Figure (5-26-a) Rupture in Stirrups for Specimen B2.

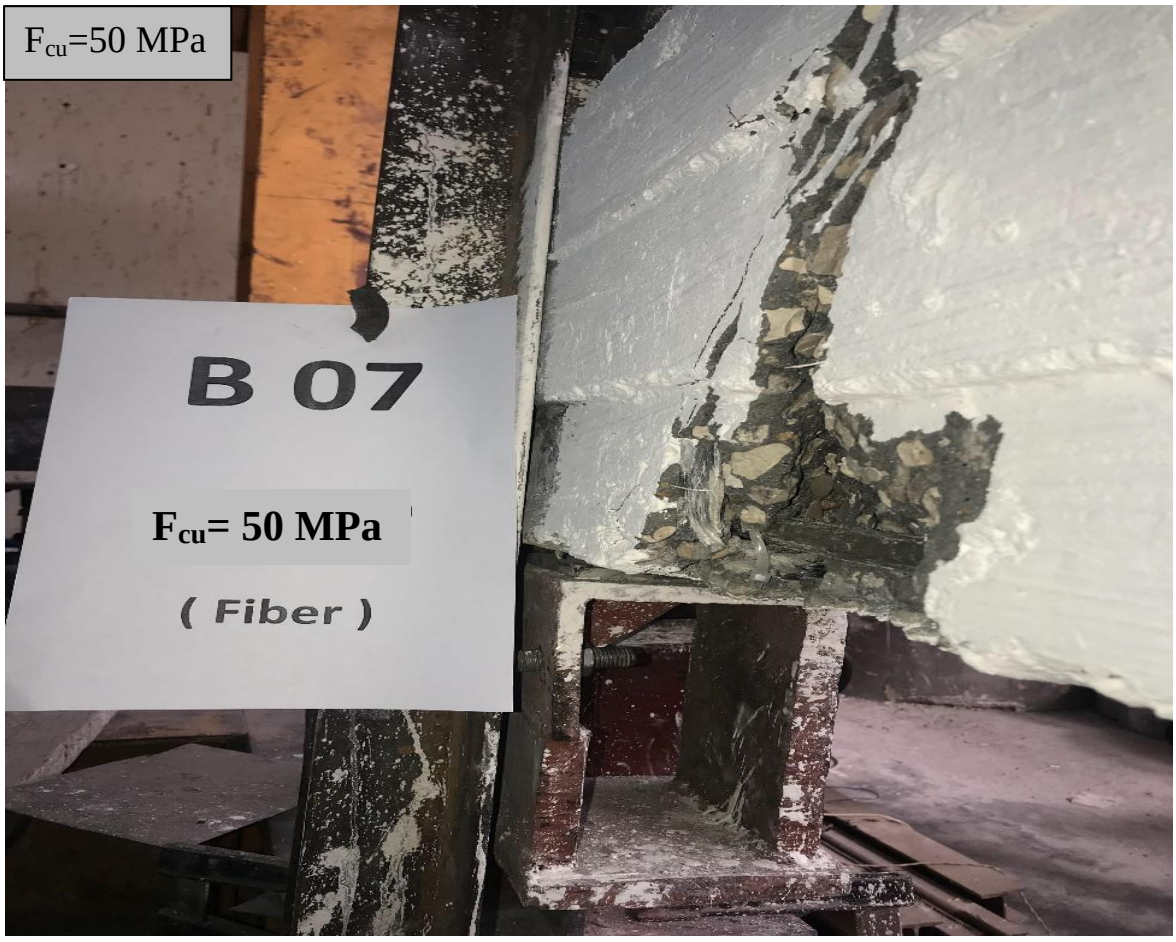

Figure (5-26-b) Rupture in Stirrups for Specimen B7.

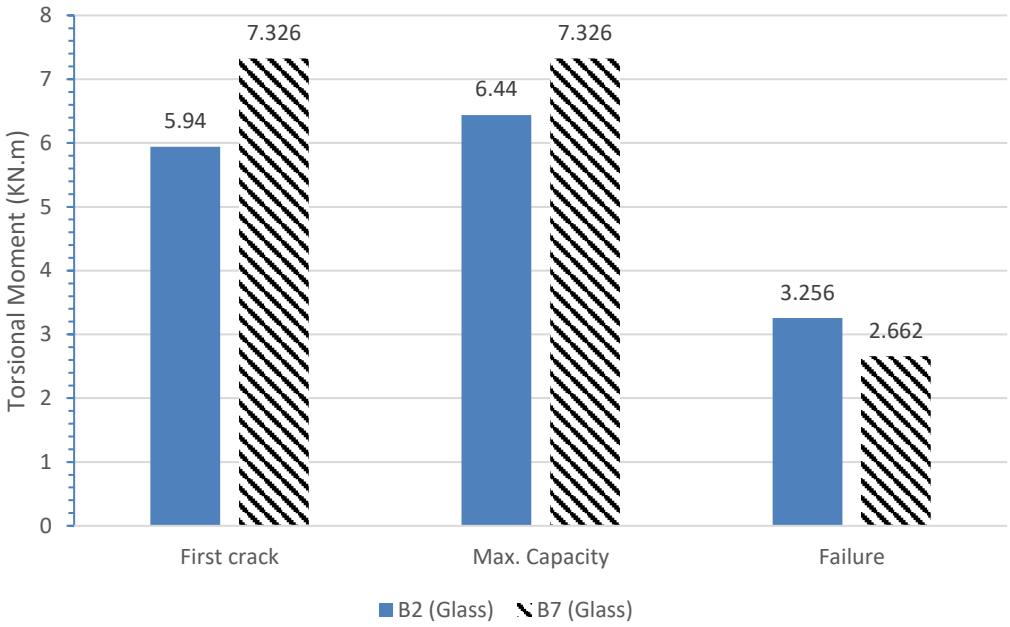

Figure (5-27) Experimental Torsional Moment for Specimens (B2 and B7).

5.2.7.2 Twist-Torsional Moment

Figures (5-28) and (5-29) show the twist-torsional moment for B2 and B7. The maximum twist for beam (B2) was $25.6*10^{-2}$ rad/m, while maximum twist for beam (B7) was $14.4*10^{-2}$ rad/m, for first and maximum capacities stage the twist were the same for B7 $2*10^{-2}$ rad/m and increased 9 % (from $0.89*10^{-2}$ rad/m to $0.97*10^{-2}$ rad/m) for B2 and in both stage the twist of B7 were little more. By comparing the results, it was clear that concrete strength had effect on the twist of beam, the twist increased for B2, which has low concrete strength, by 66.7% concrete strength from B7 concrete strength. The effect of strength increasing was clear, the increasing in concrete strength made the beam more rigid which reflected on the twist of beam (B7), made the crack for B7 at failure was little (56.25 % of B2 twist at failure) and the for first and maximum capacities stage the twist were the same for B7, the first crack met twist $2*10^{-2}$ rad/m more B2 which the resistance concrete resistance was more for B7 than B2.

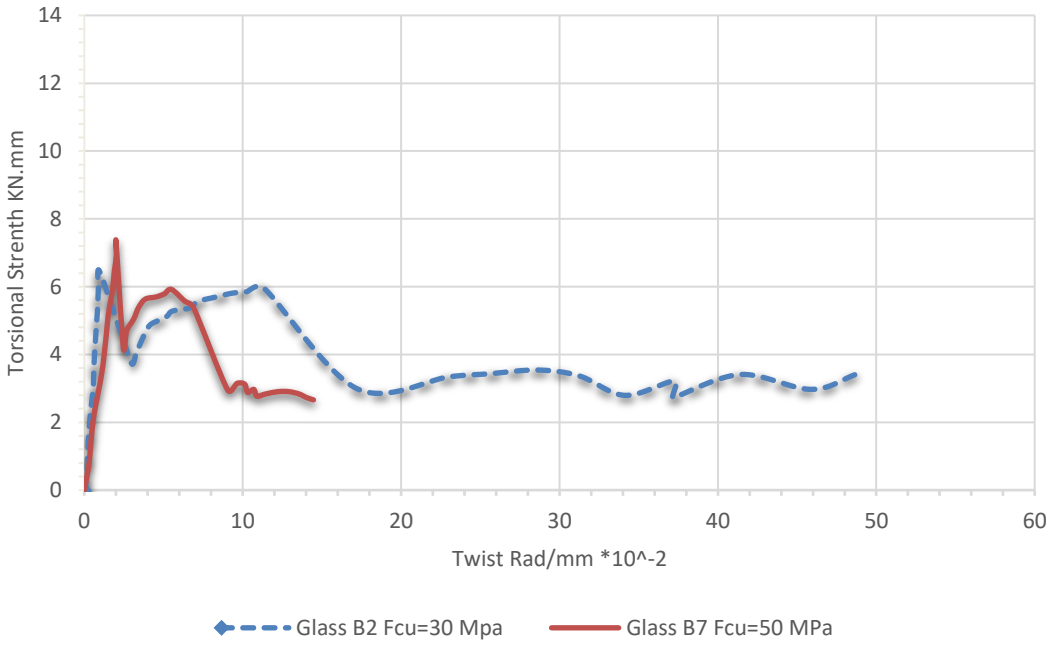

Figure (5-28) Twist-Torsional Moment Curve for B2 and B7.

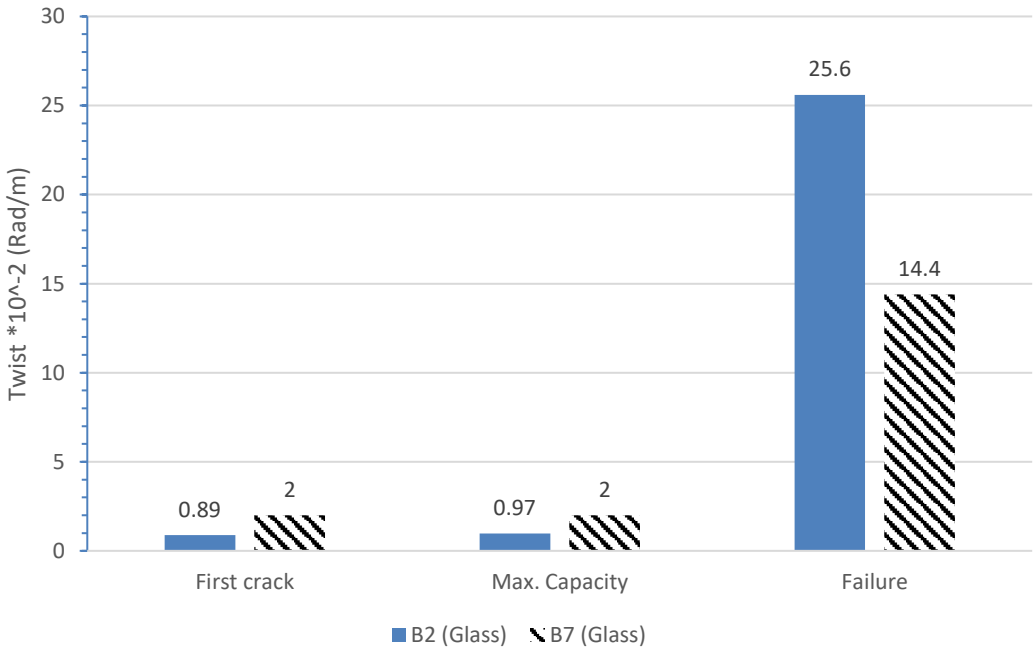

Figure (5-29) Twist for B2 and B7 at Three Phases.

5.2.8 The Load Effect in The Beams without Stirrups

This compression between B8 and B9, the two beams had the same reinforcement. The beams reinforced by steel in longitude direction without stirrups, 2 φ 10 as a compression reinforcement and 2 φ 12 as a tensile reinforcement with section 150*300 mm and concrete cover 20 mm.

B8 and B9 had F_{cu} = 30 N/mm^2 but B8 tested under torsion only and B9 tested under torsional, bending moments and shear forces.

5.2.8.1 General Behavior and Cracking Patterns

Figure (5-30) shows the cracking patterns for both beams B8 and B9 tested beam after failure. In the Figure, each crack is marked by a line representing the direction of cracking.

Comparing the crack patterns between specimens revealed that they were variable. By check B8 the crack took place in the middle span and continued to produce another crack near it but wider (all cracks in one zone) in the same crack and came wider and few cracks only created around the same crack, that has happened because the specimen was without stirrups and under pure torsion caused the cracks in one location, but for B9, the crack took place in the left side of span near the fixed torsional arm and two cracks around torsional arm and continued in the same cracks and came wider and few cracks only created around the same cracks. B9 had more cracks in more location because it was tested under shear force, bending and torsional moments caused the cracks were created near fixed torsional arm and near of concentrated load.

The experimental torsional moments are shown in Figure (5-31). Maximum capacity for beam (B8) was 5.478 KN.m, while maximum capacity for beam (B9) was 11.97 KN.m. By comparing results, it was clear that change of load types had bigger effect on the capacity, the maximum torsional moment for B9 increased from B8 maximum torsional moment, for first torsional moment, B9 increased 104.8% from B9 and at failure the torsional moment increased 148.8% from B9. That noticed that the bending moment cased height in torsional moment capacity.

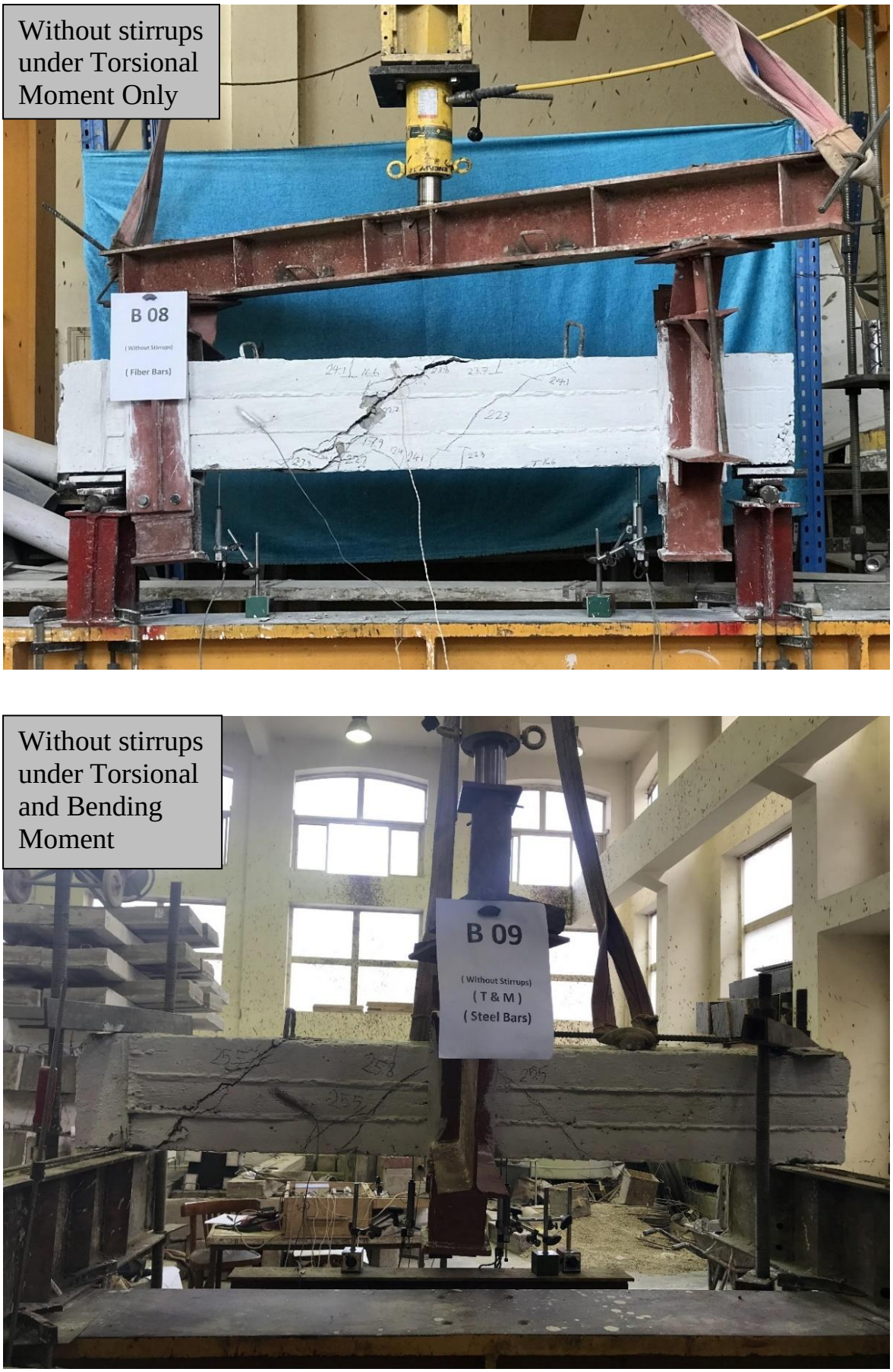

Figure (5-30) Cracks Pattern for Specimens B8 and B9.

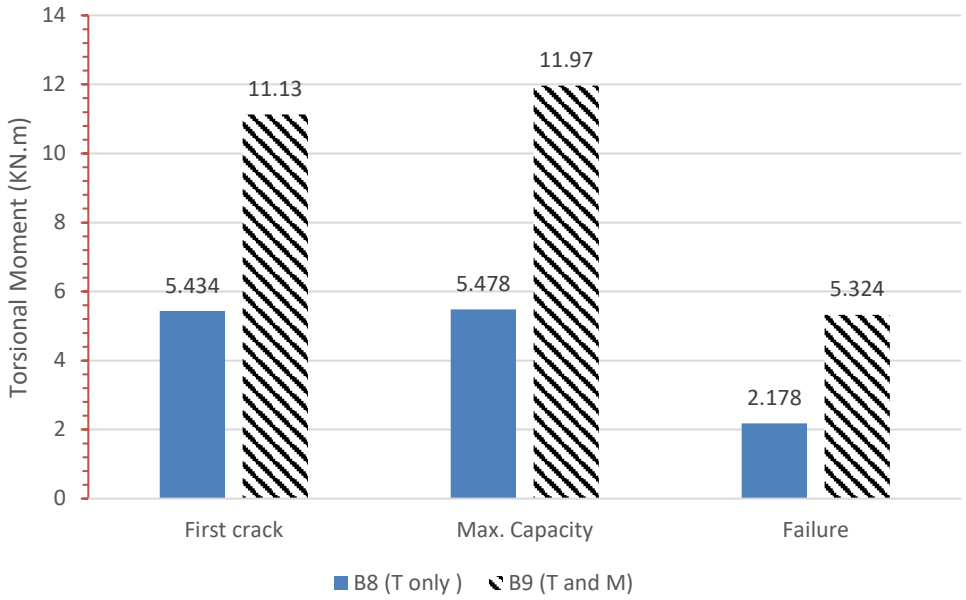

Figure (5-31) Experimental Torsional Moment for Specimens (B8 and B9).

5.2.8.2 Twist-Torsional Moment

Figure (5-32) shows the twist-torsional moment for B8 and B9. The maximum twist for beam (B8) was $7.8*10^{-2}$ rad/m, while maximum twist for beam (B9) was $18.1*10^{-2}$ rad/m. By comparing results, it was clear that change of load types had effect on the twist, the twist for B9 increased more than B8. For first crack phase, the twist for B9 increased 560% more than twist for B8, for maximum capacity phase, the twist increased 227.4% more than B8 twist and at failure the twist for B9 increased 132% more than the twist for B8 as shown in Figure (5-33). The effect for adding bending moment was clear, the twist of B9 was bigger than B8 in all phases.

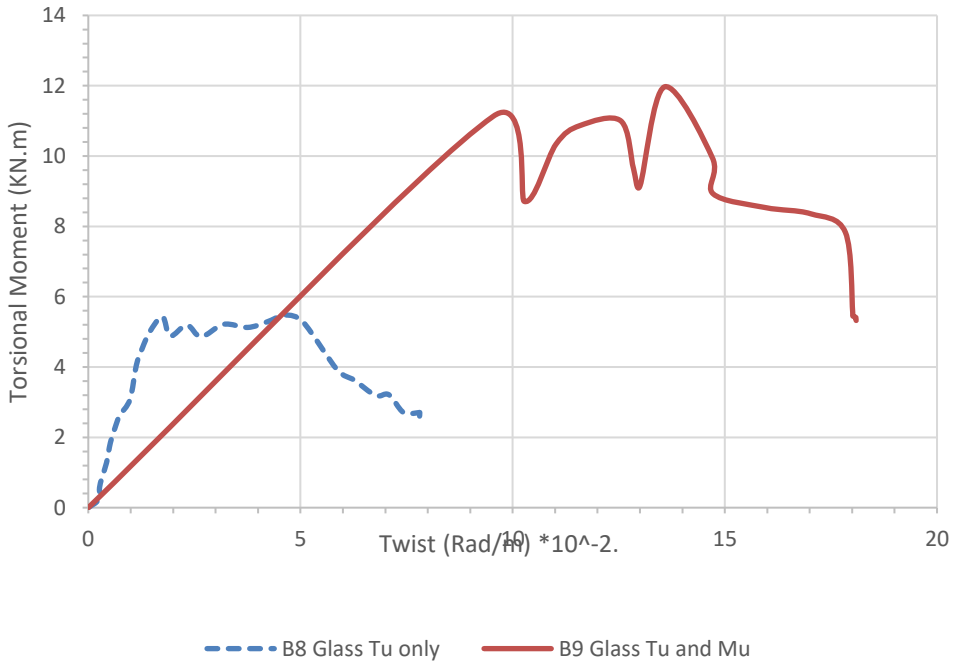

Figure (5-32) Twist-Torsional Moment Curve for B8 and B9.

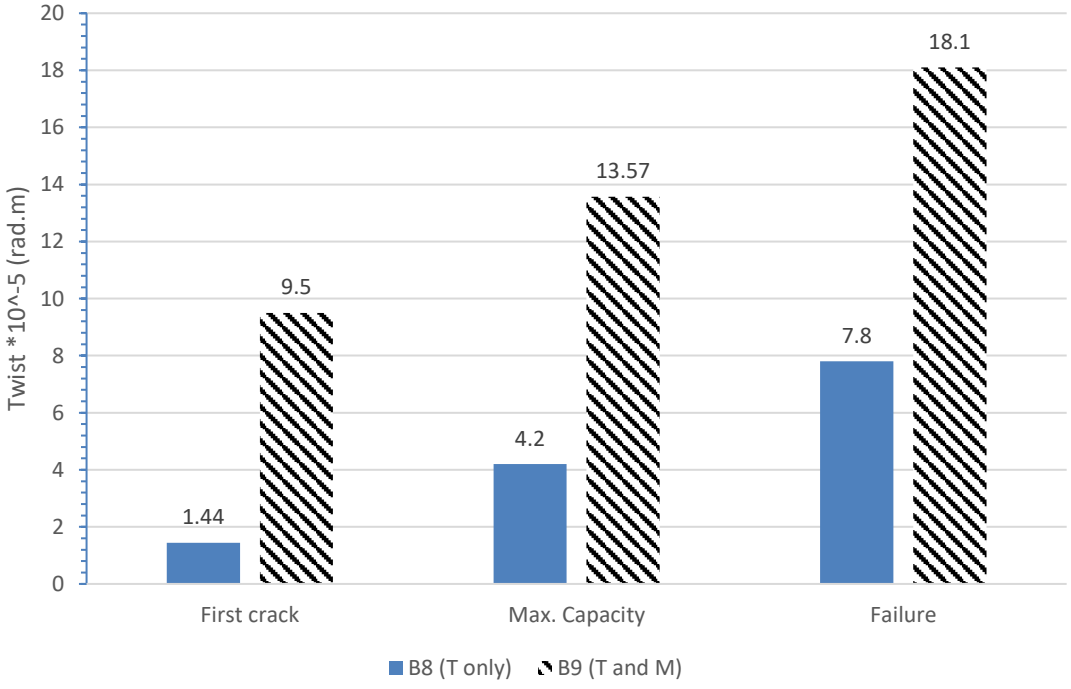

Figure (5-33) Twist for B8 and B9 at Three Phases.

CHAPTER SIX

ANALYTICAL EQUATIONS AND COMPARISON WITH TEST RESULTS

6.1 Introduction

The current research program is conducted to investigate the effect of using GFRP replacing to steel as reinforcement in longitudinal and traverses directions, change of concrete strength, stirrups configuration, spacing between stirrups, absent of stirrups, adding side bars and adding another load types for beams with and without stirrups. On the other side of research beams should be designed to make a comparison between empirical results and theoretical results and conclude new experimental factors. This Chapter contents the design of every beam by using ACI code and ECP code.

6.2 Theoretical Shear Equations

Beams will be solved as shear design for beam according to the ACI 318M-19, ECP 203-2018 and CSA A23.3-04 codes.

6.2.1 ACI Code-Torsion equations

According to the ACI Code, torsion beams must be designed using the following relationship.

$$\tau = \frac{T}{2A_0 t} \quad \textbf{Eq. (6.1)}$$

$$t = 0.75\frac{A_{cp}}{P_{cp}} \quad \textbf{Eq. (6.2)}$$

$$A_o = \frac{2A_{cp}}{3} \quad \textbf{Eq. (6.3)}$$

$$T_u \geq \varphi T_{cr} \quad \textbf{Eq. (6.4)}$$

$$T_u \geq \varphi T_{th} \quad \textbf{Eq. (6.5)}$$

$$T_{th} = 0.085\lambda\sqrt{f'_c}\left(\frac{A_{cp}^2}{P_{cp}}\right) \quad \textbf{Eq. (6.6)}$$

$$T_{cr} = 0.33\lambda\sqrt{f'_c}\left(\frac{A_{cp}^2}{P_{cp}}\right) \quad \textbf{Eq. (6.7)}$$

$\frac{A_{cp}^2}{P_{cp}}$ for reduction torsional moment

$$T_n = \frac{2A_oA_tf_{yt}}{S}cot\theta \quad \textbf{Eq. (6.8)}$$

$$T_n = \frac{2A_oA_lf_y}{P_h}tan\theta \quad \textbf{Eq. (6.9)}$$

T_n equal the smallest of Eqs. (6.8) and (6.9).

$\frac{A_{cp}^2}{P_{cp}}$ for reduction the torsional moment

From ACI318-19 the concrete section cracks at $\tau = 0.33\lambda\sqrt{f'_c}$.

So, by equaling eq. (6.1) with $0.33\lambda\sqrt{f'_c}$ we can find the torsional moment strength for concrete section, and by take θ = 45° we can find we can find the torsional moment strength for reinforced concrete section.

Where: T_u and T are the total torsional moment applied at a given section of the beam due to factored loads

Where: -

T: torsional moment.

T_t: ultimate torsional moment.

$\mathbf{T_n}$: nominal torsional moment strength, N·mm

τ: torsional stress.

A_o: gross area enclosed by torsional shear flow path, mm^2

t: wall thickness which resist the torsion, mm

A_{cp}: area enclosed by outside perimeter of concrete cross section, mm^2

P_{cp}: outside perimeter of concrete cross section, mm

T_{cr}: cracking torsional moment, N·mm

T_{th}: threshold torsional moment, N·mm

φ: the strength reduction factor, taken equal to 0.75 for torsion.

λ: modification factor to reflect the reduced mechanical properties of lightweight concrete relative to normal weight concrete of the same compressive strength.

f'_c: specified compressive strength of concrete, MPa

A_t: area of one leg of a closed stirrup, hoop, or tie resisting torsion within spacing s, mm2

A_l: total area of longitudinal reinforcement to resist torsion, mm^2

F_y: specified yield strength for non-prestressed reinforcement, MPa

F_{yt}: specified yield strength of transverse reinforcement, MPa

P_h: perimeter of centerline of outermost closed transverse torsional reinforcement, mm

S: the stirrup spacing.

φ: the strength reduction factor, taken equal to 0.75 for torsion.

f_y: Shear reinforcement yield strength

And according to the ACI Code, shear beams must be designed using the following relationship.

$$V_u \leq \varphi V_n \qquad \textbf{Eq. (6.10)}$$

Where: V_u is the total shear force applied at a given section of the beam due to factored loads and $V_n = V_c + V_s$ is the nominal shear strength, equal to the sum of the contribution of the concrete and the web steel if present. Thus, for vertical stirrups and for inclined bars.

$$Vu \leq \varphi Vc + \frac{\varphi Av\, fy\, d}{S} \qquad \textbf{Eq. (6.11)}$$

$$Vu \leq \varphi Vc + \frac{\varphi Av\, fy\, d}{S}(Sin\,\alpha + Cos\,\alpha) \qquad \textbf{Eq. (6.12)}$$

Where: -

A_v: area of shear reinforcement within spacing s, mm2

α: the angle of the stirrup with the horizontal.

φ: the strength reduction factor, taken equal to 0.85 for shear.

f_y: Shear reinforcement yield strength.

The nominal concrete shear strength contribution (containing contributions from aggregate interlock, main reinforcing bar dowel action, and un-cracked concrete) can be simplified as shown in Eq (6.4).

$$V_c = 0.17 \lambda \sqrt{f'_c}\ b_w d \qquad \textbf{Eq. (6.13)}$$

Where: b_w and d are the section dimensions, and for normal weight concrete, $\lambda = 1.0$. From those equation we can calculate the capacity for section under torsion and shear forces.

6.2.2 ECP Code - Torsion equations.

According to the ECP Code, torsional beams must be designed using the following relationships, taking in account that the critical section is from distance d/2 from the support.

$$q_{tu} = \frac{M_{tu}}{2A_o t_e} \qquad \textbf{Eq. (6.14)}$$

Where $A_o = 0.85 A_{oh}$ and te equal the smallest of eq.(6.13) or the smallest effective wall in for the concrete section.

$$t_e = \frac{A_{oh}}{P_h} \qquad \textbf{Eq. (6.15)}$$

In case of shear and torsional forces on the beams

$\sqrt{(q_u)^2 + (q_{tu})^2} \leq q_{max}$ where q_u is the applied shear force on the section. And once the $\sqrt{(q_u)^2 + (q_{tu})^2} \leq q_{max}$ for shear and torsional section or $q_{tu} > 0.06\sqrt{\frac{f_{cu}}{\gamma_c}}$, it's need to design the section to resist the applied forced, without that it's applied the min. transverse reinforcement.

$$A_{oh} = x_1 * y_1 \qquad \textbf{Eq. (6.16)}$$

$$A_{str} = \frac{M_{tu} s_t}{1.7 A_{oh} \frac{f_{ys}}{\gamma_s}}$$ **Eq. (6.17)**

Where maximum f_{ys} is equal to 400 MPa

For the additional longitudinal bars reinforcement is the bigger of eq.(6.18) and eq.(6.19)

$$A_{sl} = \frac{A_{st} p_h}{S} \frac{f_{ys}}{f_{yl}}$$ **Eq. (6.18)**

$$A_{sl\,min} = \frac{0.4 \sqrt{\frac{f_{cu}}{\gamma_c}}\, A_{cp}}{\frac{f_{ys}}{\gamma_s}} - \frac{A_{st} p_h}{S} \frac{f_{ys}}{f_{yl}}$$ **Eq. (6.19)**

M_{tu}: ultimate torsional moment, N·mm.

q_{tu}: torsional stress.

A_o: gross area enclosed by torsional shear flow path, $mm^{2.}$

t: wall thickness which resist the torsion, mm.

A_{cp}: area enclosed by outside perimeter of concrete cross section, $mm^{2.}$

P_{cp}: outside perimeter of concrete cross section, mm.

f_{cu}: specified compressive strength of concrete, MPa.

A_{str}: area of one leg of a closed stirrup, hoop, or tie resisting torsion within spacing s, mm^2

A_l: total area of longitudinal reinforcement to resist torsion, $mm2$

F_y: specified yield strength for nonprestressed reinforcement, MPa

F_{yt}: specified yield strength of transverse reinforcement, MPa

F_{yl}: specified yield strength of longitudinal reinforcement, MPa

P_h: perimeter of centerline of outermost closed transverse torsional reinforcement, mm

S: the stirrup spacing.

γ_s: Reinforcement strength reduction factor.

γ_c: Concrete strength reduction factor.

And according to the ECP Code, shear beams must be designed using the following relationship:

$V_u > v_{cu(uncracked)}$

$V_u = v_s + v_{cu(cracked)}$ **Eq. (6.20)**

$V_s = A_v (f_{yw}/\gamma_s) / b.s$ **Eq. (6.21)**

$v_{cu(cracked)} = 0.12 \sqrt{\frac{f_{cu}}{\gamma_c}}$ **Eq. (6.22)**

$V_{u\,max} = 0.7 \sqrt{\frac{f_{cu}}{\gamma_c}}$ **Eq. (6.23)**

$V_u < v_{cu(uncracked)}$

$V_u = v_{cu(uncracked)}$

$v_{cu(uncracked)} = 0.16 \sqrt{\frac{f_{cu}}{\gamma_c}}$ **Eq. (6.24)**

Where:-

V_u: the ultimate shear strength.

$v_{cu(cracked)}$: the shear strength provided by concrete after cracking.

$v_{cu(uncracked)}$: the shear strength provided by concrete before cracking.

v_s: the shear strength provided by web reinforcement.

S: the spacing between stirrups.

γ_c: the strength reduction coefficient for concrete, equals 1.5.

γ_s: the strength reduction coefficient for steel, equals 1.15.

$v_{c\,max}$: the maximum shear strength and ≤ 4.4 N/mm^2.

6.2.3 ECP 203-2005 code for Composite materials

the basic design equations for the shear capacity of RFP are:

$V_u = v_{cuf} + v_{fu}$ **Eq. (6.25)**

$q_{cuf} = 0.24 \sqrt{(f_{cu} / \gamma_c)} \cdot (\mu_f E_f / (\mu_s E s)) \ \text{N/mm}^2$ **Eq. (6.26)**

$v_{fu} = v_u - 0.5\, v_{cuf}$ **Eq. (6.27)**

$$\mu_{fq} = \frac{A_{fq}}{b.s} = \frac{q_{fu}}{\left(\frac{f_{fq}}{\gamma_f}\right)}$$ **Eq. (6.28)**

$$f_{fq} = 0.002\, E_f < f^*_{fb}$$ **Eq. (6.29)**

$$V_{u\,max} = 0.7 \sqrt{(f_{cu} / \gamma_c)}$$ **Eq. (6.30)**

Where: -

V_u: the ultimate shear strength.

v_{cuf}: the shear strength provided by concrete.

S: the spacing between stirrups.

γ_c: the strength reduction coefficient for concrete, equals 1.5.

γ_f: the strength reduction coefficient for fiber, equals 1.15.

$v_{u\,max}$: the maximum shear strength and ≤ 3.00 N/mm^2.

μ_f: Ratio of longitudinal reinforcement with FRP bars.

E_f: Moduls of elasticity for FRP bars.

μ_s: The maximum longitudinal reinforcement ratio is taken 5x10^{-4} f_{cu}

E_s: Moduls of elasticity for steel.

f^*_{fb}: It is the maximum permissible stress at the corners of the stem reinforcement according to equation (5-1).

6.2.4 CSA Code-Shear and Torsion Equations

According to the CSA A23.3-04 Code, shear and torsional beams must be designed using the following relationship for steel reinforcement concrete sections.

$$T_f > T_{cr}$$ **Eq. (6.31)**

$$T_r = \left(\frac{A_c^2}{P_c}\right) * 0.38\lambda\varphi_c\sqrt{f'_c}\sqrt{1 + \frac{\varphi_p f_{cp}}{0.38\varphi_c\lambda\sqrt{f'_c}}}$$ **Eq. (6.32)**

$$T_r > T_f$$ **Eq. (6.33)**

$$T_r = 2A_o \frac{\varphi_s A_t f_y}{S} cot\theta \quad \textbf{Eq. (6.34)}$$

$$A_o = 0.85A_{oh} \quad \textbf{Eq. (6.35)}$$

$$\theta = 29^o + 7000\varepsilon_x \quad \textbf{Eq. (6.36)}$$

$\theta = 42^o$ according to code noticed because the width of section is less than 250mm.

$$\varepsilon_x = \frac{\frac{M_f}{d_v} + \sqrt{(v_f - v_p)^2 + \left(\frac{0.9P_h T_f}{2A_o}\right)^2} + 0.5N_f - A_p f_{po}}{2(E_s A_s + E_p A_p)} \quad \textbf{Eq. (6.37)}$$

$$\beta = \frac{0.4}{1+1500\varepsilon_x} * \frac{1300}{1000+s_{ze}} \quad \textbf{Eq. (6.38)}$$

For longitudinal bars

$$F_{lt} = \frac{M_f}{d_v} + 0.5N_f + \sqrt{\left(v_f - 0.5v_s - v_p\right)^2 + \left(\frac{0.45P_h T_f}{2A_o}\right)^2} \cot\theta \quad \textbf{Eq. (6.39)}$$

According to the CSA S806-12 Code, shear and torsional beams must be designed using the following relationship for FRP sections.

$$T_r > T_f \quad \textbf{Eq. (6.40)}$$

$$T_r = \frac{2A_o \varphi_f A_{ft} f_{ft}}{S} cot\theta \quad \textbf{Eq. (6.41)}$$

$$A_o = 0.85A_{oh} \quad \textbf{Eq. (6.42)}$$

$$\theta = 30^o + 7000\varepsilon_1 \quad \textbf{Eq. (6.43)}$$

$$f_{ft} \leq 0.4f_{fu} \text{ or } 1200MPa \quad \textbf{Eq. (6.44)}$$

$$\varepsilon_1 = \frac{\frac{M_f}{d_v} + \sqrt{(v_f - v_p)^2 + \left(\frac{0.9P_h T_f}{2A_o}\right)^2} + 0.5N_f - A_p f_{po}}{2(E_f A_f + E_p A_p)} \quad \textbf{Eq. (6.45)}$$

$$M_f > (v_f - v_p)d_v \quad \textbf{Eq. (6.46)}$$

$$\varepsilon_1 > 0 \quad \textbf{Eq. (6.47)}$$

$60 \geq \theta \geq 30$ **Eq. (6.48)**

For longitudinal bars

$$F_{lt} = \frac{M_f}{d_v} + 0.5N_f + 1.3\sqrt{\left(v_f - 0.5v_{sf} - v_p\right)^2 + \left(\frac{0.45P_hT_f}{2A_o}\right)^2} \quad \textbf{Eq. (6.49)}$$

Where:

T_r: factored torsional resistance.

T_f: factored torsional moment.

A_o: area enclosed by shear flow path, including area of holes.

φ_f: resistance factor for FRP reinforcement.

φ_s: resistance factor for steel reinforcement.

A_{ft}: area of one leg of transverse FRP torsional reinforcement.

A_t: area of one leg of transverse steel torsional reinforcement.

E_p: modulus of elasticity of prestressing tendons.

S_{ze}: equivalent value of S_z that allows for influence of aggregate size.

f_{ft}: stress in FRP reinforcement under specified loads.

θ: the angle of the diagonal compressive stress.

A_{oh}: area enclosed by stirrups.

ε_1: longitudinal strain for FRP reinforcement at mid-depth of the section.

ε_x: longitudinal strain for steel reinforcement at mid-depth of the section.

β: factor accounting for shear resistance of cracked concrete.

f_{fu}: limiting compressive stress in concrete strut.

v_f: factored shear force.

v_p: component in the direction of the applied shear of the effective prestressing force or, for variable depth members, the sum of the component of the effective prestressing force and the components of flexural compression and tension in the direction of the applied shear; positive if resisting applied shear.

P_h: perimeter of centerline of outermost closed transverse torsional.

T_f: factored torsional moment.

N_f: factored axial load normal to the cross-section occurring simultaneously with V_f, including effects of tension due to creep and shrinkage (taken as positive for tension and negative for compression).

A_p: area of prestressing tendons.

f_{pu}: stress in prestressing tendon when strain in the surrounding concrete is zero.

d_v: effective shear depth, taken as the greater of 0.9 d or 0.72 h.

M_f: factored moment.

F_{lt}: longitudinal reinforcement on the flexural tension side.

v_{sf}: factored shear resistance provided by FRP shear reinforcement.

6.3 Parameters of Beams

- Compressive strength of concrete = 30 MPa, except B7 the compressive strength of concrete = 50 MPa
- Beam dimensions are 2000 × 300 × 150 mm clear span, length, and breadth thickness respectively.
- 2 ϕ 10 mm and yield strength of 360 MPa are used as compression bars and 2 ϕ 12 as tension bars and ϕ 8 for stirrups with yield strength of 240 MPa and for the steel reinforcement bars. (Assumption without RFT test)

- 2 ϕ 10 mm and yield strength of 750 MPa are used as compression bars and 2 ϕ 12 as tension bars and ϕ 8 for stirrups and for the GFRP reinforcement bars. (Assumption without RFT test)

6.4 The Analytical and Tested Results for Each Beam

Table (6-1) show the theoretical result for experimental result, ACI, ECP, CSA and percentage between experimental result and codes, the closer code is CSA. The ACI and ECP need modifications to be suitable for experimental results and also the same for CSA to be exact or semi exact for experimental results, this all can make with a lot of experimental studies to be sure that the modified equations will meet the real results. For all codes, the experimental results for steel reinforced beam and beams without stirrups were bigger than theoretical results in the other side theoretical results for GFRP reinforced beams were bigger than experimental results except B5 because B5 was tested under torsional and bending moment with shear force which cause increasing of strength to meet the theoretical results, and codes should take in the account the boundary conditions. CSA code was the closer code for the experimental result because CSA takes in calculations many of parameters affect essential in the resistance, $\boldsymbol{\theta}$ (the angle of the diagonal compressive stress), d_v (effective shear depth), f_{pu} (stress in prestressing tendon when strain in the surrounding concrete is zero), N_f (factored axial load normal to the cross-section occurring simultaneously with V_f , including effects of tension due to creep and shrinkage (taken as positive for tension and negative for compression), $\boldsymbol{T_f}$ (factored torsional moment), $\boldsymbol{v_p}$ (component in the direction of the applied shear of the effective prestressing force or, for variable depth members, the sum of the component of the effective prestressing force and the components of flexural compression and tension in the direction of the applied shear; positive if resisting applied shear), $\boldsymbol{v_f}$

(factored shear force), ε_1 (longitudinal strain for FRP reinforcement at mid-depth of the section), ε_x (longitudinal strain for steel reinforcement at mid-depth of the section), E_p (modulus of elasticity of prestressing tendons), S_{ze} (equivalent value of S_z that allows for influence of aggregate size). The previous parameters contribute to improve the expected action for strength and strain.

The results of beams are shown in Figures from (6-1) to (6-9) outlining the differences between the three analyzed codes with experimental results.

Table (6- 1) The Analytical and tested results for each beams

Beams	Type of Reinforcement	t	b	Cover	X1	Y1	Fy or Fft	Fcu	ys	ycu	Astr	St	Concrete Strength	Max Experimintal Load	Mtu ECP	Max Exp / Mtu ECP	Mtu ACI	Max Exp / Mtu ACI	Mtu CSA	Max Exp / Mtu CSA
		mm	mm	mm	mm	mm	N.mm	N.mm			mm2	mm	KN.m	KN.m	KN.m		KN.m		KN.m	
B1	Steel	300	150	20	252	102	240	30	1	1	52.26	150	8.008	13.29	3.65	2.34	3.65	3.64	3.45	3.85
B2	GFRP	300	150	20	252	102	760	30	1	1	52.26	150	5.94	6.44	11.57	0.28	11.57	0.56	8.68	0.74
B3	GFRP	300	150	20	252	102	760	30	1	1	52.26	100	3.74	7.87	17.36	0.32	17.36	0.45	13.02	0.60
B4	GFRP	300	150	20	252	102	760	30	1	1	52.26	150	6.93	6.93	11.57	0.36	11.57	0.60	8.68	0.80
B5	GFRP	300	150	20	252	102	760	30	1	1	52.26	150	6.908	11.84	11.57	0.46	11.57	1.02	8.68	1.36
B6	GFRP	300	150	20	252	102	760	30	1	1	52.26	150	5.236	5.24	11.57	0.25	11.57	0.45	8.68	0.60
B7	GFRP	300	150	20	252	102	760	50	1	1	52.26	150	5.61	7.33	11.57	0.23	11.57	0.63	8.68	0.84
B8	Steel	300	150	20	252	102	240	30	1	1	52.26	150	5.434	5.48	0.44	4.91	3.53	1.55	3.60	1.52
B9	Steel	300	150	20	252	102	750	30	1	1	52.26	150	11.13	10.87	0.44	12.01	3.53	3.08	3.60	3.02

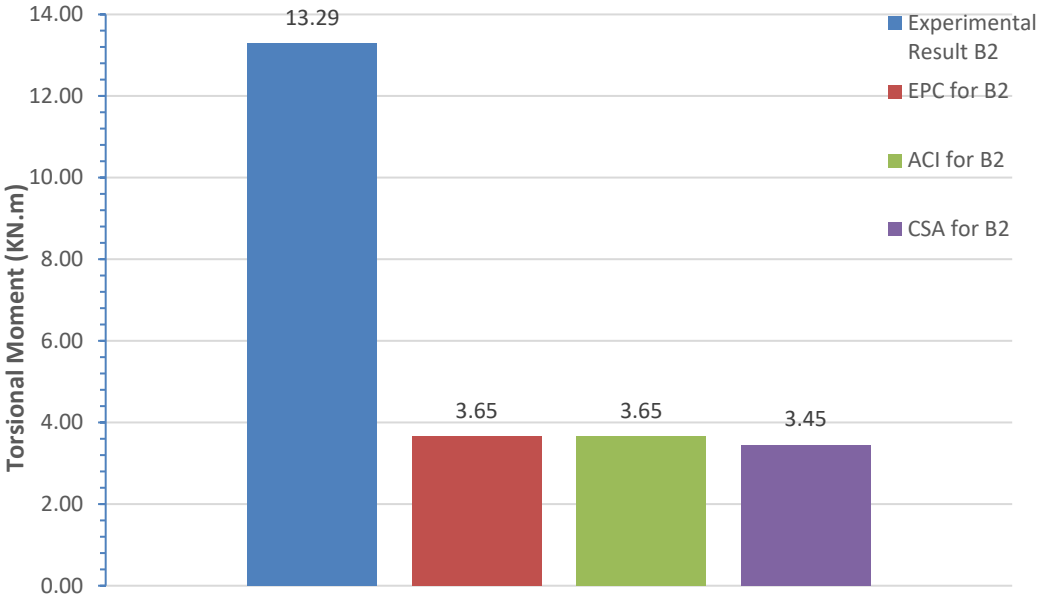

Figure (6-1) Theoretical and Test Results for Beam (B1).

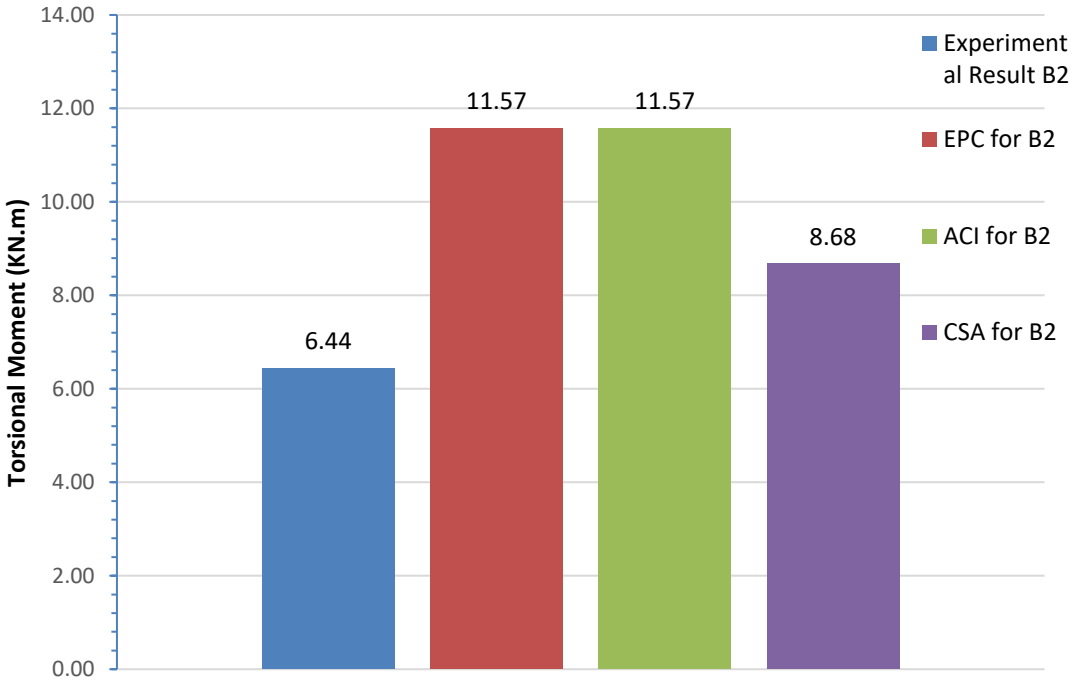

Figure (6-2) Theoretical and Test Results for Beam (B2).

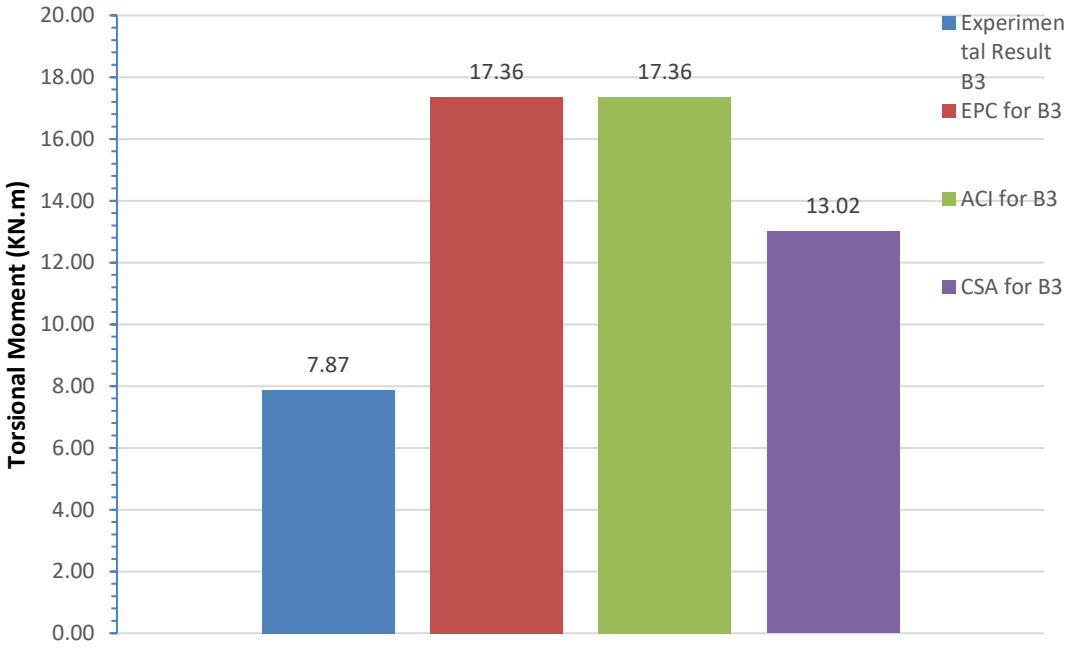

Figure (6-3) Theoretical and Test Results for Beam (B3).

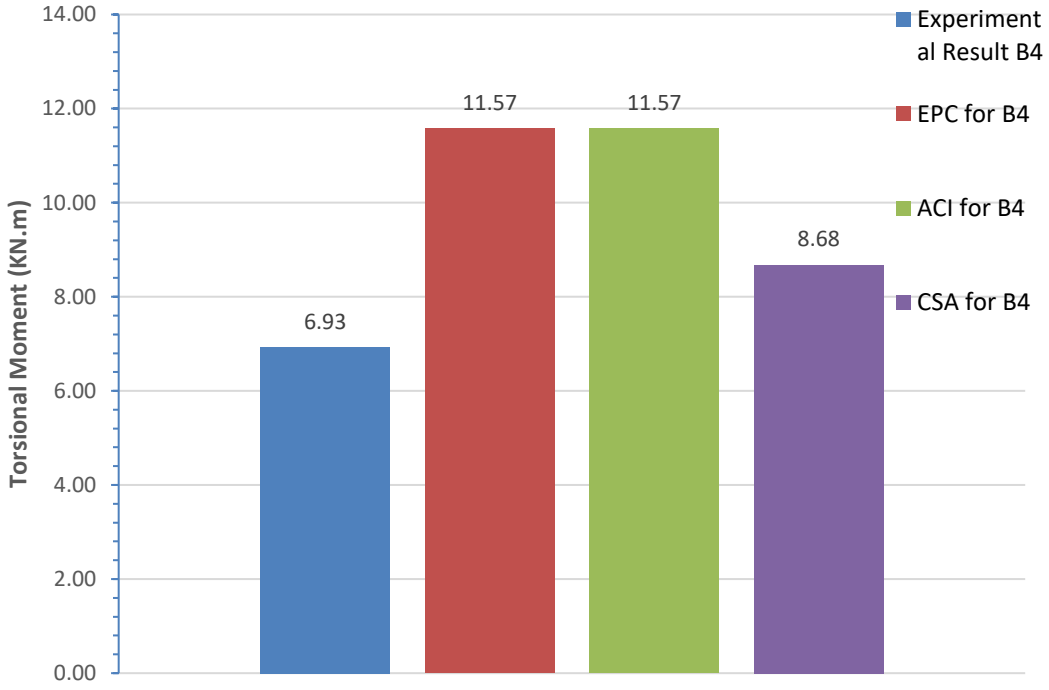

Figure (6-4) Theoretical and Test Results for Beam (B4).

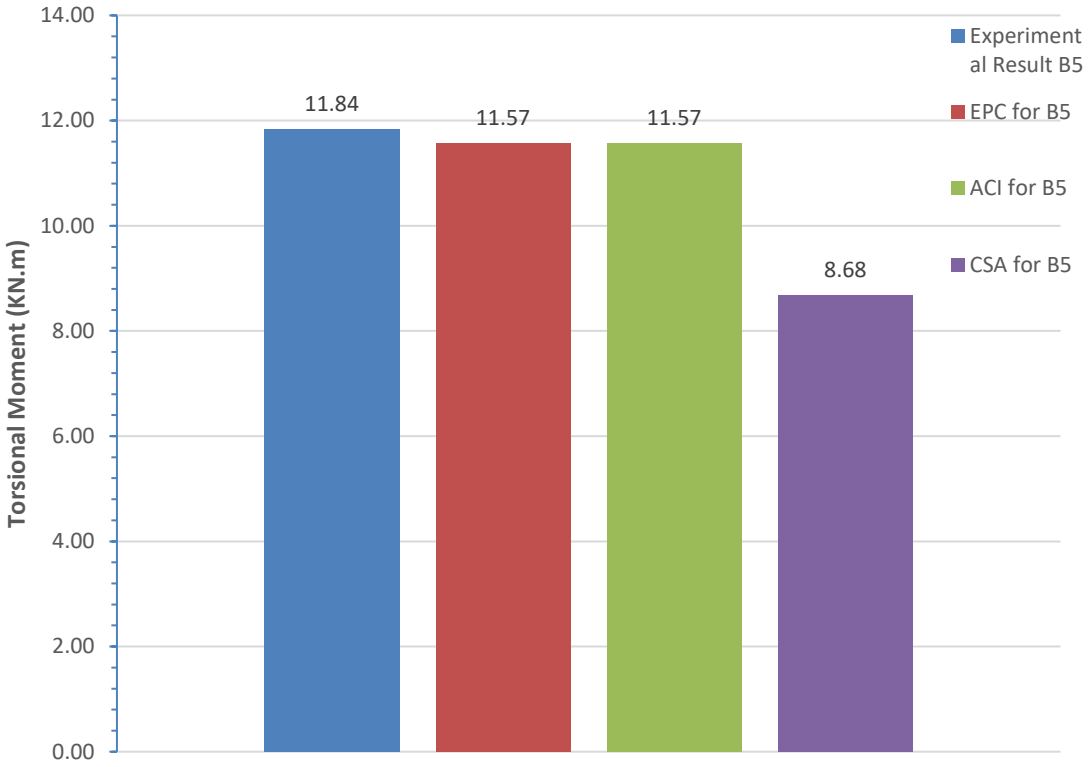

Figure (6-5) Theoretical and Test Results for Beam (B5).

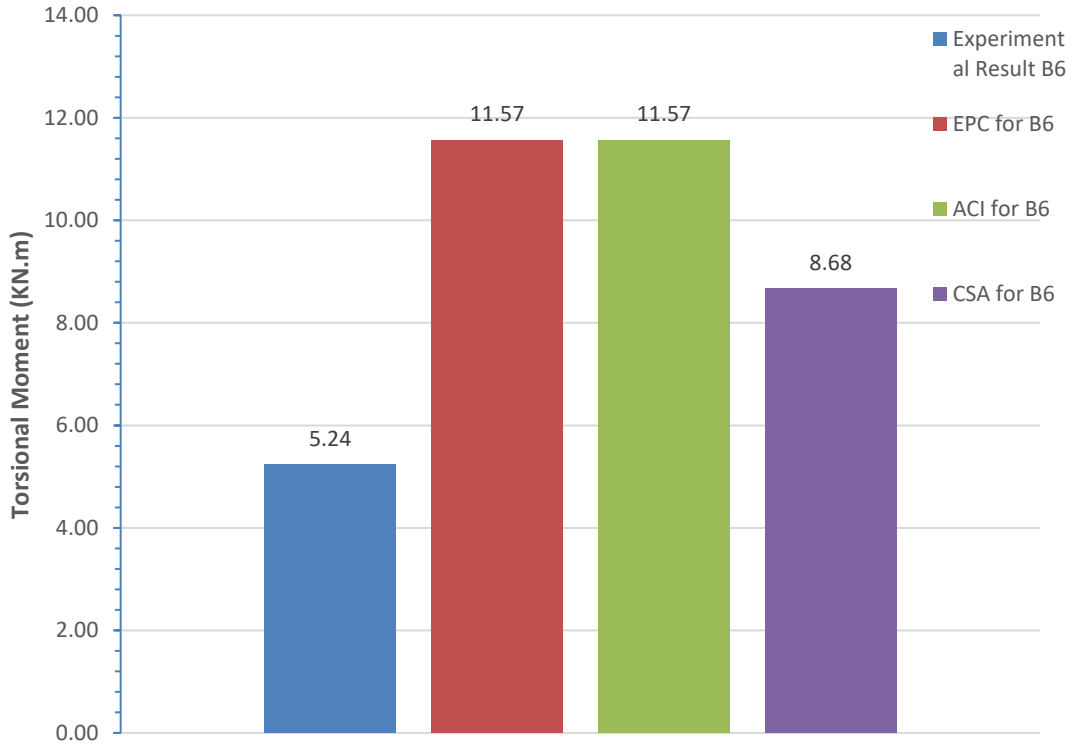

Figure (6-6) Theoretical and Test Results for Beam (B6).

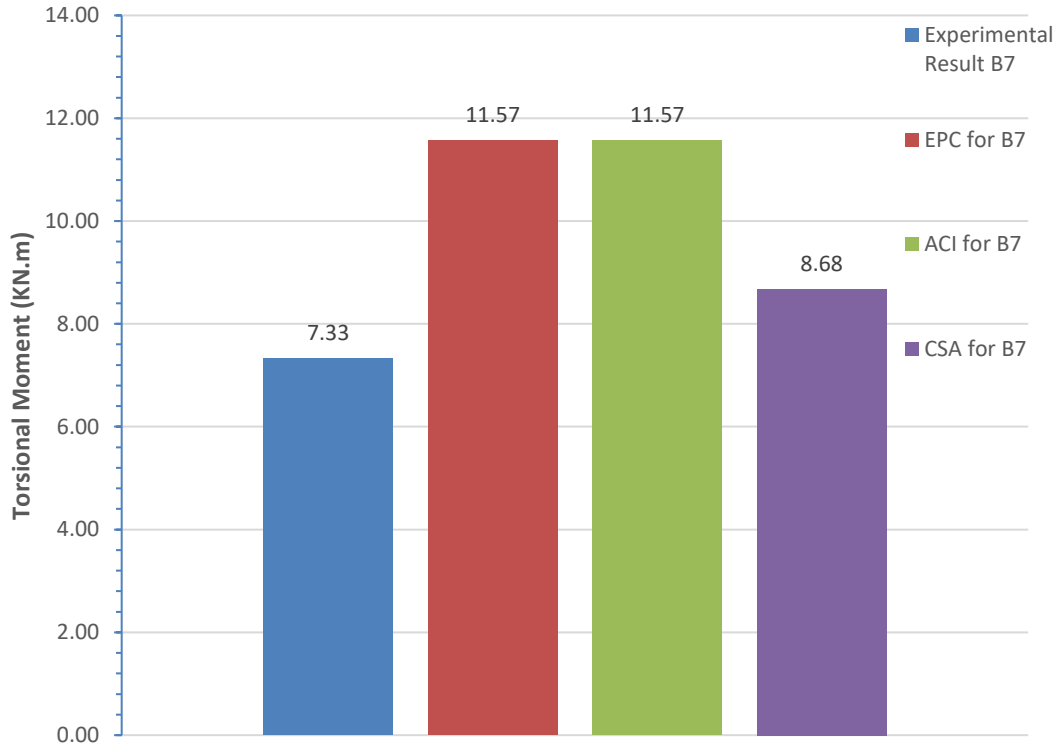

Figure (6-7) Theoretical and Test Results for Beam (B7).

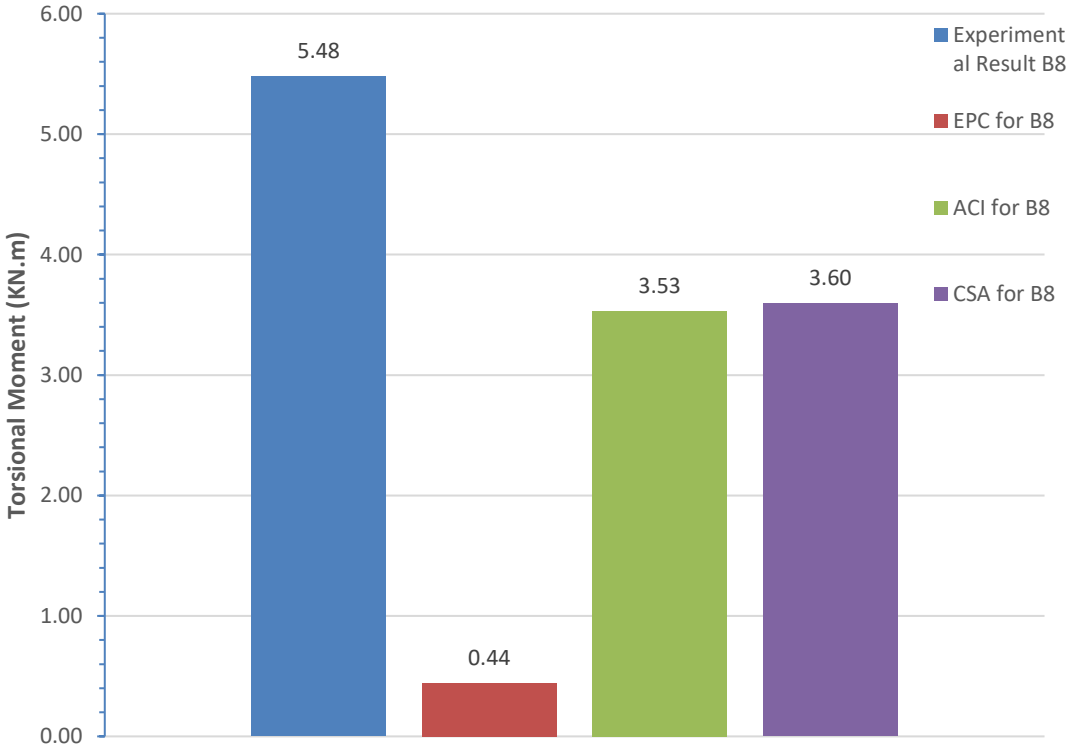

Figure (6-8) Theoretical and Test Results for Beam (B8).

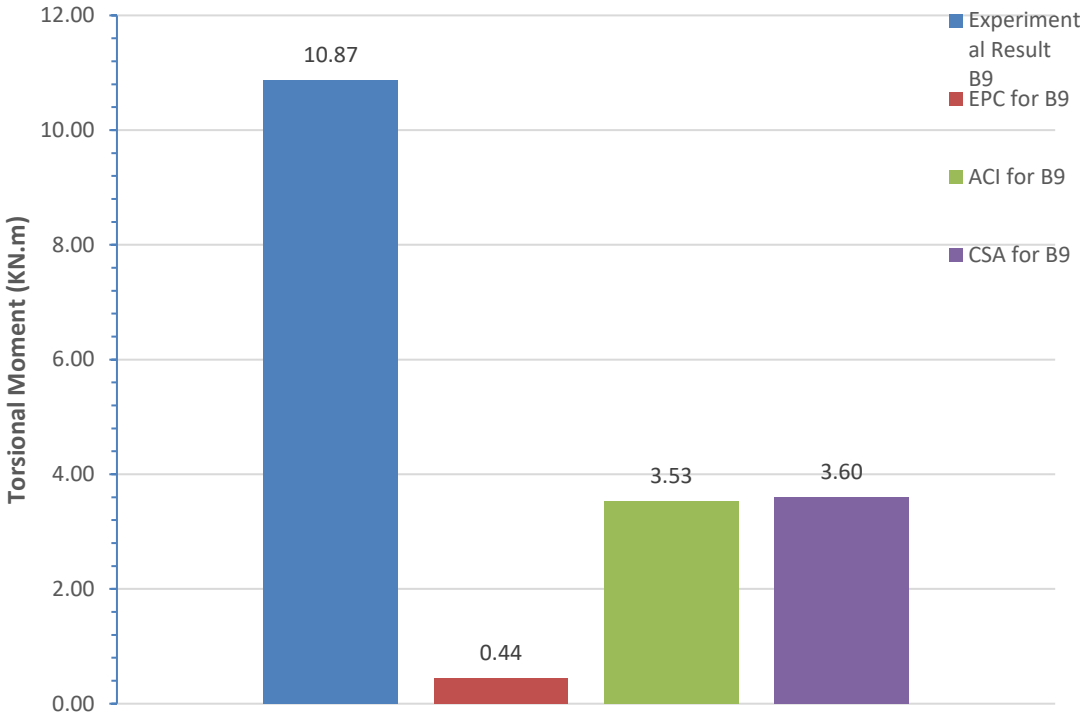

Figure (6-9) Theoretical and Test Results for Beam (B9).

CHAPTER SEVEN

CONCLUSIONS AND RECOMMENDATIONS

7.1 Summary

This study investigates the torsional characteristics of simply supported GFRP-reinforced concrete beams. Several parameters are considered in this study which are: the using variable concrete types, existence and absence stirrups, reinforcement types (steel, GFRP), stirrups configuration, stirrups spacing 150,100 mm, load types and shrinkage bars. All beams had a clear span length and were simply supported L=2000 mm and over all depth t=300 mm and width b_w =150 mm. Several results were recorded: the loading capacity, the deflections, the strain in stirrups, bars and concrrete, the crack pattern and the failure mode. This chapter summarizes the principal findings from the research conducted in this study and identifies number of future research recommendations.

7.2 Conclusions

The following are the primary results that can be taken from the current research based on the tested results: -

1. Steel reinforcement is better in resisting torsional moments and has a good behavior for distribute the load over all the beams, made the cracks over all the beam on the contrary counterpart GFRP beam cracks were around 20% of the beam.
2. Steel reinforcement makes the beam carried strength 206.5% of counterpart GRFP beam.

3. For GFRP reinforced beam, decreasing spacing between stirrups for B3 100mm spacing make the beam load more capacity by 22.2% than counterpart B2 150mm spacing.
4. For GFRP reinforced beam, change of boundary condition impacted on the behavior which clear in addition bending moment to torsional moment, the strength of B5 loaded with torsional and bending moments associated with shear force increased 84% more than the counterpart B2 loaded with pure torsion
5. For GFRP reinforced beam, decreasing the distance between the side bars improve the load distribution and crack patterns and torsional strength of beam.
6. Using inclined stirrups decreased the torsional strength because the torsional cracks are continuing and inclining so the cracks were parallel to stirrups for GFRP reinforced beam, the strengths were greatly closer with counterpart B2, vertical stirrups.
7. The maximum capacity for inclined stirrups beam reinforced by GFRP was closer to maximum capacity of beam without stirrups (only longitudinal steel bars), with increasing in strength 4.6% for B8 (longitudinal steel bars without stirrups) more than the counterpart B5 (GFRP inclined stirrups).
8. Increasing concrete strength improved the strength of beam, the increasing of concrete strength 66.7% (50MPa and 30MPa) associated with increasing of strength 14%, but the crack patterns in the first area of cracking for GFRP reinforced beam was same for both.
9. Corner effect affected on the behavior and crack pattern for GFRP reinforced beam.

10. The closer code was CSA A23.3-04 than EPC and ACI but also bigger than experimental result, because the CSA code takes in account more factors which describes the GFRP deeper.

7.3 Recommendations for future research

The recommendations for future research: -

1. Study of torsional loading for RC beams reinforced with GFRP after improving the bond between the concrete and GFRP.
2. Study effect of more different concrete strengths on the torsional capacity.
3. Study of fully beams scale under torsional loads.
4. Study of influence of change the concrete beam section on torsional capacity and behavior.
5. Revision the guideline codes are requirements for FRP RC beam under torsional loads.

References

1. Hyunjin Ju, Deuckhang Lee, Jong R. Kim, Kang Su Kim ‘’ Maximum torsional reinforcement ratio of reinforced concrete beams’’ Structures 23 (2020) 481–493.

2. A.G. Razaqpur, F. Bencardino, L. Rizzuti, G. Spadea ‘’ FRP reinforced/prestressed concrete members: A torsional design Model’’ Composites Part B 79 (2015) 144e155.

3. Japan Society of Civil Engineers, 1997, “Recommendation for Design and Construction of Concrete Structures Using Continuous Fiber Reinforcing Materials,” Concrete Engineering Series 23, A. Machida, ed., Tokyo, Japan, 325

4. Canadian Standards Association (CSA), 2012, “Design and Construction of Building Structures with Fibre-Reinforced Polymers (CAN/CSA S806),” Mississauga, ON, Canada.

5. ACI Committee 318M-2019, “Building Code Requirements for Structural Concrete (ACI 318-19),” American Concrete Institute, Farmington Hills, MI, 503 pp.

6. Imjai T, Guadagnini M, Pilakoutas K. Mechanical performance of curved FRP rebars: part I e experimental study. In: Proceedings of the 1st Asia-Pacific Conference on FRP in Structures (APFIS07), Hong Kong; 2007. p. 333e8.

7. Imjai T, Guadagnini M, Pilakoutas K. Mechanical performance of curved FRP rebars: part II e analytical study. In: Proceedings of the 1st Asia-Pacific Conference on FRP in Structures (APFIS07), Hong Kong; 2007. p. 339e44.

8. Imjai T, Guadagnini M, Pilakoutas K. Curved FRP as concrete reinforcement. Ice Eng Comput Mech 2009;162(EM3):171e8.

9. Gurdal Z, Haftka RT, Hajela P. Laminated composite materials. N.Y: John Wiley & Sons Inc.; 1999.

10. Eyptian Code of Design for Reinforced Concrete Structures, ECP 203-2019.

11.M. R. PRAKASH, SADANAND P, MANJUNATH H. R, JAGADEESH KUMAR B. G and PRABHAKARA R '' CRACKING AND TORSIONAL DUCTILITY BEHAVIOR OF HSC BEAMS'' International Journal of Civil, Structural, Environmental and Infrastructure Engineering Research and Development (IJCSEIERD) ISSN 2249-6866 Vol. 2 Issue 4 Dec - 2012 1-10.

12.Changbin Joh , Imjong Kwahk , Jungwoo Lee , In-Hwan Yang , and Byung-Suk Kim '' Torsional Behavior of High-Strength Concrete Beams with Minimum Reinforcement Ratio'' Hindawi Advances in Civil Engineering Volume 2019, Article ID 1432697, 11 pages https://doi.org/10.1155/2019/1432697.

13.Hao-Jan Chiu, I-Kuang Fang, Wen-Tang Young, Jyh-Kun Shiau '' Hao-Jan Chiu, I-Kuang Fang_, Wen-Tang Young, Jyh-Kun Shiau'' Engineering Structures 29 (2007) 2193–2205.

14. Luı´s F. A. Bernardo Æ Se´rgio M. R. Lopes '' Behaviour of concrete beams under torsion: NSC plain and hollow beams'' Materials and Structures (2008) 41:1143–1167 DOI 10.1617/s11527-007-9315-0.

15. Prabaghar, G. Kumaran '' Experiment on Torsional Behaviour of Reinforced Concrete Beams'' International Journal of Innovative Technology and Exploring Engineering (IJITEE) ISSN: 2278-3075, Volume-8, Issue-6S4, April 2019.

16.Ahmed Hassan and Laila Abd-EL Hafez '' Investigation of Torsional Behaviour of High-Strength Reinforced Concrete Sections''

World Applied Sciences Journal 33 (1): 01-13, 2015 ISSN 1818-4952© IDOSI Publications, 2015 DOI: 10.5829/idosi.wasj.2015.33.01.14569.
17.Mostofinejad, D.*, Talaeitaba, S. B., '' Nonlinear Modeling of RC Beams Subjected to Torsion using the Smeared Crack Model'' Procedia Engineering 14 (2011) 1447–1454.
18.Min-Jun Kim, Hyeong-Gook Kim, Yong-Jun Lee, Dong-Hwan Kim, Jung-Yoon Lee, Kil-Hee Kim. '' Pure torsional behavior of RC beams in relation to the amount of torsional reinforcement and cross-sectional properties'' Construction and Building Materials 260 (2020) 119801.
19.Khaldoun N. Rahal '' Torsional strength of normal and high strength reinforced concrete Beams'' Engineering Structures 56 (2013) 2206–2216.
20.Mohammad Rashidi, Hana Takhtfiroozeh '' The Evaluation of Torsional Strength in Reinforced Concrete Beam'' Mechanics, Materials Science & Engineering, December 2016 – ISSN 2412-5954.
21.Tuakta C.: Use of Fiber Reinforced Polymer Composite in Bridge Structures, Massachusetts Institute of Technology, (2005).
22. https://ale.nl/
23.Zobel H.: Mosty kompozytowe,50. Jubileuszowa Konferencja Naukowa Kiliw pan i KN PZITB, Krynica, (2004).
24.Kolding, Fiberline Design Manual, Fiberline Composites A/S, (2003).
25.Ko, F.K.; Somboonsong, W.; Harris, H.G. Fiber architecture based design of ductile composite rebars for concrete structures. In: Proceedings of the 11th International Conference of Composite Materials. Gold Coast, Australia, 1997.
26.Dong-Woo Seo, Ki-Tae Park, Young-Jun You and Sang-YoonLee, Experimental Investigation for Tensile Performance of GFRP-Steel

Hybridized Rebar, Structural Engineering Research Institute (SERI), Korea Institute of Civil Engineering and Building Technology (KICT), Goyang, 411712, South Korea; 2016.

27.Esam El-Awady, Mohamed Husain, Sayed Mandour. '' FRP-Reinforced Concrete Beams Under Combined Torsion and Flexure'' ISSN: 2319-5967 ISO 9001:2008 Certified International Journal of Engineering Science and Innovative Technology (IJESIT) Volume 2, Issue 1, January 2013.

28.Hamdy M. Mohamed and Brahim Benmokrane. '' Reinforced Concrete Beams with and without FRP Web Reinforcement under Pure Torsion'' ASCE, J. Bridge Eng., 04015070.

29.Hamdy M. Mohamed and Brahim Benmokrane. '' Torsion Behavior of Concrete Beams Reinforced with Glass Fiber-Reinforced Polymer Bars and Stirrups".

30.Jikai Zhou, Wei Shen, Shifu Wang '' Experimental study on torsional behavior of FRC and ECC beams reinforced with GFRP bars''.

31.Prabaghar and G. Kumaran. '' Theoretical study on the behaviour of rectangular concrete beams reinforced internally with GFRP reinforcements under pure torsion'' Journal of Computations & Modelling, vol.3, no.1, 2013, 1-31 ISSN: 1792-7625 (print), 1792-8850 (online) Scienpress Ltd, 2013.

- ظهر تأثير زاوية الكانات بالنسبة للكمرات المسلحة بالألياف الزجاجية حيث حدث تمزق للكانات في الزاوية خلاف انه لم يظهر في الكمرات المسلحة تسليح حديدي.

- الكود الكندي كان الأقرب للتحليل المعملي من نظيره المصري والأمريكي، ولكن أكثر في القيمة من النتائج المعملية.

الفصل الثالث: البرنامج العملي

يقدم هذا الفصل وصفاً شاملاً لتجارب المعمل التي أجريت علي بعض العينات, بما في ذلك التفاصيل المتعلقة بمراحل تصنيع العينات والموارد المستخدمة وإجراء التجارب وإعداد الاختبار وخصائص المواد وتفاصيل العينات ووصف الإعداد العملي وأجهزة القياس المستخدمة.

الفصل الرابع: نتائج الاختبارات المعملية

يناقش هذا الفصل نتائج تفصيلية للبرنامج العملي وتحليل وشرح شاملاً للنتائج المستخلصة من الدراسة.

الفصل الخامس: تحليل ومناقشة النتائج

يحتوي هذا الفصل على تحليل ومناقشة نتائج الكمرات المعملية المختبرة لفهم تأثير العوامل تحت الدراسة على سلوك الكمرات بشكل كامل من خلال مقارنة نتائج منحنيات الحمل الترخيم وحمل الانهيار وشكل الانهيار.

الفصل السادس: المعدلات التحليلية ومقارنة النتائج

يقدم هذا الفصل حساب العوزم عن طريق استخدام الاكواد الكندية للفايبر والكود الأمريكي والمصري ومقارنة النتائج بالنتائج المعملية.

الفصل السابع: التوصيات المستنتجة والاقتراحات المنبثقة

يقدم هذا الفصل نتائج هذا البحث مع التوصيات المستنتجة والاقتراحات المنبثقة من هذا البحث والتي يمكن الاسترشاد بها في المستقبل وأهم الاستنتاجات يمكن إيجازها في التالي

- في مقاومة عزوم اللي يفضل أستخدم التسليح الحديدية عن الالياف الزجاجية حيث يعطي تصرف أفضل للعينة وتوزيع منتظم للشروخ.
- الكمرات المسلحة بالتسليح الحديدية تتحمل عزوم لي اكثر من نظيرها المسلحة بالالياف الزجاجية.
- الكمرات المسلحة بالألياف الزجاجية كلما قلت المسافات في الكانات كلما تصرفت العينة بشكل أفضل من حيث الشروخ وتجمل أكثر لعزوم اللي.
- بتقديم عزوم الانحناء مع عزوم اللي بالنسبة للكمرات المسلحة بالألياف الزجاجية أدى ذلك إلي تحسن تصرف الكمرات وكذلك للكمرات المسلحة بقضبان حديدية وبدون تسليح عرضي.
- بتقليل المسافات بين قضبان التسليح بالألياف الزجاجية أدى ذلك إلي تحسن توزيع الشروخ ومقاومة عزوم اللي.
- أستخدام الكانات المائلة بالنسبة للكمرات المسلحة بالالياف الزجاجية قلل مقاومة عزوم اللي لان شروخ اللي حلزونية مستمرة ولذلك ستقابل الشروخ الكانات في نفس الزاوية وتكون الشروخ موازية للكانات مما يجعل الكانات بلا فائدة.
- المقاومة القسوة للكمرات المعرضة لعزوم اللي بالنسبة للكمرات المسلحة بالألياف الزجاجية كان قريباً في القيمة للكمرات المسلحة بتسليح حديدي طولي بدون كانات.
- زيادة مقاومة الخرسانة أدى إلي تحسين مقاومة اللي ولكن منطقة الشرخ بكل رئيسي كانت لنفس ظهور الشرخ الأول واستمر التوسع لنفس الشرخ حتي الانهيار.

ملخص الرسالة

عنوان الرسالة/

" سلوك الكمرات الخرسانية المسلحة بالألياف الزجاجية تحت تأثير عزم اللي"

“Behavior of GFRP- Reinforced Concrete Beams under Torsion”

مخلص الرسالة المقدمة من المهندس/ **عبدالله فارس نافذ سيد** للحصول علي درجة الماجيستير في الهندسة المدنية.

تحت إشراف:

أ. م. د / هاله ممدوح أسماعيل د / أحمد محمد حسن على

الملخص:

تعتبر الخرسانة المسلحة بأسياخ البوليمر المقوى بألياف الزجاج أحد توجهات عالم صناعة الهندسة لما يقدمه البوليمر المقوى بألياف الزجاج من مميزات كمقاومة الصدأ وقلة الوزن في مقابل المقاومة العالية. يساعد توفر معلومات موثوقة عن سلوك تلك المواد في انتشار استخدامها حول العالم واعتمادها في الأكواد والمراجع. على الرغم من ذلك، محدودية معرفة سلوك هذه المواد يعد عائقا في انتشار استخدمها في المنشأت الخرسانية. بالإضافة إلى ذلك، لم يتم دراسة سلوك الكمرات المسلحة بأسياخ البوليمر المقوى بألياف الزجاج تحت تأثير عزم اللي بشكل وافي. وبالتالي تهدف هذه الدراسة إلى دراسة سلوك الكمرات الخرسانية المسلحة بأسياخ من البوليمر المقوى بألياف الزجاج في كلا الاتجاهين الطولي والعرضي تحت تأثير عزوم اللي مع متغيرات مختلفة.

الهدف من الدراسة:

الهدف الرئيسي من هذه الرسالة هو سلوك الكمرات الخرسانية المسلحة بالألياف الزجاجية تحت تأثير عزم اللي مع المتغيرات التالية:

١. تتغيير نوعية التسليح
٢. نسبة التسليح العرضي بزيادة نسبة التسليح العرضي لدراسة التأثير.
٣. أضافة تسليح جانبي لدراسة تاثير أضافة تسليح جانبي وتقليل المسافات بين التسليح الطولي.
٤. تغير الاحمال بدراسة تأثير إضافة أحمال مع أحمال اللي.
٥. أستخدام كانات مائلة بأستخدام كانات مائلة بدلاً من الكانات الرئيسية.
٦. مقاومة الخرسانة بأستخدام خرسانة عالية المقاومة من المستخدمة في العينات الرئيسية.
٧. الغاء التسليح العرضي بأستخدام عينات بلا تسليح عرضي.

محتوى الرسالة:

تتكون الرسالة من سبع فصول:

الفصل الأول: مقدمة

مقدمة وعرض لأهداف للرسالة والغرض منها ومحتوياتها.

الفصل الثاني: الدراسات السابقة

يحتوي هذا الفصل على بعض الدراسات السابقة التي تخدم فكرة الرسالة في مجال البحث العلمي والنظري لتوسيع القاعدة المعرفية ودراسة تصرف الكمرات المسلحة بالألياف الزجاجية تحت تأثير عزوم اللي.

مستخلص الرسالة

عنوان الرسالة/

" سلوك الكمرات الخرسانية المسلحة بالألياف الزجاجية تحت تأثير عزم اللي"

"Behavior of GFRP- Reinforced Concrete Beams under Torsion"

مستخلص الرسالة مقدم من المهندس/ **عبدالله فارس نافذ سيد** للحصول علي درجة الماجيستير في الهندسة المدنية.

المستخلص

تعتبر الخرسانة المسلحة بأسياخ البوليمر المقوى بألياف الزجاج أحد توجهات عالم صناعة الهندسة لما يقدمه البوليمر المقوى بألياف الزجاج من مميزات كمقاومة الصدأ وقلة الوزن في مقابل المقاومة العالية. يساعد توفر معلومات موثوقة عن سلوك تلك المواد في انتشار استخدامها حول العالم واعتمادها في الأكواد والمراجع. على الرغم من ذلك، محدودية معرفة سلوك هذه المواد يعد عائقا في انتشار استخدمها في المنشأت الخرسانية. بالإضافة إلى ذلك، لم يتم دراسة سلوك الكمرات المسلحة بأسياخ البوليمر المقوى بألياف الزجاج تحت تأثير عزوم اللي بشكل وافي. وبالتالي تهدف هذه الدراسة إلى دراسة سلوك الكمرات الخرسانية المسلحة بأسياخ من البوليمر المقوى بألياف الزجاج تحت تأثير عوزم اللي بمختلف المتغيرات لكمرات مسلحة بالبوليمر المقوى بألياف الزجاج ودراسة تأثير تغيير مقاومة الخرسانة ونسبة تسليح عزوم اللي. وتأثير تداخل احمال اخري مع حمل اللي على المقاومة النهائية للكمرات لمقاومة عزوم اللي. باستخدام عوامل مختلفة تبين انه تم انهيار الجميع تحت تأثير عزوم اللي كما مصمم. الخرسانة ذات مقاومة اعلي حققت علو في المقامة النهائية لعزوم اللي بالإضافة الا انه بزيادة نسبة التسليح العرضي زادات مقاومة الكمرة لعزوم اللي وتحسن شكل الكسر الكمرات ذات الكانات المائلة كانت غير فعالة بالإضافة لضعف الترابط بين تسليح البوليمرات والخرسانة زاد من قلة فاعلية القطاع لمقاومة الخرسانة. الكمرات بدون تسليح عرضي كانت فعالة ولكن اللي الشرخ الاول فقط وبعدها تلاشى مقاومة القطاع ثم مقارنة النتائج بالأكواد الكندية والامريكية والمصرية.

الكلمات الدالة: البوليمر المقوى بألياف الزجاج, خرسانة عالية المقاومة.

كلية الهندسة بالمطرية
جامعة حلوان
قسم الهندسة المدنية

سلوك الكمرات الخرسانية المسلحة بالألياف الزجاجية تحت تأثير عزم اللي

رسالة مقدمه للحصول على درجة الماجستير في العلوم الهندسية
قسم الهندسة المدنية

مقدمه من
المهندس/ عبدالله فارس نافذ سيد امام
بكالوريوس الهندسة المدنية جامعة حلوان، مايو٢٠١٧

المشرفون:

أ.م.د. هالة ممدوح اسماعيل
أستاذ مساعد – قسم الهندسة المدنية
كلية الهندسة بالمطرية
جامعة حلوان

أ.م.د. أحمد محمد حسن علي
أستاذ مساعد – قسم الهندسة المدنية
كلية الهندسة بالمطرية
جامعة حلوان

٢٠٢٤